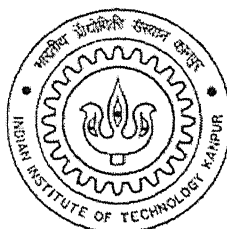# Membrane Preparation, Characterization, Modeling *and* Optimization *of* Pervaporation

A Thesis Submitted

in Partial Fulfillment of the Requirements

for the Degree of

Doctor of Philosophy
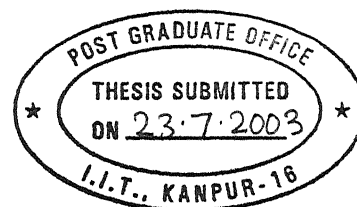
by

S. Venkata Satyanarayana

to the

Department of Chemical Engineering

INDIAN INSTITUTE OF TECHNOLOGY KANPUR

July, 2003

CERTIFICATE

It is certified that the work contained in this thesis entitled *"Membrane Preparation, Characterisation, Modeling and Optimization of Pervaporation"* by *S. Venkata Satyanarayana,* bearing roll number Y010262 has been carried out under our supervision and that this work has not been submitted elsewhere for a degree.

Dr. P.K. Bhattacharya
Professor
Department of Chemical Engineering
Indian institute of Technology, Kanpur
Kanpur-208016, (INDIA)

Dr. Ashutosh Sharma
Professor
Department of Chemical Engineering
Indian institute of Technology, Kanpur
Kanpur-208016, (INDIA)

July, 2003

SYNOPSIS

Pervaporation, a key technology for azeotropic separation, is considered to be useful for the treatment and recycling of volatile organic compounds. However, there are problems associated with membrane properties like low flux and low selectivity. Further, lack of generalized mass transport models are the other constraints, apart from cost of module. An attempt has been made, in the present thesis, to understand the basic transport mechanism and the nature of the membrane.

The present thesis has been divided into three sections constituting seven chapters. Further, chapter 1 introduces the process of pervaporation and its applications as well as organization of the thesis. The first section (chapters 2-4) deals with the membrane preparation, characterization, and separations. The second section (chapter 5) constitutes an attempt to understand the transport mechanism by conducting single component pervaporation experiments. Finally, the third section (chapters 6 & 7) concentrated on modeling, simulation, and optimization of pervaporation process. Following paragraphs describe brief summaries of chapter 2 to 7.

Positron annihilation technique, a powerful characterization tool to measure free volume and free volume fraction in polymers, was employed to estimate free volume parameters for both commercial and laboratory prepared membranes. These values may play important role in the pervaporation process and direct measurement of their sizes may

help to understand the transport mechanism behind separation. The positron lifetime spectra were analyzed, assuming 3 or 4 exponential components. Long-lived components (lifetimes in the range 1.4 to 3 ns) were found and were attributed to orthopositronium (o-Ps) pick-off annihilations in free volumes. Free volume size determinations were carried out, assuming in spherical as well as in cylindrical shapes. Further, in order to understand the changes in the characteristics of free volumes, these membranes were also studied in their soaked state (chapter 2).

Various polymeric membranes (commercial and laboratory prepared) were chosen as candidate materials for dehydration of hydrazine hydrate, the separation of which is challenging (pH~13). Further, ethyl cellulose membrane was modified by reacting with phenyl isocyanate to convert some of the -OH groups into carbamate groups. FTIR, XRD, etc., were performed to observe the modifications. Higher contact angle of water with modified membranes, compared to unmodified membranes, indicates increase of hydrophobicity. Further, sorption of both water and hydrazine hydrate in modified ethyl cellulose membrane were observed and were found to be lower compared to pure ethyl cellulose. Selective diffusion of water appears to dominate pervaporation selectivity of all the polymers. Apolar materials exhibited higher separation factors than polar materials. Contact angles of water and hydrazine hydrate were measured and their ratio was related to pervaporation selectivity (Chapter 3).

Composite membranes (PERVAP®1060 and PERVAP®1070) were utilised for hydrophobic pervaporation using toluene-water system to understand the role of support layer during pervaporation. Flory- Huggins interaction parameters (surface thermodynamic approach through contact angle measurement) as well as diffusion coefficient of toluene

with in the membrane were estimated in order to study solute – membrane interactions. Influences of operating conditions were observed on pervaporate fluxes and selectivities. The obtained values of selectivities for composite membranes suggested importance of support layer. Resistance –in-series model, along with solution –diffusion model was employed for mathematical analysis of the results (Chapter 4).

The membrane permeation of a component followed by its vaporization on the opposite face is governed by the solubility and down stream pressure. The evaporative flux of pure methanol and iso-propanol were measured using dense membranes with different free volumes and different affinities (wettabilities and solubilities) for the permeant. Solubilities of permeants in different composite membranes were estimated from the Flory-Huggins theory. The interaction parameter was obtained from the surface properties measured by the contact angle goniometery in conjunction with the acid-base theory of polar surface interactions. Interestingly, the evaporative flux for different membranes vanished substantially (20% - 90%) below the equilibrium vapor pressure in the bulk. The discrepancy was larger for smaller pore size and more wettable membranes. This observation, which cannot be explained by the existing (mostly solution-diffusion type) models of pervaporation, suggests an important role for the membrane-permeant interactions in nanopores that can lower the equilibrium vapor pressure. Indeed, the observations are found to be consistent with the lowering of equilibrium vapor pressure based on the Kelvin's equation. Thus, higher solubility or selectivity of a membrane also implies stronger permeant-membrane interactions and a greater retention of the permeant by the membrane, thus decreasing its evaporative flux. For the membrane-permeant pairs

S.V. Satyanarayana

Contents

List of Tables

List of Figures

Chapter 1

Introduction

Separation processes play an important role in the chemical industries for purifying raw materials, recovering product streams of desired purity and preventing pollution through treatment of waste streams released to the environment. It was estimated that around 30-70% of the capital cost of the chemical industry is accounted by separation processes [1]. The national research council reported more than 50 different types [1] of separation processes, including membrane based separations. Membrane processes are already well known for its relevance in the water desalination, effluent treatment, food processing, medical applications, gas separations and liquid mixture separations, etc. Membrane processes are classified with respect to the use of membranes (homogeneous or microporous), types of driving forces (difference of pressure, concentration, etc.) and nature of feed solutions (ionic, non-ionic, liquid, gas, etc.). Reverse osmosis, ultrafiltration, nanofiltration, microfiltration are pressure driven processes. Gas separation and pervaporation are other recently developed processes. An attempt has been made, in the present thesis, to understand basic transport mechanism and the nature of the membrane behind newly evolved membrane separation processes of pervaporation. The following

paragraphs, therefore, touch upon the basic phenomena and principles of the process to illustrate the intricacies involved in the process.

1.1 Pervaporation

Pervaporation is a process in which a liquid mixture is separated into its components by virtue of employing a selective (dictated by solubility) membrane. The name pervaporation in itself indicates the permeation and vaporization through the membrane. The separation is carried out using a dense or homogeneous film. The feed solution to be separated is contacted on one side of the membrane and the permeate, in vapour form, is obtained on the other side of the membrane by applying pressure lower than the saturation vapour pressure (Figure 1.1). The concentration gradient across (and within) the membrane is the driving force for the mass transport. This can be achieved by keeping the other side under dry state as compared to the feed side which is always kept under wet state. Usually, either vacuum (vacuum pervaporation) is applied or an inert gas (sweeping gas pervaporation) is passed on the other side. Besides these two modes of operation, there are several other process variants, including thermo pervaporation [2], vapour permeation [3], vacuum aided reverse osmosis [4], perstraction [5], membrane distillation [6,7], and electrically induced pervaporation [8].

Unlike other membrane processes, pervaporation involves a phase change of permeate. Therefore, the enthalpy of vaporization is the minimum amount of energy required for the process. Further, there is strong interaction between liquid feed components and membrane, resulting into high swelling of membrane. The swelled film works as a pseudo-liquid immobilized layer. Further, swelling tends to alter the membrane properties and generally leads to higher permeability and lower selectivity. The swelled

membrane allows the diffusion of feed components from one side of the membrane to other. Thus, the permeate composition is mainly determined by relative affinities of the feed components and also for their unequal mobilities within the membrane. Accordingly, permeate composition varies from that of the vapour liquid equilibrium [9].
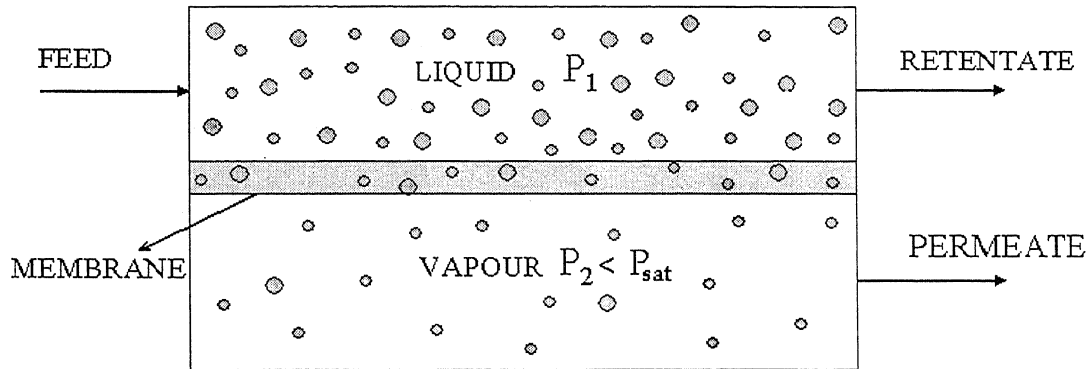
Figure 1.1 Schematic diagram of pervaporation principle

1.2 History

The phenomenon of pervaporation was first observed by Kober [10] for his experiments on evaporation of water placed in a collodion (cellulose nitrate) bag into atmospheric air. Before to this, in 1906 Kahlenberg.[11] reported some qualitative observations concerning the selective transport of hydrocarbon/alcohol mixtures through a thin rubber sheet. In 1935, Farber [12] recognized the usefulness of pervaporation for

4

separation and concentration. However, Heisler et al. [13] reported the first quantitative work for the separation of alcohol/water using cellulose film by pervaporation. Binning and co-workers [14, 15] carried out pervaporation of different mixtures and highlighted the potential application of pervaporation. A first commercial application of pervaporation, installed in Brazil, was reported in 1982 [16] for the separation of alcohol-water mixtures using G.F.T. (Gesellschaft für Trenntechnik, Homburg/Saar, F.R.G) membrane. Meanwhile, development of new membranes, experimental investigations, fundamental understandings, theoretical models, and module designs are in progress [17, 18].

1.3 Applications

Pervaporation finds several applications and may be classified into various categories as:

1. *Dehydration of liquid mixtures*; a) Azeotropic mixtures: Ethanol – water, Dioxane – water, etc.; b) Close boiling mixtures: acetic acid – water; c) Electrolytic solutions.

2. *Removal of organics from water*; a) Pollution control: toluene-water, benzene-water, etc.; b) Aroma recovery: apple juice aroma compounds, etc.; c) Wine and beer dealcoholisation.

3. *Separation of organic –organic mixtures*; a) Azeotropic mixtures: Benzene – cyclohexane, MTBE – methanol, etc.; b) Isomers: C8 isomers.

4. *Reactive pervaporation*; Removal of water from the product of esterification reactions to shift equilibrium reaction towards the product side.

5. *Hybrid process*; integrating pervaporation unit with other conventional units.

1.4 Merits and Limitations of Pervaporation

It is being considered that in addition to various applications, pervaporation may be energy efficient, pollution free, easier plant installation, maintenance, and expansion. Bravo et al. [19] ranked pervaporation third highest amongst the 31 techniques under evaluation for the fluid separation. Further, in 1983, Baker [20] had predicted that by the year 2000 all the refineries would have used pervaporation for the separation of liquid mixture. The process, however, could not fulfil its earlier promise because of low flux with dense membranes, low selectivity due to high swelling of the membrane, lack of mathematical models, lack of design of high compact modules, lack of cost estimations, fundamental understandings (particularly downstream pressure effect), etc.. Therefore, the present thesis is an attempt to seek some answers of these aspects by carrying out detailed experimentations, membrane characterizations, modelling and simulation, optimizations, etc. The broad objectives of the thesis may be described as:

➢ To prepare membranes with known and newer polymers as well as to modify. Study the modified characteristics of such membranes. Further, to characterise membranes (both prepared and commercially available) using advanced analytical techniques such as positron annihilation, contact angle, etc.

➢ To conduct experiments for the study of common as well as newer but highly important separation schemes using laboratory prepared and commercially available membranes.

➢ To develop mathematical models for prediction of flux and selectivity of few liquid mixtures.

➤ To conduct experiments and to theoretically examine the results in order to understand the basic mechanism behind separation during pervaporation and its associated problems (like air leaks).

➤ To study separation schemes, particularly in terms of design and cost analysis using advanced optimization tools.

1.5 Schematic Presentation of Thesis

The hierarchy of the present work can be presented pictorially in Figure 1.2.

1.6 Organization of Thesis

The following paragraphs describe the layout of the total work, present in the thesis (chapter wise).

The thesis has been divided into three major/minor sections. Further, chapter 1 introduces the importance, fundamental mechanism and design principle of pervaporation process, apart from potential applications. The chapter also presents organizational aspects of the thesis. Section A comprise of membrane preparation, characterization and applications of pervaporation, followed by transport mechanism (section B) and modelling, simulation and optimization (section C).

In the pervaporation studies membrane preparation and characterisation play significant role towards separations of various systems. Section A was, therefore, subdivided into three chapters (Chapter 2 to 4). Several commercial composite and dense membranes are available for pervaporation studies; hence, a work was carried out to determine the pore sizes as well as to characterise these membranes using positron annihilation technique. Chapter 2 describes the estimation of free volume/pore sizes of both the types of membranes (dense and composite) apart from laboratory cast

Characterisation of dense and composite membranes: positron annihilation technique (Chapter 2)

Membrane
A. Preparation, Characterisation& Applications

Dehydration of hydrazine hydrate: Membrane preparation, characterisation and separation (Chapter 3)

Role of composite membrane support layer: Toluene-Water system (Chapter 4)

B. Transport Mechanism

Single component permeation and solubility measurements (Chapter 5)

Hydrazine-water separation with hollow fibre module: Study of operating parameters (Chapter 6)

Modelling,
C. Simulation & Optimization

Multicomponent system (VOCs): optimization with real coded genetic algorithm (Chapter 7)

Figure 1.2 Organization Chart of Thesis

8

hydrophilic and hydrophobic membranes. The method of positron annihilations directly measures these values which proved immense help and gave better understanding towards the use of these membranes for subsequent studies of pervaporation applications.

One of the important systems that may be applied for pervaporation is dehydration of hydrazine hydrate. Hydrazine is an important inorganic chemical and separation of this compound from water by conventional process is highly energy consuming due to its formation of azeotrope. An exclusive chapter (chapter 3) has been presented for such an application. The separation of hydrazine hydrate needed special membrane preparations (modified ethyl cellulose and *apolar* polymers) and their characterizations using FTIR, XRD, contact angle measurements, etc.

Composite membranes have been used for toluene – water separation. The support layer, however, plays an important role in dictating the flux and selectivity. A detailed study was carried out to emphasis the role of support layer for the composite membranes during separation, adapting the standard toluene-water system. Chapter 4 presents such a work.

A fundamental enquiry that came to quite a few researchers, also constituted the present work which is the single component permeations of pervaporation. Therefore, in section B which constitutes single chapter (chapter 5), such a work on single component permeation was carried out with emphasis on permeant-membrane interactions. The previous models do not account this aspect. Chapter 5 addresses fundamental enquires with detailed experimentations to understand and to help to design the pervaporation process.

approach which constitutes section C. This section is divided in two chapters (Chapter 6 & 7). Chapter 7 presents a work on hydrazine-water separation with hollow fiber module in which influence of operating parameters as well as spatial variations of properties have been studied. Separate equations were developed for the feed flow either in the tube side or in the shell side for hollow fiber module. The obtained equations were solved by clubbing with solution diffusion model for estimation of flux and selectivity.

Multi-component systems are common to chemical process industries and conventional techniques require higher costs for separation. It was felt that pervaporation process may provide a contrast picture because of the basic mechanism of separation Therefore, a work was carried out to optimise the incurred cost (capital & recurring) of separation for a multicomponent system (VOC's) using real coded genetic algorithm and presented in Chapter 7.

Each chapter (2-7) is complete in itself, in terms of its own introduction, literature review, development of theory (if necessary), experimental section (if necessary), results and discussions, conclusions, references and appendix (if necessary). Therefore, each of these chapters are presented in their completeness and hence exclusive by nature.

Finally, some recommendations are made based on the work done, experiences through experimentations and is summarized in chapter 8.

References

[1]   Rakesh Agrawal, Separations: Perspective of a process developer/designer, AIChE, 47 (2001) 5.

[2]   P. Aptel, N. Challard, J. Cuny, J. Neel, Application of the pervaporation process to the separation of azeotropic mixtures, J. Membrane Sci., 1 (1976) 271-287.

[3]   R. W. Baker, N. yoshioka, J.M. Mohr, A.J. Khan, Separation of organic vapours from air, J. Membrane Sci., 31 (1987) 259-271.

[4]   M.D.C Goncalves, D. Windmoller, N.D. M. Erismann, F. Galembeck, Pressure-driven pervaporation, Sep. Sci. Tech., 25 (1990) 1079.

[5]   I. Cabasso, J. Jagur-Grodzinski, D. Vofsi, A study of permeation of organic solvents through polymeric membranes based on polymeric alloys of polyphosphonates and actylcellulose. II. Separation of benzene, cyclohexene and cyclohexane, J. Appl. Poly. Sci., 18 (1974) 205-232.

[6]   A.C.M. Fraken, S. Ripperger, Terminology for membrane-distillation, Recommendations by the European society of membrane science and technology. Issued on Jan. 1988.

[7]   N. Kjellander, Design and field tests of a membrane distillation system for seawater desalination. Desalination, 61 (1987) 19-26.

[8]   S.F. Timashev, V.V. Valuev, R.R. Salem, A.G. Strugatshaga, Pervaporation induced by electric current, J. Membrane Sci., 91 (1994) 249.

[9]   J. Neel, P. Aptel, and R. Clement, Desalination, 53 (1985) 297-396.

[10]   P.A. Kober, Pervaporation, Perstillation, and Percrystallisation, J. of Amer. Chem. Soc., 39 (1917), 9444.

[11] L. Kahlenberg, On the nature of the process of osmosis and osmotic pressure with observations concerning dialysis. J. Phys. Chem., 10 (1906) 141.

[12] L. Farber, Applications of pervaporation, Science 82 (1935) 158.

[13] E.G. Heisler, A.S. Hunter, J. Sicilliano, R.H. Treadway, Solute and temperature effects in the pervaporation of aqueous alcoholic solutions. Science, 124 (1956) 77.

[14] R.C. Binning, R.J. Lee, J.F. Jenning, E.C. Martin, Separation of liquid mixtures by pervaporation. Ind. Eng. Chem, 53 (1961) 45-50.

[15] R.C. Binning, F.E. James, How to separate by membrane permeation. Petroleum Refiner, 37 (5) (1958) 214-215.

[16] H.E.A. Bruschke, W.H. Schneider, G.F. Tusel, Pervaporation membrane for the separation of water and oxygen containing simple organic solvents. Communication, European workshop on pervaporation, Nancy, France, Sept. 21-22, 1982.

[17] A.Jonquières, R. Clément, P. Lochon, J. Néel, M. Dresch, B. Chrétien, Industrial state-of-art of pervaporation and vapour permeation in the western countries, J. Membr. Sci. 206, (2002) 87-117.

[18] X. Feng, R.Y.M. Huang, Liquid separation by membrane pervaporation: A review, Ind. Eng. Chem. Res. 36 (1997) 1048-1066.

[19] J.L. Bravo, J.R Fair, J.L. Humphery, C.L. Martin, A.F. S. Seibert, Fluid mixture separation technologies for cost reduction and process improvement, Noyes Data: Park Ridge, NJ, 1986.

[20] R. Baker, Membrane technology in the chemical industry: Future Directions. In: Membrane technology in the chemical industry, Edited by S.P. Nunes and K.-V. Peinemann, Wiley-VCH, Verlag Gmbh, Weinheim, 2001.

Chapter 2

Characterization: Positron Annihilation Lifetime Spectroscopy

2.1 Introduction

Pervaporation is a relatively new membrane separation process applied to separate liquid mixtures. The separation is carried out using dense polymeric film. The feed solution to be separated is contacted on one side of the membrane and permeate in vapour form is obtained on the other side of the membrane by applying pressure lower than the saturated vapour pressure. The mass transport mechanism through the membrane is considered complex because of the high interaction between the liquid feed components and the membrane, resulting into high swelling of the membrane. Free volume existing in membrane plays an important role in pervaporation process. Free volumes can be in the form of static holes (unfilled spaces) or created and destroyed as a result of molecular motions (dynamic free volumes), in the macromolecular network, or in the form of connected free volumes, known as pores. Principally, there are two mechanistic models to describe the mass transport: (i) Solution - Diffusion model and (ii) Pore Flow model. The solution - diffusion model is widely accepted, particularly, because of its simplicity. According to this model, pervaporation permeability is simply the product of solubility and

diffusivity. Free volume theory of diffusion when extended to polymeric systems [1-2] suggests diffusivity (of a component within the membrane) being a strong function of concentration of permeating component. Yeom and Huang [3] developed a model to predict pervaporation performance of membranes based on the free volume theory. An empirical relation connecting free volume and glass transition temperature was used to estimate the free volume fraction of the dry membrane. However, as the determination of glass transition temperatures of cross-linked and composite commercial membranes is difficult, this model may not be very useful for wider applications. In this context, a direct determination of the free volume parameters may greatly help in understanding the complex processes involved in pervaporation. Further, in their model [3], the free volume fraction of wet membrane was assumed to be the sum of free volume of the polymer and the increase in free volume due to the plasticizing action of the permeating components. The later contribution was estimated from the increase in specific free volume as the temperature is increased and hence led to increase in free volume for any membrane-permeate combination. However, the mechanism leading to expansion in free volume is related to plasticizing action and not all permeating components plasticize with membrane [4]. In these situations, the vital input parameter will be grossly incorrect. Thus, the model can be utilized only if the free volume size of the wet membrane is available from more direct and reliable measurements.

According to solution – diffusion model, the zero flux condition during pervaporation may be achieved at a downstream pressure equal to the saturation pressure of the permeating component [5]. However, our recent experiments on single component permeation through commercial membranes (Chapter 5) and work done by Vallieres, et al.,

[6] showed the importance of air leaks in pervaporation experiments. Quantitative estimation of air leaks showed the occurrence of zero flux condition well below the saturation vapour pressure during pervaporation. It was inferred that this might be due to depression of equilibrium vapour pressure within the membrane. Such depression of equilibrium vapour pressure may be estimated by Kelvin's equation [7], if we assume cylindrical pores to exist and know the effective radius of such pores.

Thus measurement of free volume size assumes an important role for understanding pervaporation process. However, free volumes of a dense membrane are generally in the size range of 1 to 6 angstrom, a direct determination of this size range is not straightforward. Positron annihilation technique [8] has developed into a powerful characterization tool for the study of free volume sizes and free volume fraction in polymeric materials. By measuring the lifetimes of the positrons, one can get fairly accurate estimates of the free volume of angstrom (2-10 Å) range. Contrary to other methods, PAS is capable of determining the holes and free volume in a polymer without being significantly interfered by the bulk. When positrons are implanted into a polymeric material, some of them interact with the electron clouds in the material to annihilate and give two gamma rays of energy 511 keV each. However, a fraction of positrons combine with the electrons to form a hydrogen-like quasi-stable atom, known as positronium and denoted as Ps. Depending upon the spin alignment, positronium could be in the form of para-positronium (p-Ps) or ortho-positronium (o-Ps). The positronium atom preferentially gets localized within the free volume cavities and annihilate after an average time characteristic of the shape and size of the free volume. Positron annihilation lifetime spectra are analyzed in terms of three lifetime components, viz: para-positronium (p-Ps)

annihilation, τ_1; free positron and positron-molecular species annihilation, τ_2; and o-Ps annihilation, τ_3. While τ_1 and τ_2 are of the order of few hundred picoseconds, τ_3 is of the order of nanoseconds. Each lifetime has an intensity I, corresponding to the fraction of annihilations taking place with the respective lifetimes. The parameters τ_3, I_3 corresponding to the decay of o-Ps provide the size-specific information for free volumes and pores.

Free volume radius r is obtained by first considering o-Ps trapped into a spherical volume with radius r_0, providing infinite potential barrier. The Schrödinger equation is solved to obtain the positronium wave function for the centre of mass motion of o-Ps in the ground state. The o-Ps pick-off annihilation rate is then calculated through a semi-empirical approach, by assuming a homogeneous electron layer with a thickness of Δr ($= r_0 - r = 0.166$ nm) adjacent to the wall and calculating the overlap of positronium wavefunction with the electron layer. Accordingly, the following expression may be obtained, which relates o-Ps pick-off lifetime, τ_3 and free volume radius [9-11].

$$\tau_3 = \frac{1}{2}\left[1 - r/(r + \Delta r) + (\frac{1}{2\pi})\sin(\frac{2\pi r}{r + \Delta r})\right]^{-1} \tag{2.1}$$

Further, the fractional free volume f, may be estimated from the following empirical relation.

$$f = CV_F I_3 \tag{2.2}$$

Where V_F is free volume and the scaling factor, C, is obtained from variation of free volume with temperature. However, in the absence of such data, it may be typically assigned a value of 1.0 [12]. Equation (2.1) can also be used for cylindrical free volume (pore) with the value of Δr set at 0.196 nm [13]. In this case, for the same lifetime value, one gets a higher value for the radius as compared to the spherical case.

In this chapter, measurement of free volume size and their fraction in the total volume of the material for a number of dry membranes as well as for wet membranes (obtained in real experimental situation) were reported.

2.2 Experimental

2.2.1 Materials

Analytical grade toluene (Ranbaxy, India), acetone (Ranbaxy, India), formamide (Loba Chemie, India), Ethyl cellulose (ethoxy content 48-49.5%: Loba-Chemie, India), cellulose acetate (Jams Chemicals, Bombay), Benzyl isocyanate (laboratory prepared) and acrylonitrile styrene butadiene (Strasis & Co, USA) were used to cast the membranes. Ethanol (Hychem, England), hydrazine hydrate (Qualigens, India) and double distilled water were used for soaking and pervaporation purpose. The commercial composite membrane PERVAP® was obtained from Sulzer Chemtech, Germany. The membrane consists of a very thin (0.5-2 μm) separating layer on top of a porous support (70-100 μm), which in turn is on top of a polymer fleece (non-woven fabric of thickness 100 μm). Another composite membrane HR-98-PP was obtained from Danish Separation Systems, Denmark.

2.2.2 Membrane Preparation

Ethyl cellulose (EC) polymer (10 g) was dissolved in toluene (90 g). The solution was centrifuged (REMI model -R 24) at 10000 rpm for 15 minutes for the removal of un-dissolved polymer and dust particles. The supernatant homogeneous solution was transferred to a conical flask (air tight) and kept for overnight for the removal of entrappe

Table 2.1 Base polymers and cross-linking level for commercial membranes.

PERVAP® is a registered trademark of Sulzer Chemtech, Germany

Membrane	Base Polymer	Cross-linking level	Reference
HR98PP	Polypropylene	-	As specified by the manufacturer
PERVAP 1060	PDMS	Not Available	[17]
PERVAP 1070	PDMS + Silicalite Zeolite	Not Available	[17]
PERVAP 2201	PVA	High	[17]
PERVAP 2210	PVA	Low	[17]
PERVAP 2256	PVA	Not Available	[17]

air bubbles. The casting of membrane was carried out on modified thin film applicator (ACME-make, India) using a glass plate. After around 24 hours of solvent evaporation at room temperature, the membrane together with the base glass plate was placed in vacuum oven for another 4 hours for the removal of residual traces of solvent. Finally, the membrane was peeled off the glass plate.

Similar procedure was followed for casting acrylonitrile butadiene styrene (ABS) membrane; by taking the polymer (16 wt %) in toluene solvent. Ethyl cellulose reacted with isocyanate membrane (ECNCO), was prepared by adding 4ml of benzyl isocyanate to 100ml of 10% polymer solution. Cellulose acetate (CA) membrane was prepared by taking 17wt% cellulose acetate in 68% acetone and 15% formamide.

2.2.3. Sorption Studies

Pre-weighed dry membranes were taken in a conical flask containing water or ethanol for sorption purpose. The flask was kept on shaking bath (model SW-23, Julabo, Germany) under 200 rpm for a longer period (6-7days) at room temperature. The membranes in conical flasks were taken out at regular intervals and were wiped with tissue paper for the removal of the adhering liquid. The wet weight of the membrane was measured. The procedure was repeated until consecutive readings of weight of wet membranes were equal. The difference of weights was presented with respect to dry weight of membranes as percentage of sorption.

2.2.4. Positron Annihilation Lifetime (PAL) Measurements

Positron annihilation experimental setup photograph is shown in Figure 2.1. The PAL measurements were carried out using a system having a resolution of 300 pico-seconds (FWHM for the ^{60}Co prompt γ-rays, under ^{22}Na window settings). This is a fast-fast coincidence system conventionally used in nuclear spectroscopy. The detector consists of fast NE111 scintillators coupled to fast RCA8575 photomultiplier tubes (PMT). The high voltage (HV) source is connected to the PMT through the PMT base. The anode pulse from the PMT is fed to the constant fraction differential discriminator (CFDD). Each CFDD generates the timing information if the detected events fall within the selected energy ranges. In the case of 'START' the energy window is set on the upper 50% of the Compton events of the 1.28 MeV γ-ray and in the case of 'STOP' the energy window is the upper 50% of the Compton events of the 0.511 MeV γ-ray. If they are coincident within the selected resolving time (50 ns) for the coincidence unit, the time-to-pulse-height-converter (TPHC) is gated to accept the delayed timing information using DELAY unit. The

Positron Annihilation Lifetime Spectroscopy
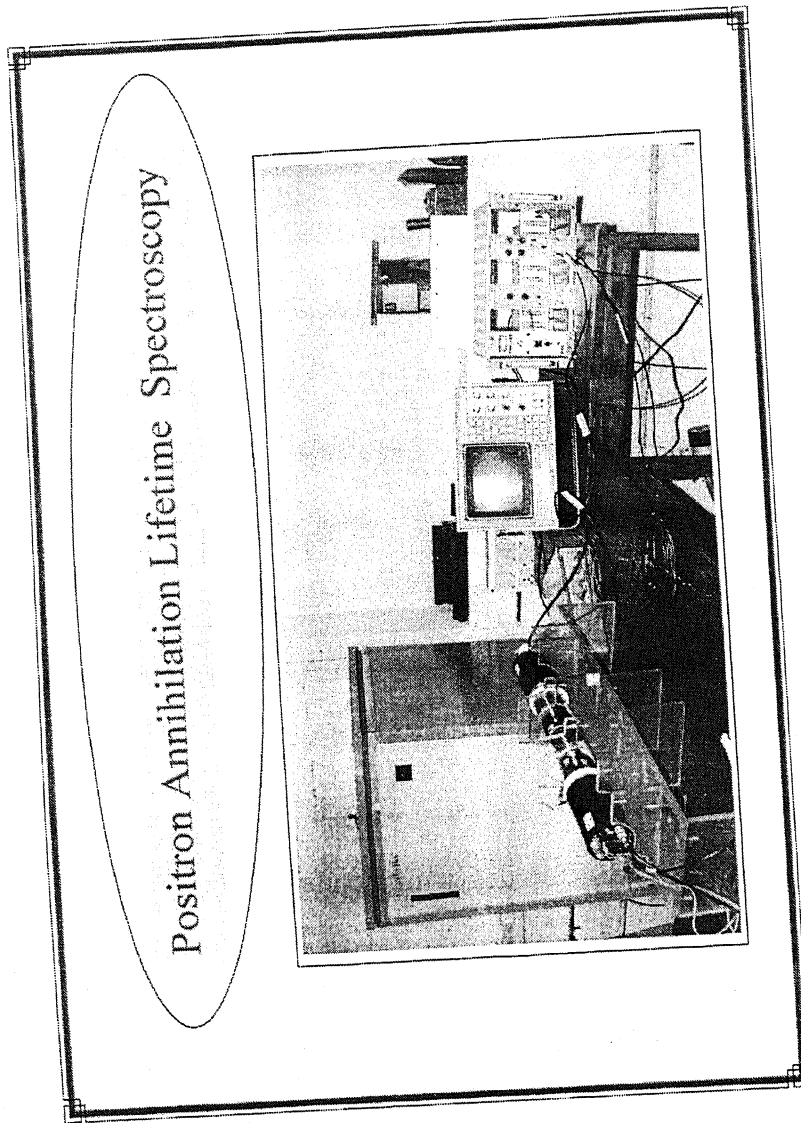
Figure 2.1 Photograph of Positron annihilation experimental setup
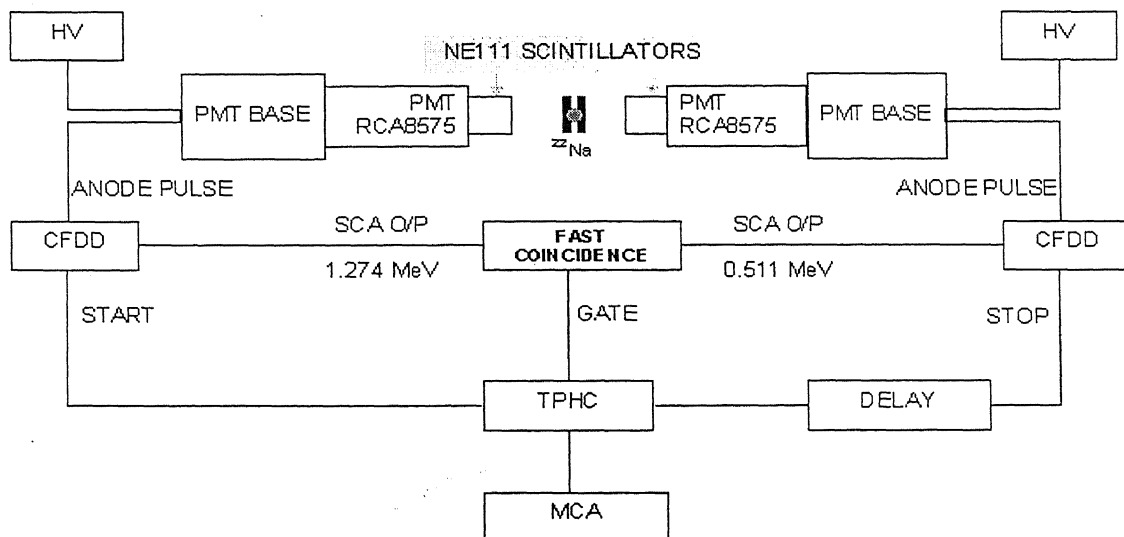
Figure 2.2 A block diagram of the positron annihilation lifetime measurement setup.

histogram of time intervals is accumulated in the multichannel analyzer (MCA). A block diagram of the system is shown in Figure 2.2.

The positron source was prepared by depositing around 2 micro-Curie aqueous ^{22}NaCl on a thin aluminium foil (thickness ~ 12μm), and covering it with an identical foil. The source was sandwiched between 13 layers (on each side) of the polymeric membrane, which were stacked together. The separating layer portion (membrane) was pealed out from the "woven fabric" for commercial membranes for positron study. For laboratory made membranes, samples (membranes) were prepared with sufficient thickness to absorb 99.9% of the positrons. The source-sample sandwich was placed between two NE111 scintillators coupled to RCA 8575 tubes. All the measurements were made at room temperature (24°C). Approximately one million counts were collected in each spectrum, and four spectra were measured for each sample. The lifetime data were analysed using PATFIT-88 programs [14]. Source correction was done for all spectra. In the case of measurements on water-soaked and ethanol-soaked samples, the soaked membranes were sealed inside a commercial polymer cover. The polymer cover was tested for its non-permeability for water and ethanol with satisfaction (0.1% loss for both the components). The positron spectra were corrected for annihilations taking place within the cover material.

2.3 Results & Discussion

The positron lifetime spectroscopy data were analysed, in general, by fitting three lifetime components. Scanning electron microscopy picture of the porous layer in the case of commercial membrane showed (Figure 2.3) pore size range of 1-10 μm. The positron
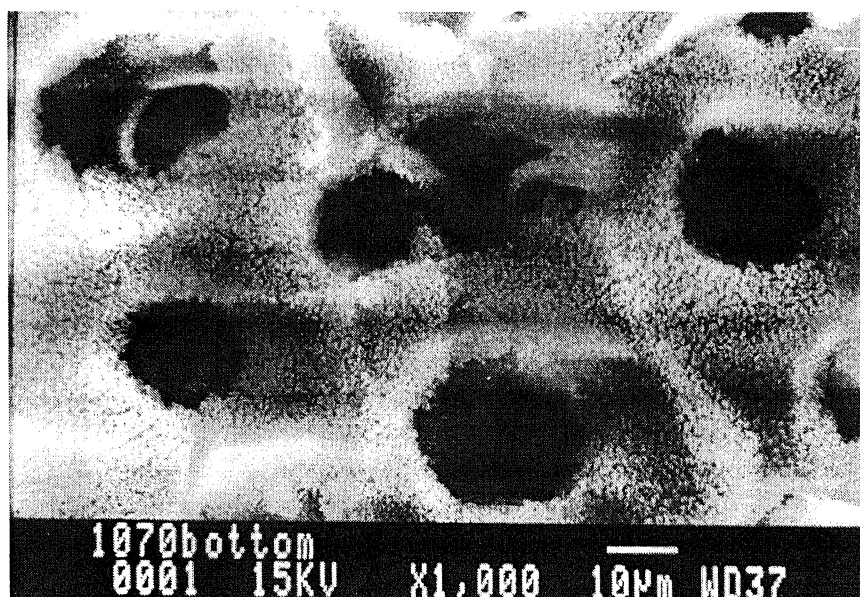
Figure 2.3 Scanning electron microscope picture of porous layer of PERVAP®1070.
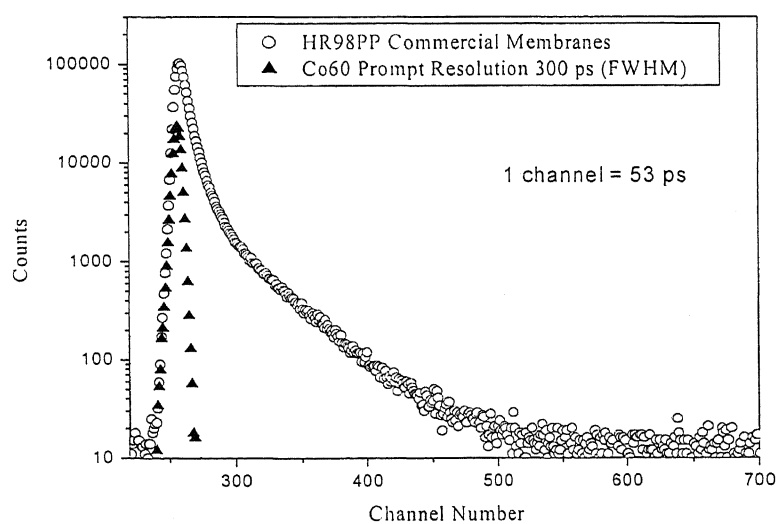
Figure 2.4 A typical positron lifetime spectrum for HR-98-PP membrane

annihilation lifetime in such large pores would be of the order of several tens of nanoseconds, which may not affect the spectrum, as recorded. Further, the density of the support layer is very small compared to dense layer. Hence, the contribution of the porous layer for the positron annihilation lifetime spectrum of the membrane in the dry state was neglected. A typical positron lifetime spectrum (a sum of decaying exponentials corresponding to the number of positron states in the material convoluted with instrumental resolution function) for the membrane HR-98-PP is shown in Figure 2.4.

2.3.1 Commercial Membranes

2.3.1.1 Dry State

The base polymer and level of cross-linking level for commercial membranes [15] are given in Table 2.1. The positron lifetime parameters and the calculated free volume parameters for commercial membranes are given in Table 2.2.

HR-98-PP membrane for which the base material is polypropylene, the free volume radius obtained from our measurements is 0.281 nm. This value is in excellent agreement with an obtained value from a mathematical model by Rosa and de Pinho [16]. Further, positron annihilations also provide the value of intensity I_3 as 15.2%, which is incidentally the largest value obtained for commercial membranes (Table 2.2), utilised for the present work. This reflects high free volume available for such commercial membrane, meant to be applied for reverse osmosis operation.

PDMS polymer is the base material for both PERVAP 1060 and PERVAP 1070. Further, an extra component in the form of silicalite zeolite is also present in PERVAP 1070. Accordingly, the positron lifetime spectrum corresponding to the later had to be fitted with four lifetime components whereas the usual three components were sufficient

Table 2.2 Free volume parameters of commercial membranes

Membrane	State	τ_3 (ns)	I_3 (%)	r (nm) (sphere)	V_f (nm^3)	F	r (nm), cylinder
HR98PP	Dry	1.96±0.01	15.2±0.2	0.281	0.093	0.014	0.324
PERVAP 1060	Dry	2.30±0.02	9.4±0.2	0.311	0.126	0.012	0.359
PERVAP 1070	Dry	2.32±0.28, τ_4:4.53±0.48	10.6±1.5 I_4:5.1±2.0	0.312 / 0.451	0.128 / 0.385	0.014 / 0.020	0.36 / 0.52
PERVAP 2201	Dry	1.64±0.04	8.3±0.4	0.249	0.065	0.005	0.288
PERVAP 2256	Dry	1.73±0.06 / 6.19±0.36	8.8±0.2 / 1.1±0.1	0.259 / 0.526	0.073 / 0.608	0.006 / 0.007	0.298 / 0.606
PERVAP 2210	Dry	1.46±0.02	9.3±0.3	0.229	0.050	0.005	0.264
PERVAP 2210	Water soaked	1.52±0.03	14.6±0.6	0.236	0.055	0.008	0.272
PERVAP 2210	Water soaked and dried	1.48±0.02	9.3±0.2	0.231	0.052	0.005	0.267
PERVAP 2210	Ethanol soaked	1.26±0.40, τ_4:3.30±0.11	4.6±1.4 I_4:8.8±0.8	0.204 / -	0.036 / -	0.002 / -	0.235 / -

for PERVAP 1060. The lifetime τ_3 was observed to be almost same (~ 2.3 ns) for both the

membranes, reflecting same size of voids in the base material. However, the presence of

zeolites for PERVAP 1070 was reflected by the lifetime measurement [8], employing an

extra component τ_4 (4.53 ns). Vankelecom et al. [17] have found that only compounds with

molecular size below 0.55 nm may permeate through silicalite zeolite. This implies the size

of pores being around 0.55 nm and our measured value of the radius of free volume

(assuming cylindrical pores) was found to be 0.52 nm.

The component values of τ_3 are found to be slightly in variance (Table 2.2) for

PERVAP 2201, 2256 and 2210. This is because of varied preparation technique of these

membranes, in spite of having same base material (PVA). PERVAP 2256 required

addition of a fourth component ($\tau_4 = 6.19$ ns) with a small intensity value (1.1%) to obtain

improved fit. Requirement of τ_4 suggests the presence of extra component on base PVA, as

this membrane is meant for organic-organic separation [18]. Comparing PVA based

membranes (2201, 2256 and 2210) to PDMS based membranes (1060, 1070) and

polypropylene based membrane (HR98PP), it was observed that the fraction of free volume

of PVA based membranes are consistently smaller than others. This is expected as the base

polymer PVA has glassy structure compared to rubbery structure of PDMS. The free

volumes are known to be larger for rubbery structures [19]. Such measurements of free

volume fractions may help to model [3] for efficient design of pervaporation process.

2.3.1.2 Wet State

As mentioned earlier, free volume may change from a dry state membrane to wet

state due to swelling. Therefore, accurate estimation of free volume of membrane under

wet state assumes importance as it eventually relates diffusivity of species within the

membrane, commonly obtained through empirical relations. Further, it was thought to examine the reversibility or irreversibility of swelling effect, due to sorption, on the free volume of the membrane. Therefore, in this paper positron lifetime measurements were carried out for sorbed (water soaked and ethanol soaked) and air dried water soaked (prior to) membrane (PERVAP 2210). The results are reported in Table 2. 2.

Following general observations may now be mentioned (as reported in literature) for information purpose only in order to enhance clarity of understanding while interpreting results of wet membranes. In polymers, positronium atoms are formed in the free volumes [20]. It is known that only about 28% [21] of the positrons, entering into bulk water, are able to form o-Ps. Whereas 22% of positrons enter into ethanol bulk to form o-Ps [22]. The probability of positronium formation in the free volumes containing water or ethanol may be smaller compared to empty free volumes. Thus, a decrease in I_3 is expected in the case of sorbed (soaked) membranes, in the absence of plasticization.

2.3.1.2a Water Soaked Membranes

Water soaked membrane (wet state) shows a positron lifetime of 1.52 ns, which is slightly greater than that observed under dry state. The intensity, I_3 is increased from 9.1 to 14.6%. Water occupying larger size pores (~10 μm) in the porous support may also contribute to positron lifetime spectrum. The lifetime of positronium in bulk water is known to be 1.81 ns [21] and the lifetime for dry state membrane (2210) is 1.46 ns. This small difference of lifetime may be insufficient for four- component fit. Therefore, the lifetime 1.52 ns (measured for the water-soaked membrane) may represent a weighted average of the two. The contribution from water may also be responsible for the increase in I_3, at least partially. The other contribution may come from the interaction of water with the

skin layer. PERVAP 2210 is highly selective for water (solubility is around 193 g of water in 100g of polymer if the skin layer is assumed to be PVA). The molecules efficiently dissolve where they contact the membrane and plasticization occurs. Plasticization can expand the existing free volumes and also it can create new free volumes. This may enhance the lifetime as well as the intensity. However, quantitative estimation is difficult because of the presence of water in the porous support as well as due to the change in the positronium formation probability, once the free volumes are filled with water.

2.3.1.2b Water Soaked and Dried Membranes

The lifetime τ_3 and its intensity I_3 are almost same for both dry as well as for dried water sorbed membrane (PERVAP 2210). Therefore it is obvious there is no change in the free volume or in other words the free volume is reversible by nature if a dry membrane undergoes sorption and then dried. However, an interesting observation was noticed with regard to amount sorption of water for PERVAP 2210 under two different conditions; i) sorption for a fresh dry membrane and ii) sorption of air-dried water sorbed (prior to) membrane. The results are reported in Table 2.3. In the first case sorption is more than 300%, whereas for the second case sorption was only 125% by weight. Therefore, it is evident that fresh polymer initially gives much higher sorption then in its repeated use for sorption. It is known that the porous support is of poly acrylonitrile material [15], which may not be much affected by water; hence, the difference in the water sorption between the two cases may be because of the changes in the sorption property of the skin layer. The fact that the positron annihilation lifetime does not show any change may be understood by noting that sorption is a thermodynamic phenomenon, which depends on the surface characteristics of the membrane; whereas, the positron annihilation lifetime measurements

in the present study provide free volume properties of the bulk of the membrane (depth-averaged information).

Table 2.3 Sorption of water in PERVAP 2210

Type	Dry weight (g)	Equilibrium weight of wet membrane (g)	% Absorption
Fresh	0.0340	0.1363	300.9
Soaked and dried	0.0340	0.0765	125.0

2.3.1.2c Ethanol Soaked Membrane

Free volume measurements were also done through sorption of ethanol on PERVAP 2210 membrane. Earlier studies [23] have showed that 2210 membrane is highly selective for water compared to ethanol. Pervaporation studies for ethanol-water system [23] with a feed of 10% of water, permeate contained more than 90% of water. This shows that ethanol is much less soluble in PERVAP 2210 membrane. Thus the value of positron lifetime τ_3 and intensity I_3 of ethanol sorbed (soaked) membrane may be expected to be nearly same as that for dry membrane. However, this is not the case as seen from Table 2.2.

A four-component fit was needed with an intense component having 3.30 ns, which is a high value. Incidentally, the positron lifetime for bulk ethanol is also known to be 3.30 ns [22]. This high value is expected, as the presence of ethanol in the larger pores of the porous support (~10 μm) contributes significantly. Further, unlike the case with water-

sorbed membrane, the lifetime for ethanol is much different from that of dry membrane. Therefore, a four component fit resolved well for such a large lifetime difference (3.3-1.46 ns) between ethanol sorbed and dry membrane conditions. The value of τ_3 (1.26 ns) corresponds to the free volume of the polymer itself. This value is smaller than 1.46 ns found for the case of the dry membrane. Correspondingly, the free volume radius is also smaller, as seen by the positrons. One of the possible reasons for this reduction in τ_3 may be because larger size free volumes are filled with ethanol as lower probability of positronium formation may contribute less lifetime spectrum.

2.3.2 Laboratory Cast Membranes

2.3.2.1 Dry State

The free volume parameters for four laboratory-prepared homogeneous membranes (EC, ECNCO, CA and ABS) were measured (through positron lifetimes) and are reported in Table 2.4. The free volume radii and the fractional free volume are observed to be larger than those for the commercial membranes. This may be due to the fact that laboratory prepared membranes were untreated, i.e., there was no cross-linking either by chemical addition or by heat treatment. Lower free volume radii may be directly related to the high selectivity of commercial membranes for specific cases. The values of fractional volume, obtained in our measurement, are in agreement with the value (ie., 2.5%) from Williams-Landel-Ferry equation [24].

Generally, the estimated pore size estimation of pervaporation membranes is little more than a nanometer [25]. The present measurements, which are more direct in nature, show that for all the membranes studied the pores are smaller than one nanometre in size. The pore sizes are found in the range of 0.2 to 0.6 nm. (water molecule size is 0.31 nm.)

Table 2.4 Free volume parameters of laboratory cast membranes

Membrane	state	τ_3 (ns)	I_3 (%)	r (nm) (sphere)	V_f (nm^3)	F	r (nm), cylinder
EC	dry	2.63±0.01	26.0±0.2	0.337	0.160	0.042	0.385
EC1	dry	2.55±0.02	22.5±0.3	0.331	0.151	0.034	0.381
ECNCO	dry	2.26±0.01	17.5±0.2	0.308	0.121	0.021	0.355
ABS	dry	2.37±0.02	21.1±0.3	0.317	0.133	0.028	0.365
CA	dry	2.16±0.02	18.8±0.3	0.300	0.112	0.021	0.345
CA	Ethanol-soaked	2.91±0.05	7.5±0.2	0.357	0.190	0.014	0.411
EC	Water-soaked	2.26±0.02	17.7±0.2	0.308	0.121	0.021	0.355

Ambient temperature variation on casting of membrane leads to vary permeability; hence, effect of such ambient temperature variation was also observed on free volume. Ethyl cellulose membranes were prepared at 30^0C (EC) and also at 25^0C (EC1). As seen from Table 2.4, EC1 has lower free volume fraction compared to EC. It may be due to the fact that at lower temperature the rate of evaporation of solvent is less and the polymer molecules get more time to rearrange themselves. This provides compact structure of the membrane and hence a lower free volume which may lead to lower pervaporation flux.

2.3.2.2 Wet State

To study the characteristics of wet membranes in terms of positron lifetimes, the EC membrane was sorbed (soaked) with water and the CA membrane with ethanol. These represent combinations where the solubility of the liquid in the membrane is small. Sorption studies made on these membranes showed that only 4 g of water dissolves in 100 g of EC and 27 g of ethanol dissolves in 100 g of CA. In water soaked EC, the positron lifetime was decreased from 2.63 to 2.26 ns whereas in ethanol soaked CA it increased from 2.16 to 2.91 ns. It may be mentioned that the lifetime of positronium decay in water (1.81 ns) is smaller than that of dry EC whereas the lifetime in ethanol (3.30 ns) is larger than that in dry CA. In the case of laboratory prepared membranes there is no porous support and the change in lifetime or the intensity reflects the changes occurred in the membrane in more direct manner.

The decrease of lifetime for the water soaked EC membrane may be indicating the lack of plasticization of the membrane. Whereas, the increase in lifetime for the case of ethanol soaked CA membrane may also be interpreted in terms of plasticization of the membrane due to filling of free volumes by the sorbate and the consequent expansion of

free volume. However, such a hypothesis may be ruled out, as ethanol is less soluble in CA membrane. At this point, similar conclusion may also be made for ethanol soaked PERVAP 2210 membrane (section 2.3.1.2c.).

The intensity I_3 decreases for both (soaked EC and CA) cases compared to corresponding dry states. This is due to presence of sorbate in the cavities, which reduces the intensity I_3. The reduction of I_3 in the case of ethanol-soaked CA is more than that in the case of water-soaked EC. This may be related to the higher solubility of ethanol in CA restricting the positronium formation more effectively. These observations show that there may be a relation between the reduction in intensity I_3 and solubility of the component in the membrane. Interestingly, our observations (shown in Table 2.4) satisfy the equation derived by MacQueen et al., [26] for the weight gain of the membranes due to sorbate, in terms of the free volume parameters. However, it should be mentioned here that the relation between the o-Ps lifetime in the free volumes containing the sorbate and their size is not straightforward.

2.4 Conclusions

Positron annihilation lifetime spectroscopy technique to estimate the free volume size establishes the existence of sub-nanometer size pores in pervaporation membranes contrary to various estimates in literature using more indirect methods. The free volume parameters, estimated for commercial membranes, may be useful for the purpose of transport modelling. The laboratory cast membranes showed higher values of free volume parameters than those for commercial membranes, which are indeed better membranes for other aspects of pervaporation process. Influence of membrane preparation conditions, like solvent evaporation temperature on the free volume fraction was studied.

Positron measurements were also made on wet state membranes. Qualitatively, a decrease in the positron lifetime in the soaked state may indicate lack of plasticization of the membrane due to the sorbate. However, quantitative estimation of free volume fractions for wet membranes, if further pursued, may help to better understand the actual phenomena behind pervaporation process.

References

[1] M.H. Cohen, D. Turnbull, Molecular transport in liquids and gases, J. Chem. Phys., 31 (1959) 1164.

[2] H. Fuzita, Diffusion in polymer-diluent systems, Fortschr.Hochpolym.-Forsch., 3 (1961)1.

[3] C.K. Yeom, R.Y.M. Huang, Modelling of the pervaporation separation of ethanol-water mixtures through cross linked poly (vinyl alcohol) membrane, J. Membrane Sci., 67 (1992) 39-55,

[4] V. Sanchez, R. Lopez, L.A. Fucugauchi, Y. Ito, Vapor sorption process in poly(ethylene terephthalate) studied by PAL, Mater. Sci. Forum 175-178, (1995) 773-776.

[5] F.W.Greenlaw, S.H. Shelden, E.V. Thompson, Dependence of diffusive permeation rate on upstream and downstream pressures, J. Membrane Sci. 2, (1977) 333-348.

[6] C. Vallieres, E. Favre, D. Roizard, J. Bindelle D. Sacco, New insights into pervaporation mass transport under increasing downstream pressure conditions: critical role of inert gas, Ind. Eng. Chem. Res. 40, (2001) 1559-1565.

[7] R.J. Hunter, Foundations of colloidal science, vol. 1, Clarendon press. Oxford, 1987.

[8] Y.C Jean., Characterizing free volumes and holes in polymers by positron annihilation spectroscopy, NATO Advanced Research Workshop, Advances with Positron Spectroscopy of Solids and Surfaces, Varenna, Italy, July 16-17,1993.

[9] S.J. Tao, Positronium annihilation in molecular substances, J. Chem. Phys., 56 (1972) 5499-5510.

36

[10] M .Eldrup, D. Lightbody, J.N. Sherwood, The temperature dependence of positron lifetimes in solid pivalic acid, Chem. Phys., 63 (1981) 51-58.

[11] H. Nakanishi, S.J. Wang, Y.C. Jean, in S.C. Sharma, (Ed.), Positron annihilation studies of fluids, World Scientific, Singapore, 1988. p.292.

[12] A.J. Hill, S. Weinhold, G.M. Stack, M.R. Tant, Eur Polym J., 32 (1996) 843.

[13] K. Ciesielski, A.L. Dawidowicz, T. Goworek, B. Jasinska, J. Wawryszczuk, Positronium lifetimes in porous vycor glass, Chem. Phys. Lett. 289 (1998) 41-45.

[14] P. Kirkegaard, N.J. Pedersen, M. Eldrup, PATFIT-88: a data processing system for positron annihilation spectra on mainframe and personal computers, Riso National Laboratory, Denmark, 1989.

[15] A.Jonquières, R. Clément, P. Lochon, J. Néel, M. Dresch, B. Chrétien, Industrial state-of-art of pervaporation and vapour permeation in the western countries, J. Membrane Sci. 206 (2002) 87-117.

[16] M.J.Rosa, M.N.de Pinho, Membrane surface characterization by contact angle measurements using immersed method, J. Membrane Sci.,131 (1997) 167-180.

[17] I.F.J. Vankelecom, J. De Kinderen, B.M. Dewitte, J.B. Uytterhoeven, Incorporation of hydrophobic porous fillers in PDMS membranes for use in pervaporation, J. Phys. Chem., 101 (1997) 5182-5185.

[18] B. Gonzalez, I.O. Uribe, Mathematical modeling of the pervaporative separation of methanol-methyl tert-butyl ether mixtures, Ind. Eng. Chem. Res., 40 (2001) 1720-1731.

[19] D.W. Van Krevelen, Properties of Polymers, Elsevier, Amsterdam, 1990.

[20] H. Cao, R. Zhang, J-P.Yuan, C-M/Huang, Y.C. Jean, R. Suzuki, T. Ohdaira, B. Nielsen, Free-volume hole model for positronium formation in polymers: surface studies, J. Phys.: Condens. Matter 10 (1998) 10429-10442.

[21] V.S Subrahmanyam, M.F. Ferreira Marques, G. Duplâtre, Effect of water-soluuble electron scavengers on positronium formation in AOT/water/isooctane microemulsions, Chemical Physics, 247 (1999) 333-340.

[22] Y.N. Molin, O.A. Anisimov, Positronium and muonium chemistry; edited by H.J.Ache, Advances in chemistry series vol.175, ACS publishers, Washington D.C.(1979).

[23] P. Praveen Kumar, Analysis of partial fluxes for the separation of ethanol-water during pervaporation, M.Tech Thesis, Indian Institute of Technology-Kanpur, India, 2002.

[24] M.L. Williams, R.F. Landel, and D.J. Ferry, The temperature dependence of relaxation mechanisms in amorphous polymers and other glass-forming liquids, J. Am. Chem. Soc., 77 (1955) 3701-3707.

[25] T. Okada, T. Matsuura, A new transport model for pervaporation, J. Membrane Sci., 59 (1991) 133.

[26] R.C. MacQueen, R.D. Granata, Positron annihilation spectroscopy of moisture sorption in protective epoxy coatings, Mater. Sci. Forum 105-110 (1992) 1649-1652.

Chapter 3

Dehydration of Hydrazine Hydrate

3.1 Introduction

Hydrazine is an important inorganic chemical with high heats of combustion and hence becomes highly useful as rocket fuels. The other main applications of hydrazine include de-oxygenation of boiler feed water, fuel cells and production of blowing agents. However, production of hydrazine which is carried out using any of the known various reaction routes still pose problems with regard to its yield and purity [1]. Ordinary distillation provides hydrazine in the form of hydrate (64%by wt of hydrazine). This form of hydrazine finds wide applications; whereas, use of hydrazine in rocket propulsion requires in the form of anhydrous hydrazine. Therefore, removal of water from hydrate state to produce anhydrous hydrazine is essential and to make it suitable for such purposes. However, conventional separation techniques for the removal of water experience difficulty as hydrazine forms an azeotrope with water at 71.5 wt % of hydrazine [2]. Further, hydrazine and water are highly polar by nature (surface tension values very close) and between them there is strong hydrogen bonding. Therefore, conventionally combinations of processes are required to seek dehydration. Theses are chemical reactions, followed by distillation or azeotropic distillation with aniline as entrainer. Still, a specific

problem remains which is the explosive nature of hydrazine vapours during distillation, apart from other limitations like high energy consumption and cost. Hence, there is a need to search alternative technologies to produce anhydrous hydrazine. Application of membrane technology is one such attempt to address the stated problems [3-5]. Pervaporation process, in particular, may be examined because of its potential to separate azeotropic mixtures.

Pervaporation is relatively a new membrane separation process that has elements common to reverse osmosis and gas separation through polymeric membranes. In pervaporation, the feed solution is contacted to one side of the membrane and permeate (in vapour form) is obtained on the other side by keeping downstream pressure lower than the saturation vapour pressure of the permeated components. Chemical potential gradient across the membrane is the driving force for mass transfer. It is used for separation of liquid mixtures, particularly for azeotropes [6], isomers [7] and organic – organic solvents [8]. Removal of trace quantities of organics from waste water is also being considered a potential area of application [9, 10]. Pervapoartion has many advantages over distillation; like ambient temperature operation, lower energy requirement, simpler equipment and lower capital costs. The ambient temperature operation of pervaporation is of significance; particularly for hydrazine – water system, as during high temperature distillation explosive decomposition of hydrazine may occur. The selection of polymer for hydrazine separation plays an important role due to high alkaline nature of hydrazine (pH>12.5) and only few polymers are available to withstand such solutions. Further, hydrazine has strong reducing and hydrolyzing effects. Ravindra et al [5] have used ethyl cellulose membrane to carry out this separation. Even though, ethyl cellulose is highly selective for water at low

concentrations of hydrazine, it is, however, have poor selectivity with 64% of hydrazine. Further, it was reported that ethyl cellulose is selective for hydrazine during sorption and selective for water during diffusion [11].

Therefore, such a problem may be addressed by selecting a membrane with high water-permselectivity. This may be achieved by increasing the sorption selectivity (water to hydrazine) or diffusion selectivity. For a better sorption ratio, hydrophilic moiety may be introduced into the polymer chain to enhance water sorption but hydrazine sorption may also increase because of high polarity of the compound. In addition to this, excessive swelling may decrease diffusion selectivity because of increase of free volume and overall selectivity may therefore decrease [12]. Various hydrophilic chitoson and modified chitoson membranes were previously used [13] and were found to have low selectivities. Again for better diffusion ratio, the hydrophobic moiety may be introduced into the polymer chain. This may, however, decrease permeation rate. Thus, with the introduction of balanced quantities of hydrophilic and hydrophobic moieties better flux and better selectivity may be obtained. In this regard, the conversion of remaining hydroxyl groups, depending on the degree of deacetylation of ethyl cellulose to carbamate group, may increase the hydrophobicity of the membrane. Such a conversion may be carried out by reacting ethyl cellulose with phenyl isocyanate [14], according to the reaction given in Figure 3.1.

The objective of the present work is to observe separation by pervaporation process at fixed operating conditions (temperature: 50°C, downstream pressure: 0.1mmHg, static feed condition) using commercial (PERVAP) and laboratory prepared (polystyrene, acrylonitrile butadiene styrene and modified ethyl cellulose) membranes. Further, the effect
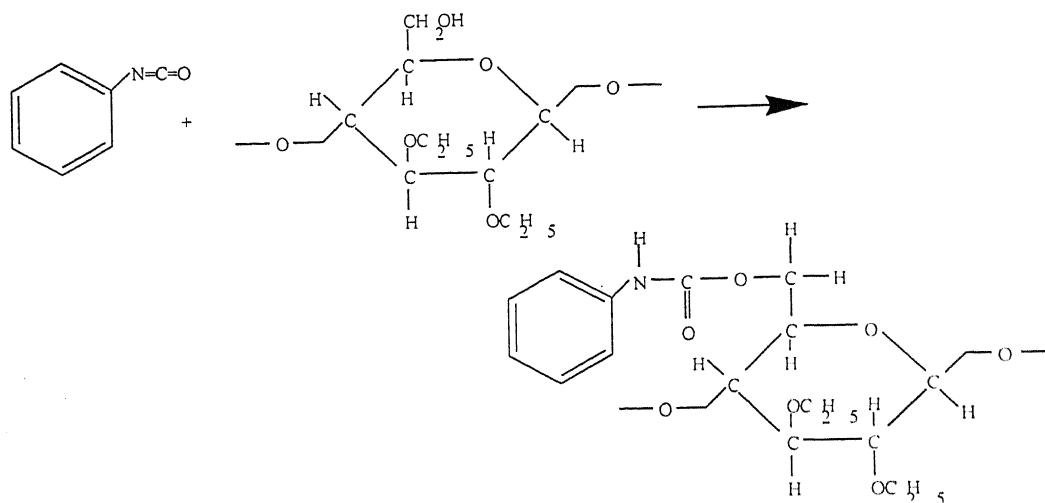
Figure 3.1 Reaction between ethyl cellulose and Phenyl Isocyanate

of amount of phenyl isocyanate (laboratory prepared) was studied on pervaporation flux and selectivity. The isocyanate dissociates into amine within few hours of preparation. Hence, freshly prepared isocyanate was used before an experiment. In order to understand the hydrophilicity/hydrophobicity of the membranes, contact angles were measured and pervaporation performance were analysed.

3.2 Experimental

3.2.1 Materials

Analytical grade toluene (Ranbaxy, India), benzene (Ranbaxy, India), benzoyl chloride (S.D.Fine, India), hydrazine hydrate (Qualigens, India), sodium azide (Hi media, India), ethyl cellulose (ethoxy content 48-49.5%: Loba-Chemie, India) and acrylonitrile

styrene butadiene (Strasis & Co, USA) were used for experimentation. Double distilled water was used for preparation of solution and for the purpose of analysis. The commercial composite membranes (PERVAP®) were obtained from Sulzer Chemtech, Germany. Such membranes consist of a porous support layer (70-100μm) on top of a polymer fleece (non-woven fabric of thickness 100μm). Further, on top of the porous support is a very thin (0.5-2μm) polymeric separating layer.

3.2.2 Preparation of Phenyl isocyanate

The reaction between benzoyl chloride and sodium azide in presence of organic medium (benzene) may produce phenyl isocyanate, according to following reaction [15, 16].
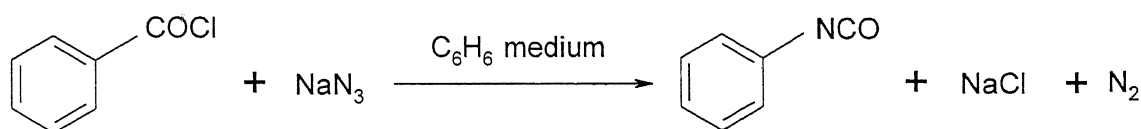
Around 60 ml of benzene (dehydrated by keeping in calcium chloride) and 35 g of sodium azide were taken in a 250ml stoppered conical flask. Further, around 70 ml of benzoyl chloride was taken in Soxhlet apparatus, having Teflon stopcock. The Soxhlet apparatus was fixed on a conical flask and benzoyl chloride was added drop wise. Flow rate of benzoyl chloride was adjusted in order to add entire benzoyl chloride in 8 hours. The reaction mixture was continuously stirred using magnetic shaker. The flask was kept in chilled ethanol. Thus, reaction temperature was maintained at 3-5°C by recirculating (Julabo bath, Germany) chilled ethanol. On completion of reaction, the whole mixture was vacuum filtered. Formation of isocyanate was ascertained through FTIR spectrum of filtrate.

3.2.3 Preparation of Membrane

Ethyl cellulose (EC) polymer (10 g) was dissolved in toluene (90 g). The solution was centrifuged (REMI model -R 24, India) at 10,000 rpm for 15 minutes for the removal of undissolved polymer. The supernatant homogeneous solution was transferred to a conical flask (air tight) and kept for overnight for the removal of entrapped air bubbles. The casting of membrane was carried out on a glass plate using a modified thin film applicator (ACME, India). After around 24 hours of solvent evaporation, the membrane was placed in vacuum oven for another 4 hours for the removal of residual traces of solvent. Similar procedures were followed for casting acrylonitrile styrene butadiene (ABS) and polystyrene (PS) based membranes, in toluene solvent with 16 wt% polymer concentrations. For modified ethyl cellulose membranes, varied quantities of phenyl isocyanate were added to ethyl cellulose polymer solution (after centrifuging). Castings of membranes were done after 24 hours of the reaction. The nomenclatures of modified ethyl cellulose (MEC) membranes with respect to amounts of isocyanate used are reported in Table 3.1.

Table 3.1 Nomenclature of modified ethyl cellulose membranes

Quantity of Phenyl isocyanate (ml in 100g of polymer solution)	0	1	2	3.2	4	5 (loss of strength)
Membrane	MEC0	MEC1	MEC2	MEC3	MEC4	MEC5

3.2.4 Contact Angle: Measurements

Equilibrium contact angles of water and hydrazine hydrate with membranes were measured in saturated environment through sessile drop method using Goniometer (Rame-Hart, inc. Imaging System, USA). Flat sheets were mounted using stainless steel holder and placed in environmental chamber. A glass syringe with a stainless steel needle was used to put the liquid drop on membrane. The angles were measured with RHI software by capturing the image with video camera. Around 5 minutes stabilization time was allowed to capture the image. Around 50 readings were then recorded in a time span of 1 second and from the average of these readings, an estimation of angle was made. Further, four or five such measurements were made for each liquid on the same membrane and the average value was noted.

3.2.5 Sorption

Pre-weighed dry membranes were taken in a conical flask containing water or hydrazine hydrate for sorption purpose. The flask was kept on shaker bath (model SW-23, Julabo, Germany) under 200 rpm for 6-7days at 50°C. The membranes in conical flasks were taken out at regular intervals and were wiped with tissue paper for the removal of adhered liquid. The wet weight of the membrane was measured. The procedure was repeated until consecutive readings of weight of wet membranes were found equal. The difference of weights was presented with respect to dry weight of membranes as percentage of sorption.

3.2.6 Analysis

Hydrazine is a hygroscopic substance which is prone to air oxidation. Further, under exposure to atmosphere it absorbs carbon dioxide and, therefore, analysis of

hydrazine sample requires proper precautions. The tedious procedure involved in Penneman method [17] of employing potassium iodate as titrant is prone to errors. Therefore, gas chromatograph method [18] was employed for analysis of hydrazine. Concentrations in both the feed and the permeate samples were measured. Gas chromatograph (Nucon, India equipped with TCD) with Puropack-Q as reference column and chromosorb-103 as main column was employed for the purpose. Both the columns are made of stainless steel having dimensions: length 6ft, outside diameter 1/8 inch and inside diameter of 2mm. The injector, detector and oven temperatures were set at 210, 220 and 170°C, respectively. Helium was used as a carrier gas at 20ml/min. Observed retention time for water was 1.94 and that for hydrazine was 2.46 minute for above stated conditions.

3.2.7 Pervaporation: Set up and Procedure

A set-up was designed and developed for the pervaporation experimental investigations and a schematic version is shown in Figure 3.2. Pervaporation test cell, made of glass, was having specially designed flanges to lodge the membrane with an effective membrane area of 50.6 cm². The membrane was kept on highly porous stainless steel support with the shiny polymeric layer (for commercial membranes) facing the feed solution. Initially fixed volume of feed solution (hydrazine hydrate of 64 wt% of hydrazine) was taken on the upper side (feed side) of the cell. Both upstream and downstream sides of the cell were heated (in order to maintain isothermal conditions around the cell [19]) and hence cell surface was covered by heating mantels. The temperatures of both the sides were controlled at 50°C, using PID controller device (Fuji, Japan). The membrane upstream side was kept at atmospheric pressure and the downstream
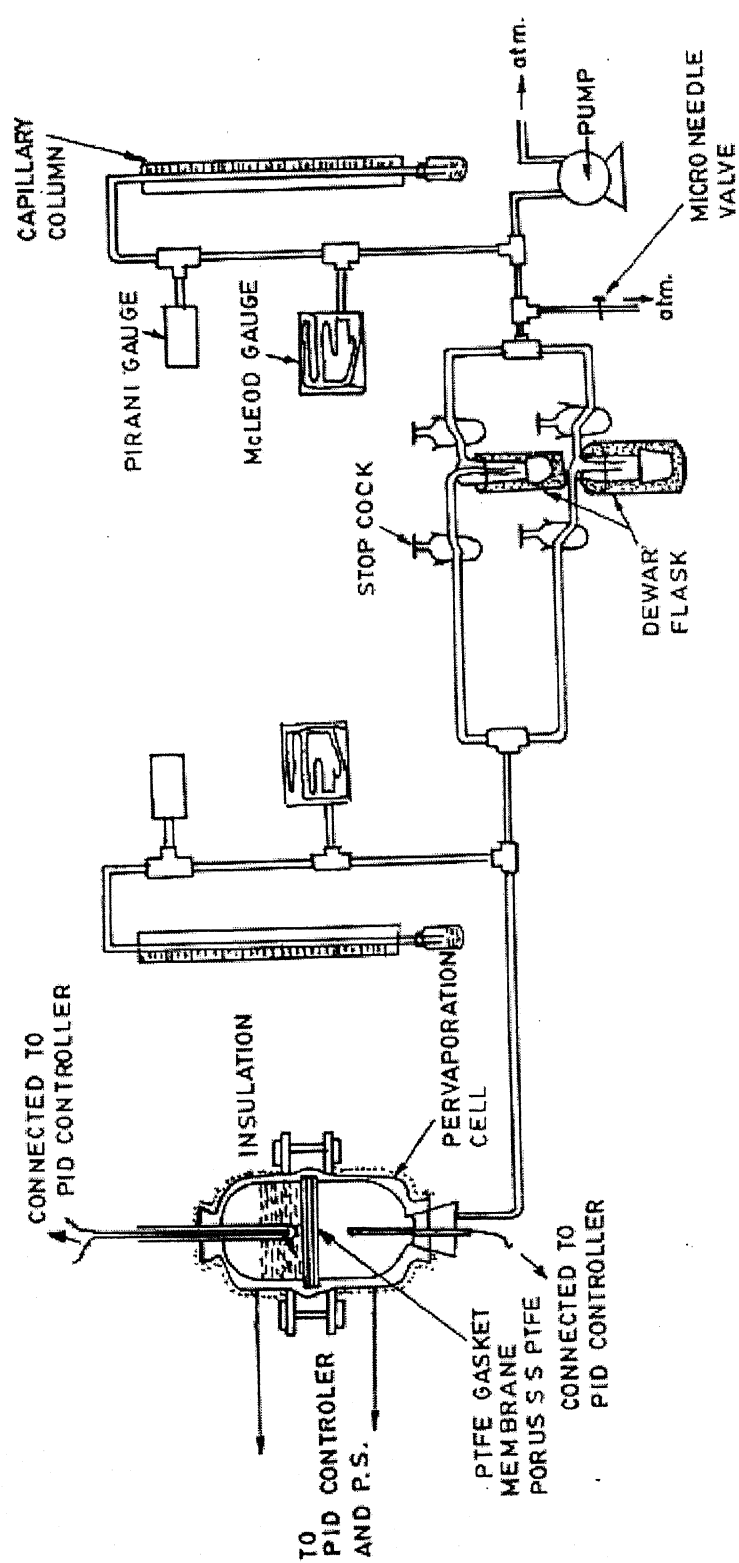
Figure 3.2 Schematic diagram of pervaporation experimental setup

side was maintained under vacuum, using a vacuum pump (Vacuum Techniques, Bangalore).

The condenser system consisted of two traps that can be used alternately, allowing the permeated pervaporate stream to be sampled continuously without interruption of the operation. The permeated vapours are condensed in the trap, which is kept in Dewar flask, filled with liquid nitrogen. The frozen permeate was collected within a specified time interval. The cold traps were brought to room temperature for measuring its weight, using a five decimal balance, to determine mass flux. Permeate was analyzed to determine its hydrazine content. Flux values and hydrazine concentration in permeate were recorded as a function of time. To minimize in measurement errors, an average of two separate consecutive readings were taken after the system reached to steady state. The average error in the total permeation mass flux was estimated around to be±3% and that for hydrazine concentration was around to be ±5.

3.3 Results & Discussion

3.3.1 Modified Ethyl Cellulose Membrane: Characterization

Ethyl cellulose membrane was reacted with different proportions of phenyl isocyanate to form modified ethyl cellulose membrane (MEC). The reaction has been described in the earlier sections. In the following section, such a modified membrane, however, using a fixed quantity of phenyl isocyanate (4 ml/100 g of polymer solution), was characterized in order to observe the modifications in comparison to unmodified form of ethyl cellulose. FTIR, XRD and positron annihilations techniques were employed for the purpose and results are discussed. Further, contact angles were also measured, not only for above stated membranes but also for various forms of modified membranes (using different

proportions of phenyl isocyanate), including other membranes, used for the work. Such a restrictive use of characterization techniques (FTIR, XRD, PAL) with a fixed type of modified membrane were carried out simply to observe the modifications due to reaction on ethyl cellulose polymer.

3.3.1.1 FTIR

The FTIR spectra were obtained for phenyl isocyanate, dry ethyl cellulose as well as modified ethyl cellulose. Vector 22 FTIR Spectrometer (Brooker, Germany) was used for the purpose.

Figure 3.3 shows the FTIR spectrum of phenyl isocyanate (obtained after the reaction of benzoyl chloride and sodium azide). The peak at $2135cm^{-1}$ corresponds to isocyanate [20] which confirms the formation of reaction (**section 2.2**). Similarly, Figure 3.4 depicts the FTIR spectrum of EC and MEC4. Ravindra et al [21] have used FTIR spectrum for EC and have explained various functional groups. In the present work, FTIR spectrum analysis was carried out in order to ascertain the modification of EC. Comparison of spectrums (Figure 3.4) show a decrease in relative intensity of –OH peak $(3476cm^{-1})$ from 0.742 (EC) to 0.585 (MEC4). Further, an extra peak was found in MEC4 at $1722.68cm^{-1}$. This peak corresponds to the carbamate group [20]. This confirms the conversion of the hydroxyl groups in the closed ring structure of EC into carbamate groups.

3.3.1.2 XRD

The packing of the original and modified ethyl cellulose membranes were investigated with wide angle X ray diffraction (WAXRD). WAXRD curves of the membranes were obtained using an Iso-Debyeflex X- ray powder diffractometer having monochromatic radiation of α- rays emitted by Cu at a wave length of 1.54 Å. Scanning
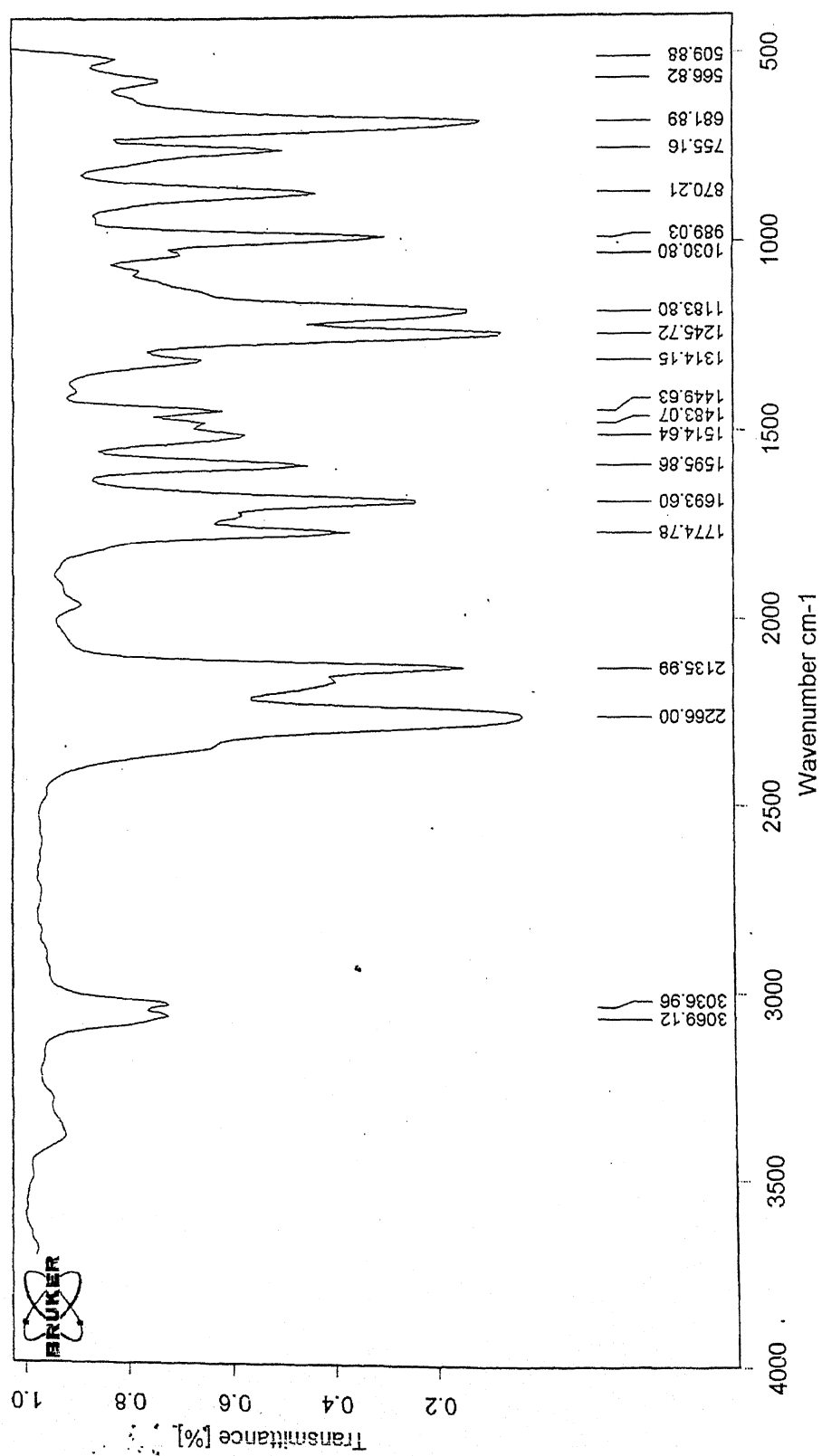
Figure 3.3 FTIR spectrum of phenyl isocyanate
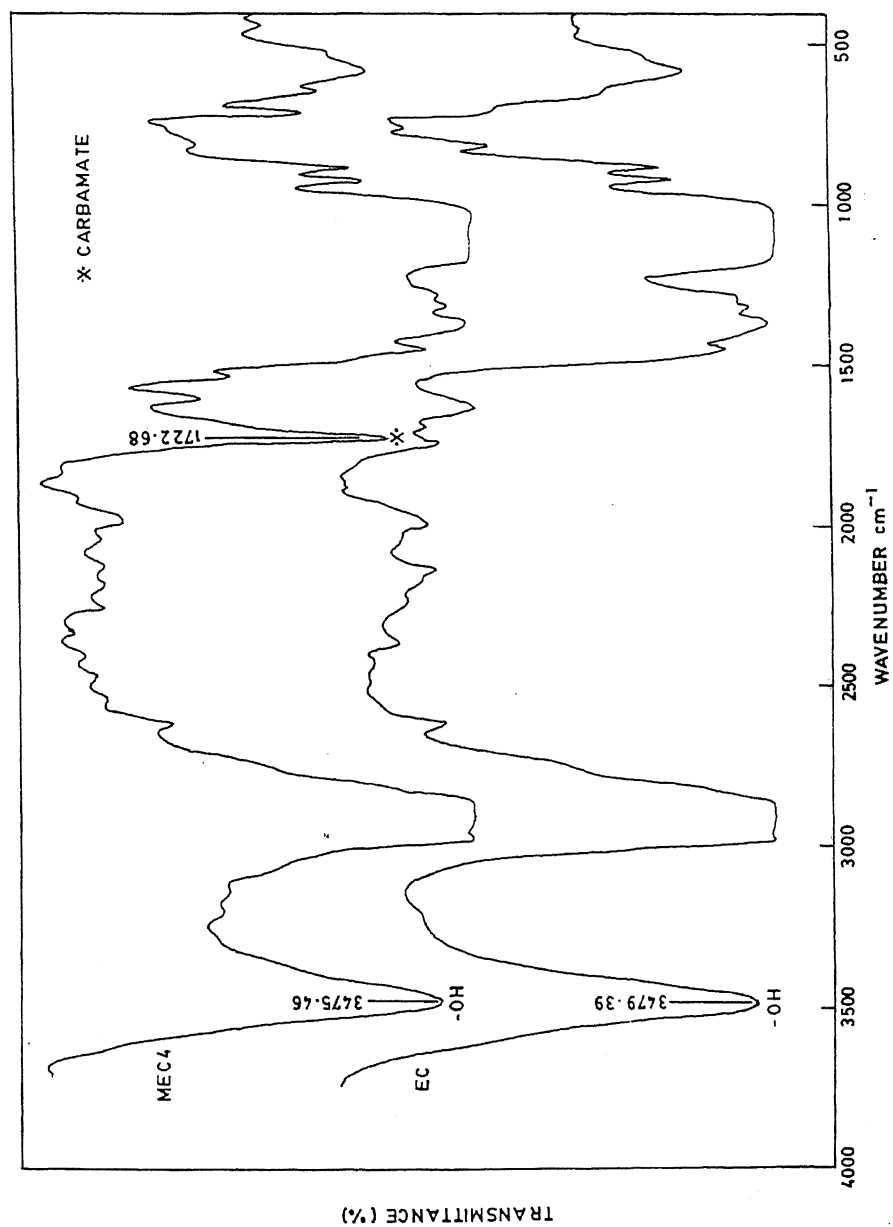
Figure 3.4 FTIR spectrum of EC and MEC4 membranes

was performed with an angle ranging from 7 to 50 at a rate of 3°/min with an accelerating voltage of 30kV and tube current of 20 mA.

Figure 3.5 shows the WAXRD spectra of EC and MEC4. Both spectra display three sharp peaks at 14, 17 and 26°. The sharp peaks suggest the semi crystalline nature of polymers. There is not much difference in the obtained spectra for EC and MEC membranes. However, one can observe a slight umbrella shape at lower angles, in addition to intensity changes (corresponding to above angles) for MEC4 membrane. Qualitatively, this change suggests that the modified ethyl cellulose membrane is slightly amorphous compared to ethyl cellulose membrane. This may, in a sense increase the flux. Further, studies on XRD spectra, particularly of detailed structures of the polymers, are insignificant for the present work.

3.3.1.3 Positron Annihilation Lifetime (PAL) Spectroscopy

The PAL measurements were carried out using a fast-fast system having a resolution of 300 pico-seconds (FWHM for the ^{60}Co prompt γ-rays, under [22]Na window settings). The positron source was prepared by depositing around 2 micro-Curie aqueous [22]NaCl on a thin aluminium foil (thickness ~ 12μm) which was covered with an identical foil. Approximately, one million counts were collected in each spectrum and four spectra were measured for each sample. The lifetime data were analysed using PATFIT-88 programs [22]. Source correction was done for all the spectra. The following expression was used to relate o-Ps pick-off lifetime (τ_3) and special free volume radius (r) [23].

$$\tau_3 = \frac{1}{2}\left[1 - r/(r+\Delta r) + (\frac{1}{2\pi})\sin(\frac{2r\pi}{r+\Delta r})\right]^{-1} \tag{3.1}$$
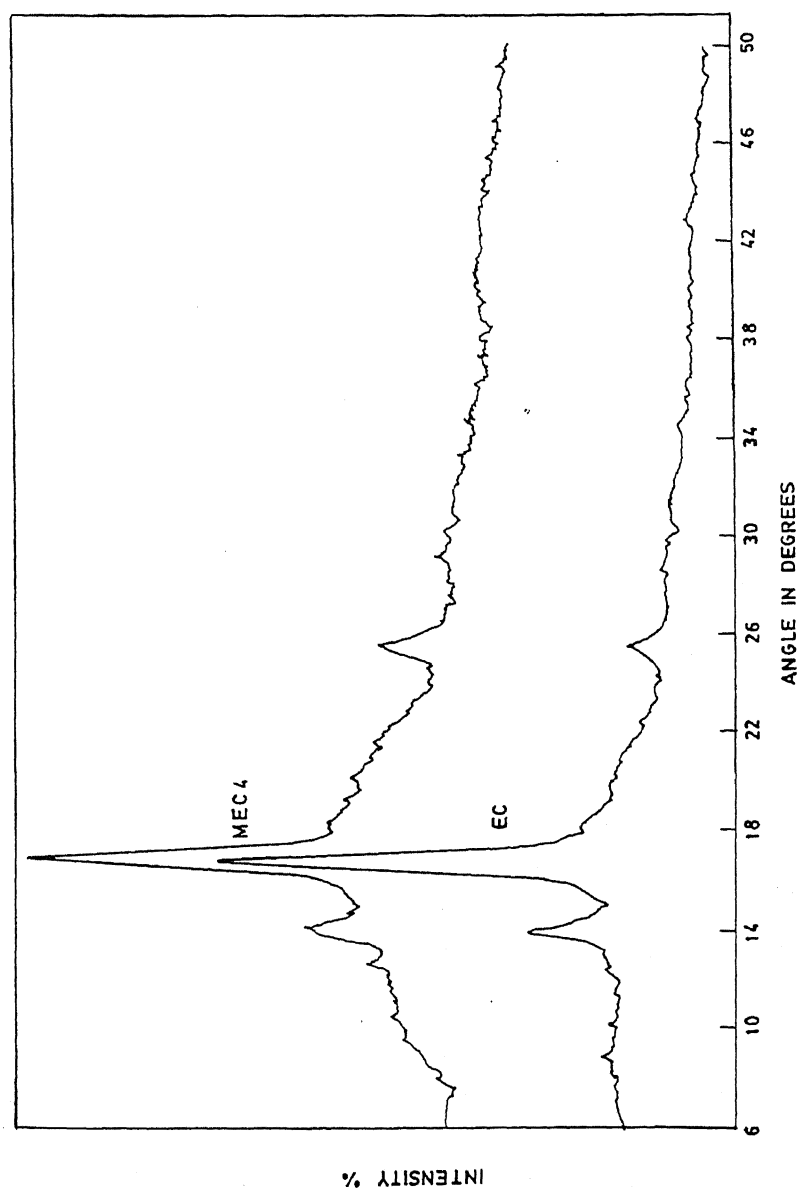
Figure 3.5 XRD spectrum of EC and MEC membranes

Where, Δr is the electron layer thickness. Further, the fractional free volume f, may be estimated from the following empirical relation [23].

$$(3.2)$$

$$f = bV_F I_3$$

Where, V_F is the free volume of the membrane and I_3 is the intensity corresponding to τ_3.

The scaling factor b, is obtained from variation of free volume with temperature. However, in the absence such data, it may be typically assigned a value of $1.0/nm^3$ [24].

Chapter 2 describes the detailed work on positron lifetime spectroscopic analysis made for varieties of dense and composite membranes in order to obtain primarily free volume parameters. In this chapter, results pertaining to ethyl cellulose and modified ethyl cellulose membranes are presented in Table 3.2 to observe the modification of the same. Ortho positron lifetime (τ_3) and intensity (I_3) were observed to be smaller for MEC4 compared to EC. Further, Table 3.2 show the calculated values of free volume fraction which was also found to be smaller for MEC4 as compared to EC. These obtained free volume parameters are in general in the same range as given for semi crystalline polymers [25]. Therefore, during modification of ethyl cellulose dense film, free volume becomes smaller and this may lead to decrease of species diffusivities within membranes which eventually reduce flux.

3.3.1.4 Contact Angle: Analysis

Contact angles of water and hydrazine hydrate were measured on different membranes and the results are tabulated in Table 3.3. The contact angles for both hydrazine hydrate and water on PERVAP® and EC were found to be lower than the contact angles for same species on MEC4, PS and ABS membranes. This suggests that EC and PERVAP®

Table 3.2 Free volume parameters of EC and MEC4 membrane

Membrane	τ_3 (ns)	I_3 (%)	r (nm)	V_f (nm^3)	f
EC	2.63±0.01	26.0±0.2	0.337	0.160	0.042
MEC4	2.26±0.01	17.5±0.2	0.308	0.121	0.021

membranes are hydrophilic by nature; whereas, other membranes are hydrophobic by nature (*apolar* nature of polymers). Further, expectedly, EC membrane on reaction with phenyl isocyanate (MEC4 membrane) changes its characteristics from hydrophilic to hydrophobic, as evidenced from increase of contact angle. This was made possible because of the introduction of phenyl group through reaction on EC.

Table 3.3 Contact angles of water and hydrazine hydrate

Membrane	Hydrazine hydrate contact angle	Water contact angle	Ratio of contact angles of water to hydrazine hydrate
Pervap 2200	30.7	65.2	2.12
Pervap 2201	23.4	30.5	1.30
Pervap 2202	30.0	51.3	1.71
EC	32.8	61.6	1.87
MEC4	66.0	95.5	1.45
PS	73.7	78.9	1.07
ABS	69.5	78.3	1.13

56

It was decided to observe the influence of varied concentrations of phenyl isocyanate (during reaction with EC membrane) on modification of EC membrane towards hydrophobicity. This was observed through the measurements of contact angles of thus formed varied MEC membranes. Accordingly, relationships were observed in terms of contact angles of water, hydrazine hydrate as well as ratio of contact angles of water to hydrazine hydrate against phenyl isocyanate concentration. Such relationships are shown in Figure 3.6. It may be observed from Figure 3.6, as the amount of isocyanate is increases contact angle of both hydrazine hydrate and water increases; but, the ratio of angles decreases. This is explained due to the fact that more and more hydroxyl groups in EC are getting converted to carbamate groups as the concentration of phenyl isocyanate increases. Further, low values of contact angles of hydrazine hydrate, compared to water for all membranes, suggests that hydrazine is strongly held by membrane compared to water. FTIR studies of feed components with ethyl cellulose membrane also led to such conclusions [21].

3.3.2 Sorption

Equilibrium sorption experiments could be conducted with dense membranes (EC, MEC, PS & ABS) only. Commercial PERVAP® membranes were all composite by nature and hence sorption experiments could not be conducted because of difficulty of distinguishing between skin and support layers. Results for water and hydrazine hydrate are reported in Table 3.4. The temperature of sorption experiments were maintained at 50°C. This was done in order to compare such sorption results with subsequent pervaporation experimental results to be conducted at the same temperature.
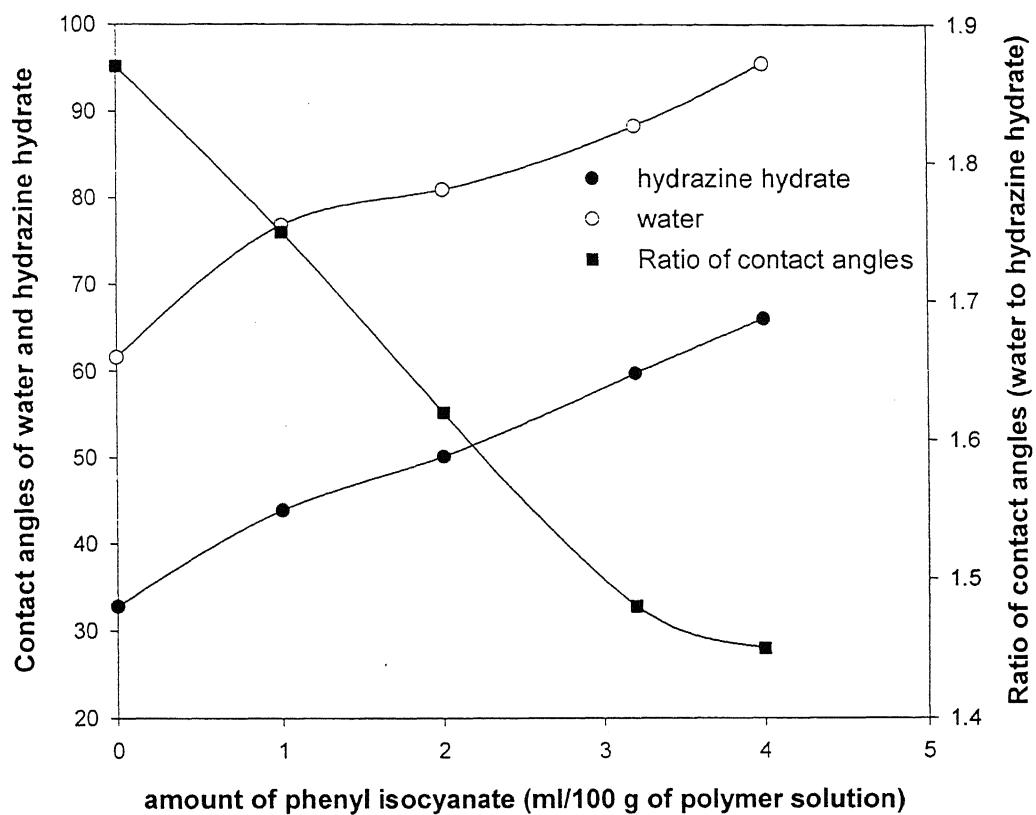
Figure 3.6 Influence of isocyanate concentration on contact angles of water and hydrazine hydrate.

Apolar membranes (ABS and PS) exhibit relatively low sorption characteristics for both hydrazine hydrate and water, reconfirming hydrophobicity. Similarly, MEC4 membrane which changed its characteristics due to the reaction with isocyanate also exhibit relatively lower sorption of water and hydrazine hydrate compared to pure EC membrane.

Table 3.4 Sorption characteristics of water and hydrazine hydrate (T=50°C)

Membrane	%Sorption of water (g/g of polymer)	%Sorption of hydrazine hydrate (g/g of polymer)	Sorption selectivity (water/hydrazine hydrate)
EC	4.01	5.21	0.681
MEC4	3.75	4.95	0.533
PS	0.11	0.22	0.390
ABS	0.299	0.505	0.482

This also indicates the increase of hydrophobicity of MEC4 due to reaction. Sorption of water and hydrazine hydrate for MEC membranes is shown in Figure 3.7, as a function of isocyanate amount. Sorption of both the species decrease with increase in isocyanate amount, to the extent that sorption of these species becomes negligible. Further, sorption selectivity was estimated assuming linear solubilities. This assumption may be considered to be valid for polar components in *apolar* polymers. Accordingly, Figure 3.7 was drawn to depict a relationship of sorption selectivity against varied isocyanate amount for MEC membranes. Further, Table 3.4 presents sorption selectivity for other membranes. From
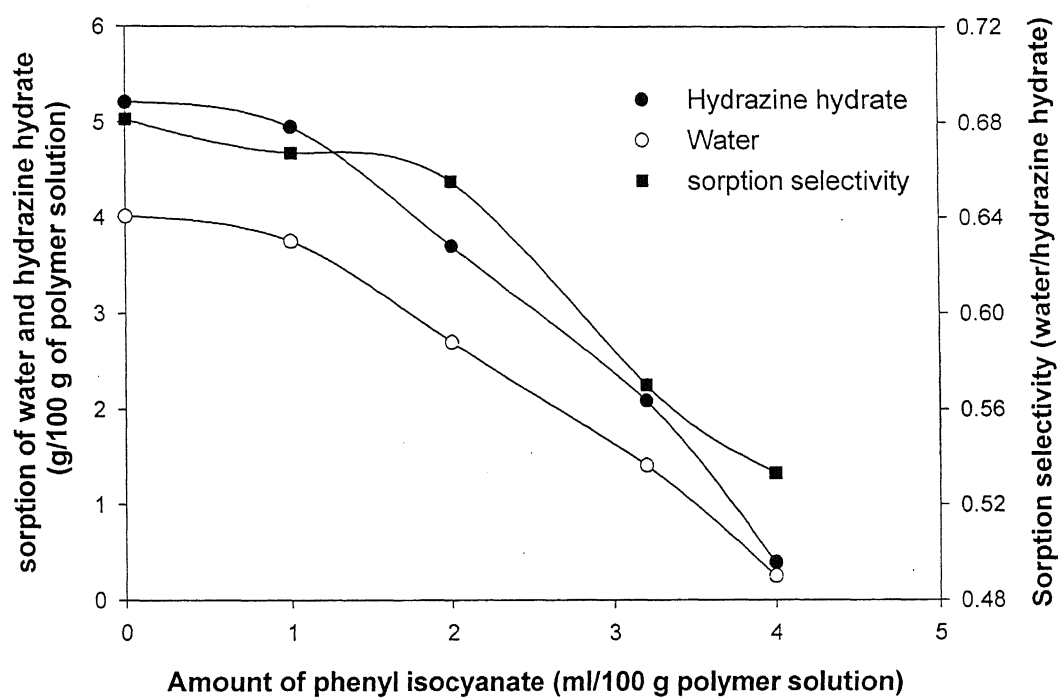
Figure 3.7 Influence of isocyanate concentration on sorption of water and hydrazine hydrate

Figure 3.7 it is observed that MEC membranes are more selective to hydrazine hydrate. Similarly, other membranes also reflect same characteristics for hydrazine (Table 3.4).

3.3.3 Pervaporation

The ability of the membrane to separate given liquid mixture is given by separation factor α_{WH}^{P} (water to hydrazine) and is defined as:

$$\alpha_{WH}^{P} = \frac{y/(1-y)}{x/(1-x)} \tag{3.3}$$

where, y and x are the mass fractions of water in permeate and feed, respectively. Further, P refers to pervaporation. Mass flux data were normalized corresponding to 5μm thickness to compare obtained flux data between commercial and laboratory made membranes. This was done using inverse relationship of flux and thickness for fixed operating conditions. Further, to compare the performance of different membrane materials the PSI value [26] of membrane was utilized. This value was calculated by multiplying permeation mass flux with separation factor.

Pervaporation of hydrazine hydrate was carried out at 50^{0}C, 0.1mmHg with static feed conditions, using different commercial and laboratory prepared membranes. The obtained flux, selectivity and PSI at quasi steady state are reported in Table 3.5. It may be mentioned here that the choice of 50°C temperature, higher than the earlier reported work with EC membrane only [5] at room temperature, was primarily to obtain an appreciable quantity of pervaporate which could enhance accuracy of analytical estimation.

It is encouraging to find (Table 3.5) and observe higher separation characteristics for hydrazine-water using MEC and other selected hydrophobic polymers. The selectivity of water to hydrazine of all the membranes, except PERVAP®2200, is higher than that the

Table 3.5 Flux, selectivity and PSI index (T=50°C; downstream pressure=0.1mmHg)

Membrane	Thickness (μm)	Actual flux (g/m²h)	Normalized flux (g/m²h for 5μm)	Selectivity	PSI (g/m²h for 5μm)
Pervap2200	2	306.00	122.4	1.09	133.4
Pervap2201	2	10.00	4.0	3.58	14.32
Pervap2202	2	78.50	31.4	1.93	60.6
EC	58	8.28	96.5	1.72	166.0
MEC4	75	5.45	81.8	3.23	262.4
PS	56	1.02	11.5	5.45	62.6
ABS	110	3.55	78.1	5.07	395.9

one may be obtained from distillation which is 1.4 at 760mmHg [2]. This indicates that pervaporation provides better selectivity compared to distillation and with the possibility of breaking azeotrope.

The results clearly show that the PSI index and selectivity of laboratory prepared hydrophobic membranes (MEC, PS, ABS) are better than that of hydrophilic membranes (PERVAP and EC). Earlier, Ravindra et al [5] obtained flux, selectivity and PSI values as 50 g/m²h (for 5μm thickness), 2.82 and 141 at room temperature for EC membrane, respectively. In the present work, flux has almost doubled but the selectivity got reduced to 61%. However, the present work obtains a PSI value of 166 which is 1.17 times higher than earlier work [5]. This small increase therefore, may be simply explained because of the choice of higher operation temperature of 50°C. Further, PERVAP 2201 membrane gave a reasonably high selectivity of 3.58; but, at the expense of flux which is very low (4 g/m²h for 5μm thickness). This is because the said membrane is supposed to be having a highly cross-linked PVA skin layer [27].

The selectivity, obtained with PS membrane, is the highest but the flux and PSI index are very low. This is because of strong hydrophobic nature of PS membrane. One may, therefore, decrease its hydrophobicity by modifying the polymer or blend with hydrophilic polymer to get better flux. In this regard, an attempt was made to blend PS and EC (both are soluble in toluene) to obtain better PSI value. However, it was observed that there was phase separation between PS and EC in toluene. This may be attributed due to the fact that entropy of mixing may be small and there may be a positive enthalpy of mixing which gives rise to positive Gibbs free energy of mixing [28]. Results are, therefore, not reported.

One of the interesting polymers (ABS), selected for the present work, gave the highest PSI value with reasonably high flux and better selectivity. ABS is a blend of glassy copolymer with rubbery domain [29]. The component acrylonitrile is hydrophilic whereas styrene and butadiene are hydrophobic by nature. Therefore, the high selectivity may be attributed due to the presence of glassy copolymer (styrene-co-acrylonitrile) and good flux may be due to the presence of rubbery domain (butadiene). Such a combination of two different contrast properties led to a high PSI index ($\approx$396). Still, there may be a possibility to improve PSI index by varying the composition of ABS polymer.

Considering the effect of modifications on EC membrane, it may be observed from Table 3.5 that MEC4 gave better selectivity and PSI index than that obtained from EC. Increased hydrophobicity may have decreased the solubility and hence swelling; this may have increased the diffusion selectivity of water to hydrazine. These results were, however, obtained with a fixed amount of isocyanate (4 ml/100 g of polymer solution). Therefore, another set of experiments were carried out to observe the influence of varying amounts of
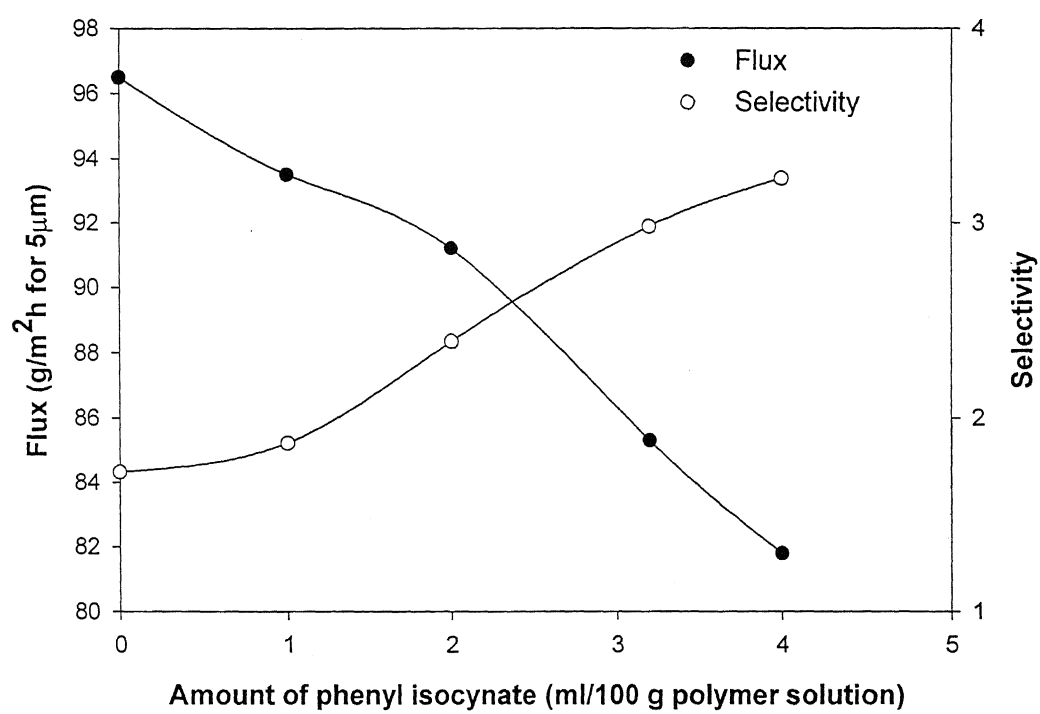
Figure 3.8 Influence of isocyanate concentration on flux and selectivity
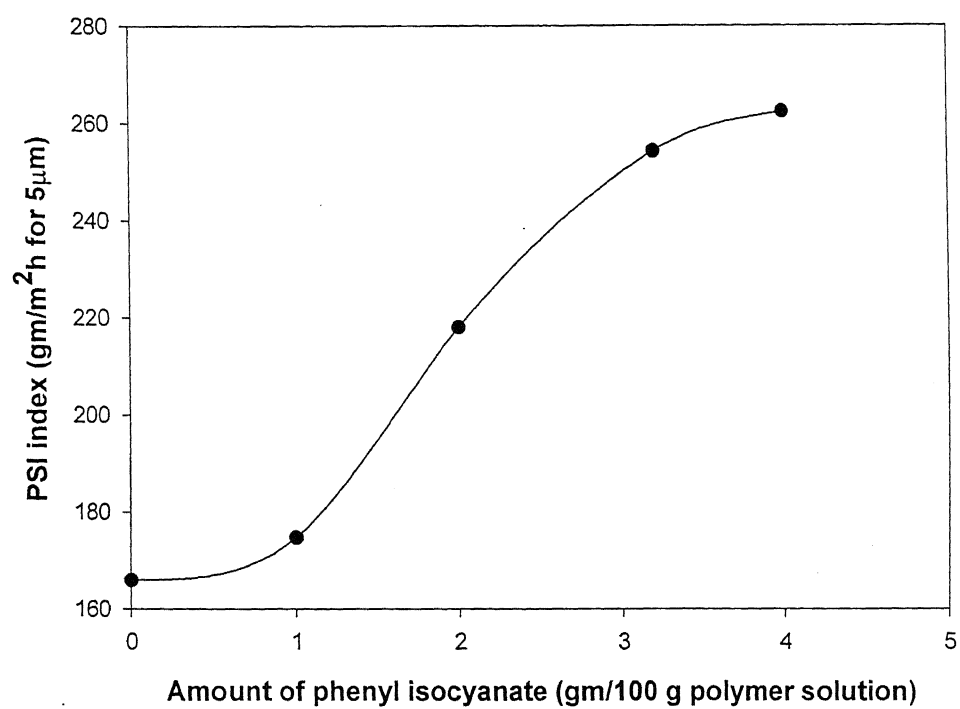
Figure 3.9 Influence of isocyanate concentration on PSI

isocynate on the modifications of EC. Figure 3.8 shows the effect of isocyanate concentration on flux and selectivity. There is around 16% decrease in flux (increase of isocyanate amount from 0 to 4ml) whereas selectivity increased up to around 92%. This is more evident from Figure 3. 9 with respect to PSI value. The figure shows a steep increase in PSI with 1 to 3.2 ml of phenyl isocyanate amount which is around to be 40 PSI/ ml of phenyl isocyanate. Overall, there is 57% increase in PSI which may be considered to be significant. However, with a significant increase of isocyanate concentration (beyond 4 ml), it was observed that the membrane casting was becoming difficult while peeling off the membrane from the casting glass plate. Therefore, membrane may have lost its physical strength.

Further, as evidenced above (section 3.3.1.4), with the increase of isocyanate amount, the contact angles of both the components increase which will decrease the adhesion force between the membrane material and feed components [30]. Decrease of adhesion force decreases the interaction between the membrane material and components. This reduces the solubility. This may also be observed while referring Figure 3.7. Therefore, decrease of adhesion forces lead to easy desorption of components. Similarly, Figure 3.6 also explains that the ratio of contact angles of water to hydrazine hydrate decreases with increase in isocyanate concentration. This infers that with increase in isocyanate concentration there is a more decrease of interaction between membrane material and water compared to interaction between membrane and hydrazine. Hence, the selectivity of water to hydrazine may increase which may be also be confirmed while referring Figure 3.8. Further, even though the hydrophobicity increases as well as free volume fraction decreases with modification of EC; there is not much decr

obtained value of flux. This may be due to the fact that the modification is providing a membrane (MEC) towards an amorphous structure as compared to semi crystalline structure of EC (as explained in section 3.3.1.2).

3.3.4 Diffusion selectivity

It may be noted while comparing Table 3.4 & 3.5 that sorption selectivity was less than one; whereas, pervaporation selectivity was greater than one. According to the solution-diffusion model [31], overall selectivity of pervaporation process α_{WH}^{P} is the product of sorption α_{WH}^{S} and diffusion selectivity α_{WH}^{D}, i.e.,

$$\alpha_{WH}^{P} = \alpha_{WH}^{S}\alpha_{WH}^{D} \tag{3.4}$$

Use of eq (3.4) is highly restricted because sorption selectivity is calculated from the pure component swelling data. However, this may be valid for very low solubilities of feed components in the membrane. Therefore, once sorption α_{WH}^{S} and overall pervaporation α_{WH}^{P} selectivities are known, diffusion selectivity α_{WH}^{D} may be estimated. The estimated diffusion selectivities values are reported in Table 3. 6. Such values are found to be greater than one. This may be attributed due to the fact that water, being the smaller molecule, diffuses very easily through the membrane compared to hydrazine. This study shows that for dehydration of hydrazine hydrate, the diffusion selectivity plays an important role as it dominants the overall selectivity. Such type of observations were earlier also made for ethanol-water separation using hydrophobic PVC [32].

The components of hydrazine and water are highly polar and hence sorption selectivity may always less than for this system. Therefore, it may be possible to get higher

Table 3.6 Diffusion selectivities

Membrane	EC	MEC1	MEC2	MEC3	MEC4	PS	ABS
Diffusion selectivity (water/hydrazine)	2.52	2.80	3.64	5.22	6.05	13.97	10.52

values of pervaporation selectivity by increasing diffusion selectivity only. Introduction of hydrophobic moiety into the polymer chain as well as thermal annealing may improve diffusion selectivity. However, such an attempt may be at the expense of flux.

3.3.5 Contact Angle versus Pervaporation Selectivity

Contact angles reflect interaction between membrane material and feed components [33]. In pervaporation, both sorption and desorption may get reflected by contact angles. Therefore, one may develop a relationship between contact angles and pervaporation selectivity in order to better understand the process. In this work, however, an attempt has been made to relate them empirically, using such available data (Table 3.3, Figure 3.6, Table 3.5 and Figure 3.8). Figure 3.10 depicts relationship between process selectivity and ratio of contact angles of water to hydrazine hydrate. Further, following exponential relationship was developed with a correlation coefficient of 0.9963.

$$\alpha_{WH}^{P} = 27.92\exp(-1.526\theta_r) \tag{3.5}$$

Where, θ_r is the contact angle ratio of water to hydrazine hydrate. This may prove useful to estimate separation factor for a polymer of unknown pervaporation performance but known contact angles.

$\alpha=27.92\exp(-1.526\theta_r)$

correlation coefficient=0.9923
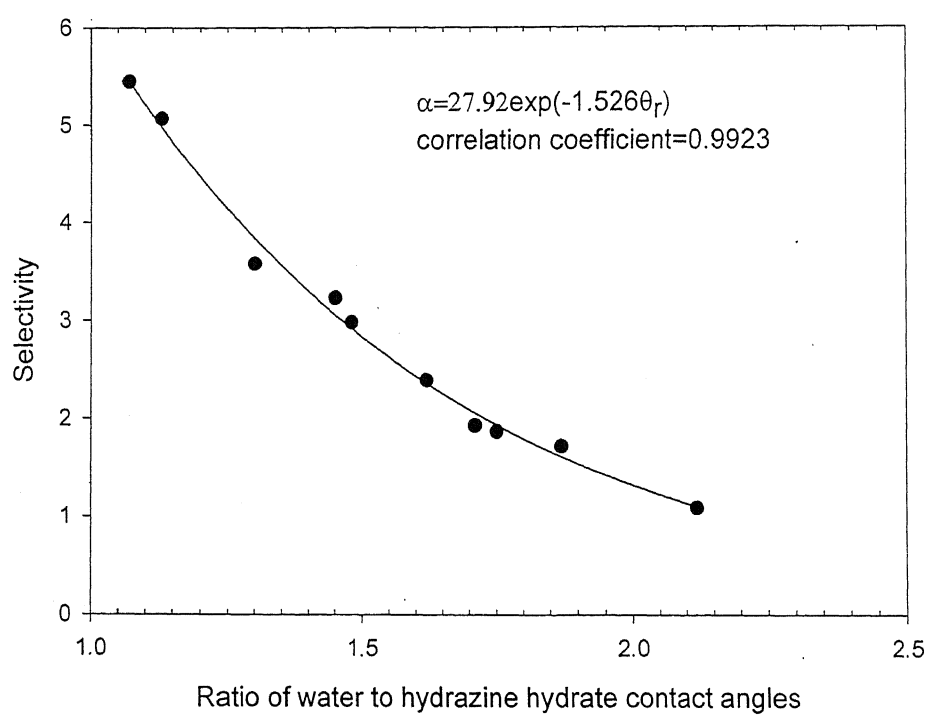
Figure 3.10 Contact angle ratio versus pervaporation separation factor

3.4 Conclusions

Separation of hydrazine-water, an azeotropic mixture, was carried out using various commercial (PERVAP®) and laboratory prepared (EC, ABS, PS) membranes. Ethyl cellulose membrane was modified by reacting with phenyl isocyanate. MEC4 membranes was characterised with the help of FTIR, XRD, PAL and contact angle measurements. Pervaporation experiments were carried out and the results were analysed with the help of sorption experiments and contact angle measurements.

FTIR spectrum analysis confirms the formation of carbamate group for the reaction of phenyl isocyanate with ethyl cellulose. XRD analysis suggested that MEC is slightly amorphous compared to EC. Positron annihilation technique successfully estimated free volume fraction, which reduced to 50% (from 0.042 to 0.021) during modification. Contact angle measurements ascertained the modification of EC towards hydrophobic characteristic. Hydrophobicity of the MEC polymer increases with increase in isocyanate concentration; however, at the expense of solubility capacity.

Pervaporation of hydrazine hydrate experiments provided encouraging results in terms of obtaining higher selectivities than the one that could be achieved through conventional distillation. MEC, PS and ABS polymeric membranes were found to be providing high selectivities. However, the PSI index suggested ABS polymer as well as MEC3 & 4, being better polymers for dehydration of hydrazine hydrate. It was observed that the diffusion selectivity plays an important role as it dominates the overall selectivity. An empirical relationship was developed to relate process selectivity and the ratio of contact angles of water to hydrazine hydrate.

70

References

[1]   E.W. Schmidt, Hydrazine and its derivatives Preparation, Properties, Applications, John Wiely & Sons, 1984, New-York.

[2]   R.Q. Wilson, H.P. Munger, J.W. Clegg, Vapour-liquid equilibrium in the binary system hydrazine/water, Chemical Eng. Progr., Symp. Series 3 (1952) 115-117

[3]   F. Wolf, P. Pollandt, R.Helmer, Diffusion behaviour of hydrazine through molecular sieve membranes (in German), Z.Chem.15 (1975) 160-161; Chemical Abstracts, 83,183856.

[4]   J.I. Dytnerskij, Membranprozesse Zur Trennung flussiger Gemische, VEB; Deutscher Verlag fur Grundstoffindustrie: Leipzig, 1977.[Cited in R. Rautenbach, R.Albrecht, "Membrane Process," John Wiely & Sons, 1989, p 368, Chichester, UK.].

[5]   R. Ravindra, S. Sridhar, A.A. Khan, Separation studies of hydrazine from aqueous solutions by pervaporation, J. Polymer Sci.: Part B: Polymer Physics, 37 (1999) 1969-1980.

[6]   A. Duggal, E.V. Thompson, Dependence of diffusive permeation rates and selectivities on upstream and downstream pressures V1. Experimental results for the water/ethanol system, J. .Membrane Sci., 27 (1986) 13-30.

[7]   M.Wessling, U.Werner, S.-T. Hwang, Pervaporation of aromatic C_8-isomers, J.Membrane Sci., 57 (1991) 257-270.

[8]   B.Cao, H.Hinode, T. Kajiuchi, Permeation and separation of styrene/ethylbenzene mixtures through cross-linked poly(hexamethylene sebacate) membranes, J.Membrane Sci., 156 (1999) 43.

[9]   E. E. B. Meuleman, J. Willemsen, M. H. V. Mulder, H. Strathaman, EPDM as a selective membrane material in pervaporation, J. Membrane Sci. 188 (2001) 235-249.

[10]   S.V. Satyanarayana, P.K. Bhattacharya, Real coded genetic algorithm for optimization of pervaporation process parameters for removal of volatile organics from Water, Ind. Engg. Chem. Res. 42(13) (2003) 3118-3128.

[11]   R. Ravindra, S. Sridhar, A.A. Khan , A.K. Rao, Pervaporation of water, hydrazine and monomethylhydarzine using ethylcellulose membranes, Polymer, 41 (2000) 2795-2806.

[12]   Fuzita. H, Fortschr.Hochpolym.-Forsch., 3 (1961) 1.

[13]   S.V. Satyanarayana, K. Kameswararao, R. Ravindra, Prem Raj Shah, A.A. Khan. Studies on the separation of ethanol-water and hydrazine-water mixtures by pervaporation, Presented in IICT, Golden Jubilee Symposium on Advances in Chemical Engg., IICT, Hyderabad, 9-11 August 1994.

[14]   Anil Kumar, R.K. Gupta, Fundamentals of polymers, McGraw-Hill, Singapore, 1998.

[15]   M.J.L. Kishore, Preparation of heterogeneous alumina catalyst covalently binding mono and bimetallic complexes for alkane isomerization, M.Tech Thesis, IIT Kanpur, 2003.

[16]   I.L. Finar, Organic chemistry, volume 1: The fundamental principles, sixth edition, ELBS/Longman, Singapore, pg no 268 & 359, 1973.

[17]   R.A. Penneman, L.F. Audrieth, Quantitative determination of hydrazine, Analytical Chemistry, 20 (1948) 1058-1061.

72

[18] L.A. Dee, A.K. Webb, Gas chromatographic separation of hydrazine mixtures and water using a stationary phase that is chemically similar to hydrazine, Anal. Chem. 39 (1967) 1165-1167.

[19] A. Hillaire, E. Favre, Isothermal and nonisothermal permeation of an organic vapour through a dense polymer membrane, Ind. Eng. Chem. Res. 38 (1999) 211-217

[20] W. Kemp, Organic Spectroscopy, PalGrave publishers, 1991, 3rd edition, China.

[21] R. Ravindra, K.R. Krovvidi, A.A. Khan, FTIR, diffusivity, selectivity and aging studies of interactions of hydrazine, water and hydrazine hydrate with the ethyl cellulose membrane, Macromolecules 30 (1997) 3288-3292.

[22] P. Kirkegaard, N.J. Pedersen, M. Eldrup, PATFIT-88: a data processing system for positron annihilation spectra on mainframe and personal Computers, Riso National Laboratory, Denmark, 1989.

[23] S.J. Tao, Positronium annihilation in molecular substances. J. Chem. Phys, 56 (1972) 5499.

[24] S. Weinhold, G.M. Stack, M.R. Tant, A.J. Hill, Effect of copolymer composition on free volume and gas permeability in poly(ethylene terephthalate)-poly(1,4 cyclohexylenedimethylene terephthalate) copolyesters. Eur Polym J., 32 (1996) 843-849.

[25] L.H. Sperling, Introduction to Physical Polymer Science; John Wiley Publishers: New-York, 1986

[26] R.Y.M. Huang, J.W. Rhim, Separation characteristics of pervaporation membrane separation processes, 2nd Chapter in Pervaporation membrane separation processes edited by R.Y.M. Huang, Elsevier publishers, The Netherlands, 1991.

[27] A. Jonquières, R. Clément, P. Lochon, J. Néel, M. Dresch, B. Chrétien, Industrial state-of-art of pervaporation and vapour permeation in the western countries, J. Membrane Sci. 206 (2002) 87-117.

[28] A.VrŸ, "J. Polymer Sci., -part A, 2 (1919) 6 sited in C. J. Van Oss, Interfacial Forces in Aqueous Media, Marcel Dekkar, New York, 1994.

[29] G.A. Morneav, W.A. Pavelich, L.G. Roettger, Bory-Warner chemicals, Kirk and Othmer Encyclopedia of Chemical Technology, Vol 1, 442-456, Wiley-interscience, New York, 1978.

[30] J. Van Oss, Interfacial Forces in Aqueous Media, Marcel Dekkar, New York, 1994.

[31] J.G. Wijmans, R.W. Baker, The solution-diffusion model: A review. J. Membrane Sci., 107 (1995) 1.

[32] H. Okuno, T. Nishida, T. Uragami, J.Polym.Sci., Polym. Phys. 33 (1995) 299.

[33] Y.M.Lee, D. Bourgeois, G. Belfort, Sorption, diffusion and pervaporation of organics in polymer membranes. J. Membrane Sci., 44 (1989) 161-181.

Nomenclature

Abbreviation

ABS   Acrylonitrile Butadiene Styrene

EC   Ethyl Cellulose

FTIR   Fourier Transform Infra-Red

MEC   Modified Ethyl Cellulose

PAL   Positron Annihilation Lifetime

PS   Poly-Styrene

PSI   Pervaporation Separation Index

XRD   X Ray Diffraction

Notation

C   constant in the equation 2

f   free volume fraction

I_3 ortho-positrionium intensity

r   spherical free volume radius (nm)

Δr electron layer thickness (nm)

V_F free volume of the sphere

x   weight fraction of water in feed

y   weight fraction of water in feed

Greek symbols

τ_3 life time of ortho-positrionium

α selectivity

Subscripts

H   hydrazine

W   water

Superscripts

D   diffusivity

S   sorption

P   pervaporation

Chapter 4

Composite Membranes for Hydrophobic PV: Study with Toluene – Water System

4.1 Introduction

Water contaminated with volatile organic compounds is encountered in several chemical industries, groundwater and site remediation applications. Conventional technologies such as air stripping and adsorption with activated carbon do not always provide a complete and economic solution for some of these waste water applications. In recent years, pervaporation [1-3] using hydrophobic membrane has been observed to be promising and potentially suitable remediation method for such applications. Pervaporation is a membrane technology utilizing a dense non-porous homogeneous polymeric film. The liquid feed solution is in contact with the membrane at the upstream side, which is at atmospheric pressure. The liquid solute selectively dissolves and diffuses in the membrane and is removed as vapour at the down stream side. The pervaporation is carried out by maintaining the downstream pressure, lower than the saturation pressure of the permeating liquid solute at that temperature. Usually a higher vacuum is maintained to carry out the operation.

Several applications of pervaporation to organic contaminants laden wastewater are reported in literature [4, 5]. Interestingly, most of these studies were conducted with

single organic component systems, such as toluene in water, etc. Certainly, this has a merit; as such an attempt may help to understand better the mechanism of pervaporation. Since, toluene is less soluble in water such studies were carried out within soluble region (less than 500 ppm). Different types of membranes (e.g., polydimethyl siloxane (PDMS), ethylene-propylene diene terpolymers (EPDM), etc.) were utilized [5, 6] for toluene- water separation. Studies on toluene-water system have used dense membranes and as per our knowledge no work has been reported having use of composite membrane which it self makes us believes to be an interesting study. This is particularly with regard to two different types of membranes (dense membranes versus thin layer interfacial polymerization over porous structure for composite membrane) which may dictate differently solute transport behaviour. Therefore, the objective of this study is to understand the role of composite nature of the membrane along with its porous support layer for toluene-water separation using PERVAP (Sulzer Tech, Germany) membranes. Accordingly, two such PERVAP membranes (1060 & 1070) were chosen, based on the measurements of contact angles of the feed components for the purpose of the present study. PERVAP membranes, however, have also been used for other systems, such as: methanol-MTBE [7], aroma compounds-water [8], butanol-water [9], etc.

Transport, through a dense membrane has been described [10]. Resistance-in-series model [11] has been widely used. Further, simplified equations for such model, were introduced for different transport steps during VOC's removal. Its simplistic approach, with the film theory to account for the mass-transfer limitations in the boundary layer, has attracted many researchers. The present work also adopts resistance-in-series model along with solution-diffusion model to analyse. However, the model

Uribe [7] that it is practically impossible to estimate the amount of sorption in commercial membranes because of the difficulty to discriminate between the active layer and the porous support layer. Hence, in order to estimate amount of sorption another objective of this study is to estimate Flory- Huggins interaction parameter using the relation between surface tension and solubility.

4.2 Theory

4.2.1 Flory - Huggins Interaction Parameter

The surface tension of the membrane surface σ_M, is composed of an apolar or Lifshitz-vander Waals (LW) and a polar or Lewis acid-base (AB) components [12].

$$\sigma_M = \sigma_M^{LW} + \sigma_M^{AB} \tag{4.1}$$

Further, following equation may be used for the acid-base surface tension component:

$$\sigma_M^{AB} = 2\sqrt{\sigma_M^+ \sigma_M^-} \tag{4.2}$$

The following general equation [13] may be used to estimate the interfacial tension between the membrane and the permeating component.

$$\sigma_{M,Li} = \left(\sqrt{\sigma_M^{LW}} - \sqrt{\sigma_{Li}^{LW}}\right)^2 + 2\left(\sqrt{\sigma_M^+ \sigma_M^-} + \sqrt{\sigma_{Li}^+ \sigma_{Li}^-} - \sqrt{\sigma_M^+ \sigma_{Li}^-} - \sqrt{\sigma_M^- \sigma_{Li}^+}\right) \tag{4.3}$$

The change in free energy per unit area for the process (in which molecules of liquid are initially present in polymer) is given by:

$$\Delta G_{Li,M,Li} = -2\sigma_{M,Li} \tag{4.4}$$

Accordingly, Flory-Huggins interaction parameter χ [14], which provides the solubility of the feed component in the membrane, in relation to Gibbs free energy [12], may be calculated from the following equation:

$$\chi_{Li,M} = -\Delta G_{Li,M,Li} S_C / kT \tag{4.5}$$

where, S_C is the minimum contactable surface area between two liquid molecules and such

values are available [15]. Further, the use of eq (4.3) requires the surface tension

components of the membrane and these can be estimated by measuring contact angle θ,

using the following version of the Young-Dupré equation [12]:

$$(1 + \cos\theta)\sigma_{Li} = 2(\sqrt{\sigma_M^{LW}\sigma_{Li}^{LW}} + \sqrt{\sigma_M^+\sigma_{Li}^-} + \sqrt{\sigma_M^-\sigma_{Li}^+})$$ (4.6)

Equation (4.6) needs to evaluate with three unknown parameters and hence measurements

of contact angles were made using three standard liquids (probe liquids). Di-iodo-methane

(essentially an apolar liquid), water (polar liquid) and ethylene glycol (or glycerol or

formamide) were used for the purpose.

4.2.2 Mass Transport

The transport mechanism of trace organics in an aqueous solution through a dense

hydrophobic membrane by pervaporation may be described by five consecutive steps, as

shown in Figure 4.1.

i). Diffusion of a penetrant from the bulk of the feed to the feed membrane interface.

ii). Dissolution of the penetrant into the membrane.

iii). Diffusion of penetrant through the membrane to the downstream side.

iv). Desorption of the penetrant as vapour at the permeate side.

v). Diffusion of penetrant from the vapour-membrane interface to the vapour permeate

bulk.

4.2.2.1 Mass Transport in the Boundary Layer

A mass balance of component i, in the feed side boundary layer over membrane surface

may be obtained at steady state. The sum of convective and diffusive flux towards

membrane surface is equal to the permeate flux of component I [5].

$$v_p x_i^F - D_i^F \frac{dx_i^F}{dz} = v_p y_{ib}^P$$ (4.7)

where v_p $(=N/\rho)$ is the velocity of the fluid perpendicular to the membrane surface, This equation is obtained after assuming that the permeate side boundary layer is neglected due to low down stream pressure. Eq (4.7) is integrated with the following boundary conditions.

$$z=\delta; \quad x_i^F = x_{is}^F$$

$$z=0; \quad x_i^F = x_{ib}^F$$

The actual separation factor of pervaporation process is calculated based on measurable concentrations of feed and permeate, according to

$$\alpha_{iw}^{act} = \frac{y_{ib}^P / y_{wb}^P}{x_{ib}^F / x_{wb}^F} \approx \frac{y_{ib}^P}{x_{ib}^F}; \quad (\because y_{wb}^P = x_{wb}^F \cong 1.0) \tag{4.8}$$
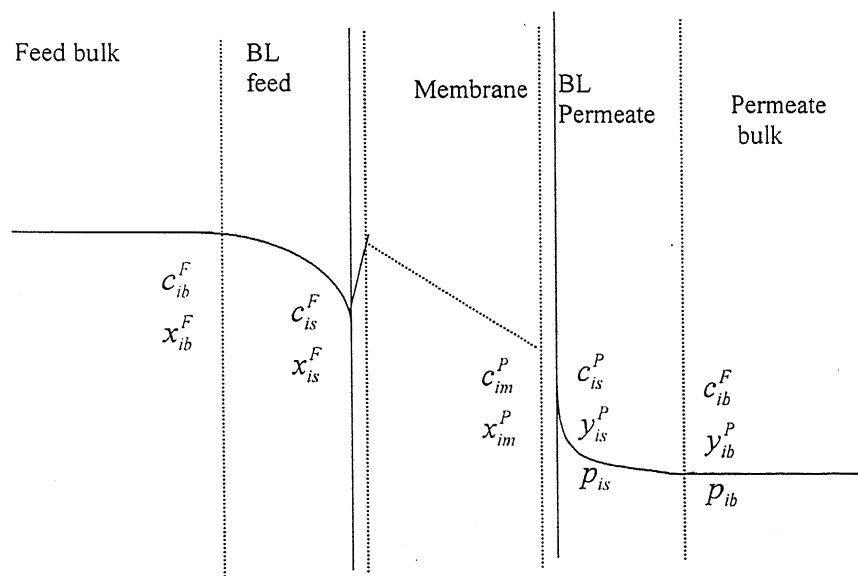
Figure 4.1 Mass transport steps during pervaporation process.

Here mole fraction of water in feed and permeate was assumed to be one because both feed and permeate are dilute solutions. The ideal or intrinsic separation factor α_{iw}^{int}, is calculated based on the membrane interface concentrations of the components.

$$\alpha_{iw}^{int} = \frac{y_{is}^{P}/y_{ws}^{P}}{x_{is}^{F}/x_{ws}^{F}} \approx \frac{y_{ib}^{P}}{x_{is}^{F}} ; (\because y_{ws}^{P} = x_{ws}^{F} \cong 1.0 \ \& \ y_{is}^{P} = y_{ib}^{P})$$

(4.9)

Assuming stagnant film theory to be valid, the mass transfer coefficient $(k_{L,i} \ D_i'/\delta)$ may be obtained by substituting the eqs (4.8) & (4.9) on integrated eq (4.7) and on rearrangement

$$k_{L,i} = \frac{v_{P}}{\ln(\frac{\alpha_{iw}^{act} - \alpha_{iw}^{int}\alpha_{iw}^{act}}{\alpha_{iw}^{int} - \alpha_{iw}^{int}\alpha_{iw}^{act}})}$$

(4.10)

4.2.2.2 Influence of Concentration and Downstream Pressure on Flux and Separation Factor

The mass transfer across the boundary layer on the feed side can be described by,

$$N_i = k_{L,i}(c_{ib}^{F} - c_{is}^{F}) = k_{x,i}(x_{ib}^{F} - x_{is}^{F})$$

(4.11)

The mass transfer across the membrane is described by Ficks law,

$$J_i = -C_i D_i \frac{d \ln a_i}{dz}$$

(4.12)

Further, the activity inside the membrane can be described as the product of the activity coefficient y_i and the mole fraction x_i. At low concentrations, activity coefficient inside the membrane may be considered to be constant and therefore,

$$J_i = -\frac{C_i D_i}{x_i} \frac{dx_i}{dz}$$

(4.13)

Eq (4.13) may be rewritten as,

$$N_i = -\rho D_i \frac{dx_i}{dz} \tag{4.14}$$

Integration of eq (4.14) across the membrane (considering the concentrations in the membrane) leads to eq (4.15) as,

$$N_i = -\rho \frac{\overline{D_i}}{l}(x_{im}^P - x_{im}^F) \tag{4.15}$$

where, $\overline{D_i}$ is the mean diffusion coefficient through the membrane. Solution-diffusion model assumes that equilibrium is at both sides of membrane interfaces include the sorption and the desorption steps. At equilibrium, chemical potential at the membrane interface is equal to the chemical potential inside the membrane. This condition is same for both feed and permeates sides. Thus, activities also get related in the same way for constant pressure in the membrane.

$$\mu_{is}^F = \mu_{im}^F \Rightarrow a_{is}^F = a_{im}^F \tag{4.16}$$

$$\mu_{is}^P = \mu_{im}^P \Rightarrow a_{is}^P = a_{im}^P \tag{4.17}$$

Further, assuming that the vapours in the permeate side behave as ideal gas,

$$a_{is}^F = \gamma_{is}^F x_{is}^F \tag{4.18}$$

and

$$a_{is}^P = \frac{py_{is}^P}{p_i^o} = \frac{py_{ib}^P}{p_i^o} \tag{4.19}$$

Equation (4.19) was obtained assuming the ratio of fugacity coefficients as well as Poynting factor to be equal to one.Hence, the concentrations inside the membrane for both sides can be obtained by combining eqs (4.16), (4.17), (4.18) & (4.19) and therefore,

$$x^F_{im} = \frac{\gamma^F_{is}}{\gamma^F_{im}} \cdot x^F_{is}$$

(4.20)

$$x^P_{im} = \frac{p}{p^o_i} \frac{y^P_{ib}}{\gamma^P_{im}}$$

(4.21)

The molar flux is then obtained by inserting eqs (4.20) and (4.21) into eq (4.15);

accordingly,

$$N_i = \frac{\rho \overline{D}_i}{l \, \gamma^F_{im} p^o_i} (\gamma^F_{is} x^F_{is} p^o_i - p y^P_{ib}) = k_{m,i}(x^F_{is} H_i - p_{ib})$$

(4.22)

Eq (4.22) was obtained assuming the activity coefficient throughout membrane is a

constant. Further, Henry's law constant $H_i = p^o_i \gamma^F_{is} = p^o_i \gamma^F_{ib}$ and mass transfer coefficient

$$k_{m,i} = \frac{\overline{P}_{m,i}}{l}$$

(4.23)

Analogous to gas separation, it is convenient to define an overall pervaporation flux in

terms of vapour pressure difference as,

$$N_i = \frac{\overline{P}_i}{l} (p^o_i \gamma^F_{ib} x^F_{ib} - p_{ib}) = K_{x,i}(x^F_{ib} - \frac{p_{ib}}{H_i}); \text{ where } K_{x,i} = \frac{\overline{P}_i H_i}{l}$$

(4.24)

At steady state, flux through each layer is same, and therefore, the overall mass transfer

coefficient may be related to film mass transfer coefficients,

$$\frac{1}{K_{x,i}} = \frac{1}{k_{x,i}} + \frac{1}{H_i k_{m,i}}$$

(4.25)

Further, the molar concentration based overall mass transfer coefficient and mole fraction

based mass transfer coefficient are related by $K_{L,i}=K_{x,i}/\rho$. In the case of downstream

pressure tending to zero ($p \rightarrow 0$), eq (4.24) becomes,

$$N_i = K_{x,i} x^F_{ib}$$

(4.26)

For two component system (organics and water), the water flux estimation is also analysed in the similar way. However, for pervaporation of dilute organic solutions, the boundary layer mass transport resistance for water is assumed to be negligible. So, the water flux can be expressed as,

$$N_W = \frac{\overline{P}_W}{l}(p_W^o \gamma_W^F x_W^F - p_{wb})$$
(4.27)

For dilute aqueous solution, γ_w^F and x_w^F may be assumed to be equal to one. If the downstream pressure is negligible, eq (4.27) can be simplified as,

$$N_W = \frac{\overline{P}_W p_W^o}{l}.$$
(4.28)

Rearranging the flux eqs (4.26) and (4.28), one can get

$$\frac{y_{ib}^P}{y_{wb}^P} = \frac{K_{x,i} x_{ib}^F l}{\overline{P}_W p_W^o}$$
(4.29)

Influence of downstream pressure on separation factor can be obtained by rearranging eqs (4.24) and (4.27) as,

$$\frac{y_{ib}^P}{y_{wb}^P} = \frac{\overline{P}_i}{\overline{P}_W} \cdot \frac{H_i}{p_W^o}[\frac{(x_{ib}^F - p\,y_{ib}^P/H_i)}{(1 - p\,y_{wb}^P/p_W^o)}]$$
(4.30)

$$\text{Let, } \beta^{perm} = \frac{\overline{P}_i}{\overline{P}_W} \quad \text{and} \quad \beta^{vap} = \frac{H_i}{p_W^o}$$
(4.31)

therefore, eq (4.30) can now be written as,

$$\frac{y_{ib}^P}{y_{wb}^P} = \beta^{perm}\beta^{vap}[\frac{(x_{ib}^F - py_{ib}^P/H_i)}{(1 - py_{wb}^P/p_W^o)}].$$
(4.32)

For dilute organic solutions, then eq (4.32) can be further written as,

$$\frac{1}{\alpha_{iw}^{act}} = \frac{1}{\alpha_{0,iw}^{act}} + (\frac{\beta^{perm}-1}{\alpha_{0,iw}^{act}})\frac{p}{p_w^0} \qquad (4.33)$$

where, separation factor at zero down stream pressure $\alpha_{0,iw}^{act} = \beta^{perm}\beta^{vap}$. The increase or

decrease of separation factor with downstream pressure depends on the value of β^{perm}.

4.2.2.3 Influence of Temperature on Flux

The relation between the temperature and flux at constant upstream and downstream

conditions is well described by Arrhenious type [16] of relation as,

$$N_i = N_{o,i}\exp(-\frac{\Delta E_i}{RT}) \qquad (4.34)$$

Similar relation may also be written for water flux.

4.3 Experimental

4.3.1 Materials

Toluene (99% purity) was obtained from Ranbaxy, India. Double distilled water

was used to prepare the feed solutions. Membranes (PERVAP®1060 &1070) were obtained

from Sulzer Chemtech, Germany. These are composite membranes consisting of a porous

support (70-100μm) on top of a polymer fleece (non-woven fabric of thickness 100μm).

On top of the porous support is a very thin (0.5-2μm) separating layer (proprietary

polymer)

4.3.2 Analysis

The toluene concentration in both the feed and the permeate samples were analyzed

through UV spectroscopy (Shimadzu, Japan) at a wavelength of 261.5 nm. The results were

also cross checked with gas chromatograph (Nuchon, India) equipped with FID. Puropack-

Q was used as reference column and chromosorb as main column. The oven, injector,

detector and oven temperatures were set at 120, 170 and 180°C and, respectively. Benzene

was used as internal standard. Nitrogen was used as a carrier gas. Retention time for benzene was 1.94 minute and that for toluene was 2.46 minute.

4.3.3 Positron Annihilation Lifetime (PAL) Measurements

The PAL measurements were carried out using a fast-fast system having a resolution of 300 pico-seconds (FWHM for the ^{60}Co prompt γ-rays, under ^{22}Na window settings). The positron source was prepared by depositing around 2 micro-Curie aqueous ^{22}NaCl on a thin aluminium foil (thickness ~ 12μm), and covering with an identical foil. Approximately 1 million counts were collected in each spectrum, and four spectra were measured for each sample. The lifetime data were analysed using PATFIT-88 programs [17]. Source correction was done for all spectra. The following expression was used to relate o-Ps pick-off lifetime and free volume radius [18].

$$\tau_3 = \frac{1}{2}\left[1 - r/(r + \Delta r) + (\frac{1}{2\pi})\sin(\frac{2\pi r}{r + \Delta r})\right]^{-1} \tag{4.35}$$

Further, the fractional free volume f, may be estimated from the following empirical relation.

$$f = bV_F I_3 \tag{4.36}$$

The scaling factor b, is obtained from variation of free volume with temperature. However, in the absence such data, it may be typically assigned [19] a value of $1.0/nm^3$.

4.3.4 Scanning Electron Microscope

The structure i.e., skin membrane thickness and pore size of the support layer were analyzed using a scanning electron microscope (SEM JEOL JSM 840A, Japan). Before taking SEM picture, the membranes were dipped in liquid nitrogen and coated with mixture of gold and Pd using a sputter coater. The membranes were positioned vertically and images were taken at accelerating voltage of 15 kV at 3×10^{-10} amperes.

4.3.5 Diffusion Coefficient

Diffusion coefficient of organic component within membrane was estimated in a specially fabricated experimental cell made of glass. The cell design and estimation procedure was presented by Barnes [20]. It consists of two stirred chambers (filled volume, V=400 ml) separated by membrane with an effective surface area of 36.78 cm^2. The chambers are held together using Perspex flanges. Feed solution was filled in one chamber and the other chamber was filled with distilled water. Heating arrangements were provided for both the chambers in order to estimate diffusion coefficients under constant and varied temperatures. The temperatures of the solutions were measured using PT-100 thermocouple. Constant temperature was maintained using proportional controller. Samples were taken at regular intervals from water chamber and analyzed for toluene content. The following equation [21] was used to estimate the diffusion coefficient.

$$C_2(t) = \frac{1}{2} C_1(0) \left[1 - e^{-2Dt/l^2} \right] \qquad (4.37)$$

4.3.6 Contact Angle Measurements

Equilibrium contact angles of toluene and 'probe liquids' in saturated environment on chosen membranes were measured by sessile drop method using Goniometer (Rame-Hart, inc. Imaging System, USA) membranes. Flat sheets were mounted in a stainless steel holder. Saturated environment was maintained by keeping the membrane holder in environmental chamber. A glass syringe with a stainless steel needle was used to place the liquid drop on membrane. The angles were measured with RHI software by capturing the image with video camera. Around 5minutes stabilization, time was allowed to capture the image. Angles (around 50) were then measured in a time span of 1 second and the average of all these angles were calculated. Further, four or five such measurements were made for each liquid on the same membrane and the average value was noted. The variation of

measured contact angles are $\pm 2^{\circ}$ with PERVAP®1060 membrane and $\pm 8^{\circ}$ with PERVAP®1070 membrane. The more variation of contact angle with PERVAP®1070 may be due to the presence of more than one component.

4.3.7 Pervaporation Experimental Set-up

Experimental set-up, designed and developed in our laboratory, was used for the pervaporation measurements, which has been shown in Figure 4.2. Pervaporation test cell of around 400ml, made of glass, was having specially designed flanges to lodge the membrane with an effective membrane area of 40.7 cm^2. The membrane was kept on highly porous stainless steel support with the shiny polymeric layer facing the feed solution. Toluene was dissolved in water by providing sufficient agitation to prepare the binary solution. A three neck round bottom flask was used to circulate feed solution to the test cell. The flask was filled with one liter of the feed solution. The solution and feed cell was heated separately to desired temperature. The temperature was controlled through a PID controller device (Fuji, Japan). Any loss of feed as vapour, formed due to heating, was recovered by placing a condenser on top of the PV test cell.

The feed solution was circulated to the upstream side of the membrane through a long capillary channel, using peristaltic pump; while retentate was sent back to the flask. Sufficient feed flow rate was maintained (around 300 ml/min). The temperature of the feed solution in the cell was measured using PT-100 thermocouple with an accuracy of $\pm 0.2\ ^{0}$C. The membrane upstream side was kept at atmospheric pressure and the downstream side was provided vacuum through the use of a pump (Vacuum Techniques, Bangalore). Total downstream pressure was measured by a Meclod/Pirani/Capillary column and was regulated with an air inlet using stainless steel micro- needle valve, located between the condensers and the vacuum pump.
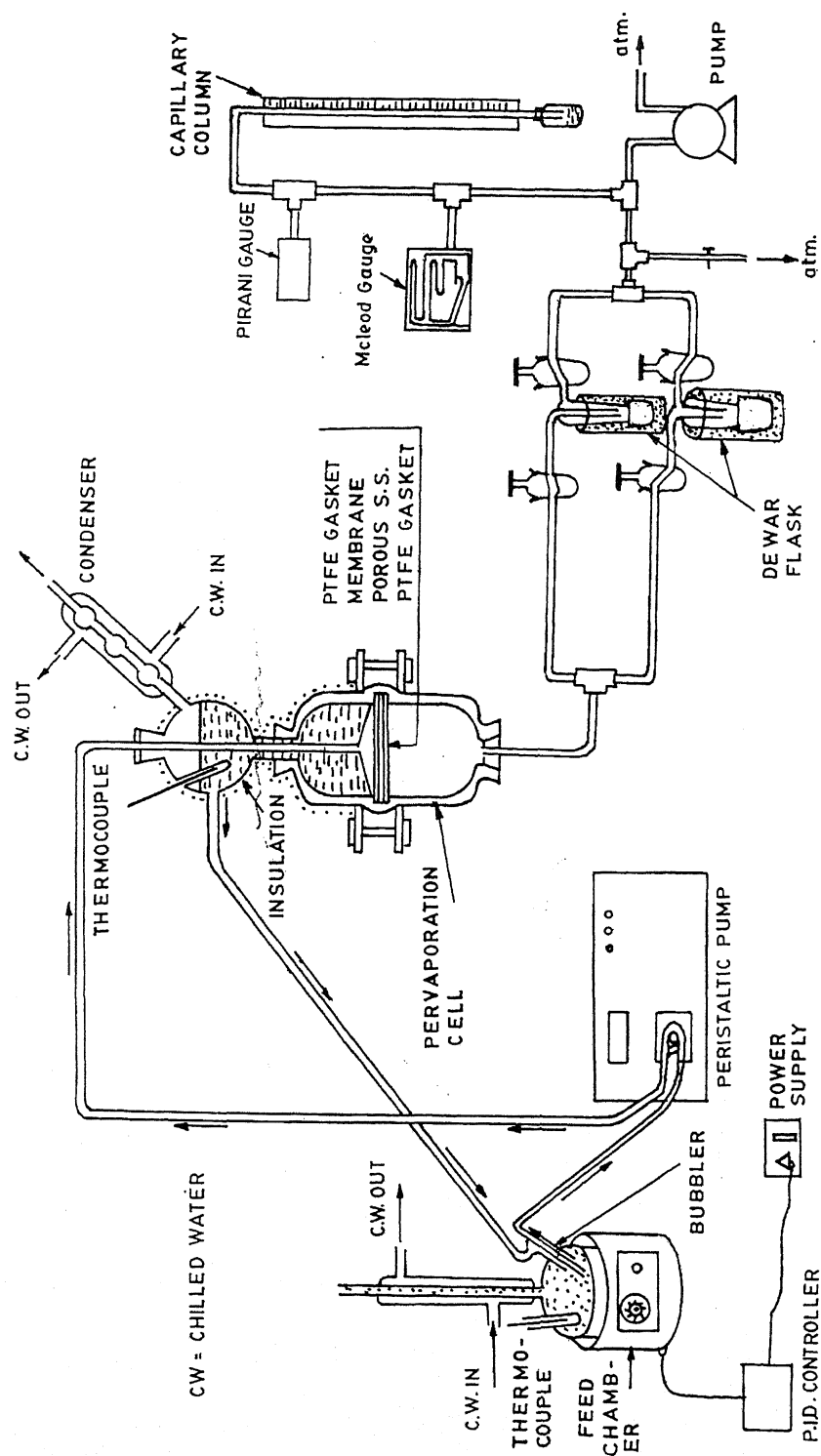
Figure 4.2 Schematic diagram of experimental setup for pervaporation.

The condenser system consisted of two traps that can be used alternately, allowing the permeated pervaporate stream to be sampled continuously without interruption of the operation. The permeated vapours were condensed in the trap by keeping it in Dewar flask, filled with liquid nitrogen. The frozen permeate was collected within a specified time interval. The cold traps were brought to room temperature for measuring its weight through a five decimal balance (Afcoset, India) to determine mass flux.

Experiments were conducted to observe the influence of independent variables: temperature (40, 50, 60°C), downstream pressure (24, 1333, 2000 Pa) and feed toluene concentration (50, 100, 200 ppm) on dependent variables: mass flux and extent of separation (toluene concentration in permeate). Flux values and toluene concentration in permeate were recorded as a function of time; however, in the present work, values obtained after around 4 hours are reported when almost no change of values was observed in the measurement. To minimize in measurement errors, an average, of three separate consecutive readings were taken after system reached to steady state. The average error in the total permeation mass flux was estimated around ±1% and that for toluene concentration was around ±5%

Further, in order to record permeate concentration under negligible concentration polarization effect, permeate samples were taken during initial period of experimentation (just around 15 minutes or so). This was done to observe and estimate intrinsic separation factor where the surface concentration would be almost equal to feed bulk concentration.

4.4 Results & Discussion

4.4.1 Composite Membrane Characterization

4.4.1.1 Positron Annihilations Technique

The positron lifetime spectroscopy analysis was made for varieties of dense and composite membranes in order to obtain primarily free volume parameters. The findings as

well as salient results have been presented in the Chapter 2. In this Chapter, however, results pertaining to P60 and P70 are utilized and presented in Table 4.1. The results show that life time (τ_3) is same for both the membranes. This indicates the polymer may be same for both the membranes. The extra lifetime (τ_4), for P70 is matching with the lifetime for zeolites [22]. Hence, the difference in the pervaporation results may be attributed due to the presence of zeolite. Further, the obtained free volume parameters are agreement with theoretical values [23].

Table 4.1 Free volume parameters and skin layer thickness of P60 and P70.

Membrane	τ_3 (ns)	I_3 (%)	r (nm)	V_f(nm3)	F	l (10^{-6} m)
P60	2.3±0.02	9.4±0.2	0.311	0.126	0.012	41.7
P70	2.32±0.28,	10.6±1.5	0.307	0.128	0.013	16.5
	τ_4:4.53±0.48	I_4:5.1±2.0	0.45	0.385	0.049	

4. 4.1.2 Scanning Electron Microscope

The Figure 4.3a & 4.3b show the SEM pictures of P60 and P70 membranes. The average thickness of the skin layers of these membranes were estimated to be 41.7 x10^{-6} m and 16.5 x10^{-6} m for P60 and P70 membranes respectively and are reported in Table 4.1. Even though, it was generally not recommended to estimate pore size of micro porous support layer through SEM pictures, nonetheless a comparative estimates was made

through SEM pictures pore sizes of support layers of two different membranes (P60 & P70)

It was observed that pore sizes for P70 membrane are higher compared to P60 membranes.

Further, it may be observed that the structure of porous layer is different for both the

membranes.

4.4.2 Solute – Membrane Interactions

4.4.2.1 Diffusion Coefficient

It is important to know the diffusion coefficient of component within the

membrane. The diffusion coefficient of toluene at different feed toluene concentration and

temperature were estimated. As per the eq (4.37), plots of time t versus

$\log[1 - 2C_2(t)/C_1(0)]$ were drawn (Figure 4.4 & Figure 4. 5) at different feed

concentrations and temperature for both P60 and P70 membranes. The slopes of these lines

along with the respective estimates of λ and l give diffusion coefficient D. The value of λ

(=effective free volume/V) was estimated by taking the effective free volume as product of

effective surface area of the membrane, membrane thickness (obtained from SEM

measurement) and free volume fraction of the membrane (obtained from positron

annihilation technique at the dry state of the membrane). The obtained values of values of

diffusivities were plotted in Figure 4.6, as function of temperature and feed concentration

for both the membranes. The obtained values are in the range of 0.78 to 28.28 $\times 10^{-9} m^2/s$.

The larger diffusion coefficients indicating that the rubbery polymers may be good

candidates for pervaporation of toluene. Further, diffusion coefficient values were found to

be 3 to 100 times lower compared to the value of diffusion coefficient of chloroform

(for100 ppm solution of chloroform) for dense PDMS membrane [21]. Even though, the

pervaporation selectivity for toluene/water and chloroform/water are in the same range for

dense PDMS membrane [11, 21], the smaller diffusion coefficients for the toluene, in the

present case, may be because of the presence of support layer of the composite membrane.
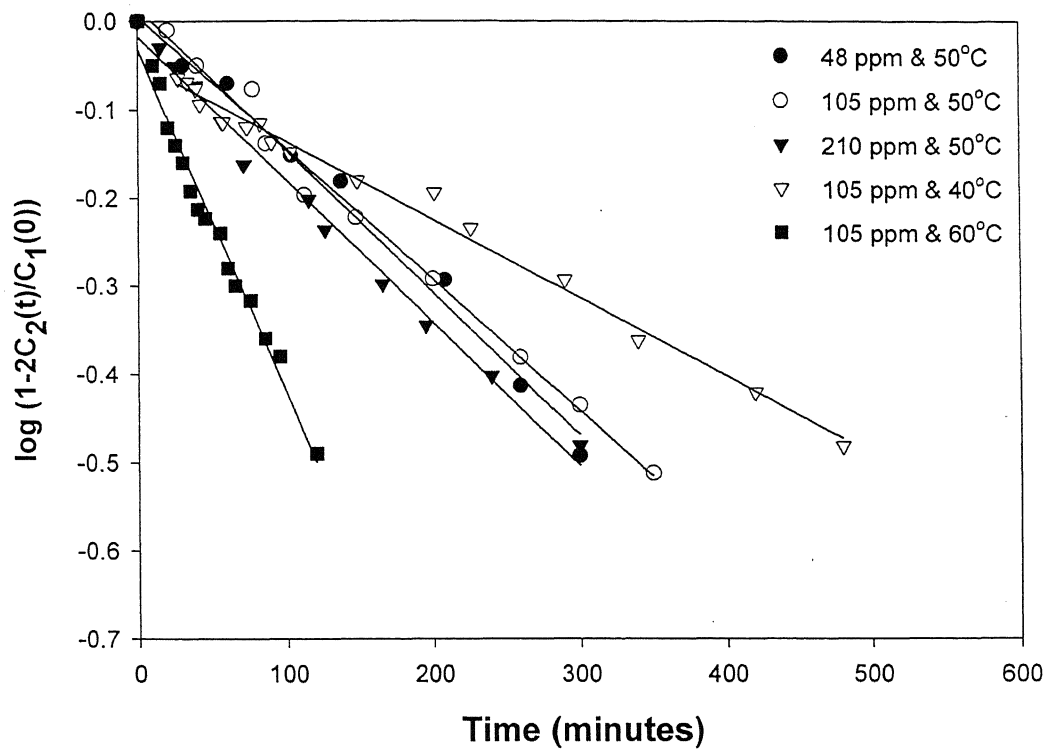
Figure 4.4 Relationship between time and log $(1-2C_2(t)/C_1(0))$ for P60 membrane.
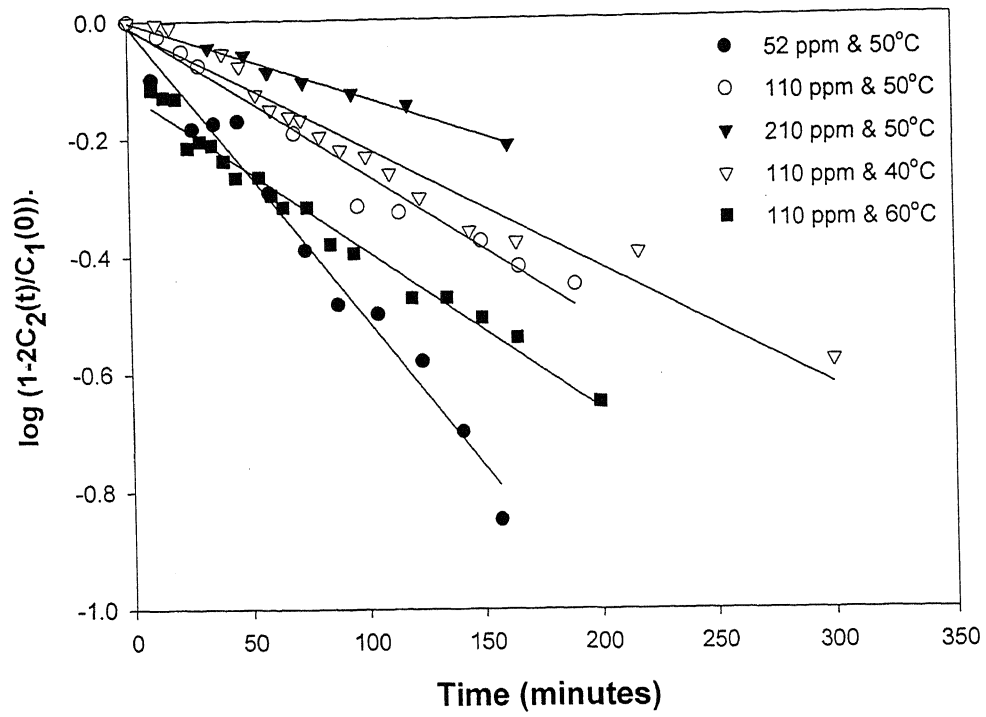
Figure 4.5 **Relationship between time and log $(1-2C_2(t)/C_1(0))$ for P70 membrane.**
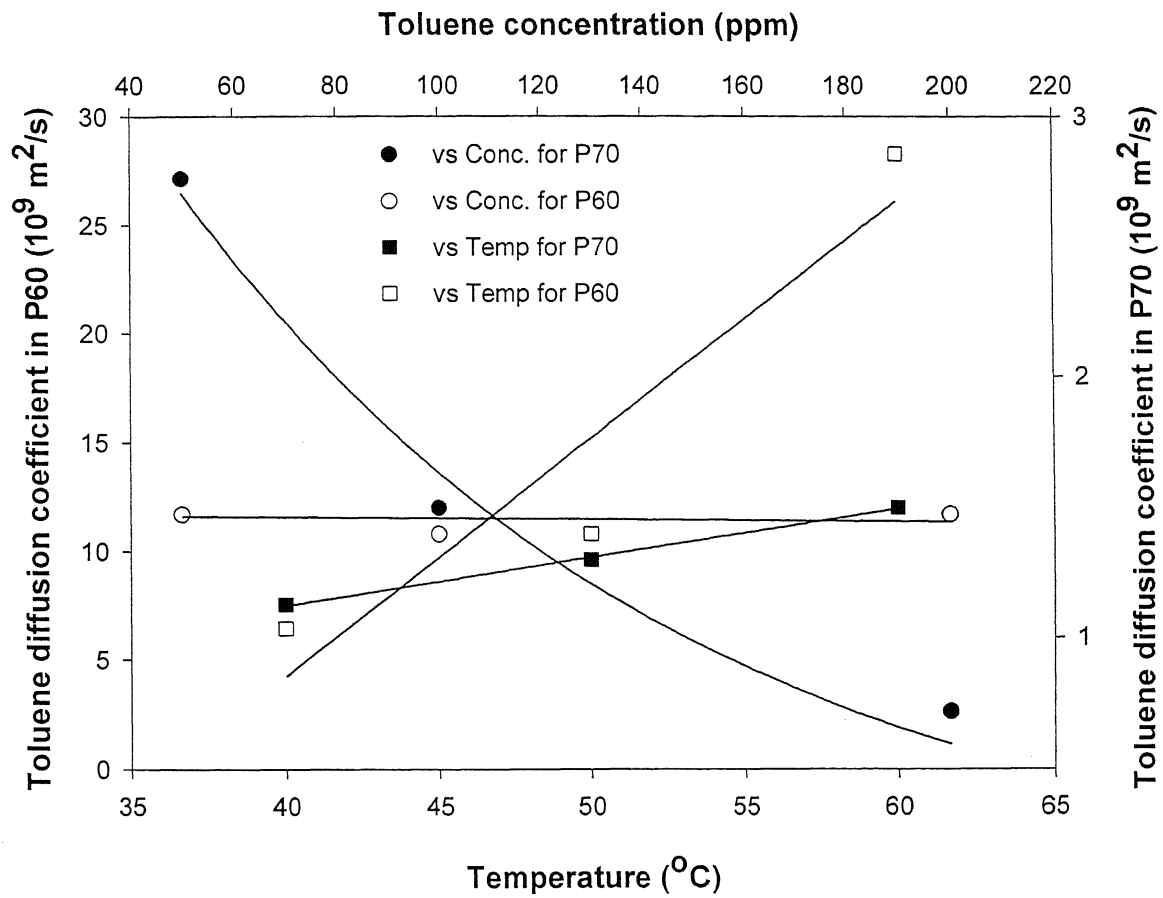
Figure 4.6 Variation of diffusion coefficient of toluene with feed toluene concentration and temperature

Further, few following observations may be made from the Figure 4.6: i) diffusion coefficient for toluene is more in P60 compared P70 membrane, ii) diffusivity of toluene is decreasing with increasing feed concentration for P70 while it was found to be independent of concentration for P60 membrane and iii) diffusion coefficient is increasing with increasing temperature for both the membranes but the increase is more for P60 compared P70.

4.4.2.2 Estimation of Flory-Huggins Interaction Parameter

The surface tension values of probe liquids at 20°C are taken from literature [12] and are reported in Table 4.2. Further, measured contact angles are reported in Table 3. Calculated values of surface tensions, using eq (4.6) and then eq (4.1) & (4.2), are also reported in Table 4.3. The obtained surface tension values suggest mono-polar nature of the chosen membranes. Flory-Huggins interaction parameters between toluene and membranes taking minimum contactable surface area, S_C for the toluene [15] as 0.44nm^2 were calculated using eq (4.5). The obtained values are reported in Table 4.3. The interaction parameter of toluene with P60 is 0.2462 which is close to the value known for PDMS[10] membrane and for P70 is 0.2556. It is known [24] that low values of interaction parameter (less than 0.5) which was found in the case of P60 & P70 suggests dissolution of skin layer with pure toluene which was indeed observed also practically. There is lot of speculations with regard to contactable surface area of water molecules. The average contactable surface area of single water [25] molecule is roughly 0.08nm^2. Using this value, interaction parameter for water was estimated and also reported in Table 4.3. The smaller value of interaction parameter between water and P70 suggests high sorption and low pervaporation selectivity compared to P60 membrane.

Table 4.2 Surface tension values of Probe liquids.

Component	γ^{LW} (mJ/m^2)	γ^+ (mJ/m^2)	γ^- (mJ/m^2)	γ (mJ/m^2)
Water	21.8	25.5	25.5	72.8
Ethylene glycol	29.0	1.9	47.0	48.0
Diodomethane	50.8	0.0	0.0	50.8
Toluene	28.5	0.0	2.3	28.5

Table 4.3 Contact angles, surface tensions of membranes and interaction parameter.

Parameters	P60	P70
θ of water	93.8	84.8
θ of ethylene glycol	78.8	64.1
θ of diodo-methane	74.8	72.0
σ^{LW} (mJ/m^2)	20.21	21.88
σ^+ (mJ/m^2)	0.026	0.66
σ^- (mJ/m^2)	5.819	7.58
σ (mJ/m^2)	20.98	26.35
Interfacial tension, σ_{iM}	1.13	1.15
χ_{iM}	0.2462	0.2501
Interfacial tension, σ_{wM}	26.12	13.85
χ_{wM}	1.0332	0.5478

4.4.3 Estimation of Mass Transfer Coefficient in the Boundary Layer

As mentioned in the experimental section, permeate samples collected for a shorter run (around 15 minutes) was analyzed and results are reported in Table 4.4. Further, pseudo steady state results are also reported in Table 4.4. Due to the large variation of selectivity with feed concentration for P70 membrane (elaborate discussion in the following sections), the shorter run results are reported only at 105ppm.

From the values of intrinsic and actual separation factors, mass transfer coefficient in the boundary layer was calculated using eq (4.10). The average value of mass transfer coefficient in the boundary layer was estimated to be 2.35×10^{-6} m/s for P60membrane and 1.00×10^{-6} m/s for P70. The obtained mass transfer coefficient is comparable to the value (6.06×10^{-6} m/s for PEBA at 25°C and 170 rpm) obtained by Raghunath et al.[5]. However, in principle, the boundary layer mass transfer coefficient is independent of membrane material but certainly a function of concentration; albeit a weak function. Selectivity of toluene was found lower for P70 compared to P60 membrane. Therefore, concentration gradient in the boundary layer was observed to be small in the case of P70 and hence lower boundary layer mass transfer coefficient. Such results were also reported by Nijhuis et al.[26] for the separation of toluene through PDMS and EPDM membrane. This was explained due to deviations during extrapolation of their results. Further, the overall flux for shorter runs was found to be slightly higher than that obtained at pseudo steady state conditions for P60 membrane. This may be due to the fact that, initially toluene concentration at the membrane surface is more. Because of this, membrane swelling (interaction coefficient 0.2462) and flux will be more. Similar observations can also be made for the slight increase of overall flux with increase in feed toluene concentration.

Table 4.4 Short run & steady state fluxes and permeate concentrations

Membrane	Feed conc. (ppm)	Short run flux (10^{-6} kmol/m^{2}s)	Short run permeate con. (ppm)	α_{iw}^{int}	Steady state flux (10^{-6} kmol/m^{2}s)	Steady state permeate con. (ppm)	α_{iw}^{act}
P60	45	5.811	1805.7	40.12	5.597	728.1	16.18
-do-	100	5.980	3821.1	38.21	5.633	1307.2	13.07
-do-	200	6.333	7020.6	35.10	5.878	2880.0	14.40
P70	105	3.631	2992.8	28.50	3.608	1090.5	10.38

However, the membrane swelling in case of P70 may be less and hence observed difference of flux between shorter and steady state run is small.

Against expectations, it is to be noted from Table 4.4 that both selectivities (intrinsic and actual) for the membranes are much lower compared to pure PDMS dense membrane [11]. Such lower values of selectivities are attributed with two facts: very thin skin layer and support layer. For elastomeric polymers the organic flux is independent membrane thickness [26] and water flux is dependent. Therefore, water flux was observed to be high. Further, low values of intrinsic selectivity are explained because of the role played by support layer: diffusion path length, pressure loss and permeate condensation. These values depend on the support structure (porosity, pore size) and material property. Feng and Huang [27] reported for the specific role of support layer in terms of separation of acetic acid – water mixtures using silicone based membranes. The homogeneous silicone-poly carbonate co-polymer membrane was found to be acetic acid selective, while silicone-poly carbonate co-polymer membrane on a micro-porous support structure was slightly water selective. Like wise, several such studies [28, 29] have reported the importance of support layer during pervaporation separation.

Further, quantitative estimation of diffusion path length and pressure drop in the support layer may be carried out, but rigorous [29]. Therefore, quantitative estimation of permeate condensation in the pores of P70 support layer was considered for the present work. An average pore size of support layer was assumed to be 25 nm which is similar to ultra filtration membranes [30]. Further, non woven fabric of the composite membrane was carefully removed and the contact angles of water and toluene on porous support were measured. The average contact angle for water is found to be 127±4 (Figure.4.7) and for toluene it was zero degrees. These values were used to estimate the saturation vapour pressure in porous support layer using Kelvin's equation [31].
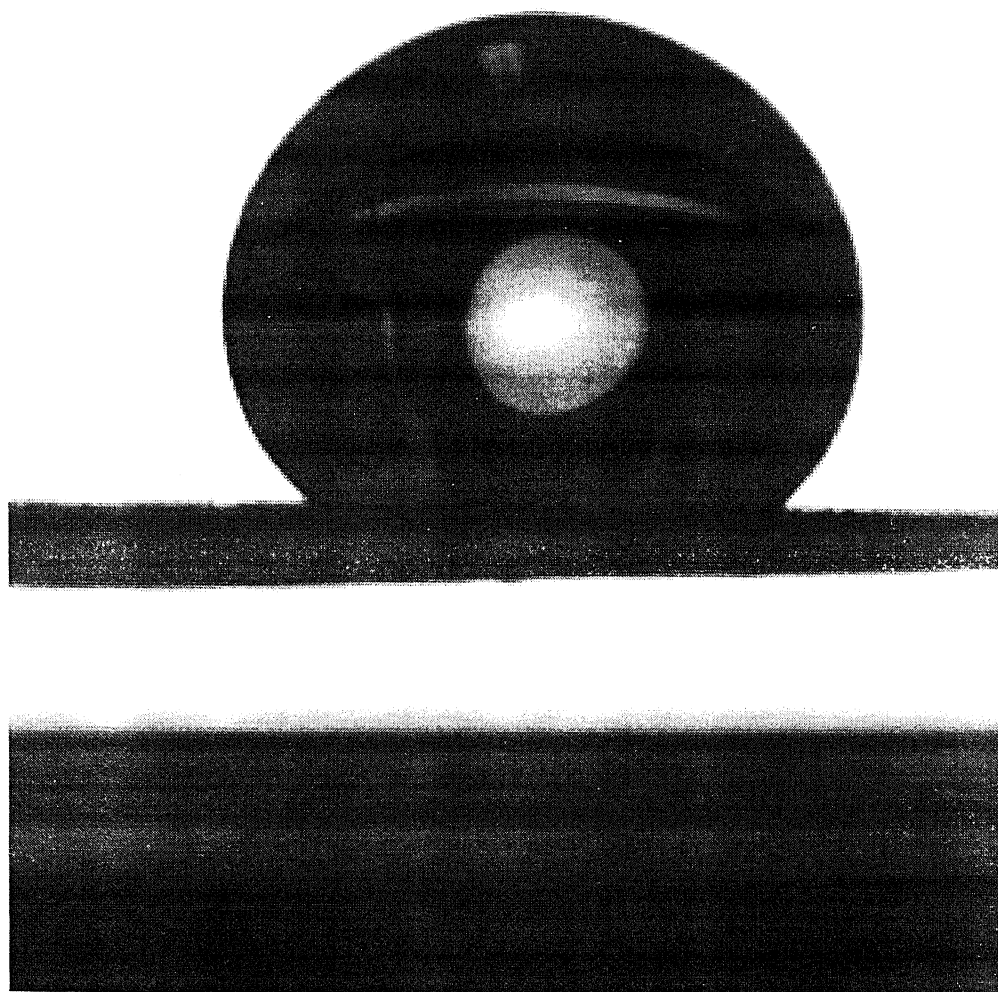
Figure 4.7 Contact angle of water on support layer of P70 membrane

$$p_{sup}^{o} = p^{o} \exp\left[-\frac{2V_{Li}\sigma_{Li}\cos\theta}{RTr_{sup}} \right] \qquad (4.38)$$

Because of the support layer, the equilibrium vapour pressure for water in the pore, increased from 92.51 to 94.63 mm of Hg, while toluene vapour pressure decreased from 92.1 to 84.6 mm of Hg. Thus, there may be toluene condensation in the support layer and this may be one of the reasons for lower selectivity as compared to dense membrane. The change in vapour pressure depends strongly on the pore size of support layer. Further, regardless of the radius of the pore of support layer water vapour pressure increases while toluene vapour pressure decreases.

4.4.4 Effect of Operating Parameters

4.4.4.1 Influence of Toluene Feed Concentration

Figure 4.8 shows the effect of feed toluene concentration on toluene flux at 50°C. Linear relationships were obtained for both membranes for the range of feed toluene concentrations chosen for the work. The toluene flux increases with increase in toluene concentration. This is because the solubility and driving force increases with increase in concentration and this trend verifies eq (4.26). However, all though the experimental values for P70 fall in straight line but the line is not passing through the origin. This may be due to the fact that, in the developed model, diffusion coefficient and activity coefficient of permeant are assumed to be independent of concentration. In general, they are concentration dependent [33] and hence simple relationship in the form eq (4.26) was obtained (detailed discussion for P70 membrane in section 4.4.4.5 regarding this aspect). Baker et al. [33] reported similar results for pervaporation of dilute aqueous solutions of toluene through silicone rubber membranes. Neglecting the initial behaviour pattern of toluene flux, a linear fit of the experimental points were obtained and as per eq (4.26), the overall mass transfer coefficient $K_{x,i}$, were estimated from the slopes of the fitted lines. The
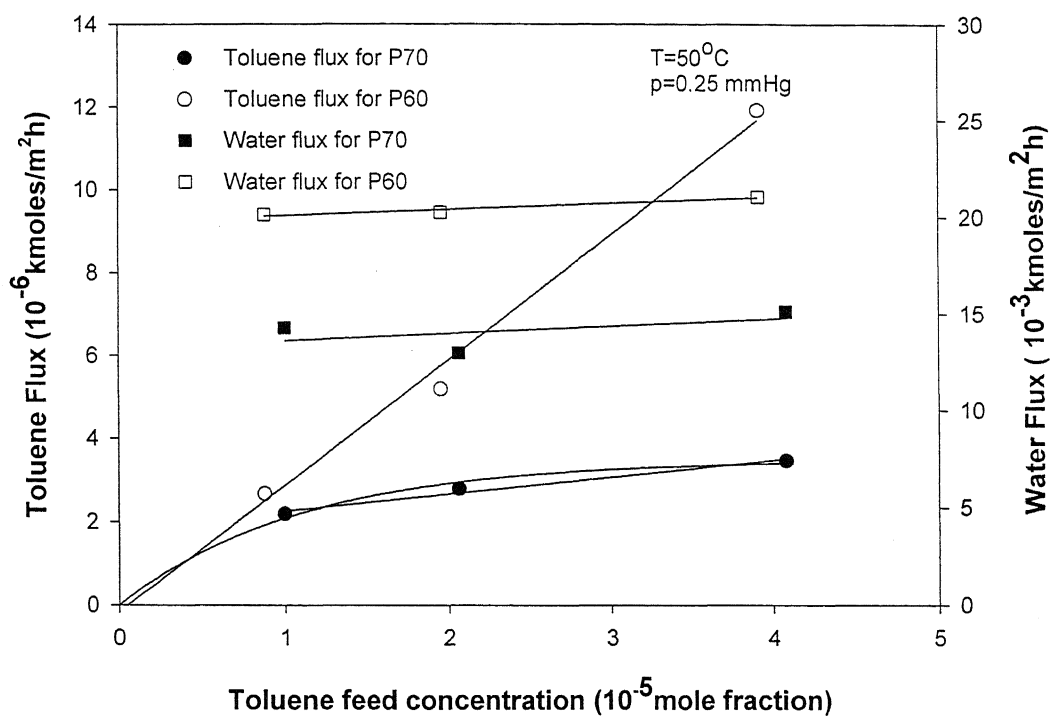
Figure 4.8 Influence of feed toluene concentration on individual fluxes

Table 4.5 Estimated values of overall mass transfer coefficients, water permeabilities and activation energies under set experimental conditions

Parameters	P60	P70	Conditions
$k_{L,i}\,(10^{-6}\,\text{m/s})$	2.35	1.00	$T=50^0C$, $p\approx0$,
$K_{L,i}\,(10^{-6}\,\text{m/s})$	1.51	0.38	$T=50^oC$, $p\approx0$,
$P_w\,(10^{-10}\text{m kmol/m}^2\text{s mmHg})$	2.48	0.64	$T=50^oC$, $p\approx0$,
$K_{L,i}\,(10^{-6}\,\text{m/s})$	1.35	0.72	$T=50^oC$, $p>0$, $x_{ib}^F = 1.95\text{x}10^{-5}$
$H_i\,(\text{mmHg})$	251.75	257.94	$T=50^oC$, $p>0$, $x_{ib}^F = 1.95\text{x}10^{-5}$
$k_{m,i}\,(10^{-6}\,\text{kmol/m}^2\text{mmHg.s})$	0.70	0.54	$T=50^oC$, $p>0$, $x_{ib}^F = 1.95\text{x}10^{-5}$
$\bar{p}_i\,(10^{-11}\,\text{m kmol/m}^2\text{ mm Hg s})$	2.93	0.89	$T=50^oC$, $p>0$, $x_{ib}^F = 1.95\text{x}10^{-5}$
$\Delta E_i\,(10^3\,\text{kJ/g})$	1.82	3.91	$p\approx0$, $x_{ib}^F = 1.95\text{x}10^{-5}$
$\Delta E_w(10^3\,\text{kJ/g})$	0.69	0.78	$p\approx0$, $x_{ib}^F = 1.95\text{x}10^{-5}$

obtained values are divided with the molar density of the solution to estimate overall mass transfer coefficient $K_{L,i,}$ and these are reported in Table 4.5. For same flow rate, overall mass transfer coefficient for P60 is higher than the one obtained for P70. Further, an attempt was made to fit P70 results using exponential and hyperbola relations and the results are found to be comparable (Figure 4.8). This non linearity may be due to exponential variation of diffusivity or Langmuir sorption with concentration or may be both. As observed from diffusion experiments (section 4.4.2.1) the diffusion coefficient of toluene in the membrane is function of feed concentration. It is to be mentioned here that Ji et al. [34] reviewed the experimental results and the models for pervaporation of various mixtures in adsorbent filled membranes. According to them, sorption may be duel – sorption.

According to eq (4.28), the water flux is independent of feed toluene concentration at higher downstream vacuum. The experimental values for water flux at high downstream vacuum and at 50°C are also shown in Figure 4.8. Almost constant water flux was observed. The deviation may be due to coupling because of swelling, which was not accounted in the developed model. Ji et al. [11] have reported constant water flux with increase feed organic concentration for the permeation of dilute aqueous solutions of toluene, methylene chloride, trichloroethane through PDMS, PEBA membranes. However, Meuleman et al. [6] have reported increase of water flux with increase in toluene concentration through EPDM membrane. Water permeability values for both the membranes were estimated and are reported in Table 4.5. The water permeability for P70 was observed lower than that for P60.

Figure 4.9 is plots of ratio of permeate concentrations of toluene to water y_i/y_w versus feed concentration x_i. According to eq (4.29), for constant overall organic permeability and water permeability, the stated ratio should provide a straight line. Figure
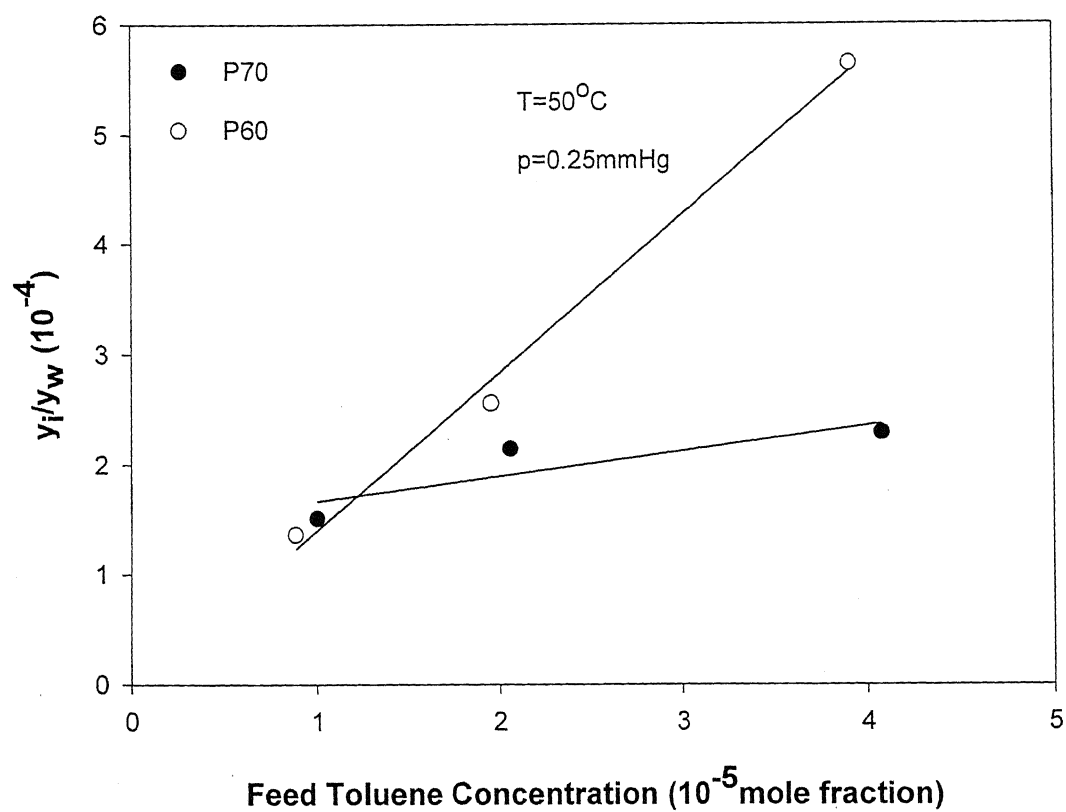
Figure 4. 9 Relationship between ratio of toluene to water (pervaporate) concentration and toluene feed Concentration.

4.9 indeed depicts such representations for both P60 and P70 membranes. However, a slight deviation was observed for P70. This may be attributed for the concentration dependence of permeability values through the membrane. Selectivity as well as total flux was observed to be higher for P60 compared to P70. This may be because of presence of zeolite in P70. However, as explained above, the obtained ratios of permeate concentrations for both the composite membranes were less compared to literature values of dense membranes [11, 27]. This observation may be because of the composite nature of membranes (as explained in section 4.4.3).

4.4.4.2 Influence of Downstream Pressure

According to eq (4.24), for constant feed concentration, a plot of N_i versus p_{ib} should be a straight line with an intercept of $K_{x,i} x_{ib}^F$ and slope of $-K_{x,i}/H_i$. The experimental values of toluene flux against downstream partial pressure of toluene are shown in Figure 4.10. A straight line was obtained in the pressure range of 0.16 to 28 mmHg. Therefore, the overall mass transfer coefficients were estimated from the intercept and are reported in Table 4.5 after dividing with molar density of the solution. These values were compared with the values obtained for feed concentration variation. Accordingly, it may be observed, that they are comparable for the P60 membrane. However, the difference is high in case of P70 membrane. Further, one can expect higher values of overall mass transfer coefficients with concentration variation (at high vacuum) compared to pressure variation because of existence of vapour phase resistance. However, the situation is reverse with this membrane. As mentioned in section 4.4.4.1 toluene flux attains plateau with concentration; hence, average concentration based overall mass transfer coefficient was found smaller than that of down stream pressure based mass transfer coefficient. Therefore, comparison between two different variations based overall mass transfer coefficients suggests that the vapour phase mass transfer resistance is negligible in the range of chosen down stream
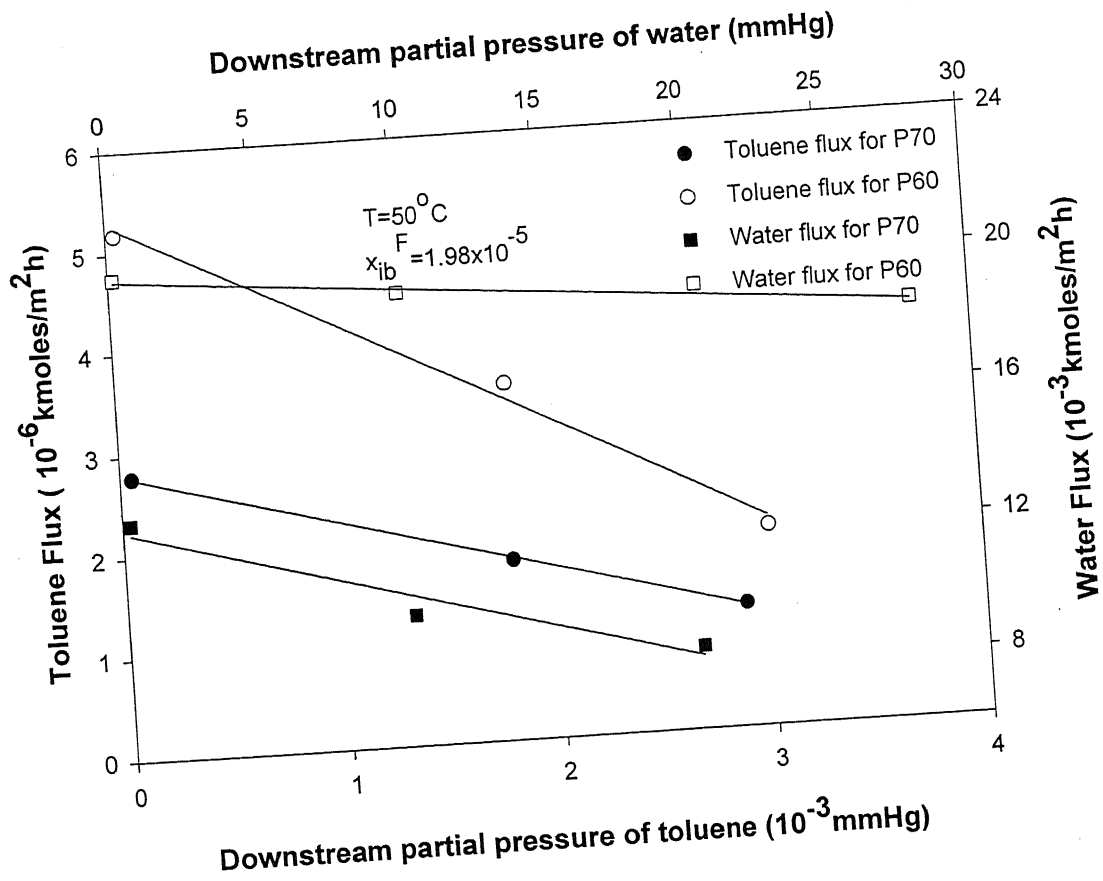
Figure 4.10 Influence of downstream partial pressures on individual fluxes.

pressures. Further, Henry's laws constant was estimated (from the slope) and are reported in Table 4.5. Henry's law constant is observed to be same (with little difference) for both the membranes. These were found to be in the similar range as reported in the literature [11, 36, 37]. The mass transfer coefficient in the membrane is also calculated using mass transfer coefficients in the boundary layer and reported in the Table 4.5. Therefore, mass transfer coefficient through the membrane $(k_{m,i} = p_i^m / l)$ is also higher for P60 and may be P60 membrane may be considered better.

Figure 4.10 also shows the variation of water flux with downstream pressure. Water flux linearly decreases with increase in downstream pressure which is agreement with theoretical behaviour (as per eq 4.27).

Figure 4.11 depicts the effect of downstream pressure on separation factor. According to eq (4.33), the reciprocal of separation factor increases with increase in downstream pressure (for β^{perm} greater than one). Brun et al. [37] have reported similar results for the separation of dilute solutions of benzene and chloroform using NBR and SBR membranes. Reverse trends have also been reported [11] using other polymeric membranes. In an interesting article Ten et al. [38] classified the systems into four classes, according to range of downstream pressures. The present system comes under the class 'A' category as per their [38] classification. Accordingly, there is a sharp decrease in permeate concentration as permeate pressure increases (from absolute vacuum); the present work indeed shows such a case.

Further, it may interest to observe from Figure 4.11 that the variation of selectivity (in terms of slope) with pressure is more for P60 compared to P70. This may be because of the drop of pressure in the support layer. Pressure drop either for viscous flow (Knudsen number < 0.01) or for molecular flow (Knudsen number > 10) in the support layer is
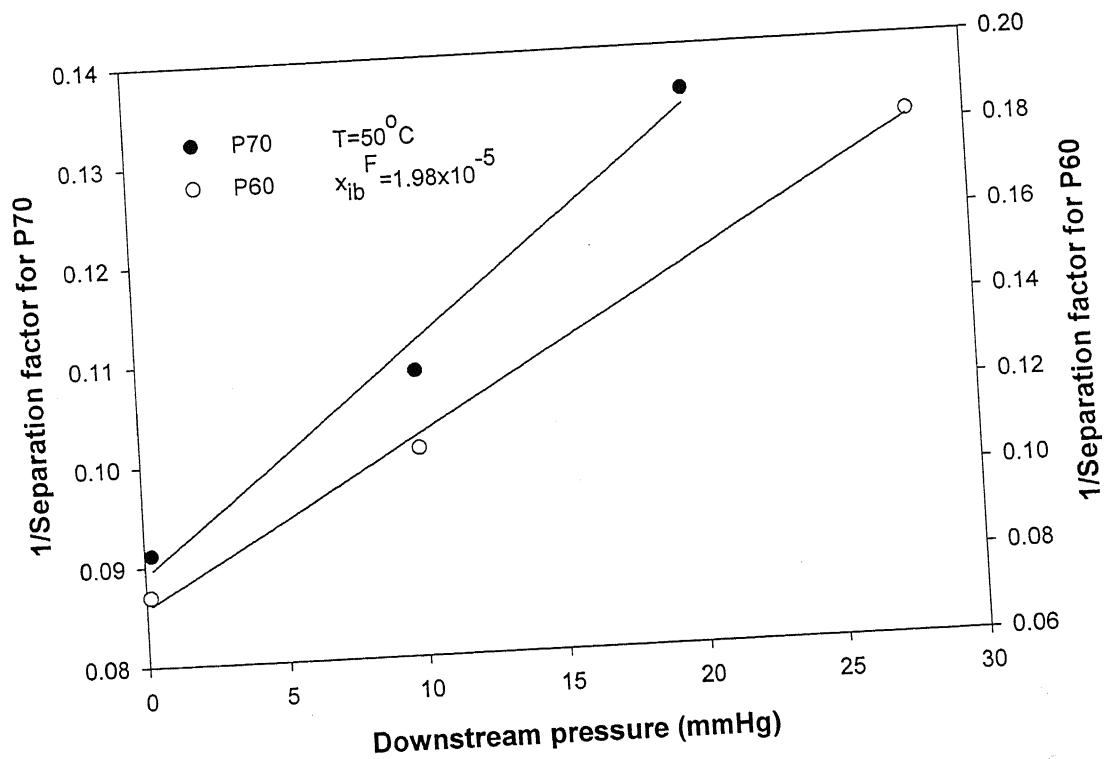
Figure 4.11 Influence of downstream pressure on separation factor.

proportional to total flux [39, 40]. The total flux obtained for P60 is higher and hence higher pressure drop. Increase in pressure drop reduces toluene flux and hence selectivity.

4.4.4.3 Influence of Temperature

Arrehenious type of temperature dependency of permeate flux was studied. Figure 4.12 is the plots of logarithmic of toluene and water fluxes versus inverse of temperature. Straight-line relationships were obtained for both the membranes. The slope of the plot gives overall activation energy for permeation of toluene and water (as per eq 4.34) and the values are given in Table 4.5. Even though, both water and toluene (Figure 4.13) flux increase with increase in temperature, but the ratios of permeate concentration of toluene to water decrease with increase in temperature. Increased water permeability at higher temperatures compared to toluene may be the explanation for the observed behaviour. Further, the increased water permeability may be because of either increase of solubility or diffusivity or may be both.

The increased water fraction in permeate dilutes permeate, resulting in decrease in separator factor. The same can also be inferred from Table 4.5; where the values of activation energies suggest faster permeation for water instead of toluene having higher activation energy. Since, membrane is more selective to toluene than water, these two opposite characteristics lower the net permeation of toluene and thus selectivity gets lowered. Further, comparing eqs (4.24) & (4.28) and taking ratios of these two fluxes at negligible downstream pressure, the selectivity (pervaporate concentration ratio) simply becomes the ratios of saturation pressures of the two components. Knowing the rate of change of vapour pressure of toluene being lower than water with increase in temperature [41, 42], the selectivity obviously decreases with increase in temperature. Therefore, pervaporation process, if carried out at lower temperature, higher selectivity may be achieved; but at the expense of toluene production rate.
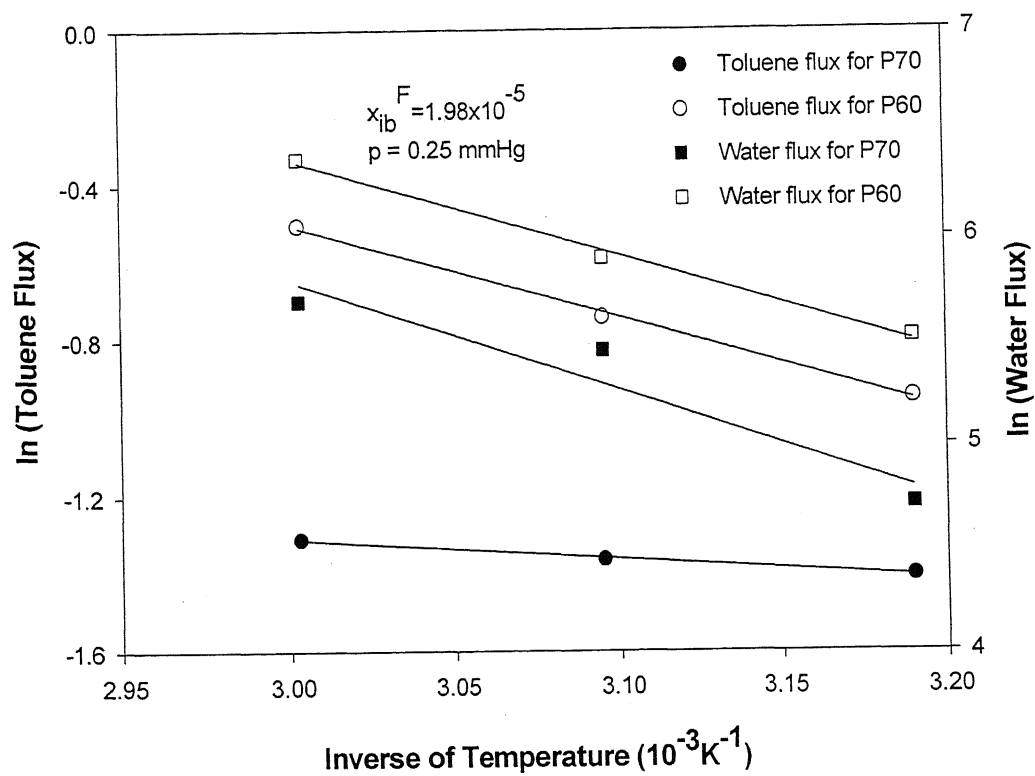
Figure 4.12 Arrhenious plot: Influence of feed solution temperature on individual fluxes.
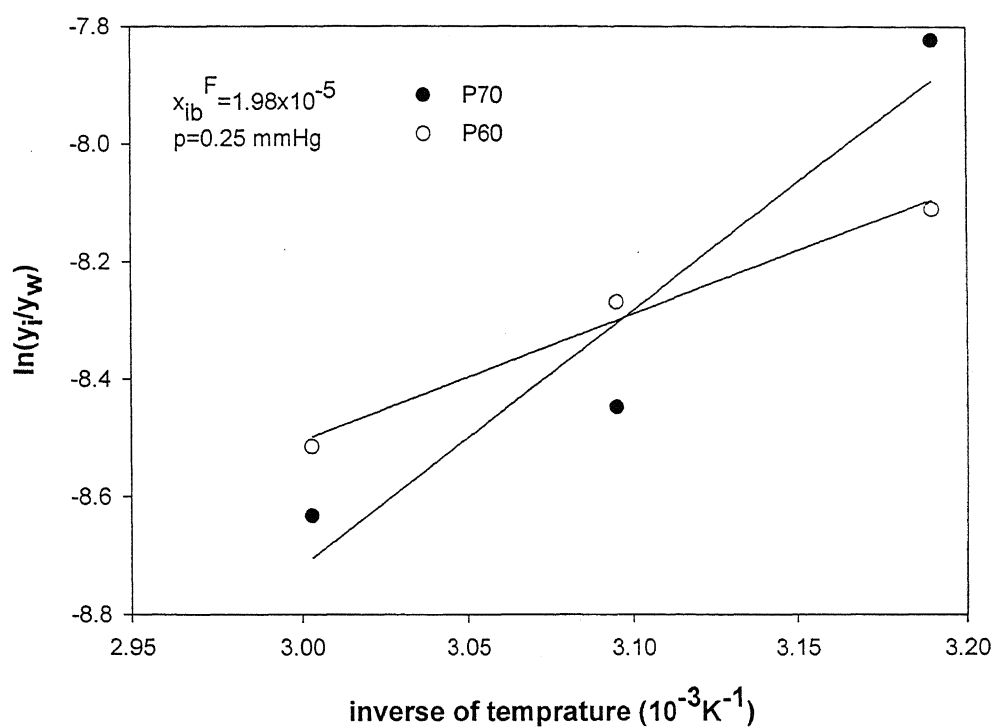
Figure 4.13 Relationship between ratio of toluene to water (pervaporate) concentration and reciprocal of temperature.

4.4.5 Performance of Membranes: A Comparison

Positron annihilations results confirmed presence of two components in the skin layer of P70 membrane. Apart from PDMS silicalite zeolites may be the second component. Silicalite zeolites known to have straight and zigzag channels connected via intersections. This may have caused difference in the results observed for the two membranes (Figure 4.8 to 4.13). The overall flux as well as toluene flux for P60 membrane was observed to be higher than P70 membrane. Similar such low values of overall flux reported for zeolite filled membranes [43-45]. This limitation on flux may be ascribed to the molecular sieving properties of the zeolites. The simulation results of adsorption of high organics (hexane) through silicalite showed the occurrence of capillary condensation of the organic components and formation of kink or step in adsorption isotherm [46]. Similarly, toluene being higher organic molecule, capillary condensation of toluene may take place which may take longer time for withdrawal. Therefore, P70 membrane has provided lower toluene flux than P60. However, Goethaert et al. [47] observed much higher chlorinated hydrocarbon flux in zeolite filled membranes compared to unfilled membranes. Further, water and overall flux reduced to less than half to that of unfilled membrane. The toluene is bigger molecule (molecular size ~ 0.6 nm) [35] compared to openings in zeolite (0.49 nm). In addition lower interaction between these two (toluene and zeolite) may be the reason for lower organic flux.

As mentioned earlier, the concentration profile obtained for P70 did not passing through the origin. This may be because at low concentration of toluene (50ppm), the molecules move freely in the channels and at high concentration (200ppm) the channels get saturated with the permeating molecules. This prevents the free movement of molecules in the channels. Therefore, toluene flux attains plateau with increasing concentration.

Further, it may be stated that at low temperature, the toluene selectivity in P70 membrane is higher compared to P60. This may be because of the absence of kink formation in adsorption isotherm at lower temperatures [48] compared to presence of kink formation at higher temperatures [49].

4.5 Conclusions

Chosen membranes were characterised using positron annihilation technique. The base polymers of skin layer for both membranes were found to be same; however, the results of P70 membrane showed the presence of an extra component (zeolites). Further, skin layer thickness was obtained from scanning electron microscope. In addition to these, diffusion coefficients of solute within membrane as well as solubilities were estimated in order to study the solute – membrane interactions. Toluene diffusivity within the membranes was observed to be independent of feed concentration for P60 while it decreased with increase in feed concentration for P70 membrane. Flory-Huggins interaction parameter of toluene with P60 membrane through surface thermodynamic approach (contact angle measurement) was found to be close to the value available (literature) for PDMS membrane.

During hydrophobic pervaporation, lower values of intrinsic and actual selectivities for composite membranes compared to dense membranes, suggested an important role played by support layer. Use of composite membranes did not show any unexpected behaviour (compared to dense membranes) under varying operating conditions during pervaporation. However, in case of P70, toluene flux attained plateau with increase in feed concentration which confirms the presence of an extra component in the skin layer.

Pervaporation experimental results were mathematically analysed with the application Henry's law and with the use of concentration independent diffusion coefficient. The results with P60 membrane adhered to such mathematical model, whereas,

the same were not observed to be valid for P70 membrane. Therefore, a simple resistance in series model may not be sufficient enough for filled membranes.

Experimental data and results may be considered to be useful for the selection of support layer for better application of composite membrane. This may necessitate simulation and optimization between the geometry and physical properties of the support layer.

4.6 Notations

a   activity

b   constant in the free volume ($1/m^3$)

C   volumetric concentration (m^3/m^3)

c   molar concentration ($kmol/m^3$)

D   diffusivity (m^2/s)

E   activation energy (J/kg)

f   free volume fraction in the skin layer

ΔG Gibbs free energy (J/m^2)

H   Henry's law constant (mmHg)

I_3 intensity in eqn. (35)

J   volumetric flux ($m^3/m^2 s$)

K_L molar concentration based mass transfer coefficient (m/s)

K_x mole fraction based overall mass transfer coefficient ($kmol/m^2$ s)

k   Boltzmann constant (J/K)

k_L molar concentration based mass transfer coefficient (m/s)

k_m mass transfer coefficient in the membrane ($kmol/m^2 mmHg.s$)

k_x mole fraction based mass transfer coefficient ($kmol/m^2$ s)

l thickness of membrane (m)

N   molar flux ($kmol/m^2 s$)

$\overline{P}$ overall average permeability ($m\ kmol/m^2.mmHg.s$)

P60   PERVAP®1060

P70   PERVAP®1070

p   downstream pressure (mmHg)

p^o saturation pressure (mmHg)

118

p^o_{sup} saturation pressure in support layer (mmHg)

$\bar{p}$ average permeability in the membrane (m kmol/m^2.mmHg.s)

R   universal gas constant (J/kmol K)

r   spherical free volume size (m)

Δr   electron layer thickness (m)

r_{sup} pore size of support layer (m)

S_c Contact surface area (m^2)

T   absolute temperature (K)

t   time (s)

V   molar volume (m^3/kmol)

V_F free volume of skin layer (m^3)

v_p velocity of the fluid (m/s)

x   liquid phase mole fraction

y   vapour phase mole fraction

z   axial coordinate

Greek Symbols

α overall selectivity

β individual selectivity

γ activity coefficient

θ contact angle in degrees

ρ molar density (kmols/m^3)

μ chemical potential

σ surface tension (J/m^2)

χ interaction parameter

δ boundary layer thickness (m)

λ constant in equation 37.

τ_3 lifetime in equation 35 (s)

Subscripts

1   solution side

2   water side

b   bulk

i   organic component

Li   liquid

M   Membrane

m   inside membrane

o   reference state

s   surface

w   water

Superscripts

AB   acid base

act   actual

F   feed side

int   intrinsic

LW   Lifshitz - vander Waals

P   permeate side

Perm   permeation

Vap   vaporization

+   electron acceptor

-       electron donor

References

[1] I. Blume, J. G. Wijmans, R. Baker, The separation of dissolved organics from water by pervaporation, J. Membrane Sci. 49 (1990) 253-286.

[2] P. Sampranpioon, R. Jiraratananon, D. Vttapap, X. Feng, R. Y. M. Huang, Pervaporation separation of ethyl butyrate and isopropanal with PEBA membranes, J. Membrane Sci. 173 (2000) 53-59.

[3] C. Viswanathan, B. Basu, J.C. Mora, Separation of volatile organic compounds by pervaporation for a binary compound combination: Trichloroethylene and 1,1,1-Trichloroethane, Ind. Eng. Chem. Res. 34 (1995) 3956-3962.

[4] C. Lipsi, P. Cote, The use of pervaporation for the removal organic contaminants from water, Environmental Progress, 9 (1990) 254-261.

[5] B.Raghunath, S.-T.Hwang, Effect of boundary layer mass transfer resistance in the pervaporation of dilute organics, J. Membrane Sci. 65 (1992) 147-161.

[6] E. E. B. Meuleman, J. Willemsen, M. H. V. Mulder, H. Strathaman, EPDM as a selective membrane material in pervaporation, J. Membrane Sci. 188 (2001) 235-249.

[7] B. Gonzalez, I.O. Uribe, Mathematical modeling of the pervaporative separation of Methanol-Methyl Tert-Butyl Ether Mixtures, Ind. Eng. Chem. Res., 40 (2001) 1720-1731.

[8] A. Baudot, I. Souchon, M. Marin, Total permeate pressure influence on the selectivity of pervaporation of aroma compounds, J. Membrane Sci. 158 (1999) 167-185.

[9] A. Baudot, I. Souchon, M. Marin, Dehydration of water/t-Butanol by pervaporation: comparative study of commercially available polymeric, Microporous Silica and Zeolite Membranes, J. Membrane Sci. 197 (2002) 309-319.

[10] E. E. B. Meuleman, B. Bosch, M. H. V. Mulder, H. Strathmann, Modelling of liquid/liquid separation by pervaporation: Toluene from water, AIChE, 45 (1999) 2153-2160.

[11] W. Ji, S. K. Sikdar, S. T. Hwang, Modeling of multicomponent pervaporation for removal of volatile organic compounds from water, J. Membrane Sci. 93 (1994) 1-19.

[12] C.J. van Oss, Interfacial Forces in Aqueous Media, Marcel Dekkar, New York, 1994.

[13] C.J. Van Oss, R.J.Good, Surface tension and the solubility of polymers and biopolymer: The role of polar and apolar interfacial free energies, J. Macromol. Sci.-Chem. A26(8) (1989) 1183-1203.

[14] P.J. Flory, Principles of polymer chemistry, Cornell University Press, New York, 1953.

[15] C.J. Van Oss, R.F. Giese, R.J.Good, The zero time dynamic interfacial tension, J. Dispersion Sci. and Technol., 23(4) (2002) 455-464.

[16] J. Neel, in R.Y.M. Huang, (Ed.), Introduction to Pervaporation: Separation Characteristics of Pervaporation Membrane Separation Processes, Pervaporation Membrane Separation Processes, Elsevier, Amsterdam, (1991) 1-110.

[17] P. Kirkegaard, N.J. Pedersen, M. Eldrup, PATFIT-88: a Data processing system for positron annihilation spectra on mainframe and personal computers, Riso National Laboratory, Denmark, 1989.

[18] S.J. Tao, Positronium annihilation in molecular substances, J. Chem. Phys, 56 (1972) 5499.

[19] S. Weinhold, G.M. Stack, M.R. Tant, A.J. Hill, Effect of copolymer composition on free volume and gas permeability in poly(ethylene terephthalate)-poly(1,4

122

cyclohexylenedimethylene terephthalate) copolyesters, Eur Polym J., 32 (1996) 843-849.

[20] C. Barnes, Diffusion through a membrane, Physics, 5 (1934) 4.

[21] Y.M. Lee, D. Bourgeois, G. Belfort, Sorption, diffusion and pervaporation of organics in polymer membranes, J. Membrane Sci. 44 (1989) 161-181.

[22] Y.C. Jean, Characterizing Free volumes and holes in polymers by positron annihilation spectroscopy, NATO Advanced Research Workshop, Advances with Positron Spectroscopy of Solids and Surfaces, Varenna, Italy, July 16-17,1993

[23] L.H. Sperling, Introduction to Physical Polymer Science, John Wiley, New-York, 1986.

[24] M.H.V. Mulder in R.Y.M. Huang, (Ed.), Thermodynamic principles of pervaporation, Pervaporation Membrane Separation Processes, Elsevier, Amsterdam, (1991) 225-251.

[25] D. Eisenberg, W. Kauzmann, The structure and property of water, Oxford Univ. Press, Oxford, 1969, pp 164-165.

[26] H. H Nijhuis, M. H. V. Mulder, C.A. Smolders, Removal of trace organics from aqueous solutions. Effect of membrane thickness, J. Membrane Sci. 61 (1991) 99-111.

[27] X. Feng, R.Y.M. Huang, Separation of isopropanol from water by pervaporation using silicone based membranes, J. Membrane Sci. 74 (1992) 171-181.

[28] J. Börjesson, H.O. E. Karlsson, G. Trägårdha, Pervaporation of a model apple juice aroma solution: Comparison of membrane performance, J. Membrane Sci. 119 (1996) 229-239.

[29] F. Lipnizki, J. Olsson, P. Wu, A. Weis, G. Trägårdha, R.W. Field, Hydrophobic pervaporation: Influence of the support layer of composite membranes on the mass transfer, Separation Sci. and Technol. 37(8) (2002) 1747-1770.

[30] S. Singh, K.C. Khulbe, T. Matsuura, P. Ramamurthy, Membrane characterization by solute transport and atomic force microscopy, J. Membrane Sci. 142 (1998) 111-127.

[31] R.J. Hunter, Foundations of colloidal science, vol. 1, Clarendon press, Oxford, 1987.

[32] J. Olsson, G. Trägårdha, Pervaporation of volatile organic compounds from water I. Influence of permeate pressure on selectivity, J. Membrane Sci. 187 (2001) 23-37.

[33] R.W. Baker, J.G. Wijmans, A.L.Athayde, R.Daniels, J.H. Ly, M. Le, The effect of concentration polarization on the separation of volatile organic compounds from water by pervaporation, J. Membrane Sci. 137 (1997) 159-172.

[34] W. Ji, S.K. Sikadar, Pervaporation using adsorbent-filled membranes, Ind. Eng. Chem. Res. 35 (1996) 1124-1132.

[35] D. T. Leighton, J. M. Cao, Distribution coefficients of chlorinated hydrocarbons in dilute air —water systems for ground water contamination applications, J. Chem. Eng. Data, 26 (1981) 382.

[36] R. C. Reid, J. M. Prausnitz, T. K. Sherwood, The Properties of Gases and Liquids, McGraw- Hill, New York, 1997.

[37] J. P. Brun, L. Larchet, R. Merlet, G. Bulvestre, Sorption and pervaporation of dilute aqueous solutions of organic compounds through polymer membranes, J. Membrane Sci. 25 (1985) 55-100.

[38] P. K. Ten, R. W. Field, Organophilic pervaporation: an engineering scienceAnalysis of component transport and the classification to behavior with reference to the effect of permeate pressure, Chemical Engg. Sci. 55 (2000) 1425-1445.

[39] R.E.Treybal, Mass-Transfer Operations, McGraw-Hill, New York, 1986 (Third Edition).

[40] M.H.V. Mulder, Basic Principles of Membrane Technology, Kluwer Academic, Dordrecht, The Netherlands, 1991.

[41] R. H. Perry, D. Green, Perry's Chemical Engineers' Hand Book, Mc-Graw Hill: New York, 1984 (Sixth edition).

[42] D.M. Himmelblau, Basic Principles and Calculations in Chemical Engineering, Prentice Hall of India, New Delhi, 1995.

[43] I. F. J. Vankelecom, J. D. Kinderen, B. M. Dewitte, J. B. Uytterhoven, Incorporation of hydrophobic porous fillers in PDMS membranes for use in pervaporation, J. Phys. Chem. B, 101 (1997) 5182-5185.

[44] T.Lamer, A. Voilley, Influence of different parameters on the pervaporation of aroma compounds. Proceedings of the 5th international conference on the pervaporation process in the chemical industry, Heidelberg, Germany, March 11-15, 1991

[45] M. Jia, K.-V. Peinemann, R.-D. Behling, Molecular sieving effect of the zeolite-filled silicone rubber membranes in gas permeation, J. Membrane Sci. 57 (1991) 289-292.

[46] B. M. Smit, T. L. M. Maeson, Commensurate 'freezing' of alkanes in the channels of a zeolite, Nature, 374 (1995) 42-44.

[47] S. Goethaert, C. Dotremont, M. Kuijpers, M. Michiels, C. Vandecasteele, Coupling phenomena in the removal of chlorinated hydrocarbons by means of pervaporation, J. Membrane Sci., 78 (1993) 135-145.

[48] U. Lohse, H. Thamm, M. Noack, B. Fahike, J. Incl. Phenom, 5 (1987) 307-313.

[49] R. E. Richard, L. V. C. Rees, Langmuir, 3 (1987) 335-340.

Chapter 5

Role of Permeant-Membrane Interactions

5.1 Introduction

Pervaporation is a relatively new membrane separation process applied to separate

liquid mixtures. The separation is carried out using dense membranes. The feed liquid

diffuses through the membrane and vaporizes on the other side where the applied pressure

is lower than the saturation vapor pressure. Recently, pervaporation has received

considerable attention from both the fundamental and applied aspects because of

tremendous upsurge in the developments of newer homogeneous membranes [1]. The mass

transport mechanism through the membrane is complex because of the high interaction

between liquid feed components and membrane, resulting into substantial swelling of the

membrane. The solution-diffusion model is widely accepted mass transport mechanism for

pervaporation [2-4] As expected, the driving force (and flux) for vaporization at the

downstream side should vanish at a downstream vapor pressure equaling the saturation

vapor pressure of the permeating component [5]. However, the existing experimental

results and their interpretations [2-11] have been somewhat equivocal on this simple

expectation because, operationally, it is the TOTAL down stream pressure (air plus vapor),

rather than the partial vapor pressure, that is maintained by a vacuum pump. To complicate

the situation, air leaks are invariably present. Recently, Vallieres et al. [12] systematically showed the importance of air leaks in a pervaporation experimental set up by passing inert gas at downstream side of the membrane. In order of have experiments that can differentiate between rival models and their interpretations, it is therefore vital to correctly estimate the downstream partial vapor pressure which also takes into account the possibility of air leaks, since vapor flux can be quite small. The experiments reported here have been designed and interpreted with special attention to these details.

On theoretical side, none of the existing models of pervaporation from dense membranes have considered the possibility of the equilibrium vapor pressure itself being reduced due to the permeate-membrane interactions. Of course, it is clear that a greater degree of interaction (also reflected in greater solubility, affinity, selectivity and wettability of the membrane) should also increase the propensity of the membrane to retain the permeant, thus decreasing its flux. In anthropomorphic terms, stronger bonds of friendship engender greater pangs of separation! Put another way, higher solubility and wettability of permeant in highly confining a membrane pores should correlate with lower equilibrium vapor pressure.

In this study, we propose to quantify the above ideas by the use of Kelvin's equation [13], applied for the first time to the pervaporation process.

$$P_{im}^{O} = P_i^{O} \exp\left[- \frac{2V_i \gamma_i \cos\theta}{RTr} \right]$$ (5.1)

Where, θ, γ, V, R and T are the equilibrium contact angle of the permeating liquid, i with the membrane, permeant surface tension, permeant molar volume, universal gas constant and temperature, respectively. Further, P_{im}^{O} and P_i^{O} are the equilibrium vapor pressure of

permeant in the membrane, m and bulk vapor pressure of the permeant, respectively. The pore radius, r is in the swelled state. Homogeneous membranes have 'pores' in the form of irregular free spaces in the polymer matrix [14]. The size of such pores should increase in a good solvent due to the swelling of the polymer [15].

Kelvin's equation predicts a decrease in the equilibrium vapor pressure (compared to its bulk value) for wettable membranes ($\theta < \pi/2$) that show high solubility and affinity for the permeant. Indeed, the experiments reported in this study show a clear and quantifiable decrease in the down stream vapor pressure where the evaporative flux becomes zero. Of course, this decrease depends on the degree of confinement (pore radius, r), which admittedly, cannot be directly measured for the dense membranes having sub-nano size pores in the swelled state. Therefore, dry membranes are characterized by positron annihilation to estimate the pores and further found a good correlation of the 'wet' pore volume (which appears in the Kelvin equation) with solubility due to the greater propensity of a membrane to swell when in a better solvent.

Therefore, the experimental objective of the this work is to carry out single component pervaporation experiments at controlled downstream pressures and well-characterized partial vapor pressures (by accounting for the air leaks) to find the depression in the equilibrium vapor pressure due to the membrane-permeate interactions. On theoretical side, we explore the possibility of interpreting the experiments in the framework of Kelvin's equation.

Towards the above ends, methanol and isopropanol were chosen as the feed components with a variety of dense membranes differing in their pore sizes, solubility and wettability. The pore sizes and contact angles were estimated using positron annihilation

technique and contact angle goniometry, respectively. The enlargement of pore size due to membrane swelling is correlated with the solubility of feed component. As noted by Gonzaliz and Uribe [16], it is not practical to directly measure the amount of sorption in composite membranes because of the difficulty to discriminate between the active layer and its porous support layer. Thus, in this study, solubility is estimated by the modified Flory-Huggins theory, which accounts for the membrane elasticity. The Flory-Huggins interaction parameter is evaluated from the polar acid-base surface tension components obtained from the contact angle goniometry using the standard probe-liquids [17-20]. For a laboratory cast cellulose acetate membrane without support layer, direct measurement of solubility was possible, and was found to be in good agreement with the estimated value.

5.2 Experimental

5.2.1 Materials

Analytical grade methanol (Merck, India), isopropanol (Qualigens, India), acetone (Ranbaxy, India), formamide (Loba Chemie, India), ethylene glycol (E-Merck, India), diodomethane (SD fine, India) and cellulose acetate (Jams Chemicals, Bombay) were used for the work. Double distilled water was used for the preparation of calibration curve and contact angle measurements. The commercial composite membrane PERVAP® was obtained from Sulzer Chemtech, Germany. The dense pervaporation membrane was a very thin (0.5-2 μm) separating layer on top of a porous support (70-100 μm), which in turn rested on top of a polymer fleece (non-woven fabric of thickness 100 μm) providing the structural support. Another composite membrane HR-98-PP was obtained from Danish Separation Systems, Denmark. Characteristics of the membranes (nature of the polymers

[21]) along with densities values [22] are reported in the Table 5.1. One type of membrane was also cast in our laboratory without the support layers as detailed below.

Table 5.1 Chemical nature and densities of membranes

Membrane	Base Polymer	Molecular weight of monomer	Density of amorphous portion (g/cc)
HR98PP	Poly Propylene	56	0.85
Cellulose acetate	-	-	1.32
PERVAP 2256*	Likely, PVA with incorporation of polar molecules*	44	1.26
PERVAP 1070	PDMS with silicalite filled zeolite	74	0.98
PERVAP 2201	PVA highly cross linked	44	1.26

* other membranes of PERVAP 22 series are PVA based [21]

5.2.2 Membrane Preparation

Cellulose acetate (CA) polymer (17 g) was dissolved in a mixture of acetone (68 g) and formamide (15 g) and kept overnight for the removal of entrapped air. The casting of membrane was carried out on a glass plate using modified thin film applicator (ACME-make, India). After around 48 hours of solvent evaporation at room temperature, the membrane together with the base glass plate was placed in a vacuum oven for another 4 hours for the removal of residual traces of solvent. Finally, the membrane was gently peeled from the glass plate.

5.2.3 Sorption Measurements

A pre-weighed dry membrane of cellulose acetate was kept in a conical flask that contained methanol for sorption purpose. The flask was kept in a water shaker bath (model SW-23, Julabo, Germany) under 200 rpm for 6 to 7 days at 20°C. The membrane in the conical flask was taken out at regular intervals and wiped with tissue papers for the removal of the adhered liquid. The wet weight of the membrane was measured. The procedure was repeated until three consecutive readings of wet membranes weight were found to be within one percent of each other. The percent sorption is based on the permeant absorbed divided by the dry weight.

5.2.4 Positron Annihilation Lifetime (PAL) Measurements

The PAL measurements were carried out using a fast-fast system having a resolution of 300 pico-seconds (FWHM for the ^{60}Co prompt γ-rays, under ^{22}Na window settings). The positron source was prepared by depositing around 2 micro-Curie aqueous ^{22}NaCl on a thin aluminum foil (thickness ~ 12μm), and covering it with an identical foil. The source was sandwiched between 13 layers (on each side) of the polymeric membrane, which were stacked together. The separating layer portion (dense membrane plus the porous support) was peeled out from the woven fabric base of the commercial membranes. Membranes prepared in our laboratory were sufficient thick to absorb 99.9% of the positrons. The source-sample sandwich was placed between two NE111 scintillators coupled to RCA 8575 tubes. The anode signals were processed in ORTEC constant fraction differential discriminators and an ORTEC time-to-pulse height converter (TPHC) generated the lifetime distribution spectra, which were recorded in a multi-channel analyzer. All the measurements were made at the room temperature (24°C). Approximately

one million counts were collected in each spectrum, and four spectra were measured for each sample.

5.2.5 Contact Angle Measurements

Advancing equilibrium contact angles of methanol, isopropanol, and the common probe liquids of the acid-base analysis (water, ethylene glycol, and diodomethane) in saturated environment on chosen membranes were measured by the sessile drop method using a contact angle goniometer (Rame-Hart, inc. Imaging System, USA). Flat sheets were mounted in a stainless steel holder. Saturated environment was maintained by keeping the membrane holder in an environmental chamber. A glass syringe with a stainless steel needle was used to place the liquid drop on the membrane. The angles were measured by capturing the image with a video camera after the angle stabilized within a few minutes. Angles (around 50) were then measured in a time span of 1 second and the average of all these angles were calculated. Further, four or five such measurements were made for each liquid on the same membrane and the average value was noted.

5.2.6 Pervaporation Experimental Set-up

Figure 5.1 shows the experimental set-up designed and fabricated in our laboratory for the pervaporation measurements. The pervaporation test cell was made of glass and had specially designed flanges to secure the membrane with an effective membrane area of 50.6 cm^2. The membrane was kept on a highly porous stainless steel support with the shiny dense polymeric layer (for commercial membranes) facing the feed solution. Initially, a fixed volume of feed component was taken in the feed chamber. To avoid non-isothermal operation [23] around the cell, both upstream and downstream side of the cell were heated separately by providing the heating mantels on the cell. The temperatures on both sides

132
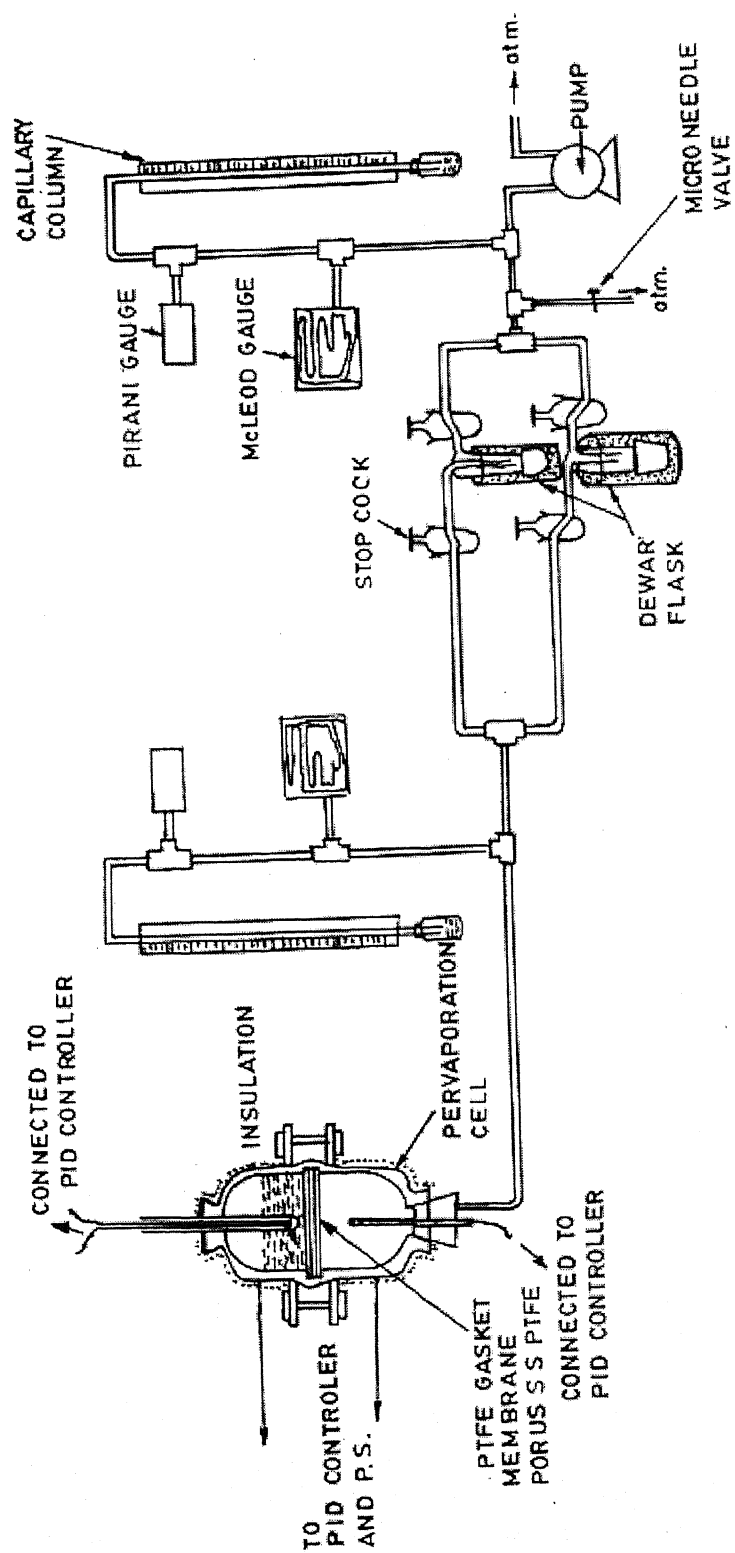
Figure 5.1 Schematic diagram of pervaporation experimental setup

were controlled by connecting heating mantles through a PID controller device (Fuji, Japan).

The membrane upstream side was kept at the atmospheric pressure and a partial vacuum was maintained at the downstream side by a vacuum pump (Vacuum Techniques, Bangalore). Total downstream pressure was regulated with an air inlet using a stainless steel micro- needle valve, located between the condensers and the vacuum pump. Downstream pressure was measured near the cell as well as near the pump using Meclod/Pirani/Capillary columns.

The condenser system consisted of two traps that could be used alternately; allowing for the collection of permeated stream continuously without interruption of the operation during the weight measurements. The permeated vapor was condensed in one of the traps, which were kept in Dewar flasks filled with the liquid nitrogen. The frozen permeate was collected periodically. The cold traps were brought to the room temperature for measuring its weight using a five decimal balance to determine the mass flux.

The experimental measurements were started only after keeping the cell for 12 to15 hours under maximum attainable vacuum (about 0.1 mm of Hg) to observe the leakage of air. Before switching over to a new trap by changing the vapor (Figure 5.1), the valves near the cell were closed. The completely evacuated condenser was then kept in the Dewar flask and the valve was opened. This procedure ensures that no residual moisture is present in the line as well as in the condenser at the time of starting the experiment. For each down stream pressure, the steady-state flux was usually reached within 3 to 5 hours, and the measurements were completed within about 3 to 12 hours depending on the flux (amount collected).

As explained above, presence of water in the permeate (air plus vapor) was expected and hence it was analyzed using a gas chromatograph (Nuchon, India) with a thermal conductivity detector. Chromosorb-102 and Puropack- Q were used as the main and reference columns, respectively. Hydrogen was used as carrier gas. The oven, detector and injector temperatures were 116, 160 and 160°C for methanol, and 200, 210 and 210°C for isopropanol. To minimize the measurement errors, an average of three consecutive readings were taken after reaching the steady state for each operating downstream pressure. For each permeate sample, a minimum of three water concentrations were measured and averaged. The average errors in the total permeation mass flux and water concentration were around ± 2% and ± 5%, respectively. Further, wet and dry bulb temperatures were tracked to obtain the room humidity.

5.3 Results and Discussion

5.3.1 Estimation of Dry Membrane Pore Sizes

The lifetime data were analyzed using PATFIT-88 programs [24]. Source correction was done for all spectra. Positron annihilation lifetime spectra were analyzed in terms of the following three lifetime components: para-positronium (p-Ps) annihilation, τ_1; free positron and positron-molecular species annihilation, τ_2; and o-Ps annihilation, τ_3. While τ_1 and τ_2 are always of the order of few hundred picoseconds and are rather immaterial for the calculation of pore sizes, τ_3 is of the order of nanoseconds and relates to the polymer free volume or pore size. Each lifetime has an intensity I, corresponding to the fraction of annihilations taking place with the respective lifetimes. The parameters τ_3, I_3 corresponding to the decay of o-Ps provide the size-specific information for free volumes and pores. The commercial PERVAP 1070 and PERVAP 2256 membranes provided very

poor fits with a mono-modal τ_3, but a bimodal τ_3 fit was entirely satisfactory, indicating a bimodal pore size. The o-Ps lifetimes and intensities thus obtained are reported in the Table 5.2. The following expression was used to relate o-Ps pick-off lifetime, τ_3 and an equivalent cylindrical pore radius r (Å) [25].

$$\tau_3 = \frac{1}{2}\left[1 - r/(r + \Delta r) + (\frac{1}{2\pi})\sin(\frac{2r\pi}{r + \Delta r})\right]^{-1} \tag{5.2}$$

where, Δr (=0.196 nm) is the electron layer thickness [26]. The pore radii thus obtained are also reported in Table 5.2. The sub-nanometer pore sizes obtained for dry membranes are in general agreement with the range of values reported for the dense membranes [1]. Also, as indicated by the bi-modal fits to the commercial membranes, PERVAP 1070 indeed seems to contain two pore sizes [21]. Although the chemical structure of PERVAP 2256 is confidential [21], the positron lifetimes similarly indicate the presence of bimodal pores.

Table 5.2 Positron parameters and pore radius of membranes

Membrane	τ_3 (ns)	I_3 (%)	r (nm),
HR98PP	1.96±0.01	15.2±0.2	0.324
Cellulose acetate	2.16±0.02	18.8±0.3	0.345
PERVAP 2256	1.73±0.06	8.8±0.2	0.298
	6.19±0.36	1.1±0.1	0.606
PERVAP 1070	2.32±0.28,	10.6±1.5	0.360
	τ_4:4.53±0.48	I_4:5.1±2.0	0.520
PERVAP 2201	1.64±0.04	8.3±0.4	0.288

5.3.2 Estimation of Solubilities

The measured advancing equilibrium contact angles of the permeants used, as well as the probe liquids on the various membranes are reported in the Table 5.3. The contact angles of probe liquids with membrane were used to calculate the surface tension components (LW, acid-base, and total) of the membrane by the method of van Oss, Good and Chaudhury [27, 28], as summarized in the eqs. (5.A.1), (5.A.2) and (5.A.6) of the appendix. The surface tension components of the probe liquids were taken from a recent paper [19,29] (see Table 5.4). The values of surface tension components for different membranes thus obtained are reported in Table 5.5. For the cellulose acetate membrane, surface tension component values are in agreement with the literature values [17]. Some difference may be attributed to the membrane roughness, and membrane preparation conditions (e.g., solvent used, degree of actylation). Empirical Flory-Huggins interaction parameter between the feed components (methanol or isopropanol) and the membranes used were calculated using eq (5.A.5), taking minimum contactable surface area, S_C for the methanol [30] to be 0.20 nm^2 and for the isopropanol [30] as 0.3 nm^2. The contactable surface area was estimated by extrapolating its value in comparison with the S_c of a related alkane. The interaction parameters thus calculated are reported in Table 5.6. The required surface tension values of the feed components were taken from literature [31, 17] and are reported in Table 5.4.

The interaction parameter obtained from a direct measurement of solubility of methanol in a laboratory prepared cellulose acetate membrane was also found to be in agreement with the value reported in Table 5.6. Direct sorption experiments measured the solubility to be 38.98 g of methanol/100 gm of cellulose acetate. The following modified

Table 5.3 Contact angles of permeants and probe liquids with membranes

Membrane	water	Ethylene glycol	Diodo-methane	methanol	Iso-propanol
HR98PP	82.1	45.5	67.7	31.2	17.4
PERVAP 1070	84.8	64.1	72.0	15.2	0.0
PERVAP 2256	72.0	76.0	36.8	31.9	-
PERVAP 2201	48.2	47.3	45.4	0.0	-
Cellulose acetate	37.5	18.2	24.2	0.0	-

Table 5.4 Surface tension components of permeants and probe liquids

Component	γ^{LW} (mJ/m^2)	γ^+ (mJ/m^2)	γ^- (mJ/m^2)	γ (mJ/m^2)
Water	21.8	25.5	25.5	72.8
Ethylene glycol	29.0	1.9	47.0	48.0
Diodomethane	50.8	0.0	0.0	50.8
methanol	18.2	0.06	77.0	22.5
Iso-propanol	17.3	0.00	0.0	17.3

138

Table 5.5 Surface tension components of the membranes

Membrane	γ^{LW} (mJ/m^2)	γ^+ (mJ/m^2)	γ^- (mJ/m^2)	γ (mJ/m^2)
HR98PP	24.28	2.84	4.00	31.02
PERVAP 1070	21.88	0.66	7.58	26.35
PERVAP 2256	41.23	3.05	3.16	47.43
PERVAP 2201	36.87	0.055	38.38	39.77
Cellulose acetate	46.42	0.03	41.71	48.65

Table 5.6 Interaction parameters and solubility of permeants in the membrane

Membrane	Component	σ_{im}	χ_{im}	φ_{pm}	Solubility (g /100 g of polymer)
HR98PP	MeOH	-19.07	-1.886	0.423	127.0
Cellulose Acetate	MeOH	6.84	0.676 0.887*	- 0.394	- 38.37
PERVAP2256	MeOH	-16.39	-1.621	0.537	54.17
PERVAP1070	MeOH	-6.69	-0.662	0.502	80.14
PERVAP2201	MeOH	3.31	0.327	0.761	27.32
HR98PP	IPA	7.33	1.087	0.694	34.17
PERVAP1070	IPA	4.74	0.703	0.731	110.67

* experimental

equation was used to calculate the Flory-Huggins binary (component-membrane) interaction parameter, χ_{ip}.

$$\chi_{ip} = -\frac{\ln(1-\varphi_{pm}) + \varphi_{pm}}{\varphi_{pm}^2} \qquad (5.3)$$

Where, φ_{pm} is the volume fraction of polymer, p in the swollen membrane. This procedure yields χ_{ip} for cellulose acetate and methanol to be 0.886, which is within the experimental errors of its value in Table 5.6. The difference of about 0.2 in interaction parameter by both methods (experimental and estimated from surface tension components) may be attributed to a host of complexities in the determination of solubility from the contact angle measurements. Among other things, contact angles are affected by the membrane roughness and the presence of pores, as well as whether the drop is captive or sessile. Even more important is the uncertainty in the estimation of contactable surface area, which increases by the formation of molecular clusters [29]. For example, increasing S_c by only about 25% increases the value of interaction parameter to 0.85, which is close to the experimental value. Since direct measurements of solubility are not possible for composite membranes, the surface thermodynamic approach employed here appears to be promising at least in semi-quantitative determinations and especially in comparing the different membranes within a consistent framework.

The eq (5.3) is applicable only for the interaction parameter values substantially higher than 0.5. In case of strong feed-membrane interactions ($\chi < 0.5$), excessive membrane swelling occurs resulting in an elastic restoring force by the polymer network. In this case, original Flory-Huggins equation is modified to include the elastic free energy [32].

$$\ln(1 - \varphi_{pm}) + \varphi_{pm} + \chi_{ip}(\varphi_{pm})^2 + \frac{V_i \rho}{M_c}\left[(\varphi_{pm})^{1/3} - 0.5\varphi_{pm}\right] = 0 \qquad (5.4)$$

Where, ρ is the density of the swollen membrane. Further, M_c is the monomer molecular weight [33]. The eq (5.4) is valid for interaction parameter values of less than 0.5, including negative values. Solubilities (reported in Table 5.6) of methanol and isopropanol in various membranes were estimated using eqs (5.3) and (5.4) with the help of data given in the Table 5.1.

5.3.3 Pervaporation

Single component pervaporation experiments were carried out with methanol and isopropanol using different membranes at different temperatures. Initially, feed liquid (methanol) was filled in the cell and kept under complete vacuum for 10 hours without collection of permeate. Then the valves between the membrane and the condenser were closed leading to accumulation of vapor on the downstream side. The downstream pressure rapidly rose to the saturation vapor pressure of methanol within 3 hours due to the permeation of methanol and thereafter, there was a slow increase of pressure. This slow increase may be attributed to the air leaks in the experimental set up. This air leakage occurs due to the permeation of air through the free volumes of tubes and possibly, through the joints, even though all care was taken to make them tight. Valiries et al. [12] also observed the same situation. In view of this, and especially, as shown below, when the suction due to the vacuum pump is turned on, the possible presence of air leaks must be accounted for in the analysis and interpretation of results.

Figure 5.2 shows the variation of partial methanol flux against partial downstream pressure of methanol for PERVAP 2256, HR98PP, PERVAP 1070, cellulose acetate, and PERVAP 2201 membrane. In Figure 5.2, methanol flux should be read as the value
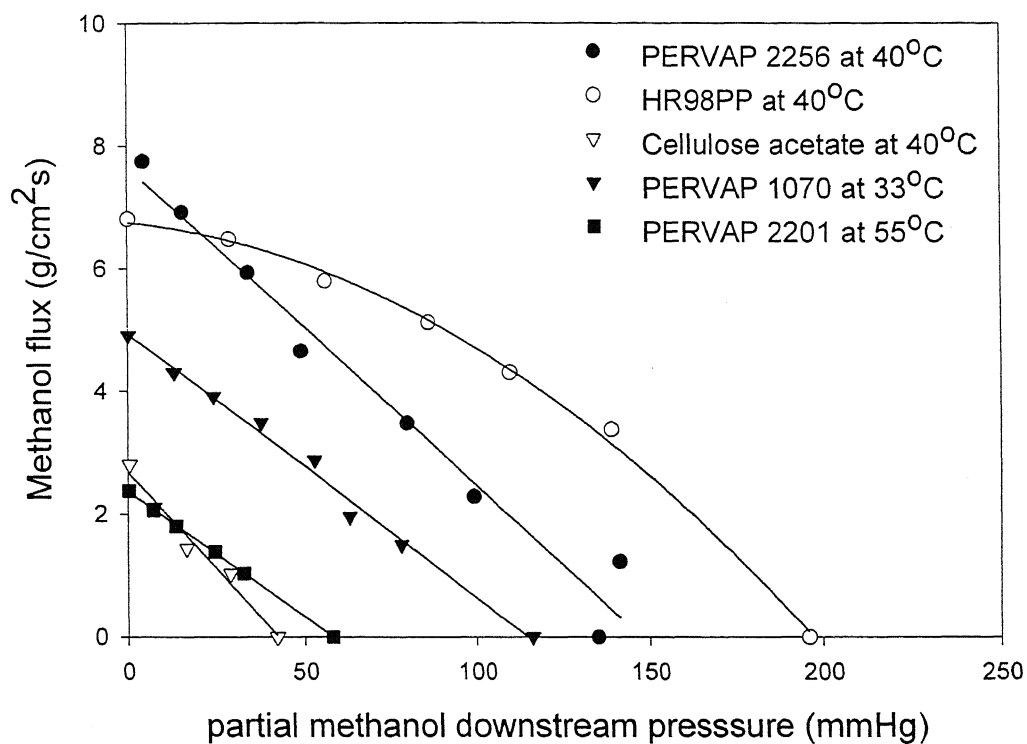
Figure 5.2 Variation of methanol flux with the partial downstream pressure of

methanol for HR98PP, PERVAP 2256, PERVAP 1070, Cellulose acetate

and PERVAP 2201.

multiplied by 10^{-5} for HR98PP and PERVAP 2256, for PERVAP1070 and cellulose acetate

it is 10^{-6} and for PERVAP 2201 it is 10^{-7}. The following procedure was used to calculate

the partial flux of methanol and the partial downstream pressure of methanol.

Concentration of water in permeate was measured by a gas chromatograph and hence the

amount of water in permeate was calculated. Air Humidity (g of water/g of dry air) was

noted from the humidity chart [34] with the help of dry and wet bulb temperatures. Thus,

the amount of air permeation was calculated, which finally provided the partial fluxes and

partial downstream pressure values for the permeant after correcting for the air leaks.

Diffusivity of methanol in all the membranes used, except HR98PP, showed an

ideal behavior in that the diffusivity (or permeability) is independent of concentration,

because of which the permeant flux decays linearly with the downstream partial pressure,

as predicted by the solution-diffusion model with a constant diffusivity [5]. A different

behavior was obtained for HR98PP membrane, where a nonlinear decrease in flux

corresponds to a concentration dependent diffusivity [12]. The already very low

experimental values of the flux in Figure 2 were extrapolated to zero flux conditions, which

provided the corresponding equilibrium partial vapor pressures for different membranes.

These equilibrium vapor pressures are summarized in the Table 5.7. The equilibrium partial

pressures are well below the bulk saturation vapor pressure of the methanol at the

temperatures noted in the table. The depression of equilibrium vapor pressure is due to the

contact angle of methanol on the high solubility membranes being well below 90 degrees,

which can substantially decrease the equilibrium vapor pressure in tight pores (see Kelvin's

equation, eq. 5.1).

Table 5.7 Equilibrium vapour pressure over a membrane, spreading coefficients and pore radii of the membranes

Membrane	Component	Temp (C)	p_i^o (mmHg)	$p_{i,pore}^o$ (mmHg)	V_i (10^{-2} m³/mol)	γ_i (mJ/m²)	θ	S_{im} (mJ/m²)	r_{Kelvin} (nm)	$r_{positron}$ (nm)
HR98PP	MeOH	40	265.8	196.0	4.14	20.98	31.2	-	1.873	0.324
Cellulose Acetate	MeOH	40	265.9	42.0	4.14	20.98	0.0	19.63	0.700	0.345
PERVAP 2256	MeOH	40	265.9	135.0	4.14	20.98	31.9	-	1.063	0.298 / 0.606
PERVAP 1070	MeOH	33	190.2	116.0	4.11	21.53	15.2	-	1.318	0.360 / 0.520
PERVAP 2201	MeOH	55	516.3	58.0	4.22	19.80	0.0	13.96	0.477	0.288
HR98PP	IPA	50	179.8	48.5	7.91	19.33	17.4	-	0.828	0.324
PERVAP 1070	IPA	33	72.5	36.0	7.75	20.65	0.0	5.26	2.255	0.360 / 0.520

MeOH: Methanol, IPA: Isopropanol

Similarly, Figure 5.3 depicts the influence of downstream pressure on isopropanol flux for PERVAP 1070 and HR98PP. Similar to HR98PP-methanol system, the PERVAP 1070-isopropanol system provided a nonlinear decrease of flux with pressure. PERVAP 1070 is zeolite filled PDMS membrane and the results are also in agreement with the literature values for the PDMS-isopropanol system [12]. The equilibrium partial vapor pressures for isopropanol, which correspond to zero flux condition, are also reported in the Table 5.7. The equilibrium partial pressure is again substantially below the bulk saturation pressure and depends on the membrane. These results clearly indicate that the permeant-membrane interactions have to be considered during pervaporation and these should be accounted in the models used for predicting the flux and selectivity.

5.3.4 Estimation of swelled membrane pore sizes and their correlation with dry membrane pore sizes

Pore radii of the membranes can be estimated using a modified Kelvin's equation, which is also valid for the case when the contact angle is zero and therefore, Young's equation cannot be used. The fundamental form of the Kelvin equation written in terms of the spreading coefficient, S is:

$$P_{im}^{o} = P_i^{o} \exp\left[-\frac{2V_i(\gamma_i + S_{im})}{RTr} \right]$$

(5.5)

Where,

$$S_{im} = \gamma_m - \gamma_{im} - \gamma_i$$

(5.6)

where, γ_m and γ_{im} (given by eq 5.A.3) are the surface tension of the membrane and interfacial tension, respectively. The spreading coefficient can also be represented in terms of the equilibrium contact angle, whenever it is nonzero, by the Young's equation:
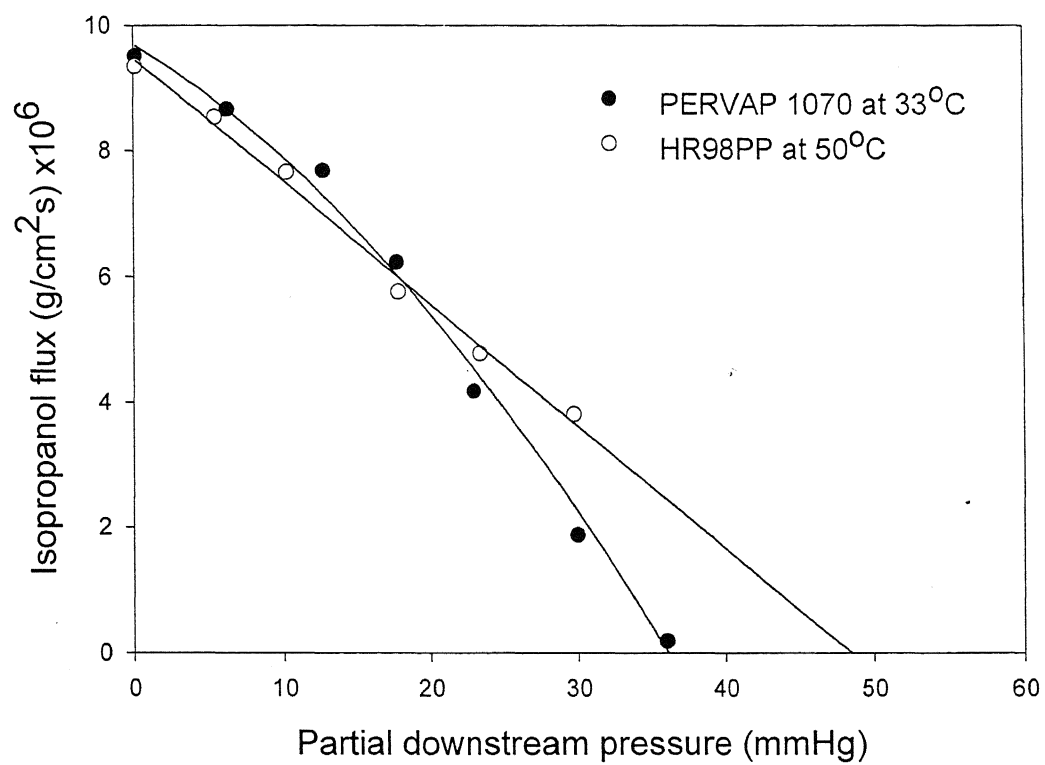
Figure 5.3 Variation of isopropanol flux with the partial downstream pressure of isopropanol for HR98PP and PERVAP 1070 membranes.

$$\cos\theta = 1 + \frac{S_{im}}{\gamma_i} \qquad\qquad (5.7)$$

Thus, for a nonzero contact angle, a more familiar form of the Kelvin's equation, eq (5.1), is readily obtained.

Pore radii were estimated using Kelvin's equation, eq (5.5), together with the equilibrium vapor pressures and the spreading coefficients (or contact angles for finite angles) reported in Table 5.7. Spreading coefficients for zero contact angle cases were calculated from eq (5.6) by using the surface tension parameters given in Table 5.5. The required molar volume and surface tension values of feed components were taken from the literature [35] and are also reported in Table 5.7.

The pore sizes thus calculated from Kelvin's equation range from 0.3 nm to 2 nm for different membranes in their swelled state. The comparison of pore sizes by two methods (Kelvin's equation and positron annihilations), shows some agreement for methanol in PERVAP 2201 and cellulose acetate membranes. However, substantial and seemingly random differences between the two pore radii (wet and dry) occur for other membranes and feed components. Several issues need to be considered in these comparisons. Positron annihilation technique provides an average pore size, whereas Kelvin's equation is weighted heavily in favor of larger pore sizes. This is because pervaporation from the smaller pores is ineffective due to their very low equilibrium vapor pressure and the flux is mainly through larger pores. Further, the positron annihilation data was taken at 20°C whereas pervaporation data were at higher temperatures. It is known, that as the temperature increases, the thermal motion of polymer chain segments increases, and this provide more empty space between polymer molecules.

The single most important factor however is that the pore size estimated by positron annihilation technique is only for dry membranes, whereas Kelvin's equation estimates the pore size for wet, swelled membranes with increased free volume/pore size [15]. Clearly, a correlation between the swelled pore size and solubility may be anticipated. Further, it is observed from Table 5.7 that the estimated pore size by Kelvin's equation is different even for the same membrane (PERVAP 1070 or HR98PP) when different feed components (methanol or isopropanol) are used. It would appear that this difference is due to the different solubility as well as swelling characteristics of the same membrane with different feed components. In what follows, we test the hypothesis that the swelled pore sizes are correlated to the solubility of a permeant in a membrane.

5.3.5 Relationship between solubility and wet pore radius

The swelled volume in a membrane may have a correlation with the solubility of permeant in the membrane. If one assumes the expansion of the free volume, modeled as Kelvin's cylindrical pores, to be in the radial direction, the pore expansion volume is: $\left[r_{Kelvin}^2 - r_{positron}^2 \right]$. Figure 5.4 shows the variation of the swelled volume with solubility. An excellent correlation (correlation coefficient > 0.99) indeed seem to confirm the hypothesis that the swelled pore sizes obtained from Kelvin's equation depend strongly on solubility and may have little in common with the dry pore sizes, except in the systems with low solubility.

5.4 Conclusions

Influence of downstream pressure on single component permeation by pervaporation is studied for a variety of membrane-permeant pairs. Since pervaporative flux is usually small, at least in a laboratory experiment setting, air leaks must be quantified
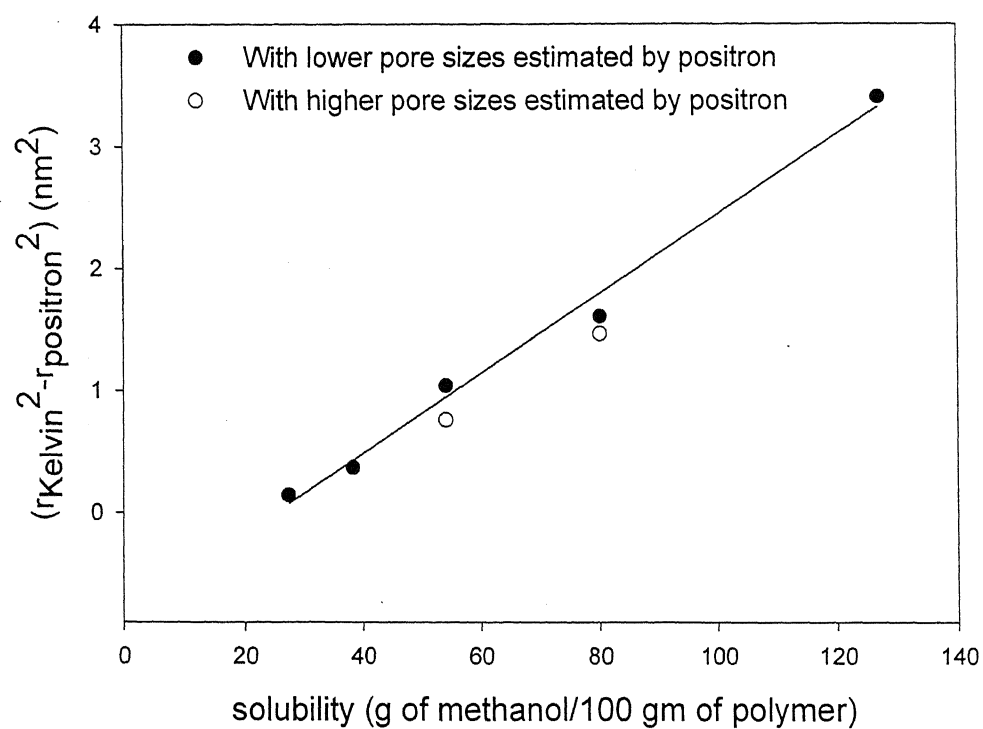
Figure 5.4 Relationship between increase in membrane volume due to swelling (for methanol) and solubility

for a proper analysis and interpretation of experiments. After doing this, it is shown that the equilibrium vapor pressure, corresponding to the zero flux condition in the pervaporation, can be substantially lower than the bulk saturation vapor pressure of the feed component. The depression in the equilibrium vapor pressure varies systematically with the wettability and surface properties of the membrane, and can be interpreted with the help of Kelvin's equation. The pore sizes obtained from the positron annihilation for dry membranes are of sub-nanometer size, as expected for dense pervaporation membranes. In contrast, the pore sizes for wet, swelled membranes obtained from Kelvin's equation are larger, in the range of sub-nanometer to nanometer. As expected, the pore sizes of the dry and wet membranes show better agreement for the membranes in which the solubility of the feed component is less. Interestingly, a linear relationship is observed between solubility and the increase in the membrane volume due to swelling. The results show the importance of membrane-permeant interfacial interactions leading to a lowering of the equilibrium vapor pressure, which needs to be incorporated in the models of pervaporation flux.

5.5 Notations

V	molar volume (m^3/mole)
r	pore radius (m)
Δr	electron layer thickness (m)
R	universal gas constant (J/mol K)
T	temperature (K)
p^0	saturation vapor pressure (Pa)
k	Boltzmann constant (J/K)
M	molecular weight (kg/mol)
M_c	molecular weight between two cross links (kg/mol)
S	spreading coefficient (J/m^2)
ΔG	Gibbs free energy (J/mol)
S_c	contactble surface area (m^2)

Greek symbols

χ	interaction parameter
τ	life time (s)
ρ	density (kg/m^3)
σ	surface tension (J/m^2)
θ	contact angle
φ	volume fraction

Subscripts

i	component
p	polymer

m   membrane

Li   probe liquid

Superscripts

LW   Lifshitz-Van Der Waals

AB   acid-base

+   electron acceptor

-       electron donar

5.6 Appendix

The surface tension of the membrane surface γ_M, is composed of an apolar or Lifshitz-vander Waals (LW) and a polar or Lewis acid-base (AB) components [17,36].

$$\gamma_m = \gamma_m^{LW} + \gamma_m^{AB} \tag{5.A.1}$$

Further, following equation may be used for the acid-base surface tension component:

$$\gamma_m^{AB} = 2\sqrt{\gamma_m^+ \gamma_m^-} \tag{5.A.2}$$

Where γ_m^+ and γ_m^- are the electron acceptor and electron donor surface tension components of the membrane. The following general equation [36] may be used to estimate the interfacial tension, γ_{im} between the membrane and the permeating component.

$$\gamma_{im} = \left(\sqrt{\gamma_m^{LW}} - \sqrt{\gamma_i^{LW}}\right)^2 + 2\left(\sqrt{\gamma_m^+ \gamma_m^-} + \sqrt{\gamma_i^+ \gamma_i^-} - \sqrt{\gamma_m^+ \gamma_i^-} - \sqrt{\gamma_m^- \gamma_i^+}\right) \tag{5.A.3}$$

The change in free energy per unit area, ΔG_{imi} for the process (in which molecules of liquid are initially present in polymer) is given by:

$$\Delta G_{imi} = -2\gamma_{im} \tag{5.A.4}$$

Accordingly, Flory-Huggins interaction parameter χ_{im} [32], which provides the solubility of the feed component in the membrane, in relation to Gibbs free energy [17], may be calculated from the following equation:

$$\chi_{im} = \frac{-\Delta G_{imi} S_c}{kT} \tag{5.A.5}$$

where, S_c, and k are the contactable surface area between the permeant molecules, and Boltzmann constant (1.38048×10^{-23} J/K), respectively. Further, the use of eq (5.A.3) requires the surface tension components of the membrane and these can be estimated by measuring contact angle θ, using the following version of the Young-Dupré equation [17]:

$$(1 + \cos\theta)\gamma_{Li} = 2(\sqrt{\gamma_m^{LW}\gamma_{Li}^{LW}} + \sqrt{\gamma_m^+\gamma_{Li}^-} + \sqrt{\gamma_m^-\gamma_{Li}^+}) \qquad\qquad (5.A.6)$$

Equation (5.A.6) needs to evaluate with three unknown parameters and hence measurements of contact angles were made using three standard liquids (probe liquids). Di-iodo-methane (essentially an apolar liquid), water (polar liquid) and ethylene glycol (or glycerol or formamide) were used for the purpose.

154

References

[1]   H.E.A. Brüschke in S.P. Nunes and K.-V. Peinemann (Ed.), State –of art of pervaporation processes in the chemical industry: Membrane Technology in the Chemical Industry, Wiley-Vch, Weinheim, Germany, 2001.

[2]   C.H. Lee, Theory of reverse osmosis and some other membrane permeations, J. Appl. Polym. Sci. 19 (1975) 83.

[3]   M.H.V. Mulder, C.A. Smolders, On the mechanism of separation of ethanol/water mixtures by pervaporation. I.Calculations of concentration profiles. J. Membrane Sci. 17 (1984) 289

[4]   T. Kataoka, T. Tsuru, S. Nakao, S. Kimura, Permeation equations developed for prediction of membrane performance in pervaporation, vapour permeation and reverse osmosis based on the solution-diffusion model. J. Chem. Eng. Jpn. 24 (1991) 326

[5]   F.W. Greenlaw, R.A. Shelden, E.V. Thompson, Dependence of diffusive permeation rates on upstream and downstream pressures. J. Membrane Sci. 2 (1977) 141.

[6]   T. Okada, T. Matsuura, A new transport model for pervaporation. J. Membrane Sci. 59 (1991) 133.

[7]   W.S. Wu, W.W.Y. Lau, G.P. Rangaiah, S. Sourirajan, Pervaporation of water and ethanol using a cellulose acetate butyrate membrane. J. Colloid Interface Sci. 160 (1993) 502.

[8]   M. Yoshikawa, Y.P. Handa, D. Cooney, T. Matsuura, Anomalous Physcicochemical Properties of ethanol in a polymeric membrane, Makromol. Chem. Rapid Commun. 11 (1990) 387-391.

[9] R.K. Tyagi, A.E. Fouda and T. Matsuura, A pervaporation model: membrane design, Chemical Eng. Sci. 50 (1995) 3105-3114.

[10] M. Wessling, U. Werner and S.T. Hwang, Pervaporation of C8-isomers, J. Membrane Sci, 57 (1991) 257.

[11] X. Feng and R.Y.M. Huang, Permeate pressure build-up in shellside- fed hollow fiber pervaporation membranes, Canadian J. Chem. Eng., 73 (1995) 833-843.

[12] C. Vallieres, E. Favre, D. Roizard, J. Bindelle, D. Sacco, New insights into pervaporation mass transport under increasing downstream pressure conditions: critical role of inert gas, Ind. Eng. Chem. Res. 40 (2001)1559-1565.

[13] R.J. Hunter, Foundations of colloidal science, vol. 1, Clarendon press. Oxford, 1987.

[14] S. Sourirajan and T. Matsuura, Reverse Osmosis/Ultrafiltration Process Principles: National Research Council Canada, Ottawa,1985.

[15] Fuzita. H, Fortschr.Hochpolym.-Forsch., 3 (1961) 1.

[16] B. Gonzalez and I.O. Uribe, Mathematical Modeling of the Pervaporative Separation of Methanol-Methyl Tert-Butyl Ether Mixtures. Ind. Eng. Chem. Res., 40 (2001) 1720- 1731.

[17] C.J. van Oss, Interfacial Forces in Aqueous Media, Marcel Dekker, New York, 1994.

[18] V. León, A. Tusa, Y.C. Araujo, Determination of the solid surface tensions I. The platinum case. Colloids and surfaces A: Physicochemical and Eng. Aspects, 155 (1999) 131-136

[19] M. Rankl, S. Laib, S. Seeger, Surface tension properties of surface coatings for application in biodiagnostics determined by contact angle measurements, Colloids and Surfaces B: Biointerfaces 30 (2003) 177-186.

[20] D.Y. Kwok, The usefulness of the Lifshitz- van der Waals/acid-base approach for surface tension components and interfacial tensions, Colloids and surfaces A: Physciochemical and Eng Aspects, 1999, 156, 191-200.

[21] A. Jonquières, R. Clément, P. Lochon, J. Néel, M. Dresch, B. Chrétien, Industrial state-of-art of pervaporation and vapor permeation in the western countries, J. Membrane Sci. 206 (2002) 87-117.

[22] D.W. Van Krevelen, Properties of Polymers, Elsevier, Amsterdam, 1990.

[23] A. Hillaire, E. Favre, Isothermal and nonisothermal permeation of an organic vapour through a dense polymer membrane, Ind. Eng. Chem. Res. 38 (1999) 211-217

[24] P. Kirkegaard, N.J. Pedersen, M. Eldrup, PATFIT-88: a data processing system for positron annihilation spectra on mainframe and personal computers, Riso National Laboratory, Denmark, 1989.

[25] S.J.Tao, Positronium annihilation in molecular substances. J. Chem. Phys, 56 (1972) 5499.

[26] K. Ciesielski, A.L. Dawidowicz, T. Goworek, B. Jasinska, J. Wawryszczuk, Positronium lifetimes in porous vycor glass, Chem. Phys. Lett. 289 (1998) 41-45.

[27] C.J. van Oss, R.J. Good, M.K. Chodhary, Langmuir, 4 (1988) 884.

[28] C.J.van Oss, L. Ju, M.K. Chodhary, R.J. Good, Chem. Rev. 88 (1988) 313.

[29] C.J. van Oss, R.F. Giese, R.J. Good, The zero time dynamic interfacial tension, J. Dispersion Sci. and Tech. 23(4) (2002) 455-464.

[30] C.J. van Oss, Personal communication

[31] J.J. Jasper, J. Phys. Chem.Ref. Data, 1 (1972) 841.

[32] P.J. Flory, Principles of polymer chemistry; Cornell University Press: New York, 1953.

[33] E. E. B. Meuleman, B. Bosch, M. H. V. Mulder, H. Strathmann, Modelling of liquid/liquid separation by pervaporation: Toluene from water. AIChE, 45 (1999) 2153-2160.

[34] R.E. Treybal, Mass-Transfer Operations; McGraw-Hill Publishers: New York, 1986 (Third Edition).

[35] T.E. Daubert, R.P. Danner, Physical and thermodynamic properties of pure chemicals, Hemisphere publishing corporation, New York, 1989.

[36] L.H. Lee, Relevance of film pressures to interfacial tension, miscibility of liquids, and Lewis acid-base approach, J. Colloid Interface Sci, 214 (1999) 64-78.

[37] C.J Van Oss, R.J. Good, Surface Tension and the solubility of polymers and biopolymer: The role of polar and apolar interfacial free energies. J. Macromol.SCI.-CHEM., A26(8) (1989) 1183-1203.

Chapter 6

Hydrazine – Water through Hollow Fiber Module: Modeling and Simulation

6.1 Introduction

The separation of hydrazine-water mixture is a problem of immense importance. Hydrazine and its derivatives have wide ranging applications, i.e., from commercial to non-commercial application. One of the major non-commercial applications of the anhydrous form of hydrazine is in the form of rocket fuel in guided missiles and space shuttles. Among major commercial applications, hydrazine solutions are used as blowing agents and for the preparation of agricultural chemicals and pharmaceuticals. Methods (various reaction routes) for the production of hydrazine contain large amounts of water as reaction product [1]. Removal of water by conventional separation techniques (example distillation in the presence of dehydrating agents or azeotropic distillation) to produce anhydrous hydrazine is highly energy intensive due to the formation of maximum boiling azeotrope at 71.5 % by wt. of hydrazine. Therefore, there is a necessity to search for newer separation technique. One such alternative is pervaporation which overcome some of the problems associated in conventional processes [2]. Pervaporation is relatively a new membrane separation process that has elements common to reverse osmosis and membrane gas separation. It is used for separation of liquid mixtures like azeotropes [3], isomers [4], close

boiling mixtures [5], and volatile organics [6], apart from established industrial applications [7, 8] of dehydration of alcohols.

Hydrazine-water pervaporation work is very scare and only one such experimental work is available using ethyl cellulose membrane [2]; however, the work doesn't report any modelling of the process. In order to mathematically model the process, the mass transport mechanism should be clearly understood. However, the mass transport of mixtures through a polymeric membrane is generally considered to be complex as systems are often highly interactive. The equations that govern the transport phenomena are highly system dependent and there is no universal model to represent all kinds of pervaporation processes. Hence, one of the objectives of this work is to develop a detailed model simply based on solution-diffusion mechanism for hydrazine – water system. Accordingly, the Flory-Huggins equations were used to estimate the volume fraction profiles in the membrane and the required interaction parameters between membrane and solute were estimated using solubility data [2]. Further, liquid-liquid interaction parameter was estimated using vapour-liquid equilibrium data [9] and Brun's version model [10] was considered for diffusivity variation with concentration. Unknown model parameters (diffusion coefficient at infinite dilution concentration, plasticization coefficients) were estimated using least square error minimization of the experimental data [2]. The developed model is an extension of the earlier model [11], applicable at high downstream vacuum and for an average volume fraction of the component in the membrane. The present model considered the volume fraction variation inside the membrane for flux estimation using a discrete analog [12]. Therefore, developed model may also be applicable for higher downstream pressures (low vacuum).

At present mainly plate and frame module is used for industrial application due to its ease in installation. Economical aspects as well as low separation area to volume ratio have led to the development of other alternative modules. Hollow fibre or spiral wound modules are found to be attractive in this regard [13]. These modules provide higher area per unit volume and therefore higher flux is achieved which are attractive for large scale industrial applications [14]. Further, the modules may also be used along with distillation columns for the development of hybrid pervaporation-distillation process that is economically more favourable than the conventional separation scheme [15]. Between hollow fiber and spiral wound membrane modules, the disadvantage associated with spiral wound module is that the flat membrane needs mechanical support while hollow fiber membrane is self-supporting [16]. However, in hollow fiber module there is a distinct possibility of built of permeate pressure [17] which reduces the flux. Such a phenomena, has been studied for a better understanding of the pervaporation process through hollow fiber module.

In recent work [18], it was found that the pervaporation of multicomponent VOC's mixtures through hollow fiber module required lower cost compared to single organic component present in water with feed flow in tube side. However, results are available for both tube and shell sides feed flows [19, 20], using hollow fiber module and no specific advantages/disadvantages of these configurations were discussed. Hence, the second objective of this work is to study the effect of feed flow on process performance for hydrazine – water separation. Model formulations were made considering mass, momentum and energy balance of both the feed and the permeate sides.

The developed model consists of a set of coupled non-linear ordinary differential equation with mixed boundary conditions. The solution of these equations is non-trivial and requires specialized numerical technique, which is also a problem specific. The coupled algebraic and differential permeate flux equations are solved at each spatial step of the differential balance equations using an iterative method. The simulations were carried out to estimate the axial variation of properties like downstream pressure, feed flow rate, retentate temperature, permeate and retentate concentrations, etc. Further, a study was made to understand the sensitivity of separation parameters to operating conditions. Finally, a comparison between performance for feed flow in the tube side and the shell side is discussed.

6.2 Theory

Five consecutive steps may describe the transport of solute from bulk feed side to bulk permeate side during in pervaporation and are shown schematically in Figure 6. 1.

1. Transport of a component from the bulk of the feed to the membrane surface.

2. Sorption of the component into the membrane.

3. Diffusion of the component in the membrane phase.

4. Desorption of the component as vapour on the permeate side of the membrane.

5. Transport of the component from the membrane surface to the permeate bulk.

6.2.1 Transport Through the Feed Boundary Layer

The mass transfer across the liquid boundary layer at the feed side of the membrane can be described by eq (6.1). The physical properties of the feed components and membranes are tabulated in Table 6.1.

$$J_i = k_{L,i} \rho_{sl} \left[w_{ib}^F - w_{iI}^F \right] \tag{6.1}$$

The mass transfer coefficient $k_{L,i}$ for the hollow fiber module can be estimated using the following correlations [21]:
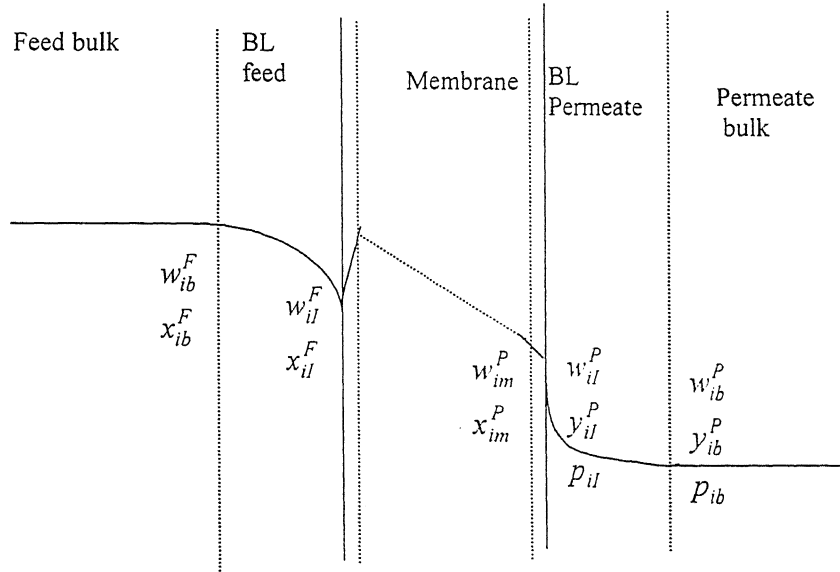
Figure 6. 1 Mass transport steps during pervaporation process

6.2.1.1 Tube Side Feed Flow

$$Sh = \frac{k_{L,i} d_{tube}}{D_{ij}} = 0.683 Re^{0.466} Sc^{1/3} \qquad Re < 4000 \qquad (6.2)$$

$$Sh = \frac{k_{L,i} d_{tube}}{D_{ij}} = 0.193 Re^{0.618} Sc^{1/3} \qquad 4000 < Re < 40000 \qquad (6.3)$$

$$Sh = \frac{k_{L,i}d_{tube}}{D_{ij}} = 0.0266Re^{0.805}Sc^{1/3} \qquad Re > 40000 \qquad (6.4)$$

6.2.1.2 Shell side Feed flow

$$Sh = \frac{k_{L,i}d_{tube}}{D_{ij}} = 0.24Re_{max}^{0.64}Sc^{1/3} \qquad (6.5)$$

6.2.2 Phenomenological Description: Solution- Diffusion Model

The solution- diffusion model is widely accepted mechanism to describe the transport of component through dense polymeric membranes. According to this mechanism, pervaporation involves steps 2-4 (given above under theory) are predominant during pervaporation.

6.2.2.1 Liquid-Liquid Interaction Coefficient

The interaction parameter between the two liquid components may be calculated using excess functions [22].

$$\frac{\Delta G_{mix}}{RT} = x_{ib}^F \ln x_{ib}^F + x_{jb}^F \ln x_{jb}^F + \frac{\Delta G^E}{RT} \qquad (6.6)$$

The free energy of mixing of the binary mixture can be calculated using Flory-Huggins theory [23].

$$\frac{\Delta G_{mix}}{RT} = x_{ib}^F \ln \varphi_{ib}^F + x_{jb}^F \ln \varphi_{jb}^F + \chi_{ij}\varphi_{ib}^F\varphi_{jb}^F \left[x_{ib}^F + x_{jb}^F \frac{V_j}{V_i} \right] \qquad (6.7)$$

Further, the excess Gibbs free energy can be expressed as [24],

$$\frac{\Delta G^E}{RT} = x_{ib}^F \ln \gamma_{ib}^F + x_{jb}^F \ln \gamma_{jb}^F \qquad (6.8)$$

The liquid phase activity and activity coefficients were estimated from vapour-liquid equilibrium data using one parameter Margules equation [24].

$$RT\ln\gamma_{ib}^{F} = A\left[x_{jb}^{F}\right]^{2} \text{ and } RT\ln\gamma_{jb}^{F} = A\left[x_{ib}^{F}\right]^{2} \tag{6.9}$$

Combining the eqs (6.6-6.9) one can obtain the relation for the binary liquid – liquid interaction parameter and it is given by eq (6.10).

$$\chi_{ij} = \frac{1}{x_{ib}^{F}\varphi_{jb}^{F}}\left[x_{ib}^{F}\ln\left\{\frac{x_{ib}^{F}}{\varphi_{ib}^{F}}\right\} + x_{jb}^{F}\ln\left\{\frac{x_{jb}^{F}}{\varphi_{jb}^{F}}\right\} + \frac{Ax_{ib}^{F}x_{jb}^{F}}{RT}\right] \tag{6.10}$$

The Margules constant A, for hydrazine-water system was determined with vapors -liquid equilibrium data using the following equation.

$$P = x_{ib}^{F}P_{i}^{sat}\exp\left[\frac{A}{RT}\left\{x_{jb}^{F}\right\}^{2}\right] + x_{jb}^{F}P_{j}^{sat}\exp\left[\frac{A}{RT}\left\{x_{ib}^{F}\right\}^{2}\right] \tag{6.11}$$

Where, P is the total vapor pressure of the binary mixture and the saturation vapor pressures for the components were calculated using Antoine's equations [25, 1].

$$\log P_{i}^{sat} = 8.07 - \frac{1730.63}{T - 39.58} \text{ and } \log P_{j}^{sat} = 7.81 - \frac{1680.75}{T - 45.26} \tag{6.12}$$

Where, P^{sat} is in mmHg and T is in K. The eq (6.11) is a function of temperature, total vapour pressure and liquid phase mole fractions with constant of Margules parameter. The Margules constant A was estimated by solving the following nonlinear optimization problem using the VLE data of hydrazine-water. The problem can be represented as

$$\min\left[\sum_{k=1}^{K} f\left\{T_{k}, P_{k}, x_{ib,k}^{F}, x_{jb,k}^{F}, A\right\}\right] = 0 \tag{6.13}$$

Where, N is the number of experimental VLE data points and the values were taken from literature [10] at constant pressure of 760 mmHg (Table 6.2). Eq (6.13) was solved using MATLAB non-linear unconstrained optimisation routine **fminsearch**. The value of A was found to be -5606.6 J/mol. Using, this value, liquid-liquid interaction coefficient was calculated from eq (6.10) and the value was found to be – 2.265. The high negative value of interaction coefficient infers strong affinity between water and hydrazine.

6.2.2.2 Solute-Membrane Interaction Parameters

The solubility of the pure component in the membrane can be predicted based on Flory- Huggins theory [23]. The following modified version may be used to calculate the solubility [26] in terms of a binary system like membrane and component.

$$\ln a_{im} = \ln\left[1 - \varphi_{pm}\right] + \left[1 - \frac{V_i}{V_p}\right]\varphi_{pm} + \chi_{ip}\varphi_{pm}^2 \qquad (6.14)$$

Where, χ_{im} is the interaction coefficient between solute and membrane. These values were estimated using solubility of the pure feed components for ethyl cellulose membrane [27]. The values found to be 2.5 and 1.8 for water-ethyl cellulose and hydrazine-ethyl cellulose membranes.

Now, for two component system, the volume fraction and the activity of components in the membrane for ternary system (membrane and two components) may be related by the following eqs (6.15) & (6.16).

Table 6.1 Pure component physical property data

Property	Water	Hydrazine	Ethyl Cellulose
Liquid density (kg/m^3)	996.5	1002.6	1100
Liquid viscosity (cP)	0.9	0.9	-
Gas viscosity (cP)	0.0108	0.009	-
Latent heat of vaporization (J/kg)	2.26x10^6	1.357x10^6	-
Specific heat (J/kg K)	4200	3092	-
Molecular Weight (g/gmol)	18	32	89448*
Molecular Weight between two cross links of polymer (g/gmol)	-	-	140*

* values are taken from ref 2

Table 6.2 Vapour – Liquid equilibrium data of hydrazine – water mixture at

atmospheric pressure [10]

at T (K)	373.0	376.0	380.0	387.0	389.8	391.1	392.2	392.8
x_j	0.00	0.10	0.20	0.30	0.40	0.45	0.50	0.55
y_j	0.00	0.02	0.05	0.13	0.24	0.31	0.39	0.48
at T (K)	393.0	392.4	391.7	391.1	390.2	388.0	386.6	
x_j	0.60	0.65	0.70	0.75	0.80	0.90	1.00	
y_j	0.56	0.64	0.71	0.78	0.85	0.93	1.00	

x_j - Hydrazine mole fraction in feed y_j - Hydrazine mole fraction in distillate

$$\ln a_{im} = \ln\varphi_{im} + \left[1 - \varphi_{im}\right] - \varphi_{jm}\frac{V_i}{V_j} - \varphi_{pm}\frac{V_i}{V_p} + \left[\chi_{ij}\varphi_{jm} + \chi_{ip}\varphi_{pm}\right]\left[\varphi_{jm} + \varphi_{pm}\right]$$

$$-\chi_{jp}\frac{V_i}{V_j}\varphi_{jm}\varphi_{pm} + \frac{V_i\rho_p}{M_c}\left[1 - \frac{2M_c}{M}\right]\left[\varphi_{pm}^{1/3} - 0.5\varphi_{pm}\right]$$

$$(6.15)$$

$$\ln a_{jm} = \ln\varphi_{jm} + \left[1 - \varphi_{jm}\right] - \varphi_{im}\frac{V_j}{V_i} - \varphi_{pm}\frac{V_j}{V_p} + \left[\chi_{ij}\varphi_{im}\frac{V_j}{V_i} + \chi_{jp}\varphi_{pm}\right]\left[\varphi_{im} + \varphi_{pm}\right]$$

$$-\chi_{ip}\frac{V_j}{V_i}\varphi_{im}\varphi_{pm} + \frac{V_j\rho_p}{M_c}\left[1 - \frac{2M_c}{M}\right]\left[\varphi_{pm}^{1/3} - 0.5\varphi_{pm}\right]$$

$$(6.16)$$

Further, the sum of the volume fraction in the membrane is equal to one, i.e.,

$\varphi_i + \varphi_j + \varphi_p = 1$. The first four terms on the right hand side of eqs (6.15) & (6.16) describe

the entropy of mixing whereas the fifth and sixth terms describe the enthalpy of mixing.

Further, the last term describes the elasticity phenomenon that opposes swelling. The

elastic term is necessary as the cross-link points may get elongated because of swelling of

polymeric chains. This may exert a force in the polymeric network [28]. In this work,

interaction parameters are assumed to be constant as per original Flory-Huggins theory.

6.2.2.3 Flux

According to solution diffusion model, the flux of the component, in absence of

flow coupling and external forces, is proportional to its chemical potential gradient.

$$J_i = -\rho_{sl}\frac{D_{im}^T}{RT}\varphi_{im}\frac{d\mu_{im}}{dX}$$

$$(6.17)$$

Where, D_i^T is the thermodynamic diffusion coefficient and it is a function of concentration

of component in the membrane. Further, the chemical potential is given by,

$$\mu_{im} = \mu_{oim} + RT\ln a_{im} + V_i \left[P - P_o \right] \qquad (6.18)$$

The variation of pressure inside the membrane was neglected and it was taken to be the pressure of upstream pressure. Substitution of eq (6.18) into eq (6.17) leads to eq (6.19) after rearrangement.

$$J_i = -\rho_{sl} D_{im}^T \varphi_{im} \frac{d\ln a_{im}}{d\varphi_{im}} \frac{d\varphi_{im}}{dX} = -\rho_{sl} D_{im} \frac{d\varphi_{im}}{dX} \quad \text{where} \quad D_{im} = D_{im}^T \frac{d\ln a_{im}}{d\ln\varphi_{im}} \qquad 6.19)$$

The diffusion coefficient was considered to vary exponentially with volume fraction of components [10].

$$D_{im} = D_{im}^0 \exp\left[b_{ii}\varphi_{im} + b_{ij}\varphi_{jm} \right] \qquad (6.20)$$

Substitution of eq (6.20) in eq (6.19) leads to eq (6.21).

$$J_i = -D_{im}^0 \rho_{sl} \exp\left[b_{ii}\varphi_{im} + b_{ij}\varphi_{jm} \right] \frac{d\varphi_{im}}{dX}. \qquad (6.21)$$

Similar equation may also be written for component *j*. Expression for *b* was obtained by Mulder [29] by differentiating Flory- Huggins eqs (6.15) & (6.16), with volume fractions. Whereas, Meuleman et al. [12] solved eq (6.21) using the discrete analogue method which, however, took large computational time. Therefore, it was felt necessary to use different method to solve eq (6.21) with less computational time providing same results. The present work uses again the discrete analogue method; however, by modifying the algorithm. Accordingly, the membrane was subdivided into *n* layers with thickness of ΔX and instead of activity, volume fraction was calculated at each subdivision, using eq (6.21). This provides distinct advantage, compared to Meuleman algorithms [12] that it does not require the solution of non-linear eqs (6.15) & (6.16) at each subdivision.

$$\varphi_{im}^{(n-1)} = \varphi_{im}^{(n)} + \Delta X \frac{J_i}{D_{im}^0 \rho_{sl} \exp\left[b_{ii}\varphi_{im}^{(n)} + b_{ij}\varphi_{jm}^{(n)}\right]} \qquad (6.22)$$

On the downstream side the activities were assumed to be equal to their partial pressure to saturation vapour pressures, since at very low pressure the fugacity coefficient as well as Poynting factor is equal to one. Hence, the activity of the component is given by (neglecting vapour phase resistance),

$$a_{ib}^p = a_{iI}^p = y_{ib}^P \frac{p}{P_i^{sat}} = \frac{J_i}{J_i + J_j} \frac{p}{P_i^{sat}} \qquad (6.23)$$

At equilibrium, chemical potential at the membrane interface is equal to that inside the membrane. This condition is same for both the feed and the permeate sides. Thus, activities also get related in the same way, i.e., $a_{is}^p = a_{im}^p$ & $a_{is}^F = a_{im}^F$. Further, permeate flux was calculated in an iterative manner due to the difficulty of writing a single equation. The following paragraph describes the procedure adapted to estimate flux.

Starting from the downstream side, the vapour phase activity was calculated using eq (6.23). The activity at the membrane interface on the downstream side is equal to the activity in the vapour phase. Thus, the volume fraction at the membrane interface was estimated by solving eqs (6.15) & (6.16) in an iterative way. The volume fraction at location (n-1) inside the membrane was calculated from the values of volume fraction at location (n) using eq (6.22). The procedure was continued till we reach the upstream side of the membrane. The activity inside the membrane was again calculated using eqs (6.15) & (6.16). These activities were compared with the corresponding activities in the liquid phase which was calculated using eq (6.1). The procedure is repeated till a convergence is observed with respect to assumed and calculated values of fluxes.

Model parameters (diffusion coefficient at infinite dilution and plasticization coefficients) were estimated using experimental flux data (Table 6.3) at different concentrations of hydrazine-water through ethyl cellulose membrane. Given a set of N data points, 2N equations are obtained by writing separate equations for component *i* & *j*. The parameters were determined by solving the non-linear least square optimisation expression.

$$\min \sum_{k=1}^{K} (J_k - J_k^*)^2 = 0 \qquad (6.24)$$

Where J^* is the experimental fluxes. MATLAB nonlinear unconstrained optimization routine **fminsearch** was used to determine the parameters. The estimated parameter values are listed in Table 6.4. Three Pareto sets are tabulated which were generated using different initial guess values.

6.2.3 Model Development: Mass, Momentum and Energy Balances along with Solution – Diffusion Model

To describe the hollow fibre module transport behaviour, a mathematical model was formulated by writing mass, momentum and energy balances. The transport equation was derived for the retentate (feed) as well as for the permeate side of the module as the flux depends on feed and permeate side conditions. The permeation through the membrane takes place in the radial direction. The transport equation was derived with the following assumption. The radial and axial diffusion were considered to be negligible compared to convection. The feed side variation was averaged in the radial direction. The VLE parameters were assumed constant in the axial direction [16].

Table 6.3 Experimental data of flux and selectivity obtained with ethyl cellulose membrane [2]

wt% hydrazine	0.20	0.30	0.40	0.64	0.70	0.85
$J \ (kg/m^2 s) \ x10^5$	4.721	4.162	1.111	0.833	0.833	1.305
α	250.0	127.8	22.2	5.6	8.3	8.6

Table 6.4 Estimated Pareto sets of model parameters

Pareto Set for Diffusion Model Parameters			
Parameters	Set 1	Set 2	Set 3
$D_{im}^0 \ (m^2/s) \ x10^{13}$	3.24	3.05	3.36
b_{ii}	72.64	111.67	110.53
b_{ij}	0.37	1.02	0.46
$D_{jm}^0 \ (m^2/s) \ x10^{12}$	4.43	1.36	2.06
b_{ji}	0.55	1.29	1.49
b_{jj}	36.76	35.58	32.61

6.2.3.1 Tube Side Feed Flow

6.2.3.1a Feed Side

The retentate (feed) side pressure and the radial average velocity for the case of

feed flow in the tube (Figure 6.2a) were obtained, combining with mass balance with

appropriate boundary condition for velocity and using the lubricating assumption [31] of

Naviers Stoke's equation [31]. The fluid was assumed to be incompressible. The detailed

derivations are given in Appendix 6.A.1.
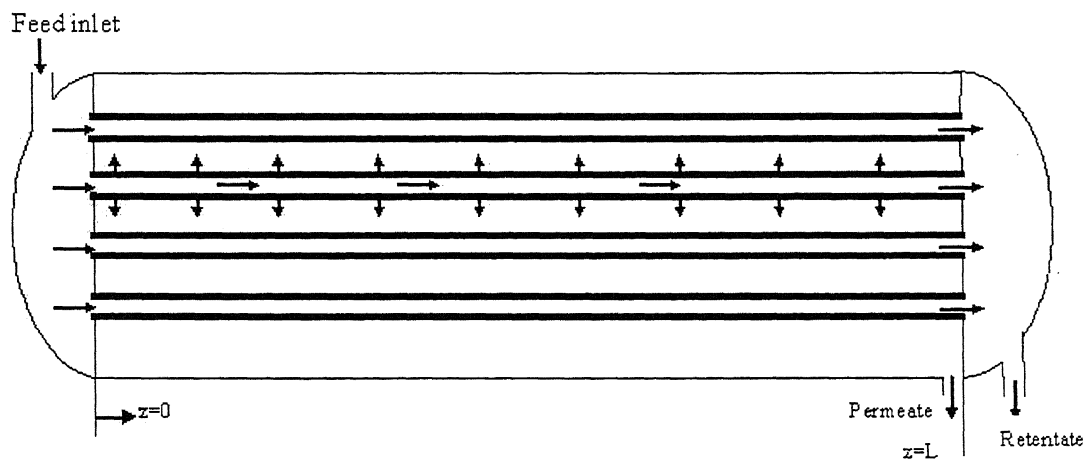
Figure 6.2a Hollow fiber module with tube side feed flow

$$\frac{dP^F}{dz} = -\frac{8\eta_{sl}v}{R_{tube}^2} \tag{6.25}$$

$$\frac{dv}{dz} = -\frac{2J}{R_{tube}\rho_{sl}} \tag{6.26}$$

The mass balance on substitution of velocity variation gives equation, which govern the composition variation of retentate (feed).

$$\frac{dx_{ib}^F}{dz} = \frac{2\rho_{jl}V_{sl}\left[Jx_{ib}^F - \frac{J_i V_{sl}\rho_{sl}}{M_i}\right]}{M_j v R_{tube}\rho_{sl}} \tag{27}$$

The feed side energy balance was derived by equating the energy removed from the feed stream to the energy consumed to vaporize permeate. The equation was obtained with the assumption of constant heat capacity and constant heat of vaporization, neglecting the small change in sensible heat.

$$\frac{dT}{dz} = -\frac{2J\lambda_{sl}}{\rho_{sl}v R_{tube}C_{p,sl}} \tag{6.28}$$

The pressure, velocity, composition, and temperature of eqs (6.25-6.28) are subject to the following initial conditions:

$$P(0) = P_{in}; \quad v(0) = v_{in}; \quad x_{ib}^F(0) = x_{in}; \quad T(0) = T_{in} \tag{6.29}$$

6.2.3.1b Permeate Side

The permeate side mass, species and momentum balance provide coupled differential equation in terms of velocity, composition and pressure. Separating each after rearrangement, the following equations are obtained (details in Appendix 6.A.1).

$$\frac{dy_{ib}^P}{dz} = \frac{2RT^P NR_{tube}\left[\dfrac{J_i M_{sv}}{M_i} - Jy_{ib}^P\right]}{pR_{shell}^2 uM_j} \qquad (6.30)$$

$$\frac{du}{dz} = \frac{2RT^P NR_{tube}\left[\dfrac{RT^P J_i M_{sv}}{M_i} - \dfrac{RT^P J_i M_j}{M_i} - RT^P Jy_{ib}^P - Ju^2 M_j y_{ib}^P\right]}{pR_{shell}^2 y_{ib}^P M_j\left[M_{sv}u^2 - RT^P\right]}$$

$$\qquad - \frac{4M_{sv}u^3 fR_{shell}}{\left[M_{sv}u^2 - RT^P\right]D_e L} \qquad (6.31)$$

$$\frac{dp}{dz} = \frac{2RT^P NR_{tube}u\left[M_{sv}Jy_{ib}^P - \dfrac{M_{sv}^2 J_i}{M_i} + M_j Jy_{ib}^P + \dfrac{M_j J_i M_{sv}}{M_i}\right]}{R_{shell}^2 y_{ib}^P M_j\left[M_{sv}u^2 - RT^P\right]}$$

$$\qquad + \frac{4pM_{sv}u^2 fR_{shell}}{\left[M_{sv}u^2 - RT^P\right]D_e L} \qquad (6.32)$$

The friction factor may be estimated by the flowing equation [14]

$$f = \frac{9.5}{Re^{0.83}}; \qquad \text{Where,} \qquad Re = \frac{\rho_{sv}uD_e}{\eta_{sv}} \qquad (6.33)$$

The differential eqs (6.30), (6.31), and (6.32) for the composition, velocity and pressure are subject to the following boundary conditions.

$$y_{ib}^P(0) = \frac{J_i(0)}{J(0)}; \qquad u(0) = 0; \qquad p(L) = p_{ap}. \qquad (6.34)$$

Where z=0 and z=L denote the inlet point of feed and the outlet point of permeate collection, respectively. p_L is the applied permeate pressure.

6.2.3.2 Shell Side Feed Flow

6.2.3.2a Feed Side

The retentate side mass, momentum and energy balances for the case of feed flow in the shell side (Figure 6.2b) on simplification yield the following equations in terms of composition, velocity, pressure and temperature.
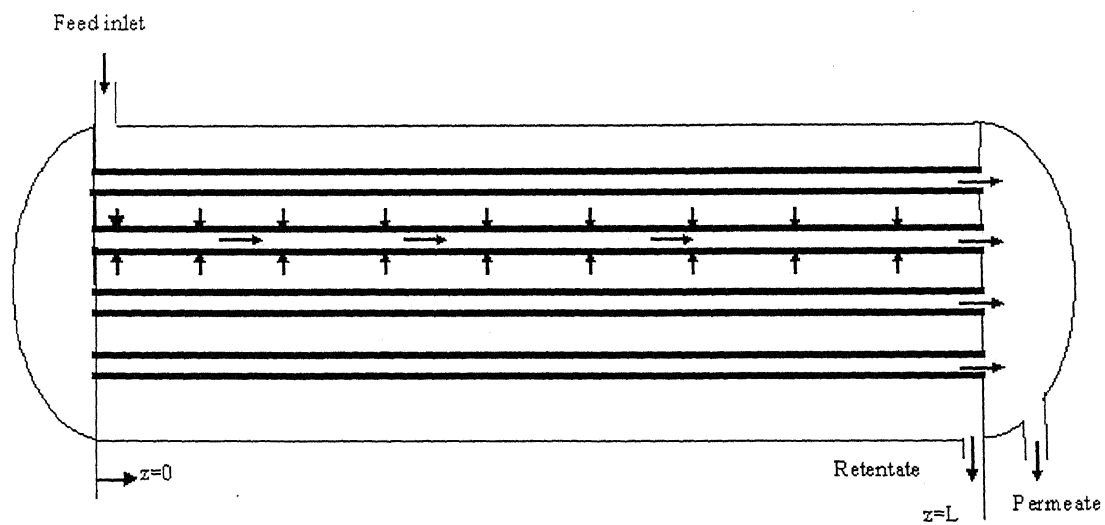
Figure 6.2b Hollow fiber module with shell side feed flow

$$\frac{dx_{ib}^F}{dz} = \frac{2N\left[R_{tube} + t\right]}{vR_{shell}^2} V_{sl} \left[\frac{x_{ib}^F J}{M_{sl}} - \frac{J_i}{M_i}\right]$$ (6.35)

$$\frac{dv}{dz} = \frac{-2\left[R_{tube} + t\right]N}{R_{shell}^2} \left[\frac{M_j}{\rho_{jl}} \frac{J}{M_{sl}} + \left\{\frac{M_i}{\rho_{il}} - \frac{M_j}{\rho_{jl}}\right\} \frac{J_i}{M_i}\right]$$ (6.36)

$$\frac{dP^F}{dz} = \frac{-2f\rho_{sl}v^2}{D_e} + \frac{2N\left[R_{tube} + t\right]M_i M_j u \left[\frac{1}{\rho_{il}} - \frac{1}{\rho_{jl}}\right]\left[\frac{x_{ib}^F J}{M_{sl}} - \frac{J_i}{M_i}\right]}{R_{shell}^2 \left[\frac{M_i x_{ib}^F}{\rho_{il}} + \frac{M_j x_{jb}^F}{\rho_{jl}}\right]}$$

$$+ \frac{4N\left[R_{tube} + t\right]\rho_{sl}v}{R_{shell}^2} \left[\frac{M_j}{\rho_{jl}} J + \left\{\frac{M_i}{\rho_{il}} - \frac{M_j}{\rho_{jl}}\right\} J_i\right]$$ (6.37)

$$\frac{dT}{dz} = -\frac{2N(R_{tube} + t)J\lambda_{sl}}{\rho_{sl}vR_{shell}^2 C_{p,sl}}$$ (6.38)

The eqs (6.35- 6.38) are also subject to the initial conditions given by eq (6. 29).

6.2.3.2b Permeate Side

The similar mass, species and momentum balance for the permeate side provides coupled differential equation in terms of velocity, composition and pressure. Separation each after rearrangement, the following equations are obtained.

$$\frac{dy_{ib}^P}{dz} = \frac{2RT^P \left(\frac{J_i M_{sv}}{M_i} - Jy_{ib}^P\right)}{pR_{tube}uM_j}$$ (6.39)

$$\frac{du}{dz} = \frac{2RT^P\left[\dfrac{RT^PJ_iM_{sv}}{M_i} - \dfrac{RT^PJ_iM_j}{M_i} - RT^PJy_{ib}^P - Ju^2M_jy_{ib}^P\right] - 2pM_{sv}u^3fy_{ib}^PM_j}{pR_{tube}y_{ib}^PM_j\left[M_{sv}u^2 - RT^P\right]}$$

(6.40)

$$\frac{dp}{dz} = \frac{2RT^Pu\left[M_{sv}Jy_{ib}^P - \dfrac{M_{sv}^2J_i}{M_i} + M_jJy_{ib}^P + \dfrac{M_jJ_iM_{sv}}{M_i}\right] + 2pM_{sv}u^2fy_{ib}^PM_j}{R_{tube}y_{ib}^PM_j\left[M_{sv}u^2 - RT^P\right]}$$

(6.41)

Further, the pressure drop in the potting length is given by,

$$\Delta p = \frac{2f\rho_{sv}[u(1)]^2L_{pot}}{R_{tube}}$$

(6.42)

Where L_{pot} is the potting length and assumed a value of 0.01 m. The friction factor is computed as [14],

$$f = \frac{16}{Re} \quad \text{where} \quad Re = \frac{\rho_{sv}uR_{tube}}{\eta_{sv}}$$

The eqs (6.39), (6.40), and (6.41) are also subject to the boundary conditions given by eq (6.34).

6.3 Solution Technique

The permeate pressure at the feed entrance side of the module (i.e. z=0) is guessed. With the initial condition of feed composition, feed temperature and the guessed value of permeate side pressure the permeate flux was calculated (following the technique discussed in section 6.2.2). The transport model equations were integrated for a small step Δz using the previous flux value; this gives new values for the process parameters (i.e. v^F, T^F, x_{ib}^F,

y_{ib}^{p}, T^{P}, p). These values were then used for the estimation of new value of permeate flux which was used again for the integration of the transport model equations from Δz to $2\Delta z$. The procedure was continued until we reach the point of permeate collection which is at the other end of the module. The obtained value of the permeate pressure (p(L)) was compared with the boundary condition (p(L)=p_{ap}). If the two values converge within a tolerance limit of ε, the simulation was stopped; else, the entire procedure was repeated with a different guessed value of permeate pressure. It has been found that a good guess value may be obtained by,

$$p(0)^{new} = p_{ap} + p(0)^{old} - p(L)^{old}$$

The above technique was implemented by writing computer code in FORTRAN language. The nonlinear algebraic equations and coupled ordinary differential equation were solved using NAG library. The 'D02EJF' subroutine was used for solution of the coupled differential equations. This subroutine uses variable-order and variable-state method for implementing the Backward Differentiation Formulae (BDF). The nonlinear algebraic equations were solved using 'C05NBF' subroutine. This subroutine uses Powell hybrid method for finding the roots. Required computational time required for the simulation was dependent upon the initial guesses for permeate pressure, permeate flux and tolerance limit. But on an average for a relative tolerance of 10^{-5}, it was about 1 min on 'sg4' server. The configuration of this server is SGI Origin 200, Four R12000 270 MHZ processors, 1 GB RAM, GB HDD. The operating system is IRIX 6.5

6.4 Results & Discussion

6.4.1 Spatial Variation

The obtained solution-diffusion model parameters were used to predict the performance of the hollow fiber module using the developed model equations for the separation of hydrazine water mixture. The hollow fiber module parameters and operating conditions, used for the simulation, for both tube and shell sides flows are listed in Table 6.4 & 6.5.

Table 6.5 Chosen model parameters and operating conditions for simulation

Parameter	Value	Parameter	Value
x_{in}	0.64	L (m)	1
F_{in} (m^3/s)	2.77×10^{-3}	R_{shell} (m)	0.3
T_{in}(K)	300	R_{tube} (m)	7.5×10^{-4}
P_{ap} (Pa)	100	t (μm)	10
T_{ap} (K)	300	N	40000

6.4.1.1 Composition Variation: Retentate (Feed) Side

The variation of retentate (feed) side water composition as a function of position is shown in Figure 6.3. The feed side composition of water shows a linear decrease along the length for both sides of feed flows. However, the change in composition is very small because of single pass and low permeation through the ethyl-cellulose membrane. Further,

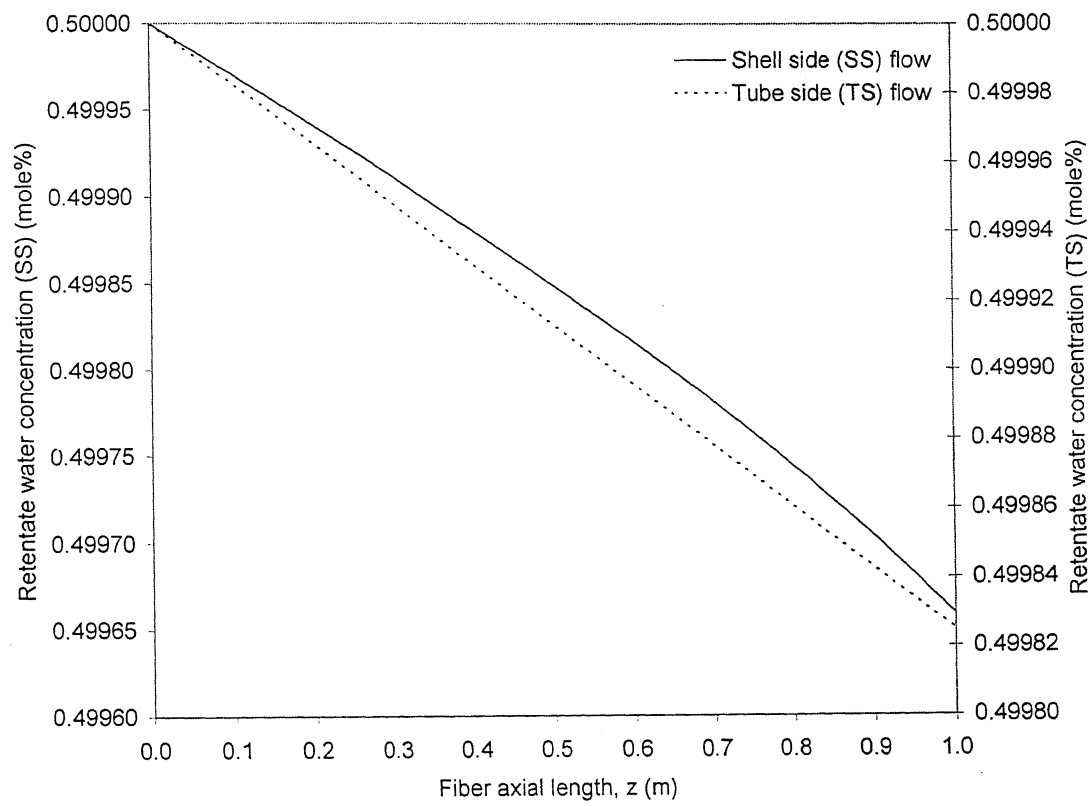**Figure 6. 3 Feed side water concentration as a function of fiber length axial position**

(at x_f = 50 mole%; feed flow rate = 2.77 x 10^{-3} m^3/s; p = 100 Pa; t = 10 μm;

r_{shell} = 0.3 m; r_{tube} = 750 μm; N = 40,000)

the decrease in composition of water is more for the case of shell side, which is due to larger permeation in case of shell side flow. Obviously, this is because of larger permeation in the shell side which is due to larger available permeation area; since permeation takes place on the outer surface of the tube.

6.4.1.2 Temperature Variation: Retentate (Feed) Side

The variation of feed side temperature as a function of position is shown in Figure 6.4. The feed side temperature decreases linearly along the length for both the cases of feed flows. The permeate is getting vaporized by taking latent heat from the feed side. Temperature is decreasing from 300 to 299.6 K for the feed flow in the shell side whereas for the case of feed flow in tube side temperature decreased from 300 to 299.8 K The larger decrease of temperature for the case of shell side flow is because of the larger available permeation area. Further, the temperature drop suggests the use of inter stage heating with multiple modules.

6.4.1.3 Pressure Variation: Permeate Side

Figure 6.5 shows the ratios of local point permeate pressure to applied pressure along the fiber length. The ratio decreases parabolically for both the cases of feed flows, i.e., the permeate pressure is building up along the fiber length from the entry point of downstream pressure (at z=L). The ratio is 6.02 for the case of feed flow in the shell side and 1.38 for the case of tube side. It may be mentioned here that Feng et al. [17] experimentally observed the said ratio to be 45 for 1 meter length of fiber for the permeation of isopropanol through silicon rubber. Naturally, the ratio depends on the permeability of the membrane. The increase of pressure build up will reduce the permeate flux due to the decrease of driving force. This is one of the major problems for the use of
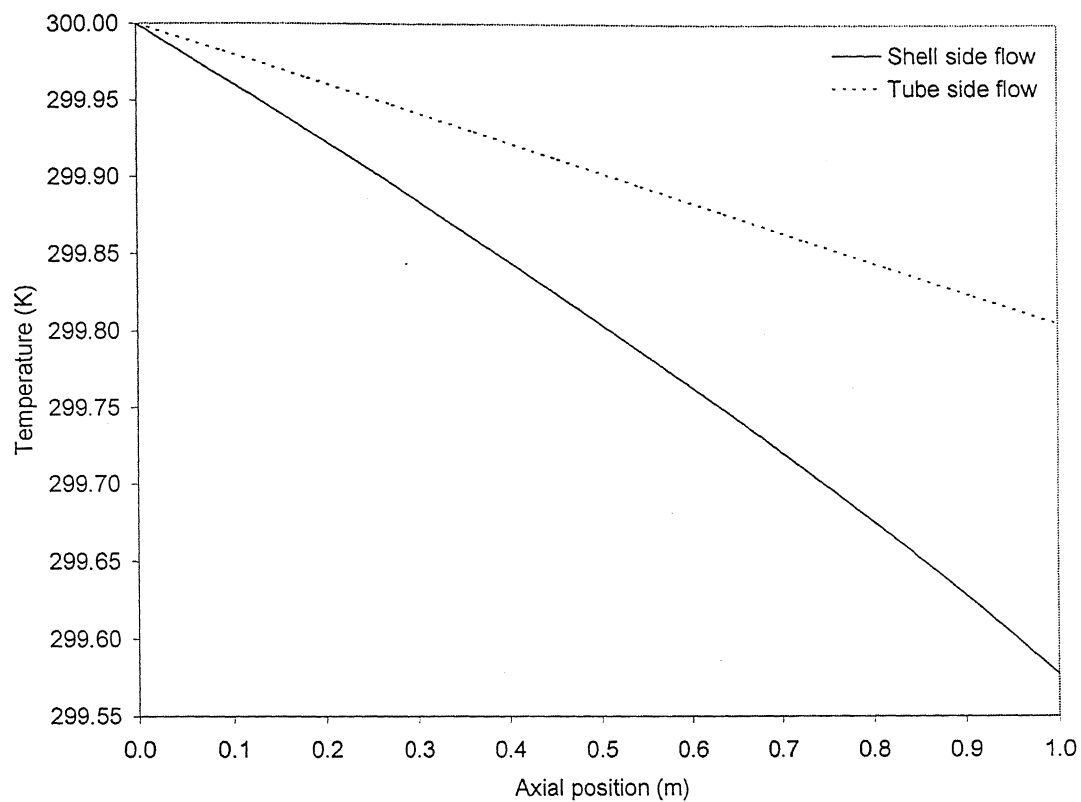
Figure 6.4 Feed side temperature as a function of fiber length axial position

(at x_f = 50 mole%; feed flow rate = 2.77 x 10^{-3} m^3/s; p = 100 Pa; t = 10 μm;

r_{shell} = 0.3 m; r_{tube} = 750 μm; N = 40,000)

hollow fiber modules for the pervaporation process. However, only small increase of permeate pressure build up for the pervaporation of hydrazine- water may not be a problem for the use of hollow fiber modules for its separation. The effect of permeate pressure build up may be reduced by increasing fiber diameter but at the cost of high membrane area packing density. One may attempt to optimize the fiber dimensions for the hollow fiber module.

6.4.1.4 Pervaporate Collection Velocity Variation: Permeate Side

The variation of pervaporate collection velocity along the length for both sides feed flows is plotted in Figure 6.6. The pervaporate collection velocity increases along the length for both the cases. The increase in velocity is 11.5 m/s for the case of shell side feed flow whereas it is 4.6 m/s for case of feed flow in the tube side. Further, it may be observed that in case of shell side flow the velocity shows a sudden jump at rear end of the module. The increase in velocity in the two cases is due to available permeate side pressure gradient along the length (permeate side). The larger increase in the case of shell side feed flow is because of the larger pressure gradient in this case. The sudden jump in velocity at the rear end is caused by the steep decrease in pressure at that end. Further, it may be mentioned here that the increase of fiber length and decrease of fiber diameter to reduce the cost of module leads to increase of collection velocity. At higher collection velocities (close to sonic velocities) it is difficult to operate/handle the module and becomes one of the most important operational constraints.

6.4.1.5 Composition Variation: Permeate Side

Figure 6.7 shows the variation of the permeate side composition with fiber length. The permeate composition of water increases along the length in both the cases of feed
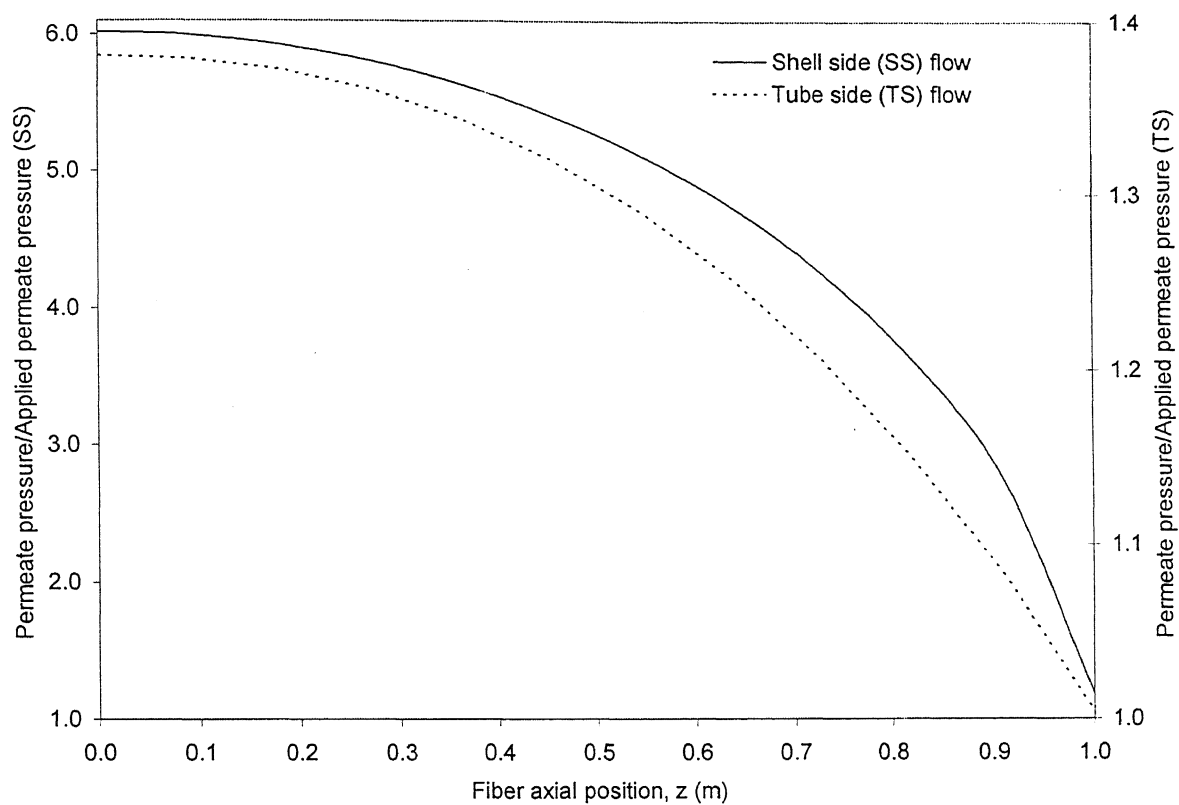
Figure 6.5 Ratio of downstream pressure to applied pressure as a function of fiber

length axial position

(at $x_f = 50$ mole%; feed flow rate = 2.77×10^{-3} m^3/s; p = 100 Pa; t = 10 μm;

$r_{shell} = 0.3$ m; $r_{tube} = 750$ μm; N = 40,000)

Figure 6.6 Permeate velocity as a function of fiber length axial position

(at $x_f = 50$ mole%; feed flow rate = 2.77×10^{-3} m^3/s; p = 100 Pa; t = 10 μm;

$r_{shell} = 0.3$ m; $r_{tube} = 750$ μm; N = 40,000)

flow. The increase in permeate composition of water is due to the dominating effect of downstream pressure (more vacuum). The water permeation flux at lower downstream pressure is so high (Figure 6.5) that it overcomes the decrease in composition due to increase in permeate composition of water as well as decrease in feed composition of water.

6.4.1.6 Flux Variation

Figure 6.8 shows the variation of hydrazine, water and total fluxes with fiber length. All the fluxes are increasing along the fiber length for both the cases of feed flow. However, the increase is observed to be marginal in case of tube side feed flow. The increase of fluxes is due to the decrease in downstream pressure along the fiber length. At $z=L=1$ m, the total, water, and hydrazine fluxes are 5.36×10^{-6}, 4.32×10^{-6}, and 1.04×10^{-6} kg/m^{2}s, respectively for the feed flow in the shell side; whereas, for the tube side, these values become 5.43×10^{-6}, 4.39×10^{-6}, and 1.04×10^{-6} kg/m^{2}h, respectively. It is clearly evident that the tube side fluxes are little bit higher than shell side. This is attributed due to fact that there is higher water concentration in the feed at $z=1$ m (Figure 6.3).

The ratio of local total flux to local total flux at $z=1$ m (J_t /$J_t(1)$) as a function of position is shown in Figure 6.9. Similarly ratio of water fluxes as well as hydrazine fluxes are also shown in Figure 6.9. The ratio of total permeation flux increases for both cases of feed flow due to the dominating effect of the rapid decrease in permeate pressure along the fiber length (Figure 6.5). The ratio of hydrazine as well as water permeation fluxes also increases along the length. However, the increase in ratios of fluxes is more for shell side flow. This is because of a larger decrease in permeate pressure for the case of shell side flow in addition to more available area.
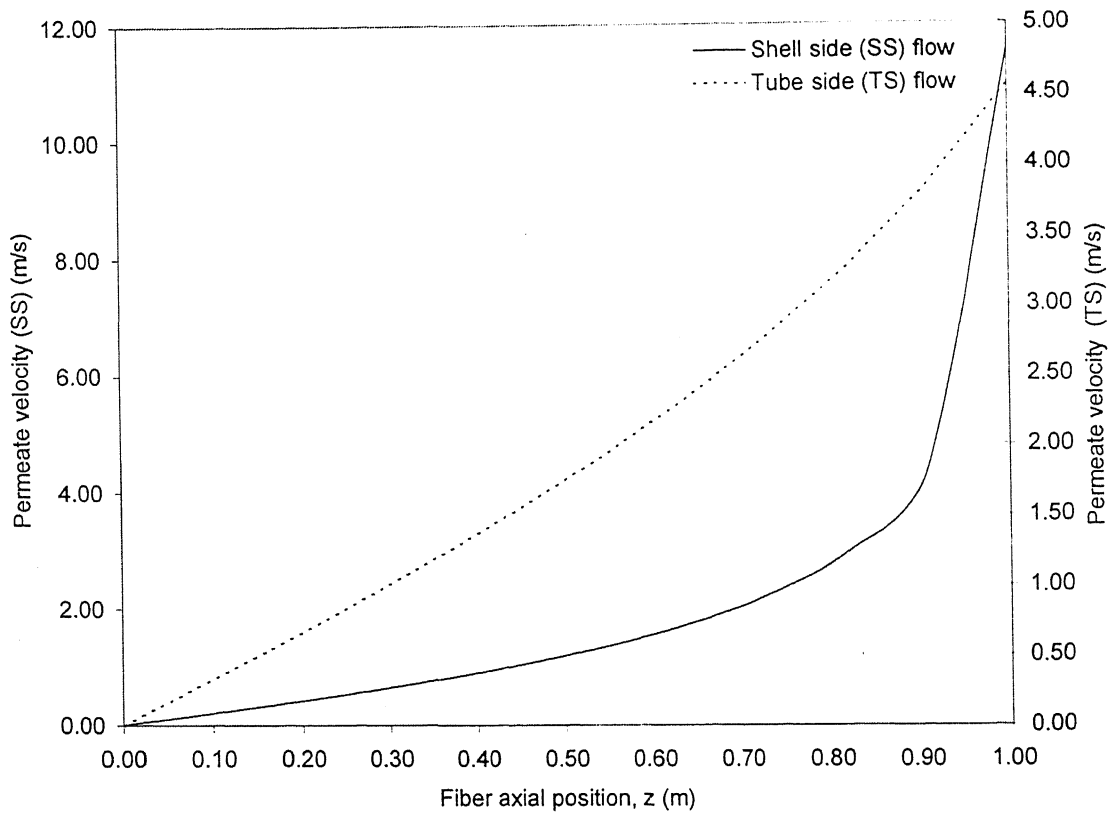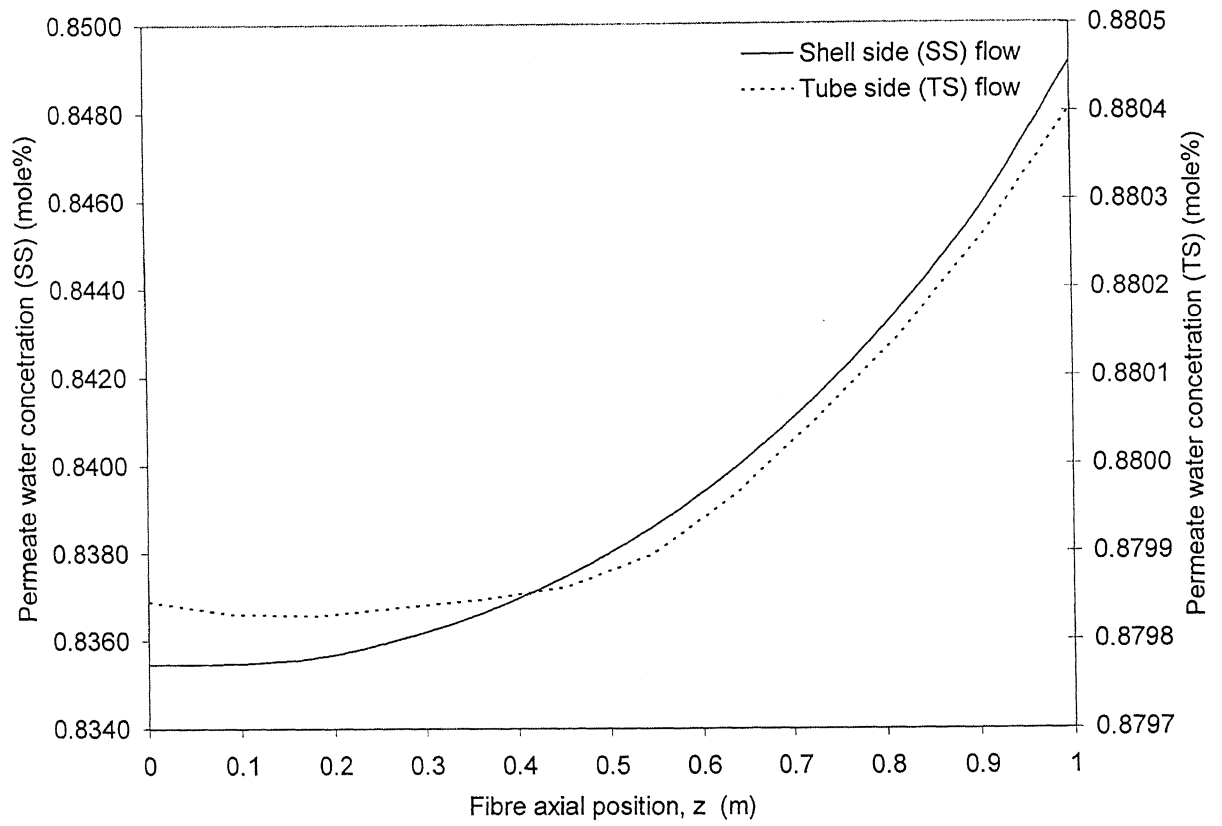
Figure 6.7 Permeate water concentration as a function of fiber length axial position

(at $x_f = 50$ mole%; feed flow rate = 2.77 x 10^{-3} m³/s; p = 100 Pa;

t = 10μm; $r_{shell} = 0.3$ m; $r_{tube} = 750$ μm; N = 40,000)
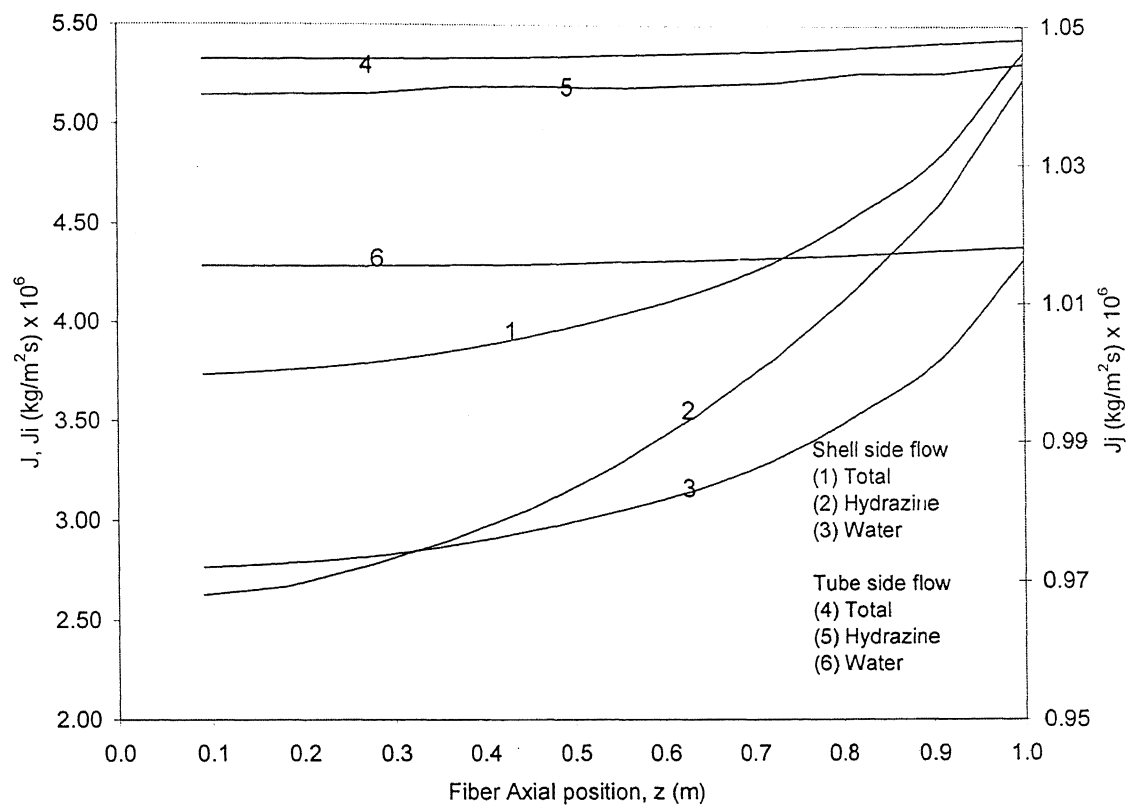
Figure 6.8 Hydrazine, water, and total flux as a function of fiber length axial

position

(at x_f = 50 mole%; feed flow rate = 2.77 x 10^{-3} m^3/s; p = 100 Pa;

t = 10μm; r_{shell} = 0.3 m; r_{tube} = 750 μm; N = 40,000)
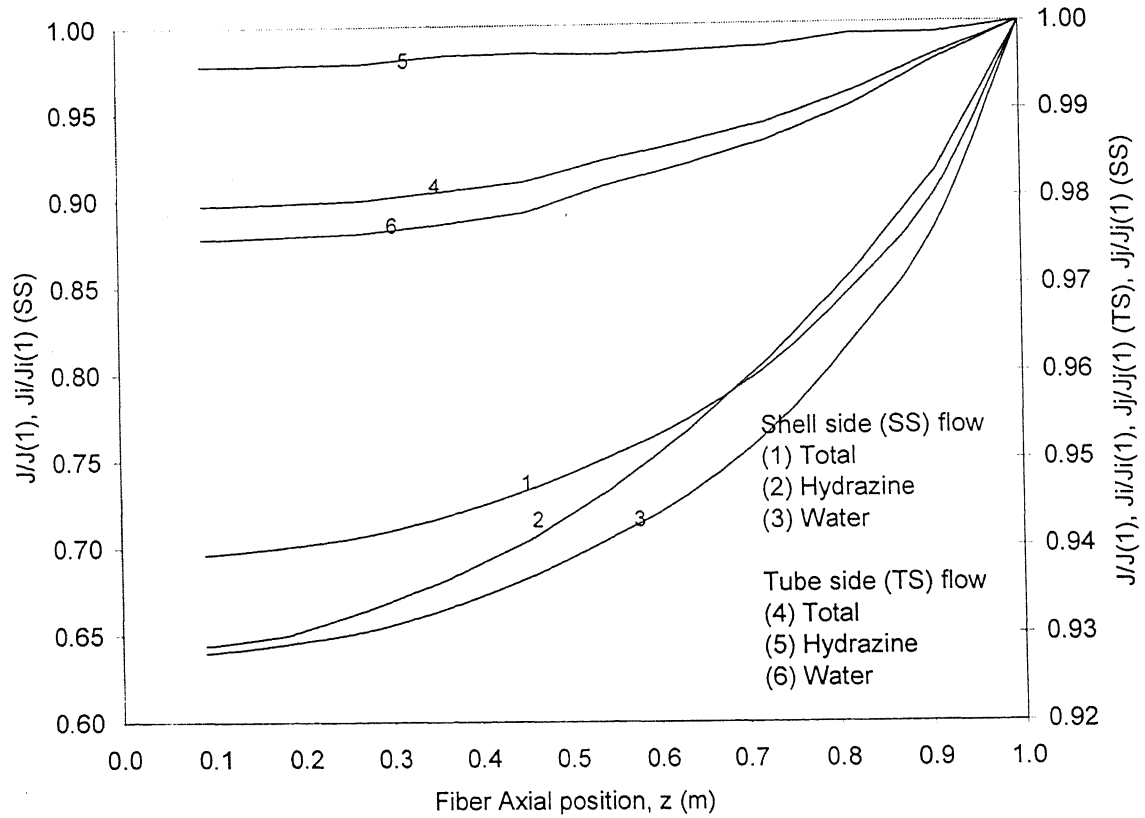
Figure 6.9 Relationships between fractional flux (flux w.r.t. corresponding flux at

z=1 m) and fiber length axial position

(at x_f = 50 mole%; feed flow rate = 2.77 x 10^{-3} m^3/s; p = 100 Pa;

t = 10μm; r_{shell} = 0.3 m; r_{tube} = 750 μm; N = 40,000)

6.4.2 Comparison Between the Shell Side and Tube Side Feed Flow

The drop in the permeate pressure is more in the case of shell side flow due to larger frictional losses caused because of the low Reynolds number of permeate flow in tubes. The frictional losses are comparatively less when the permeate flows in the shell side for the case of tube side feed flow. The larger pressure gradient of permeate in the tubes for the case of the shell side feed flow causes abnormal increase in pervaporate collection velocity. This restricts the use of shell side feed flow configuration at very low downstream pressure (high vacuum) which increases collection velocity to large value. So despite the separation advantages, the operational constraints become restricting for feed flow at shell side. However, although there is lower separation with tube side flow, but the range of operability is large which may be advantageous. The feed side pressure drop is larger than that was observed in shell side flow, resulting in larger feed pumping cost and thus may be disadvantageous.

6.4.3 Effect of Operating Variables

The separation capability was investigated over a range of feed composition, feed flow rate, permeate pressure, and membrane thickness. The properties of interests are the selectivity, 'α' and permeate to feed flow ratio, ϕ.

$$\phi = \frac{F^P}{F^F} \qquad\qquad \alpha = \frac{y_{ib}^P \left[1 - x_{ib}^F \right]}{x_{ib}^F \left[1 - y_{ib}^P \right]}$$

The ratio, ϕ gives a better understanding for interpreting separation. It depicts the fraction of feed that has been purified. Being a ratio, it can be used for comparing the permeation

in modules with different feed flows. The module parameters, used for simulation are given in Table 6.5.

6.4.3.1 Effect of Feed Concentration

Figure 6.10 shows the effect of feed water concentration on permeate to feed flow ratio for both the cases of feed flow (shell and tube side). The said ratio decreases and then increases, exhibiting minima at 30 wt% (43.2 mole%) water concentration for shell side feed flow whereas for tube side feed flow the minima observed at 27.5 wt% (40.27 mole%). It has been explained earlier that as the water concentration increases, the solubility decreases, and diffusivity increases. These two opposite trends result in minima of permeate flux at 30 wt% water concentration. Experimentally, Ravindra et al.[2] obtained the minima at 36 wt% concentration of water. The difference may be attributed due to fact that limited experimental flux data are available in this range of water concentrations (Table 6.3). Further, permeate to feed flow ratio is smaller in the case of tube side flow as compared to shell side flow. This is because of larger separation area available for shell side feed flow (as explained in section 6.4.1.1) as against tube side flow.

Figure 6.11 shows the effect of feed concentration on selectivity. The selectivity of the membrane increases with increase in composition of water for either of the flows. This continuous increase of selectivity with increase in water composition may be explained because of decrease of swelling and increase of diffusion coefficient. It is interesting to predict that at very low composition of water (i.e. less than 20 wt. %), hydrazine permeation becomes more than that of water, and hence, results into selectivity value of less than one for both shell as well as tube side feed flow. Therefore, analogous to distillation, here also there is formation of azeotrope during pervaporation of hydrazine-
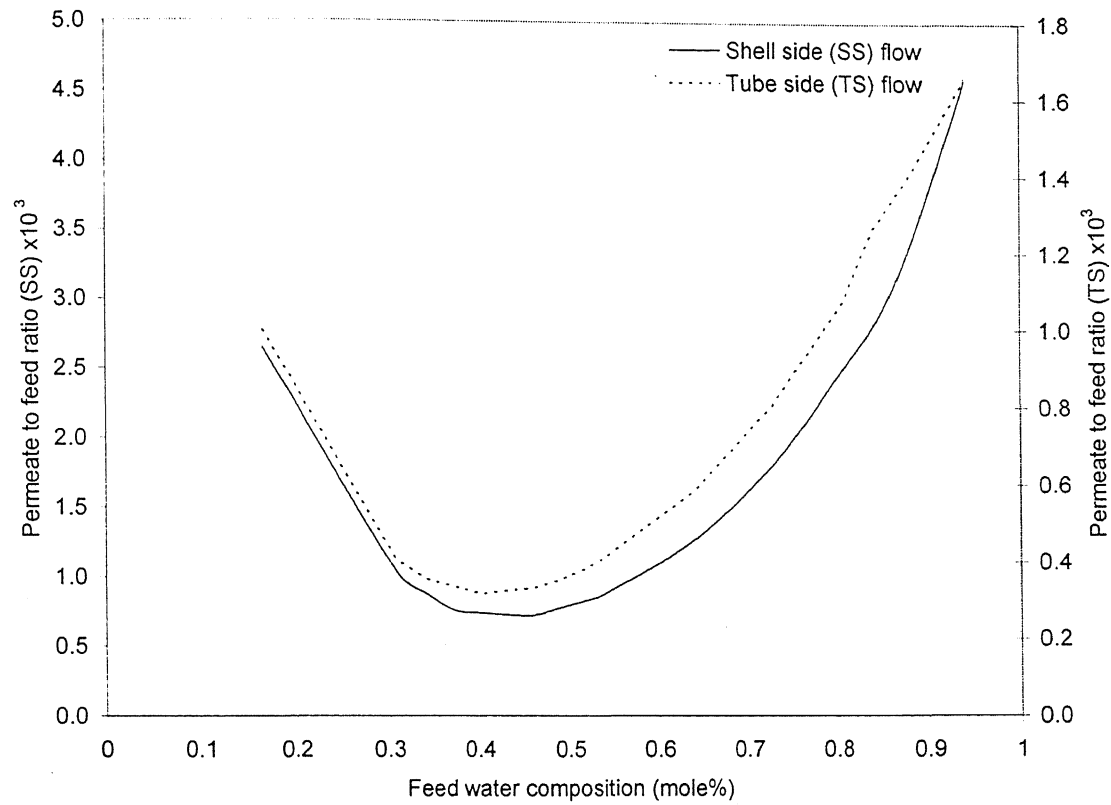
Figure 6.10 Influence of water feed concentration on permeate to feed flow ratio (φ)

(at feed flow rate = 2.77 x 10^{-3} m^3/s; p = 100 Pa; t = 10 μm; L = 1 m;

r_{shell} = 0.3 m; r_{tube} = 750 μm; N = 40,000)
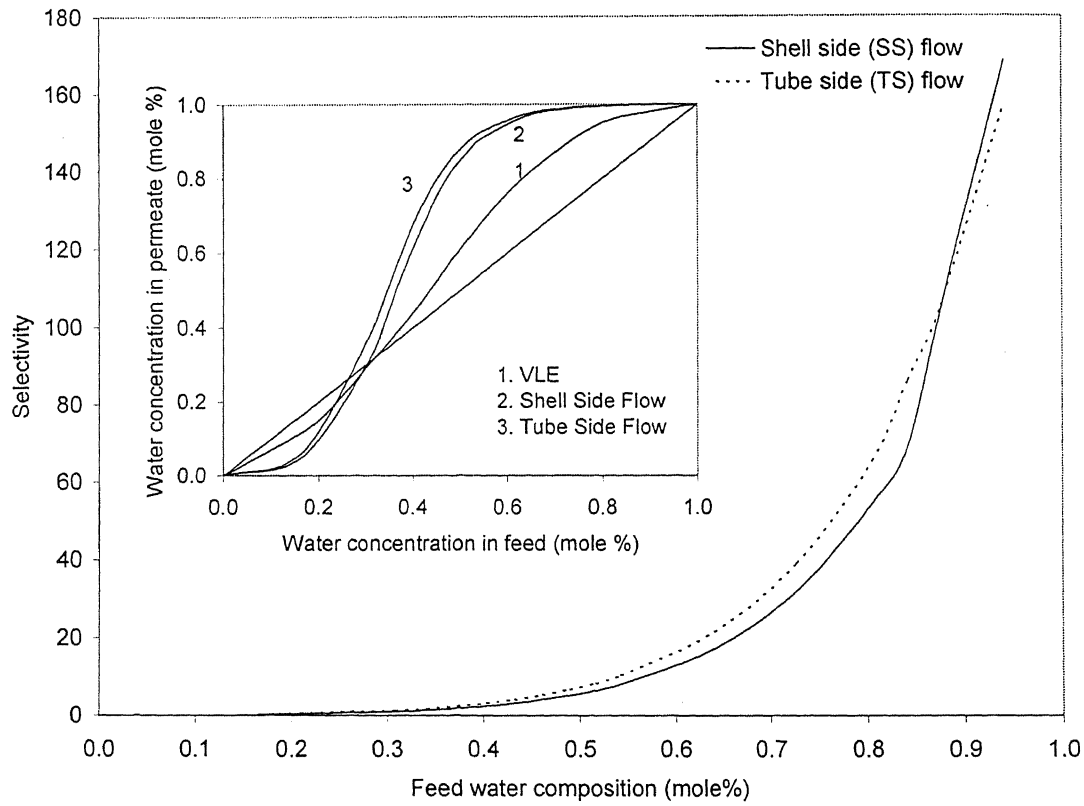
Figure 6.11 Influence of feed water concentration on selectivity

(at feed flow rate = 2.77 x 10^{-3} m^3/s; p = 100 Pa; t = 10 μm; L = 1 m;

r_{shell} = 0.3 m; r_{tube} = 750 μm; N = 40,000)

water mixtures. Such a phenomena has earlier also been demonstrated by other authors [32-35] for systems like ethanol-water, etc. Still, pervaporation provides an advantage with shifting of azeotropic concentration of water. The shift is from 28.5 (by distillation) to 17.5 wt% for tube side flow (refer inset of Figure 6.11). In case of shell side feed flow the azeotrope is observed at 28.5% which is similar VLE. Further, shifting as well as complete avoidance of azeotropic formation is possible with the selection of much improved selective membranes.

6.4.3.2 Effect of Feed Flow Rate

Figure 6.12 shows the effect of feed flow rate on the permeate to feed flow ratio. The ratio continuously decreases with feed flow rate. This may be because of increase in flow rate there is increase of mass transfer coefficient through the boundary layer. This will increase the concentration of water at the membrane surface and may become equal to bulk concentration at higher flow rates. The increase of water concentration at the membrane surface decreases the solubility of feed solution in the membrane and this decreases the flux through the membrane.

Figure 6.13 shows the effect of feed flow rate on selectivity. The selectivity of the membrane slightly increases with increase in feed flow rate. This may be explained due to increase in mass transfer coefficient which causes higher permeation flux of water. However, the selectivity was observed to be marginally higher for the case of tube side flow as against shell side flow. This may be due to the variation of water concentration in the boundary layer which is smaller because of lower permeation through the membrane for the case of tube side flow. Further, it may be also due to larger permeate pressure drop

Figure 6.12 **Influence of feed flow rate on permeate to feed flow ratio** (φ)
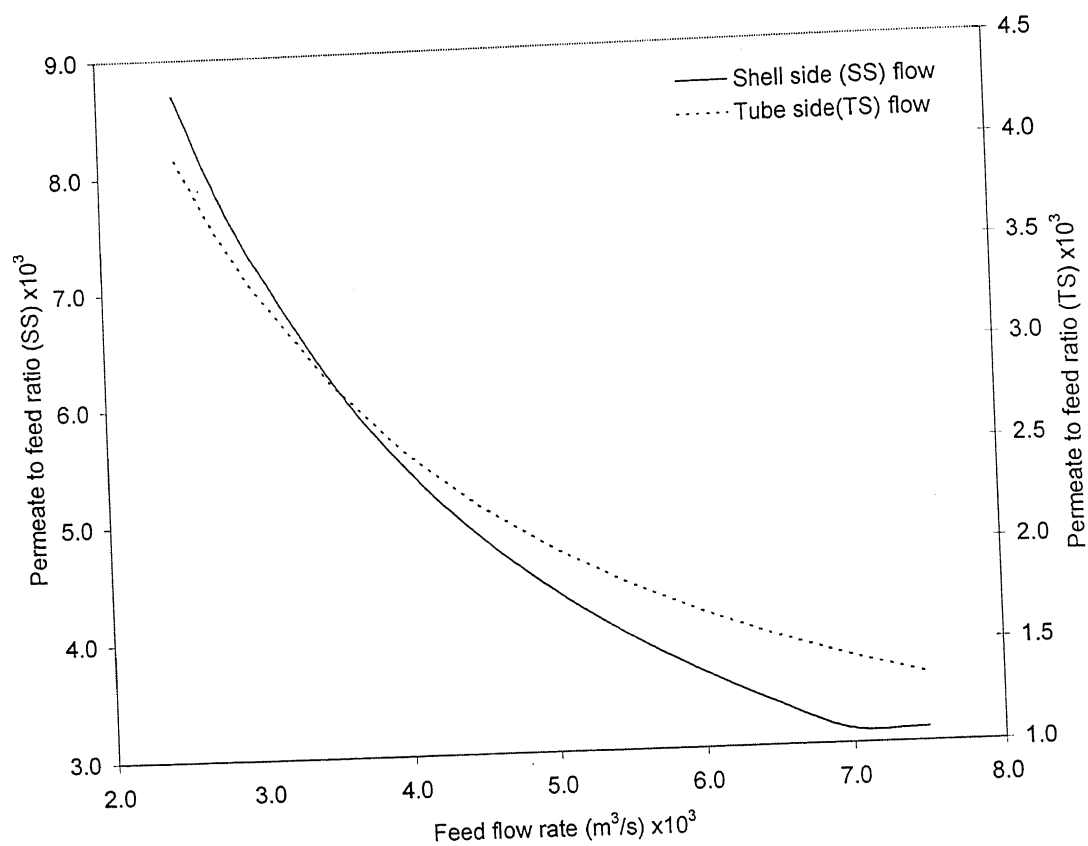
(at x_f = 50 mole%; p = 100 Pa; t = 10 μm; L = 1 m; r_{shell} = 0.3 m;
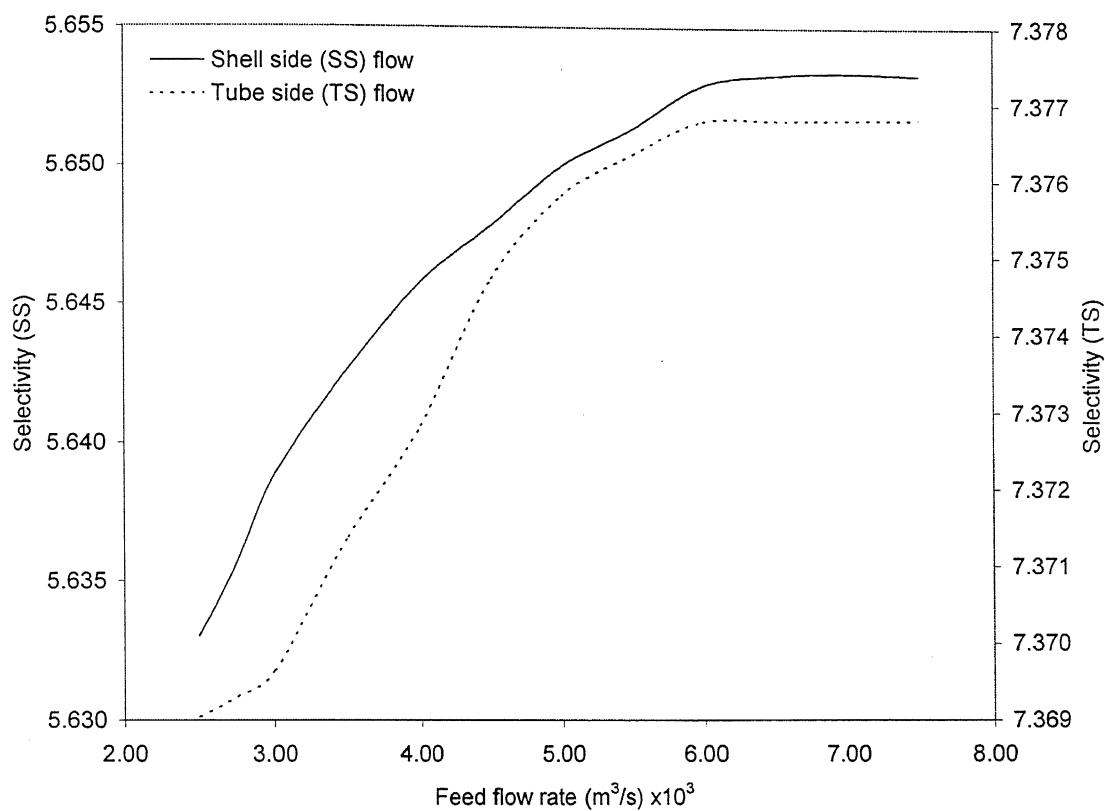
r_{tube} = 750 μm; N = 40,000)

Figure 6.13 Influence of feed flow rate on selectivity

(at $x_f = 50$ mole%; $p = 100$ Pa; $t = 10$ μm; $L = 1$ m; $r_{shell} = 0.3$ m;

$r_{tube} = 750$ μm; $N = 40,000$)

in the case (Figure 6.5) of shell side feed flow which may have resulted in lowering water flux.

6.4.3.3 Effect of Permeate Pressure

The effect of downstream pressure on permeate to feed ratio is shown in Figure 6.14. Permeate to feed ratio decreases with increase in downstream pressure with obvious reasoning and approaches zero around 1600 Pa. Further, permeate to feed ratio is twice for the shell side flow compared to tube side flow, because of larger separation area available for shell side flow. Likewise, the effect of downstream pressure on selectivity is shown in Figure 6.15 and the results depict an almost linear decrease of selectivity. The increase in downstream pressure results in decrease in flux. The decrease is more for water flux compared to hydrazine flux resulting in lower separation factor at higher downstream pressure.

6.4.3.4 Effect of Membrane Thickness

The effect of membrane thickness on permeate to feed flow ratio is shown in Figure 6.16. An exponential decay trend is observed. The ratio instantly decreases from 14×10^{-4} to 4.0×10^{-4} within a thickness of 20μm for shell side flow whereas this value in this range of membrane thickness changed from 7.2×10^{-4} to 1.8×10^{-4} for tube side flow. Such decrease is obviously because of higher diffusional resistance with increase in thickness.

There is not much effect of membrane thickness on selectivity values for shell side as well as for tube side feed flow, as shown in Figure 6.17. However, values of selectivity pass through maxima at 50 μm for the tube side feed flows and there is no maxima observed in the case of shell side feed flow. Ravindra et al. [2] found such a maxima value at 45 μm thickness; however, they had limited experimental data points in this zone.
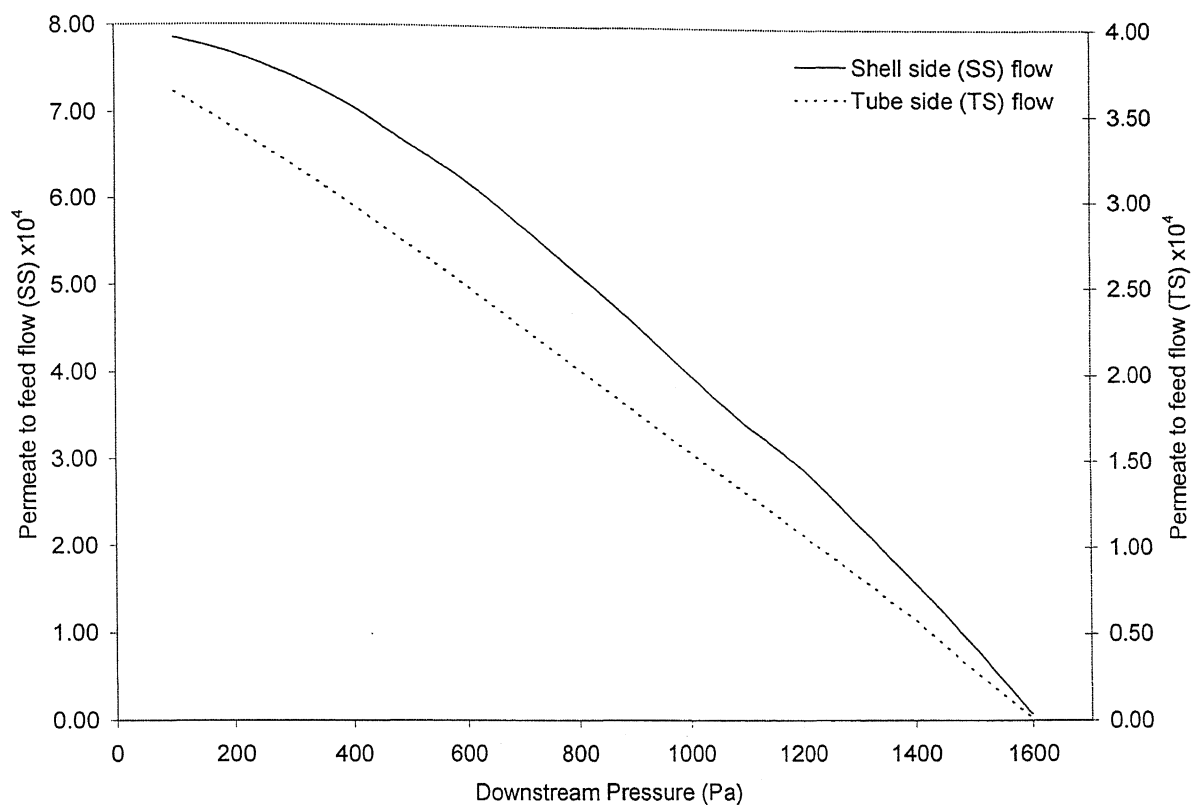
Figure 6.14 Influence of downstream pressure on permeate to feed ratio (ϕ)

(at $x_f = 50$ mole%; feed flow rate $= 2.77$ x 10^{-3} m^3/s; $t = 10$ μm; $L = 1$ m;

$r_{shell} = 0.3$ m; $r_{tube} = 750$ μm; $N = 40,000$)
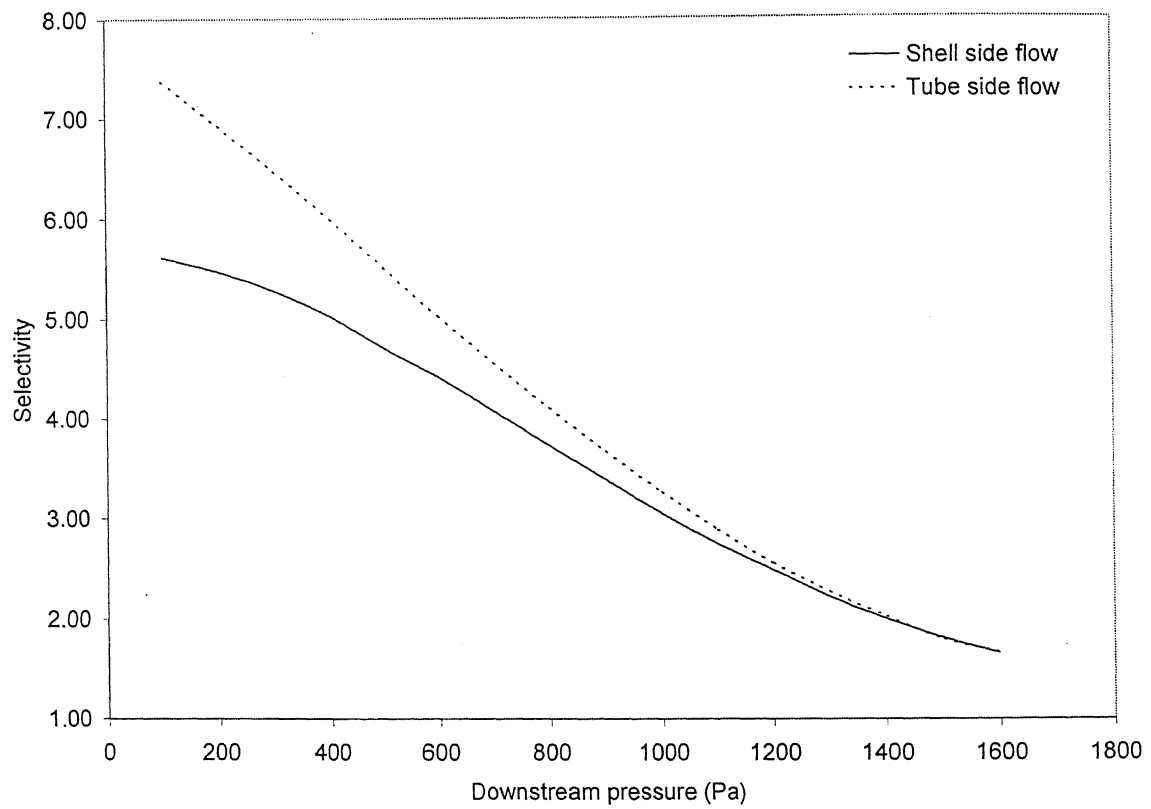
Figure 6.15 Influence of downstream pressure on selectivity

(at x_f = 50 mole%; feed flow rate = 2.77 x 10^{-3} m^3/s; t = 10 μm; L = 1 m;

r_{shell} = 0.3 m; r_{tube} = 750 μm; N = 40,000)
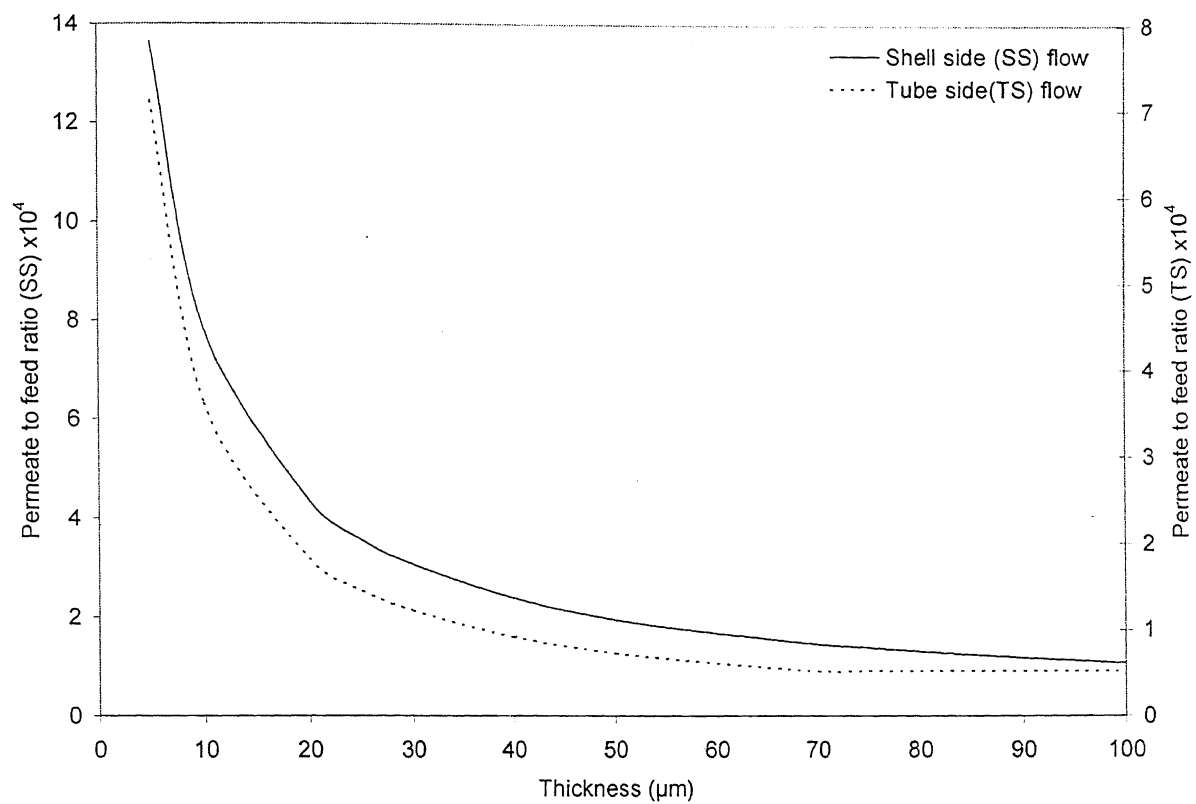
Figure 6.16 Influence of membrane thickness on permeate to feed ratio (ϕ)

(at x_f = 50 mole%; feed flow rate = 2.77 x 10^{-3} m^3/s; p= 100 Pa; L = 1 m;

r_{shell} = 0.3 m; r_{tube} = 750 μm; N = 40,000)
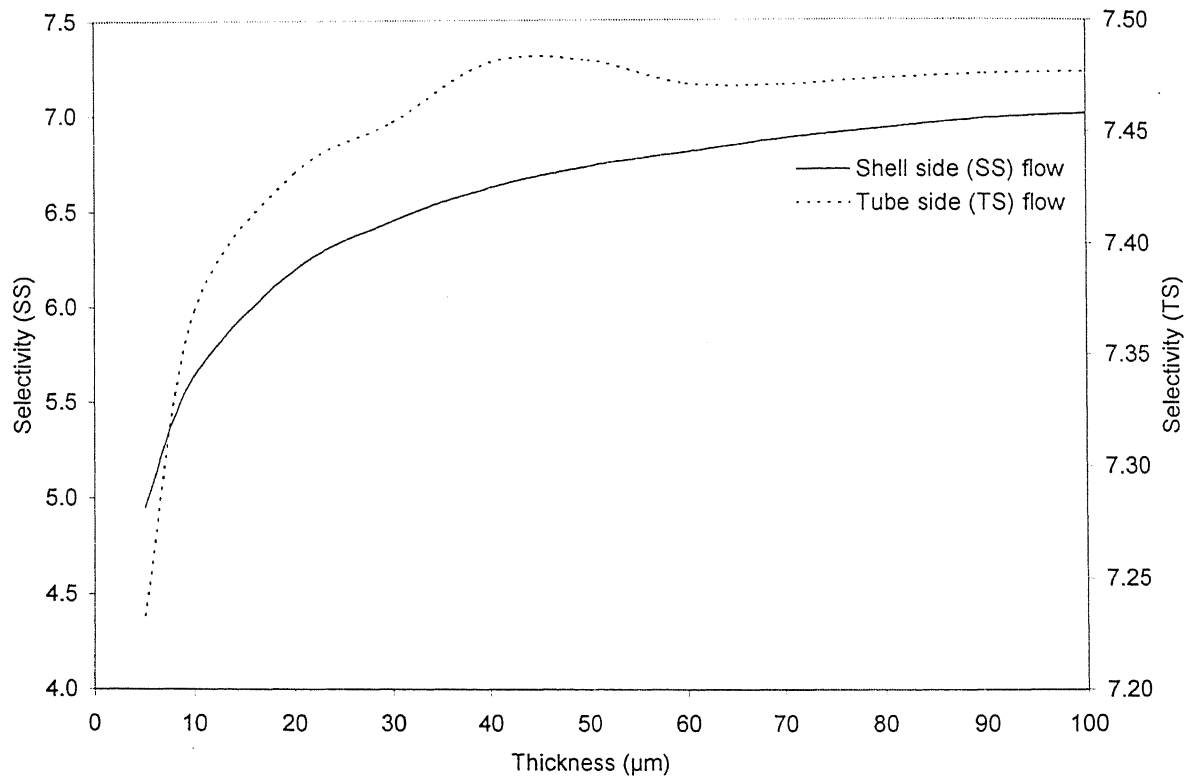
Figure 6.17 Influence of membrane thickness on selectivity

(at $x_f = 50$ mole%; feed flow rate $= 2.77 \times 10^{-3}$ m^3/s; p$= 100$ Pa; L $= 1$ m;

$r_{shell} = 0.3$ m; $r_{tube} = 750$ μm; N $= 40,000$)

6.5 Conclusions

Detailed mathematical formulations were derived, combining solution-diffusion model with mass, momentum and energy balances. Simulated results were obtained from developed models. The spatial property variations were observed in a hollow fiber module for hydrazine-water separation during pervaporation. For chosen conditions, the shell side feed flow operation was found to provide better selectivity and flux compared to tube side feed flow. However, the shell side feed flow was observed to be restricted (operational constraint). Simulated results depicted formation of azeotrope at 17.5 wt% water concentration for tube side feed flow, against azeotropic water concentration of 28.5 wt% as experienced by distillation. Results suggest use of better selective membrane or hybrid process for the separation of hydrazine water mixture.

M_c molecular weight between two cross-links (kg/mol)

N   number of tubes

n   molar flux (mol/m²s)

P   pressure (Pa).

P^{sat} saturation pressure (Pa)

p   downstream pressure (Pa)

Q   volumetric flow rate (m³/s)

R   universal gas constant (J/mol K)

R_{shell} radius of the shell (m)

R_{tube} radius of the tube (m)

Re   Reynolds Number $\left[= \dfrac{\rho_{sl} v d_{tube}}{\eta_{sl}} \right]$

Re_{max} Maximum Reynolds number $\left[= \dfrac{\rho_{sl} v d_{tube}}{\eta_{sl}} \dfrac{h_{tube}}{h_{tube} - d_{tube}} \right]$

r   radial coordinate for hollow fiber

Sc   Schmidt Number $\left[= \dfrac{\eta_{sl}}{\rho_{sl} D_{ij}} \right]$

Sh   Sherwood Number

T   temperature (K)

t   membrane thickness (m)

u   permeate velocity (m/s)

v   feed velocity (m/s)

V   molar volume (m³ /mol)

206

w   weight fraction

X   axial coordinate in solution – diffusion model

x   mole fraction in liquid phase.

y   mole fraction in vapor phase.

z   axial coordinate for hollow fiber

(0)   module entrance

(1)   module exit

Greek Letters

γ activity coefficient

χ Flory-Huggins Interaction Parameters

φ volume fraction in membrane.

μ Chemical Potential

η Viscosity (Pa-s)

ρ density (kg/m^3)

λ latent heat of vaporization (J/kgmol)

τ shear stress (Pa)

Δ differential increment

Subscripts

ap   applied

b   bulk

I   interface

i   water

in   inlet

j	hydrazine
l	Liquid phase mixture
m	membrane
p	polymer
r	radial component
o	reference state
s	mixture
v	vapor phase mixture
z	axial component

Superscripts

F	feed side
P	permeate side
n	location
-	average/molar
*	experimental

6.7 Appendix

6.7.A.1 Tube Side Feed Flow

6.7.A.1.1 Momentum Balance at Feed Side

The solution of the axial component of Naviers Stoke's equation under the lubricating assumption gives the feed side velocity and pressure equations. According to lubricating assumption [30] when liquid flows in long narrow channels or in thin films, they often have the characteristics of being unidirectional and dominated by viscous stress. The other terms in the Naviers Stoke's equation are neglected based on order of magnitude analysis. The solution is the 'z' component Naviers Stoke's equation, assuming pressure gradient to be independent of radial variation:

$$\frac{1}{\eta_{sl}}\frac{\partial P^F}{\partial z} = \frac{1}{r}\frac{\partial}{\partial r}\left[r\frac{\partial v_z}{\partial r}\right] \tag{6.A.1}$$

Further, following are the boundary conditions:

$$\text{Radial symmetry} \quad r = 0 \quad \frac{\partial v_z}{\partial r} = 0 \tag{6.A.2}$$

$$\text{No slip boundary condition} \quad r = R_{tube} \quad v_z = 0 \tag{6.A.3}$$

Therefore, the z component of velocity is obtained as:

$$v_z = -\frac{1}{4\eta_{sl}}\frac{dP^F}{dz}\left[R_{tube}^2 - r^2\right] \tag{6.A.4}$$

The feed side volumetric flow rate, Q is calculated as:

$$Q(z) = 2\pi \int_0^{R_{tube}} v_z r \, dr = -\frac{\pi}{8\eta_{sl}}\frac{dP^F}{dz}R_{tube}^4 \tag{6.A.5}$$

The radial averaged velocity, $\bar{v}_z$ is:

$$\overline{v}_z = -\frac{1}{8\eta_{sl}}\frac{dP^F}{dz}R^2_{tube}$$

(6.A.6)

The z component of velocity can now be rewritten as:

$$v_z = 2\overline{v}_z\left[1-\left\{\frac{r}{R_{tube}}\right\}^2\right]$$

(6.A.7)

The equation (6.A.6) can be rearranged to obtain eq (6.25). Further, the θ component of velocity is zero; the continuity equation under the assumption of incompressible fluid takes the form.

$$\frac{\partial v_z}{\partial z}+\frac{1}{r}\frac{\partial}{\partial r}\left[rv_r\right]=0$$

(6.A.8)

The radial component of velocity can be obtained by solving the above equation with the boundary condition:

at r=0, v_r=0

(6.A.9)

Hence, $$v_r = -2\frac{d\overline{v}_z}{dz}\left[\frac{r}{2}-\frac{r^3}{4R^2_{tube}}\right]$$

(6.A.10)

The radial component of velocity at r=R is equal to the permeation velocity and which is given by eq (6.26).

6.7.A.1.2 Mass Balance at Feed Side

Taking a feed side mass balance on the ith species over the differential element Δz as,

$$n_{iz}\big|_z\,\pi R^2_{tube}-n_{iz}\big|_{z+\Delta z}\,\pi R^2_{tube}-\frac{J_i\,2\pi R_{tube}\Delta z}{M_i}=0$$

(6.A.11)

Where, n_{iz} is the feed side component molar flux. By doing Taylor expansion,

$$\frac{dn_{iz}}{dz} = -\frac{2J_i}{R_{tube}M_i} \qquad (6.A.12)$$

The molar flux can be expressed as:

$$n_{iz} = \overline{\rho_{sl}} x_{ib}^F \overline{v_z} \qquad (6.A.13)$$

Further, the liquid molar density $\overline{\rho_{sl}}$ is given by:

$$\overline{\rho_{sl}} = \frac{1}{\left[\dfrac{M_i x_{ib}^F}{\rho_{il}} + \dfrac{M_j x_{jb}^F}{\rho_{jl}}\right]} = \frac{1}{V_{sl}} \qquad (6.A.14)$$

Substituting eqs A.13 and A.14 in eq A.12,

$$\frac{x_{ib}^F}{V_{sl}}\frac{d\overline{v_z}}{dz} + \overline{v_z}\frac{M_j}{\rho_{jl}}\frac{1}{V_{sl}^2}\frac{dx_{ib}^F}{dz} = -\frac{2J_i}{R_{tube}M_i} \qquad (6.A.15)$$

Rearranging eq (6.A.15), eq (6.27) may be obtained explicitly in terms of composition variation.

6.7.A.1.3 Energy Balance at Feed Side

The differential energy balance can be written as:

$$\rho_{sl}\overline{v_z}C_{p,sl}(T-T_0)\big|_z \pi R_{tube}^2 - \rho_{sl}\overline{v_z}C_{p,sl}(T-T_0)\big|_{z+\Delta z}\pi R_{tube}^2$$
$$-2\pi R_{tube}\Delta z J\left[\lambda_{sl} + C_{p,sl}(T-T_0)\right] = 0 \qquad (6.A.16)$$

Neglecting sensible heat due to small change in temperature of the feed mixture and assuming specific heat $C_{p,sl}$, latent heat λ_{sl}, liquid density ρ_{sl} and feed velocity $\overline{v_z}$ to be constant with temperature, eq (6.28) was obtained.

6.7.A.1.4. Momentum Balance: Permeate Side

The permeate side momentum balance can be written as [31]

$$\frac{dp}{dz} + \frac{d\tau_{zz}}{dz} + \frac{d(\rho_{sv}u^2)}{dz} = 0 \qquad (6.A.17)$$

Where τ_{zz} depends on fanning friction factor, f as:

$$\frac{d\tau_{zz}}{dz} = \frac{2f\rho_{sv}u^2}{D_e}\frac{D_{shell}}{L} \qquad (6.A.18)$$

Further, vapor mass density $\rho_{sv} = \frac{pM_{sv}}{RT^P}$. Where, M_{sv} average molecular weight of the permeate and it is calculated by:

$$M_{sv} = y_{ib}^P M_i + y_{jb}^P M_j \qquad (6.A.19)$$

Substituting τ_{zz}, ρ_{sv}, M_{sv} in (6.A.17) and expansion of the derivative produces:

$$\left[M_{sv}u^2 + RT^P\right]\frac{dp}{dz} + 2M_{sv}pu\frac{du}{dz} + pu^2\left[M_i - M_j\right]\frac{dy_{ib}^P}{dz} = -\frac{2f\rho_{sv}u^2}{D_e}\frac{2R_{shell}}{L}RT^P \qquad (6.A.20)$$

6.7.A.1.5 Mass Balance: Permeate Side

The overall mass balance on the permeate side can be written as:

$$\rho_{sv}u\Big|_z \pi R_{shell}^2 - \rho_{sv}u\Big|_{z+\Delta z}\pi R_{shell}^2 + JN2\pi R_{tube}\Delta z = 0 \qquad (6.A.21)$$

After Taylor expansion and substitution of ρ_{sv}, the following expression is obtained:

$$\frac{d}{dz}\left[\frac{pu\left\{M_i y_{ib}^P + M_j(1-y_{ib}^P)\right\}}{RT^P}\right] = \frac{2J}{R_{shell}^2}NR_{tube} \qquad (6.A.22)$$

On further simplification, eq A.22 can be written as:

$$M_{sv}u\frac{dp}{dz} + pM_{sv}\frac{du}{dz} + pu\left[M_i - M_j\right]\frac{dy_{ib}^P}{dz} = \frac{2J}{R_{shell}^2}NR_{tube}RT^P \qquad (6.A.23)$$

Similarly, the molar species balance yields the following equation:

$$\frac{d}{dz}\left[y_{ib}^P \overline{\rho_{sv}} u\right] = \frac{2J_i}{R_{shell}^2 M_i} NR_{tube} \tag{6.A.24}$$

Where, the molar density, $\overline{\rho_{sv}} = \frac{p}{RT}$. On substituting $\overline{\rho_{sv}}$ and expanding, the following equation is obtained.

$$y_{ib}^P u \frac{dp}{dz} + y_{ib}^P p \frac{du}{dz} + pu \frac{dy_{ib}^P}{dz} = \frac{2J_i}{R_{shell}^2 M_i} NR_{tube} RT^P \tag{6.A.25}$$

The eqs (6.A.20), (6.A.23), and (6.A.25) is simplified using matrix inversion such that each equation contains a single derivative, providing eqs (6.30), (6.31), and (6.32).

6.7.A.2 Shell Side Feed Flow

Momentum, mass, and energy balances were derived similar to the procedure described above for tube side flow.

References

[1] E.W.Schmidt, "Hydrazine and its derivatives Preparation, Properties, Applications," John Wiely & Sons, 1984, New-York.

[2] R. Ravindra, S. Sridhar, A.A. Khan, Separation studies of hydrazine from aqueous solution by pervaporation, J. Polymer Sci., 37 (1999)1969

[3] A.Duggal, E.V.Thompson, Dependence of diffusive permeation rates and selectivities on upstream and downstream pressures V1. Experimental results for the water/ethanol system, J. Membrane Sci., 27(1986) 13-30.

[4] M.Wessling, U.Werner, S.-T. Hwang, Pervaporation of aromatic C_8-isomers, J. Membrane Sci., 57 (1991) 257-270.

[5] S. Matsui, D.R. Paul, Pervaporation separation of aromatic/aliphatic hydrocarbons by crosslinked poly(methyl acrylate-co-acrylic acid) membranes, J. Membrane Sci., 195 (2002) *229-245*.

[6] E. E. B. Meuleman, J. Willemsen, M. H. V. Mulder, H. Strathaman, EPDM as a selective membrane material in pervaporation, J. Membrane. Sci. 188 (2001) 235-249

[7] U. Sander, P. Soukup, Design and operation of a pervaporation plant for ethanol dehydration, J. Membrane Sci. 36 (1988) 463-475

[8] T. Asada, Dehydration of organic solvents, some actual results of pervaporation plants in Japan. Communication. Third. Intern. Conference on pervaporation processes in the chem.. Industry. Nancy, France. Sept.19-22, 1988.

[9] R.Q. Wilson, H.P Munger, J.W. Clegg, Vapour- Liquid equilibrium in the binary system hydrazine/water, Chemical Eng. Progr., Symp. Series, 3 (1952) 115-117.

[10]   J.P. Brun, C. Larchet, G. Bulvestre, B. Auclair, Modeling of the pervaporation of binary mixtures through moderately swelling, non reacting membranes, J. Membrane Sci. 23 (1985) 257.

[11]   B. Cao, M. A. Henson, Modeling of Spiral wound pervaporation modules with application to the styrene/ethylbenzene mixtures, J. Membrane Sci., 197 (2002) 117-146.

[12]   E. E. B. Meuleman, B. Bosch, M. H. V. Mulder, H. Strathmann, Modelling of liquid/liquid separation by pervaporation: Toluene from water, *AIChE,* 45 (1999) 2153-2160.

[13]   X. Feng, R. Y. M. Huang., Liquid separation by membrane pervaporation, a review, Ind. Engg. Chem. Res. 36 (1997) 1048

[14]   R., O. Crowder, E. L. Cussler, Mass Transfer resistance in hollow fiber pervaporation, J. Membrane Sci., 173 (1998) 145.

[15]   J. Bausa, W. Marquardt, Shortcut design methods for hybrid membrane/distillation processes for the separation of nonideal multicomponent mixtures, Ind. Eng. Chem. Res, 39 (2000) 1658-1672.

[16]   P. J. Hickey, C. H. Gooding, Modeling spiral-wound membrane module for the pervaporation of volatile organic compounds from water, J. Membrane Sci., 88 (1998) 47.

[17]   X. Feng, R.Y.M. Huang, Permeate pressure build-up in shell side fed hollow fiber pervaporation membranes, Can. J. Chem. Eng., 73 (1995) 833.

[18] S.V. Satyanarayana, P.K. Bhattacharya, Real coded genetic algorithm for optimization of pervaporation process parameters for removal of volatile organics from water, Ind. Engg. Chem. Res. 42(13) (2003) 3118-3128.

[19] J. Sheng, J.C. Mora, Pervaporation and dehydration of water-ethanol mixtures by mean of cuprophon hollow fiber membranes, Desalination, 71 (1991) 80.

[20] W. Kazunori, K. Sunao, Pervaporation performance of Hollow Fiber chitosan polyacrylonitrile composite membrane in dehydration of Ethanol, J. Chem. Eng. Japan, 17 (1992) 25.

[21] E.L Cussler, Diffusion : Mass transfer in Fluid Systems, Cambridge University Press, First south Asian Edition, New Delhi, 1998.

[22] J.M.Prausnitz, R.N. Lichtenthaler, E.G. Azevedo, Molecular thermodynamics of Fluid-Phase Equilibria, Prentice-Hall, Englewood Cliffs, NJ, 1986.

[23] P.J. Flory, Principles of polymer chemistry, Cornell University Press, Ithaca, New York, 1953.

[24] J.M. Smith, H.C. Van Ness, M.M. Abbott, Introduction to chemical engineering thermodynamics, McGraw-Hill: New York, 1996 (Fifth edition).

[25] R. H. Perry, D. Green, Perry's Chemical Engineers' Hand Book, Sixth edition, McGraw Hill, New York, 1984.

[26] M.H.V. Mulder, T. Franken, C.A. Smolders, Preferential sorption versus preferential permeability in pervaporation, J. Membrane Sci., 22 (1985) 155.

[27] R. Ravindra, S. Sridhar, A.A. Khan, A. K. Rao, Pervaporation of water, hydrazine and monomethylhydrazine using ethyl cellulose membranes, J. Polymer Sci., 41 (2000) 2795.

[28] M. Fels, R.Y. M. Huang, Diffusion coefficients of liquids in polymer membranes by a desorption method, J. Applied Polymer Sci., 14 (1970) 523-536.

[29] M.H.V. Mulder, C.A. Smolders, On the mechanism of separation of ethanol/water mixtures by pervaporation: I. Calculation of concentration profiles, J. Membrane Sci., 17 (1984) 289.

[30] W.H. Deen, Analysis of Transport Phenomena, Oxford, NewYork, NY, 1998.

[31] R.B.Bird, W.E. Stewart, E.N. Lightfoot, Transport Phenomena, John Wiley & Sons: New York, 1960.

[32] Q.T. Nguyen, A. Maazous, R. Clement, Azeotropic points in pervaporation: A physico-chemical phenomena or an apparent behaviour. Abstracts of the 1987 International congress on membranes and membrane processes, Tokyo (Japan), June 8-12, 1987, 9(31), 572-573.

[33] G.F.Tusel, H.E.A. Bruschke, Use of pervaporation systems in the chemical industry, Desalination, 53 (1985) 327-38.

[34] R. Rautenbach, C. Herion, M. Franke, Abdul-Fattah, A. Asfour, M. Bemquerer-Costa and E. Bo, Investigation on mass-transport in asymmetric pervaporation membranes, J. Membrane Sci., 36 (1988) 445-462.

[35] R. Bakish, W. Schneider; Modelling of transport phenomena in pervaporation membranes. Proceedings of the first Intern. Confer. on pervaporation processes in the Chem. Ind. Atlanta, Georgia, U.S.A. 23-26, 1986. Edited by Bakish materials corporation, Englewood, N.J. 07631, U.S.A, 133-141.

Chapter 7

Real Coded Genetic Algorithm for Optimization of Process Parameters for Removal of Volatile Organics from Water

7.1 Introduction

Volatile organic compounds (VOCs) released from process industries create serious water and air pollution problems. Conventional processes like air stripping, carbon adsorption, chemical oxidation, incineration, etc., are found [1] to be partially successful; particularly, when the concentration of the VOCs is very low in contaminated stream and quantity of effluent is large. Pervaporation is fast emerging as a viable unit operation for the separation of organic components present in water. The process may not only address the problem of pollution, it may also recover valuable organics. The term "volatile organic compound" generally refers [2] to organic compounds which have boiling points less than 100°C and /or vapour pressures greater than 1mm Hg at 25°C. Water treatment applications are reported [3] to use membranes made of organophillic polymers, such as silicone-rubber. Such membranes exhibit high permeability for organic compounds while restricting passage of water. Therefore, VOCs in permeate may be present by orders of magnitude compared to water. The concentrations of VOCs in permeate may often cross beyond their solubility limits which during condensation may separate into an aqueous and an organic phase,

facilitating an easier possibility of recovering the organic fractions. Further, during pervaporation, the presence of multi-components may be advantageous due to sharing of downstream pressure by all components [4] which in turn increase their permeation. Whereas in contrast, during carbon adsorption, removal efficiency is reduced due to competitive adsorption [5] and limited activated sites for multi-component VOC's - water mixture.

Commercialization of multi-component pervaporation process requires a thorough study of many factors that affect the process performance. These are downstream pressure, membrane thickness, Reynolds number, feed concentration and effluent flow rate, etc. The present study has been undertaken to extend the work of Ji et al. [4] for optimization of process variables of pervaporation. A shell and tube heat exchanger type of hollow fiber module was adopted for the purpose. The feed was considered to be a mixture of toluene (Tol), 1, 1, 1-trichloroethane (TCE) and methylene chloride (MC) in water. Optimum parameters were estimated for 90% toluene removal without recycling the permeate. Genetic algorithm was applied for the solution of this complex, nonlinear multivariable optimization problem as there were more chances to obtain true global minima [6] with this technique. Whereas, Ji et al[4] used the Powell's technique to optimize a particular process variable (keeping other variables fixed) for single component system (i.e. water -toluene). Powell's method works on single variable search method [7] and there is no guarantee for true global minima for multivariable problem.

The conventional optimization methods generally are associated with disadvantages like: i) convergence dependency on the initial solution, (ii) getting stuck to a suboptimal solution, (iii) separate algorithm for each problem, (iv) inefficient for discrete search space problems, (v) inefficient for simultaneous use on parallel machine,

(vi) point by point approach, and (vii) requirement of unimodel or multimodel assumption. Genetic algorithms (GA) overcome these disadvantages. Further, GAs are suitable for parallel implementations. In real optimization problems, most computational time is spent in evaluating solutions; with multiple processors overall computational time may get reduced substantially [7].

A genetic algorithm [6] is a non-traditional search and optimization method and finding important applications in engineering optimization. It mimics the principles of genetics and the Darwinian principles of natural selection (i.e. survival of the fittest). Further, genetic algorithm is a computer simulation which works on the constant size of population of individuals, called search space. The initial population of individuals are stochastically selected, recombined, mutated and either eliminated or retained, based on their relative fitness. This algorithm finds applications where exist discontinuities and vast multimode noise search space. A simple genetic algorithm mainly consists of three operators: Reproduction, Crossover, and Mutation. Initially, in an initial population, individuals are generated randomly. Each individual is evaluated according to the fitness function (objective function). Then reproduction operation is carried out by choosing individuals according to their relative fitness. High fitness individuals are selected more number of times, which is proportional to the relative performance. Reproduction alone cannot introduce any new individual into the population. Crossover and mutation operations are performed to generate new individuals.

The crossover operator is believed to be the main search operator and the purpose of this operator is two fold. Initially random strings, representing the problem variables, are searched thoroughly. Good portions of these strings are then combined to form better strings. Thus, crossover operation is carried out between two strings and is called 'parents'. Two new strings are formed by the exchange of substrings between

'parents' and are called 'children'. The children produced may or may not be good compared to parents, depending on whether or not the crossing site falls in appropriate place. Hence, every crossover may not create better solutions but this may also not cause problem. If bad children are created, they will be eliminated in the next reproduction operation and hence will have a short life. On the other hand, if good children are produced, it is likely to get multiplied in the next reproduction operation. Thus, this operation tends to enable the evolutionary process to move towards 'promising' region on the search space. This is exactly similar to the biological process where complex life forms from the simple ones [8]. Now, considering two parents which are represented by 01101011 and 00111101; if a single point crossover operator with the crossover site falls along the string length at fourth site (randomly selected) then, two children is produced and the process is described below.

0110:1011   0111:1101

                        ───────────►

0011:1101   0010:1011

'Parents'   'Children'
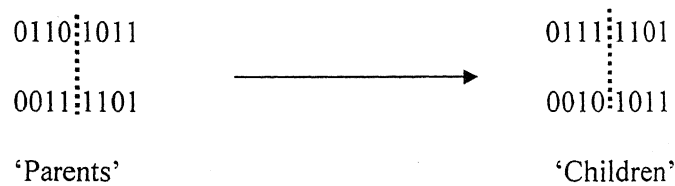
Mutation operation is similar to the crossover operator and provides the new strings in the sample by changing the value of the variable. Mutation operation keeps the diversity and prevents premature convergence to local optima. Further, it creates a point in the neighbourhood of the current point, thereby achieving local search around the current solution. Both the parents considered above are having '0' in the left position. If the true optimum solution requires '1' in that position, then neither reproduction nor crossover operation will be able to create '1' in that position. In this case the mutation operation provides the required change by replacing '0' to '1'.

In binary coded genetic algorithm, string length depends on the precision. For higher precision, the string length and population size requirement is more [9],

increasing the computational complexity. Further, fixed coding scheme is used to code the decision variables and the bounds; variable bounds must be such that they bracket the optimum variables. In many problems, this information is not known *apriori*. Hence, in this work we have used real coded genetic algorithm. Real parameters are used directly and optimization is easier when compared to binary coded GAs. However, in this case the main problem arises how to use a pair of real parameters to create a new pair of offspring and how to perturb a variable for the mutation? Herreara et al. [10] have provided a good overview of many real parameters used for crossover and mutation operators.

In the present work, the real coded genetic algorithm consists of tournament selection method[11], simulated binary crossover [12, 13] and polynomial mutation [14] operators. The simple genetic algorithm flow chart is given in the Figure 7.1. In real coded genetic algorithm, the difference between the crossover and mutation lies in the number of parent solutions used in the perturbation [9]. If only one parent is used then it is mutation and for more than one parent it is crossover. Further, perturbation is predefined in case of mutation and range of perturbation is adaptive in the case of crossover.

The main objective of the present work is to apply real coded genetic algorithm to single component system and compare the obtained results with values reported by Ji et al. [4]; then, extending the method for multi-component system. Further, for both systems, i.e. single and multi components, global optimum points were obtained.
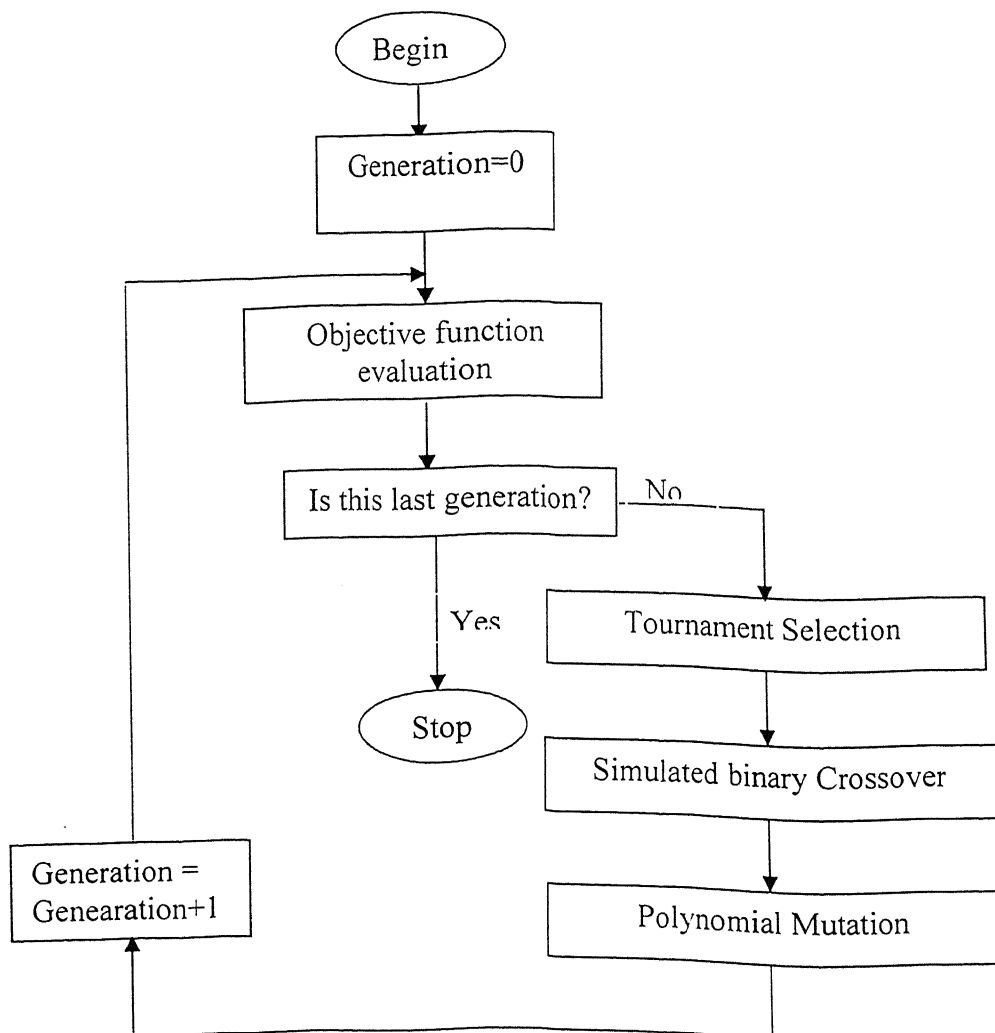
Figure 7.1 Flow chart of genetic algorithm

7.2 Theory

7.2.1 Process Model

7.2.1.1 Mass Balance

The formulations were taken from literature [4] which were developed for single component system. Therefore, for multi-component system, formulations were modified. The total feed, if subjected to hollow fiber may be divided into two flows: retentive flow and permeate flux.

Overall Mass balance:

$$-\rho dq = N dA_m \tag{7.1}$$

For organic compound, (i=1,2...i)

$$d(qC_i) = -N dA_m \tag{7.2}$$

Rearranging eq (7.1) & (7.2),

$$q \frac{dC_i}{dA_m} = \frac{C_i N}{\rho} - N \tag{7.3}$$

7.2.1.2 Permeation Flux

The organic flux can be expressed [5] in terms of overall mass transfer coefficient,

$$N_i = K_i(C_i - \frac{p_i}{H_i}) = K_i(C_i - \frac{py_i}{H_i}) \tag{7.4}$$

For pervaporation of dilute solution, liquid boundary mass transfer resistance for water is negligible. Hence,

$$N_w = L_{p,w}\left(\frac{p_w^0 - p_w}{l}\right) = L_{p,w}\left(\frac{p_w^0 - py_w}{l}\right) \tag{7.5}$$

and

$$N = \Sigma N_i + N_w \qquad \text{(where } i = 1, 2, 3) \tag{7.6}$$

7.2.1.3 Overall Mass Transfer Coefficient

According to resistance-in-series model, the total resistance is the sum of the boundary layer resistance, membrane resistance and vapor phase resistance. Generally vapour phase resistance is negligible in comparison to other two resistances [15], hence,

$$\frac{1}{K_i A_m l} = \frac{1}{k_{l,i} A_F l} + \frac{1}{L_{P,i,m} H_i A_m}$$ (7.7)

For $Re < 2100$, k_l can be calculated from Leveque equation [16],

$$Sh = 1.62 \, Re^{0.33} \, Sc^{0.33} \left[\frac{2r_i}{L}\right]^{0.33}$$ (7.8)

For $Re > 4000$,

$$Sh = 0.026 \, Re^{0.80} \, Sc^{0.33}$$ (7.9)

Further, eq (7.7) may be written as,

$$\frac{1}{K_i l} = \frac{1}{k_{l,i} r_i \ln(r_o/r_i)} + \frac{1}{L_{P,i,m} H_i}$$ (7.10)

Therefore,

$$K_i l = \frac{L_{P,i,m} H_i}{E_i + 1}$$ (7.11)

where, $E_i = \dfrac{L_{P,i,m} H_i}{k_{l,i} r_i \ln(r_o/r_i)}$ (7.12)

Substituting eq (7.11) into eq (7.4),

$$N_i = \frac{L_{P,i,m}(C_i H_i - p_i)}{(E_i + 1)l} = \frac{L_{P,i,m}(C_i H_i - py_i)}{(E_i + 1)l}$$ (7.13)

Further, substituting eq (7.5), (7.6) & (7.13) into eq (7.1) and eq (7.3), respectively as,

$$\frac{1}{2\pi} \frac{dq}{dz} = -\sum_{i=1}^{3} \frac{L_{P,i,m}}{(E_i + 1)} \frac{(x_i H_i - py_i/\rho)}{\ln(1 + l/r_i)} - \frac{L_{P,w}}{\rho} \frac{(p_w^0 - py_w)}{\ln(1 + l/r_i)}$$ (7.14)

$$\frac{q}{2\pi}\frac{dx_i}{dz} = x_i \left[\sum_{j=1}^{3} \frac{L_{P,i,m}}{(E_i+1)} \frac{(x_iH_i - py_i/\rho)}{\ln(1+l/r_i)} + \frac{L_{P,w}}{\rho} \frac{(p_w^0 - py_w)}{\ln(1+l/r_i)} \right] - \frac{L_{P,i,m}}{(E_i+1)} \frac{(x_iH_i - py_i/\rho)}{\ln(1+l/r_i)}$$

(7.15), (7.16), (7.17)

The above expressions were obtained in terms of three equations (eq 7.15, 7.16 & 7.17) for i=1,2,3. Solving eqs (7.14) to (7.17), the variation of flow rate, concentration of components along the axial direction of fiber for a given feed flow rate and inlet concentrations of components may be obtained.

7.2.2 Cost Model

7.2.2.1 Capital cost

Capital cost is estimated using the *Hand-Guthrie Bare Module Method* [17]. The bare module (BM) cost includes all the expenses incurred in creating a working unit and all auxiliary piping, instruments and support within the unit. This cost also includes freight duties, taxes and engineering expenses. The major equipment required for pervaporation process is the membrane module, feed pump, vacuum pump and condenser. So the total capital cost may be estimated by,

$$\alpha_{capital} = b_{mod}(\alpha_m + \alpha_{mod} + \alpha_{feedpump} + \alpha_{vacuumpump} + \alpha_{condensor}) \quad (7.18)$$

Assuming, a suggested [18] price of $100/m^2 for a commercial hollow fiber membrane,

$$\alpha_m = 100A_m \quad (7.19)$$

Whereas, cost of $100/m^2 for a typical hollow fiber membrane module may be taken [5] and hence,

$$\alpha_{mod} = 100A_m \quad (7.20)$$

Further, cost of feed pump may be estimated [17] as,

$$\alpha_{feedpump} = 26,700(24*3600q/50,000)^{0.53} \quad (7.21)$$

Similarly, cost of vacuum pump was estimated [17] as,

$$\alpha_{vacuumpump} = 4,200(60GRT_o/P_o)^{0.55} \tag{7.22}$$

where, T_o and P_o are standard temperature and pressure. Cost of permeate condenser was calculated from the cost of carbon steel shell and tube condenser [17], where the condenser tube length was 3.66m. Accordingly,

for $0 < A_{condensor} < 22.30$,

$$\alpha_{condensor} = 1176.7 + 128.1 A_{condensor} \tag{7.23}$$

where,

$$A_{condensor} = \frac{\sum\limits_{j=1}^{4} G_j \left[(\Delta H)_j + C^v_{p,j} (\Delta T)_P \right]}{U (\Delta T)_F} \tag{7.24}$$

The value of U was taken [19] to be 9.52×10^{-3} kJ/sm^{2}K for streams condensed by Ammonia.

7.2.2.2 Treatment Cost

The treatment cost (TC) was estimated, based on four aspects; 1) Capital Depreciation (CD), 2) Maintenance and labour requirement (ML), 3) Membrane replacement (MR), and 4) Energy Consumption (EC).

$$\alpha_{TC} = {}^{(Fr)}CD \, \alpha_{capital} + {}^{(Fr)}ML \, \alpha_{capital} + \alpha_{MR} + \alpha_{EC} \tag{7.25}$$

To cover depreciation and taxes (CD), a value [19] of 15% of installed total capital cost was assumed. The annual maintenance and labour costs were taken [19] to be 10% of the total capital cost. Further, a membrane life of three years [18] was assumed. Therefore,

$$\alpha_{MR} = 100 A_m/3 \tag{7.26}$$

Energy consumption consists of pumping feed, vacuum pumping and vapour condensation. Therefore,

$$\alpha_{EC} = (e)t \left[\frac{W_F}{\eta_F} + \frac{W_{vaccum}}{\eta_{vaccum}} + \frac{W_{condensor}}{\eta_{condensor}} \right] \tag{7.27}$$

where, W_F is power for the feed pump and it was taken [20] as the product of flow rate q and flow pressure drop Δp,

$$W_F = q\Delta p \tag{7.28}$$

In pervaporation, downstream pressure was maintained by efficient condensation of permeate. The condensation temperature controls the downstream pressure. Due to limited solubility of organics in water, permeate may be obtained in two phases. Further, it was assumed that equilibrium was reached among vapour organics and aqueous phases, therefore,

$$f_i^v = f_i^l \tag{7.29}$$

$$\Sigma p_i(T) = \Sigma p_i^O \gamma_i^\infty x_i = \Sigma p_i^O y_i^{org} \tag{7.30}$$

$$p_w \approx p_w^O \tag{7.31}$$

$$p = \sum_i p_i(T) + p_w(T) \approx \sum_i p_i^O(T) y_i^{org} + p_w^O(T) \tag{7.32}$$

A vacuum pump was used to remove the inert gas and assumed to operate at 10% of the total operating time. The work done by the vacuum pump is therefore,

$$W_{vaccum} = 0.1 G \frac{k}{k-1} RT \left[\left(\frac{P_o}{p} \right)^{\left[k - \frac{1}{k} \right]} - 1 \right] \tag{7.33}$$

Further, energy balance on the condenser gives the energy consumption,

$$W_{condensor} = \sum_{j=1}^{4} \left[G_j((\Delta H)_j + C_{P,j}^v (\Delta T)_P) \right] \tag{7.34}$$

Hence, including all the cost equations (from 7.18 to 7.34, excluding 7.25) along with the standard data were put into eq (7.25). Thus, the treatment cost equation was

obtained. Therefore, in eq (7.25), treatment cost becomes function of inlet flow rate, Reynolds number, downstream pressure, permeate flow rate and membrane area. Further, membrane area and permeate flow rate are functions of membrane thickness, feed concentration, downstream pressure, Reynolds number and removal fraction (defined as the concentration difference between the inlet and outlet of the module to the inlet concentration). A single objective treatment cost equation thus obtained was minimized.

It may be stated at this point that according to Deb [9], if a relative preference among the objectives is known for a specific problem, there is no need to formulate and solve a multi objective optimization problem. A simple weighted sum approach can be adopted for such cases. Therefore, a single objective function was utilized for the present work as the main objective is to study the optimization of process variables for multi-component system. However, one may attempt to solve a multi objective function to find multiple pareto-optimal solutions, depending upon the situation. For example, if one of the costs being more significant or dominating than others (like energy over other costs which may be relevant depending upon the availability of exact membrane plant data, geographical location, etc.), then multi-objective approach may be applied.

7.3 Solution Technique and Optimization

The main objective is to minimize treatment cost subjecting to the operating variables (q, Re, l, p, x_i) to the following selected minimum and maximum values:

$2.77*10^{-3} < q < 5.77*10^{-3}$

$20 < Re < 7000$

$-5*10^{-6} < l < 10^{-4}$

$0.2 < p < 4.0$

$2*10^{-6} < x_{Tol} < 9.8*10^{-5}$

$$2*10^{-6} < x_{TCE} < 9.7*10^{-5}$$

$$2*10^{-6} < x_{MC} < 4.01*10^{-3}$$

The minimum and maximum values were chosen in such a way that the values below and above of those become practically insignificant during pervaporation. For example, maximum toluene concentration chosen in the effluent is the solubility limit of toluene in water, i.e. 500ppm ($x_{Tol}=9.8*10^{-5}$). Poly (dimethylsiloxane) membrane was chosen for the separation and permeabilities of different species were taken from literature [3] which are given in Table 7.1. Toluene removal fraction of 0.9 was assumed. Binary diffusion coefficients of organic components in water were estimated [21] from Wilke-Chang equation and are given in Table 7.2. Vapour pressures were calculated [22] from Antoine's equation.

Calculation of treatment cost requires membrane area, total and individual permeate fluxes. The differential eqs (7.14 to 7.17) were solved by a fourth-order Runga-Kutta method [23]. However, evaluation of the right hand side of the differential equation required permeate compositions which were calculated by dividing eq (7.4) with eq (7.5) and using $\sum y_i = 1$. The resultant algebraic equations were solved using Newton–Raphson technique [23], considering hollow fiber module to be series of mixed elements. Accordingly, the permeate stream composition and permeate flow rate were calculated for each element. Further, mass balance equations gave the feed stream composition of the second element. The procedure was repeated until 90% reduction of toluene concentration was achieved. Now to optimize the process variables, a real coded genetic algorithm was used. The bounds of variables are directly specified in genetic algorithm program. The computations were performed on the *Linserv, Red Hat 7.0 release* modified *UNIX* operating system (useful for parallel programming under

Table 7.1 PDMS membrane permeability for feed components [3] (T=30°C).

Compound	Permeability (10^{-8}) mol-m/m^{2}kPa s
Toluene	5.28
Trichloroethane	1.58
Methylene Chloride	1.82
Water	2.32

Table 7.2 Physical properties of feed components (T=30°C).

Compound	Heat Capacity J/mol K	Heat of Vaporization kJ/mol	Henry's Constant kPa m^3/mol	Diffusion Coefficient (10^{-9}) (m^2/s)
Toluene	157.44	37.56	0.7358	1.97
Trichloroethane(1,1,2)	145.09	37.65	2.1115	2.56
Methylene Chloride	128.35	28.54	0.1181	2.57
Water	34.25	43.76	-	-

Linux with specifications: *Proliant* ML350 P III, 800 MHZ processor, Dual CPU, 128 MB RAM). The CPU time was around 4 hours.

7.4 Results & Discussion

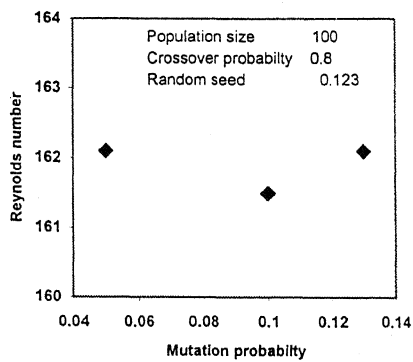### 7.4.1 Genetic Algorithm Parametric Study

Genetic algorithms are stochastic optimization techniques. Population size, crossover probability, mutation probability and random seed may affect the optimum values. Figure 7.2 (a, b, c, & d) shows the effect of these parameters on optimized Reynolds number in a multi-component system. These plots (Figure 7.2 a, b, c & d) have been depicted for optimized Reynolds number against population size, crossover probability, mutation probability and random seed, respectively. It is clear that these variables do not affect the optimized Reynolds number. However, there is marginal effect of population size on the Reynolds number. As the population size increases, optimum Reynolds number also increases. Generally, it is believed [9] that the bigger population size will provide better optimum results. Harika et al. [24] have provided certain general steps for the selection of population size. It can be further observed from Figure 7.2d; as the random seed is changing from 0.123 to 0.500, the optimum Reynolds number is varying, however in marginal numbers. This study clearly shows that there is not much effect of GA parameters on obtained optimum value for this optimization problem. Therefore, fixed GA parameters were used for present work. Parameters used for the study are given in Table 7.3. Earlier [25, 26] also, fixed GA parameters were used to solve chemical engineering optimization problems. However, a caution has to be taken, even for a simpler problem, that any choice of arbitrary parameter setting may not necessarily work well. Qi and Palmieri [27] systematically studied the effect of GA parameters on different problems.
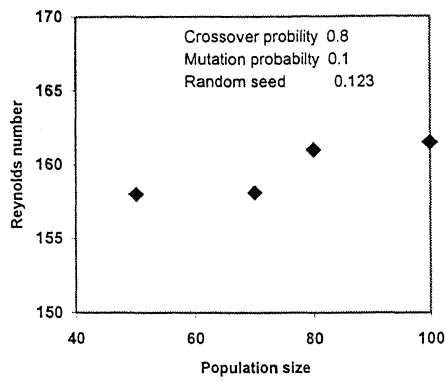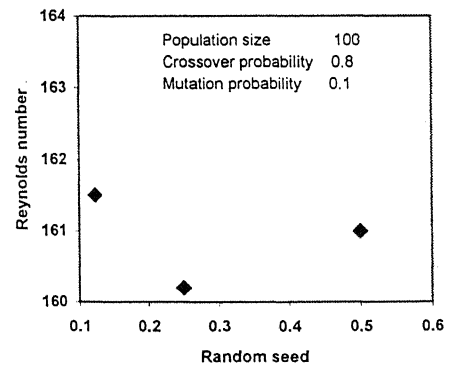
(a)
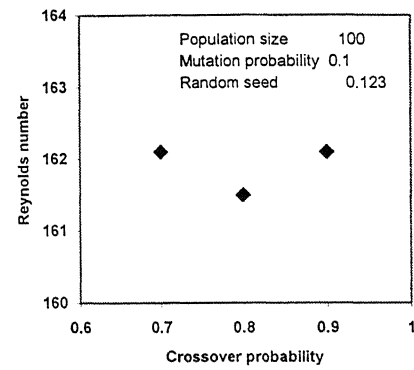
(b)

(c)

(d)

Figure 7.2 Effect of genetic algorithm parameters on Reynolds number in multi-component system (a) population size (b) crossover probability (c) mutation probability (d) random seed

Table 7.3 Selected Computational Parameters of Real Coded Genetic Algorithm

No of Variables	7
Population size	100
Maximum generations	50
Distribution index for crossover	10
Distribution index for mutation	10
Cross over probability	0.800
Mutation probability	0.100
Random seed	0.123

7.4.2 Single Organic Component System

7.4.2.1 Effect of Process Parameters

Optimization of process variables for single organic component system using real coded genetic algorithm was carried out and the results were compared to the values obtained by Ji et al [4]. Figure 7.3 shows the effect of Reynolds number on treatment cost for 90% toluene removal from 500 ppm feed toluene solution using 100μm fiber diameter. The optimum Reynolds number was estimated to be 230, close to the value of 250, obtained by Ji et al. [4]. The difference may be due to the new optimization technique and the properties used. For the full range of *Re* studied inset of Figure 7.3 may be referred. Figure 7.4 shows the effect of Reynolds number on treatment cost in the turbulent region. The treatment cost increases with increase in Reynolds number which may be due to increase in feed pumping costs. The global optimum was found in the laminar region. Similar conclusions were also made by them [4]. Distribution of various costs at optimum points is given in Table 7.4. Figure 7.5 shows the effect of Reynolds number on treatment cost for a fiber diameter of 400μm. Increasing the fiber diameter, the liquid film mass transfer coefficient decreased and
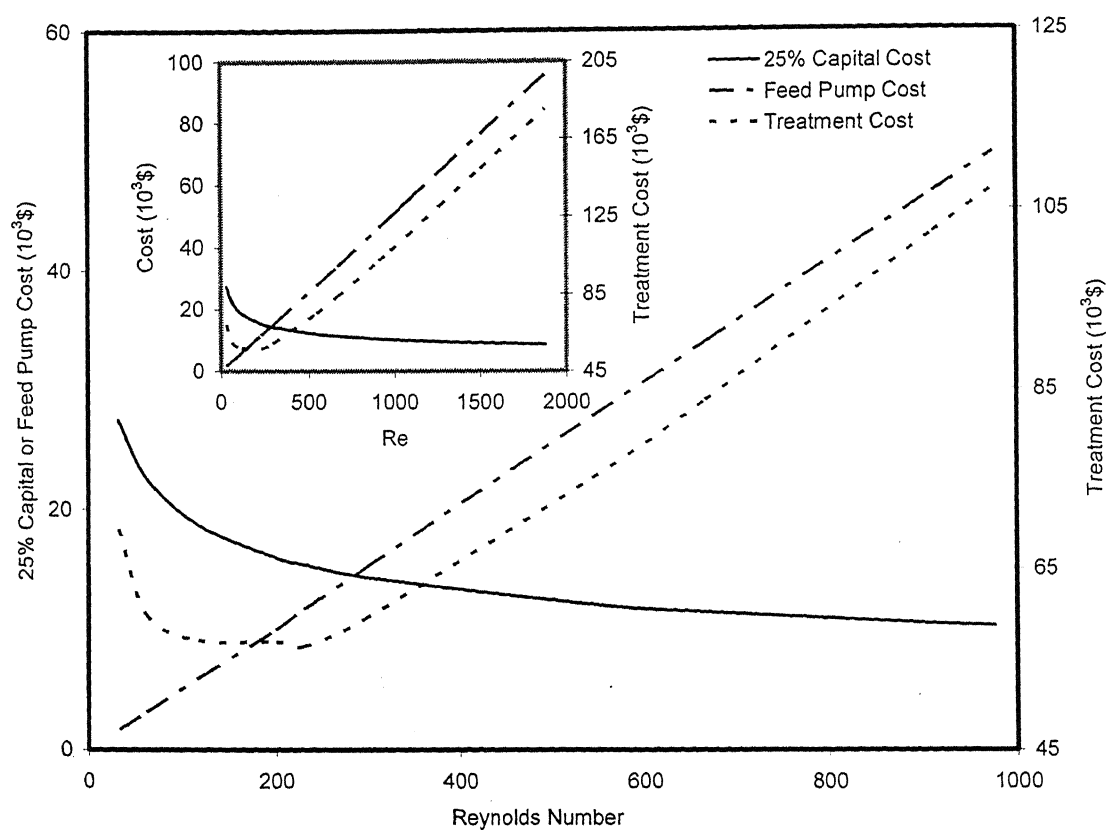
Figure 7.3 Effect of Reynolds number on cost under laminar flow for single

organic component system.

(at q=16m^3/h, l=25μm, p=1kPa, x$_{Tol}$=500ppm, r$_i$=100μm.)
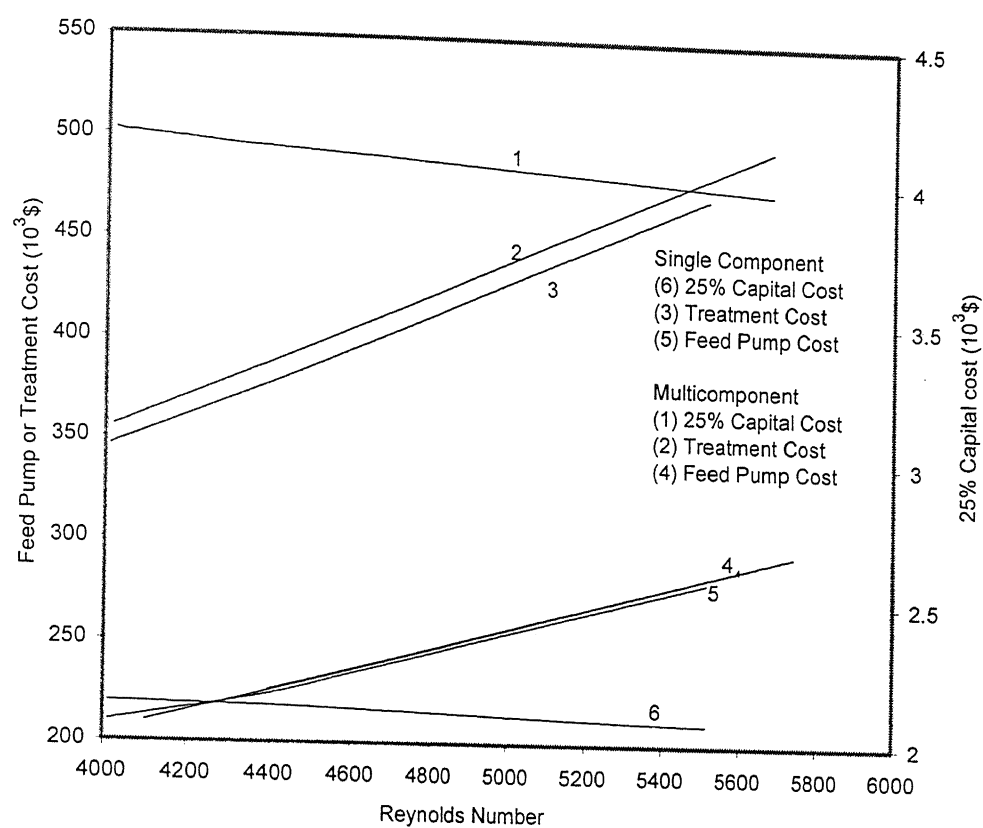
Figure 7.4 Effect of Reynolds number on cost under turbulent flow.

(at q=16m^3/h, *l*=25μm, p=1kPa, x$_{Tol}$=500ppm, r$_i$=100μm.)

Figure 7.5 Effect of Reynolds number on cost under different flow regimes at

400μm fiber diameter.

(at q=16m³/h, l=25μm, p=1kPa, x_{Tol}=500ppm, r_i=400μm.)

Table 7.4 Estimated costs at optimum points under other fixed variables.
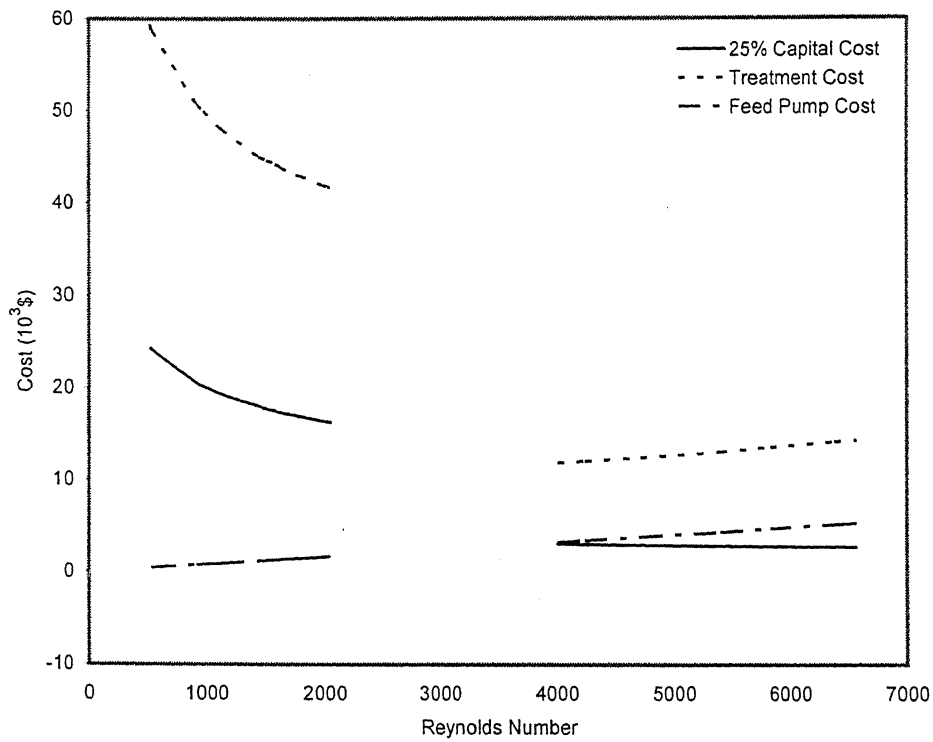
q (10⁻³) (m³/s)	Re	l (μm)	P (kPa)	x_Tol ppm	x_TCE ppm	x_MC ppm	25% Capital cost (10³$)	Membrane cost (10³$)	Condensation + vacuum cost (10³$)	Feed pump cost (10³$)	Treatment cost (10³$)
4.444	**231.0**	25	1.00	500.0	0	0	1.55	5.047	16.70	19.7	57.07
1.397	**191.9**	**62**	**3.16**	**360.8**	**0**	**0**	6.26	3.307	1.50	5.1	16.25
4.444	**161.5**	25	1.00	500.0	720.0	19400	22.32	5.535	31.05	13.8	72.74
4.444	**4009.8**	25	1.00	500.0	720.0	19400	4.16	3.004	6.84	343.5	354.88
4.444	161.5	**84**	1.00	500.0	720.0	19400	22.21	8.068	19.58	13.7	62.66
4.444	161.5	**84**	**4.00**	500.0	720.0	19400	19.45	5.835	20.03	13.7	59.12
1.444	**121.2**	**95**	**1.78**	**351.6**	**399.3**	**2698**	6.64	3.179	2.80	3.3	15.99

(Note: Optimum points are given in bold numerals)

membrane area increased. In this case, global optimum got shifted to turbulent region. These results were also similar to the earlier [4] obtained results. Effect of feed flow rate on specific treatment cost is shown in Figure 7 6. The specific treatment cost decreases slightly with increase in feed flow rate and the observations were confirmed [4]. Figure 7.7 shows the effect of feed toluene concentration on treatment cost. Treatment cost is marginally increasing with feed concentration.

7.4.2.2 Global Optimum

For global optimum analysis, all process variables were varied simultaneously. The obtained results at global points are reported in Table 7.4. It was observed that the capital cost and feed pumping cost dominated the total treatment cost. Hence, the total cost appears to be sensitive to the assumptions of the costs, chosen for module, equipment, pumping efficiency and electricity. Distribution of various costs for this system is shown in Figure 7.8 in the form of Pie chart.

7.4.3 Multi Organic Component System

Optimization of process variables for multi-component system (consisting of toluene, trichloroethane and methylene chloride) was carried out at 90% toluene removal with hollow fiber diameter of 100μm.

7.4.3.1 Effect of Process Parameters

7.4.3.1a Influence of Feed Side Reynolds Number

The effect of feed side Reynolds number on the process economics is shown in Figure 7.9, at fixed values of other variables. It is observed that the treatment cost (25% .of capital plus pumping costs, etc) initially decreases with increase in Re; however, soon this cost sharply increases with increase in Re. Hence, a minima is observed at Re of 161. This may be attributed due to the fact that as Re increases, the mass transfer

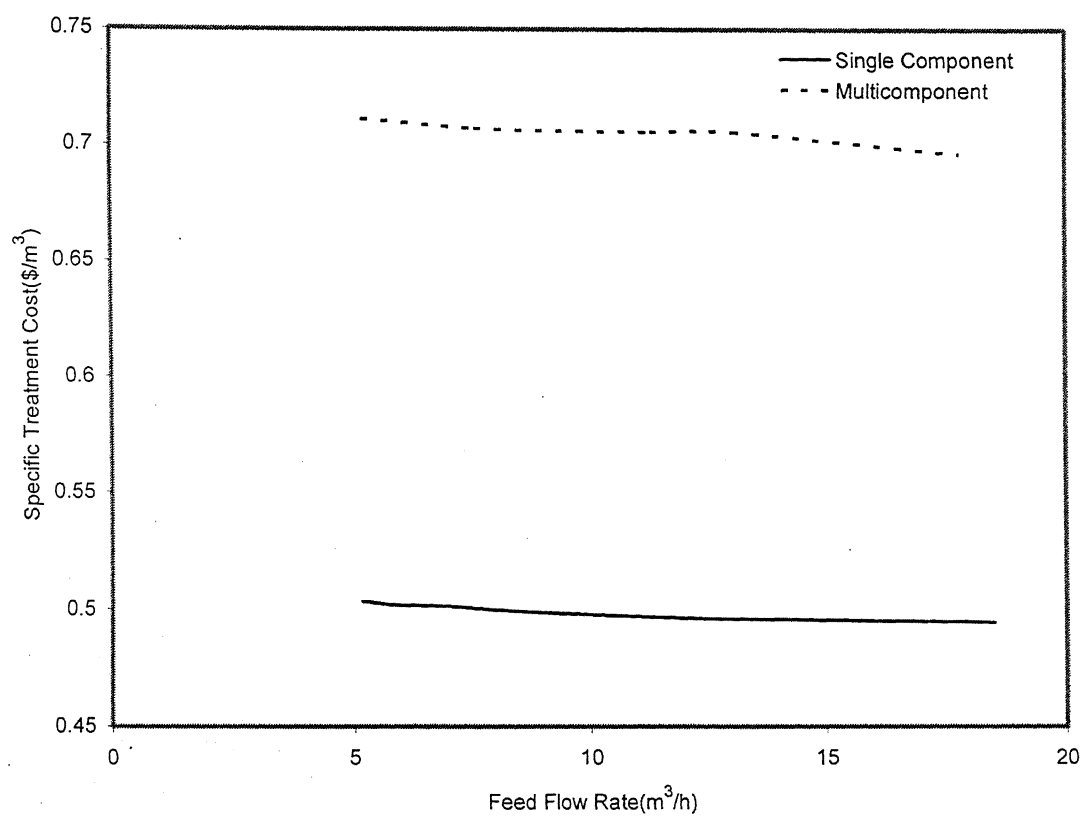**Figure 7.6 Effect feed flow rate on specific unit treatment cost**

(Re=230, l=25µm, p=1kPa, x_{Tol}=500ppm, r_i=100µm.; conditions

for single component system)

(Re=161, l=84µm, p=4kPa, x_{Tol}=500ppm, x_{TCE}=720ppm,

x_{MC}=19400ppm, r_i=100µm.; conditions for multi-component system)
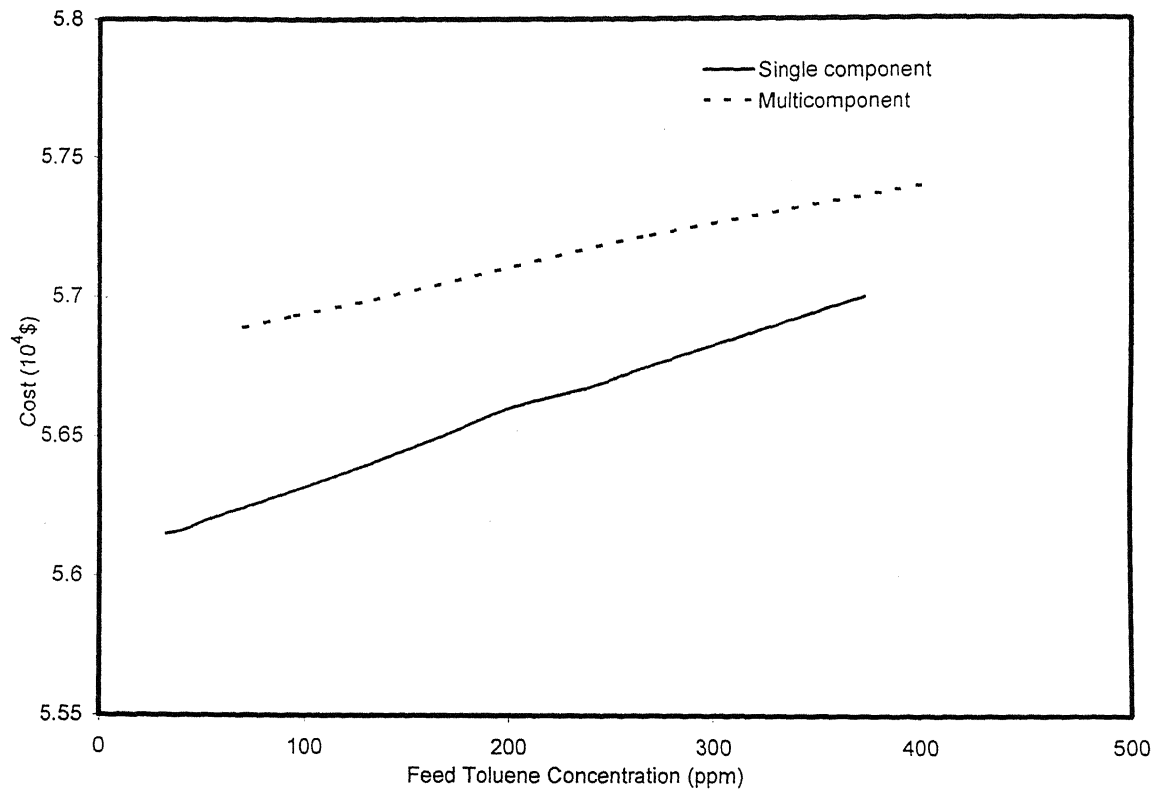
Figure 7.7 **Effect toluene feed concentration on treatment cost.**

(Re=230, q=16m^3/h, l=25μm, p=1kPa, r$_i$=100μm.; conditions for single

component system)

(Re=161,q=16m^3/h, l=84μm, p=4kPa, x$_{TCE}$=720ppm, x$_{MC}$=19400ppm,

r$_i$=100μm.; conditions for multi-component system)

1:25% Capital Cost
2:Feed Pumping Cost
3:Membrane Replacement
Cost
4:Condensation+Vacuum

2
(31.81%)

1
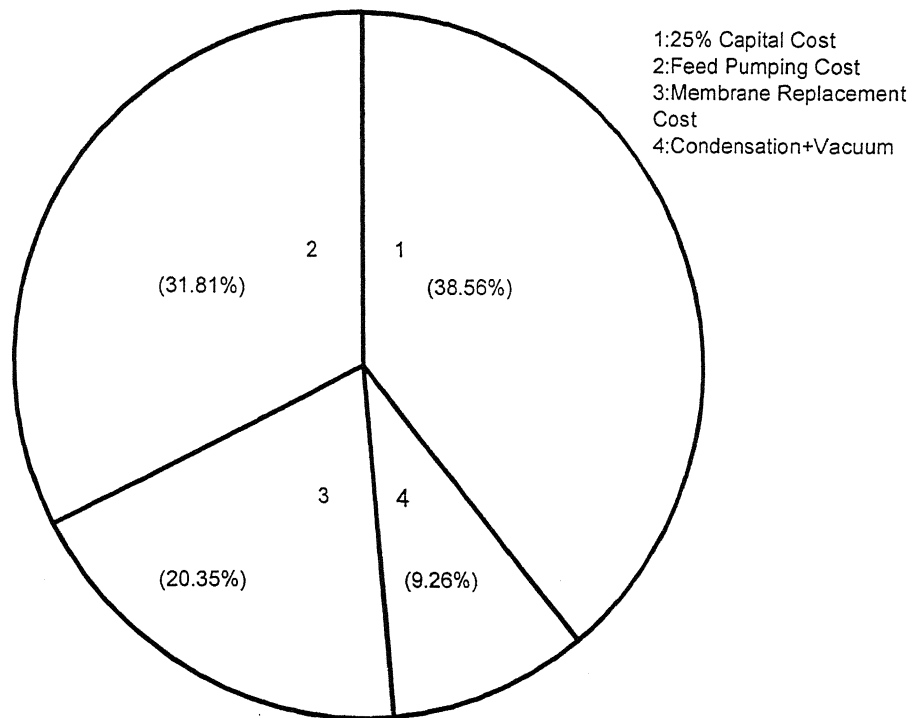(38.56%)

3
(20.35%)

4
(9.26%)

Figure 7.8 Distribution of various costs at global optimum point for single Component system.

242

coefficient in the liquid boundary layer increases which increases the overall mass transfer for a given membrane. Therefore, for fixed removal fraction of toluene, membrane area decreases. The decrease in membrane area decreases the capital cost. However, feed pumping cost increases rapidly due to the increase of pressure losses. So, operating cost increases. These two opposing trends results in an optimal value of Reynolds number of 161.5. For the full range of *Re* studied, the inset of Figure 7.9 is to be referred. Further, Figure 7.4 shows the variation of treatment cost in turbulent region. In turbulent region the mass transfer coefficients are very high because of which the requirements of membrane area and capital cost decrease. However, increase in Reynolds number increases enormously the cost of pumping the feed. Subsequently, therefore, the treatment cost increases sharply. Hence, the global optimum was found to be in the laminar region. In this study, binary diffusion coefficients were used to study the process economics. Use of diffusion coefficients in multi-component mixtures may further reduce the optimum Reynolds number due to similar nature of organic components.

7.4.3.1b Influence of Membrane Thickness

Process economics are greatly affected by the membrane thickness. Organic compounds have high affinity for silicone rubbers. With these types of polymers, the liquid film resistance may be the rate-limiting step. As a result, for poor hydrodynamic conditions, the thickness of silicone rubber may have little effect on organic flux; whereas, there may be significant reduction of water flux. The effect of membrane thickness on the treatment cost is shown in Figure 7.10. It is observed that initially treatment cost decreases significantly with increase in membrane thickness; whereas, the cost attains plateau at higher thickness (refer inset of Figure 7.10). This may be explained due to the fact that flux is high with thinner membranes. This reduces the
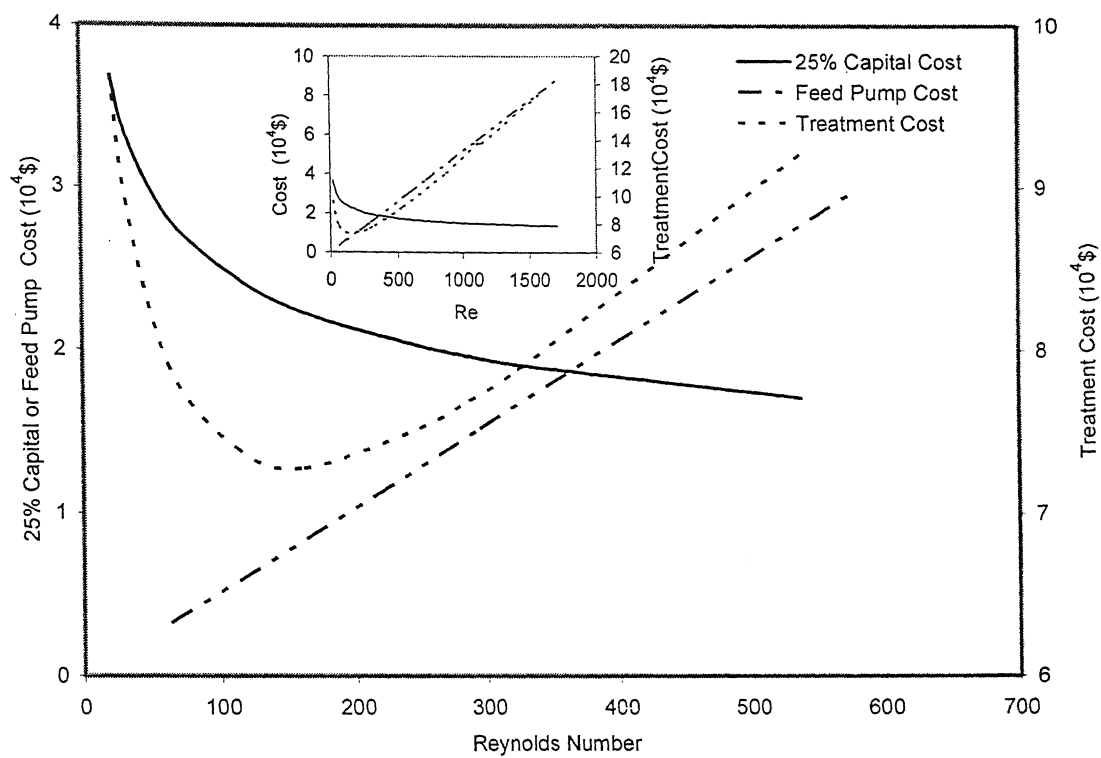
Figure 7.9 Effect of Reynolds number on cost under laminar flow for multi-component system.

(at q=16m³/h, *l*=25μm, p=1kP.a, x_{Tol}=500ppm, x_{TCE}=720ppm,

x_{MC}=19400ppm, r_i=100μm.)

membrane area and the capital cost for a given separation. However, the treatment cost becomes higher due to high-energy costs for vapour pumping and condensation. Further, from Table 7.4, it may be observed that the cost, including condensation along with vapour pumping ($19.58*10^3$), is larger than the other treatment costs (membrane costs $8.068*10^3$). Hence, treatment cost is more sensitive to condensation cost. Decrease in thickness of membrane increases treatment cost and to some extent increase in membrane thickness decreases the treatment costs. It may therefore, provide an optimum thickness of membrane. Such an optimization calculation provided the thickness of membrane as 84μm. This is too large a value as compared to the membrane thickness of single component system (25μm) [4]. Total treatment cost appears to be more sensitive to condensation energy for multi component system which may have resulted in high optimum thickness. The reason behind our earlier discussion for the case of higher membrane thickness is that the condensation cost is less for multi-component system.

7.4.3.1c Influence of Downstream Pressure

Effect of down stream pressure on process economics is shown in Figure 7.11. It is observed that treatment cost continuously decreases with increase in downstream pressure. This may be perhaps as down stream pressure increases, both water and organic flux decrease with increase in selectivity [3]. So, with the increase in downstream pressure, for fixed removal fraction of toluene, there may be marginal increase in membrane area, capital cost and membrane replacement cost. However, on other side, the sum of the vacuum pumping and condensation energy costs decrease significantly. These two opposite trends resulted in an optimum pressure of 4 kPa which is highest permissible downstream pressure. Further, in multi component system, the
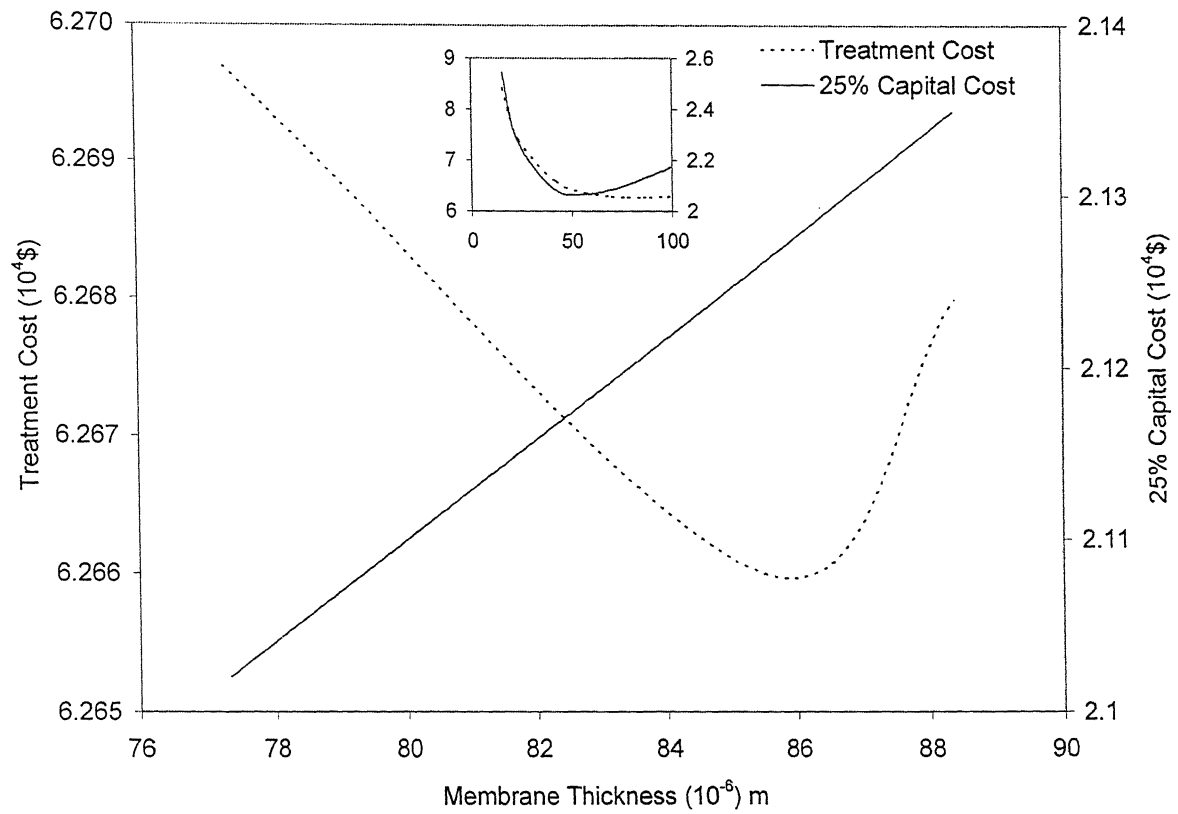
Figure 7.10 Effect of membrane thickness on cost for multi-component system.

(at Re=161, q=16m^3/h, p=1kPa, x_{Tol}=500ppm, x_{TCE}=720ppm,

x_{MC}=19400ppm, r_i=100μm.)

total downstream pressure is shared by all the components; thus the driving force for a particular component increases and this reduces the membrane area requirement. Hence, membrane replacement cost becomes less compared to single component system. However, on the other hand, cost of condensation increases, since other permeating components need also to be removed. Moreover, from Table 7.4, it may also be observed that treatment cost is more sensitive to condensation energy; hence, relatively high optimum pressure of 4 kPa was obtained for multi-component system as compared to 1.6 kPa for single component [4] system.

7.4.3.1d Sensitivity Analysis

The feed concentration and quantity of effluent may vary considerably depending on the source of the waste stream. So, it was felt necessary to study the effect of these parameters on process economics. Figure 7.6 also shows the effect of feed flow rate on specific unit treatment cost (treatment cost per cubic meter of flow rate) at optimum variables. It is evident that specific treatment cost decreases slightly with increase in feed flow rate. Therefore, an inference may be obtained that the process of pervaporation may be more economic dealing with larger flow rates of waste stream. Further, it can also observed from the graph that the increase in specific treatment cost is around $0.2\$/m^3$ for multi-component system compared to single organic component.

Further, the sensitivity of the treatment cost with respect to feed toluene concentration (at 90% toluene removal) is shown Figure 7.7. The graph shows that there is marginal increase in cost (~ $500) and hence optimal treatment cost may be considered to be independent of feed concentration. Similar types of results were also obtained for single component system. Further, from Figure 7.7, it may be observed that for fixed removal fraction of toluene, total treatment cost is almost same. Therefore, the presence of other components may not affect the process economics. In a sense, it may

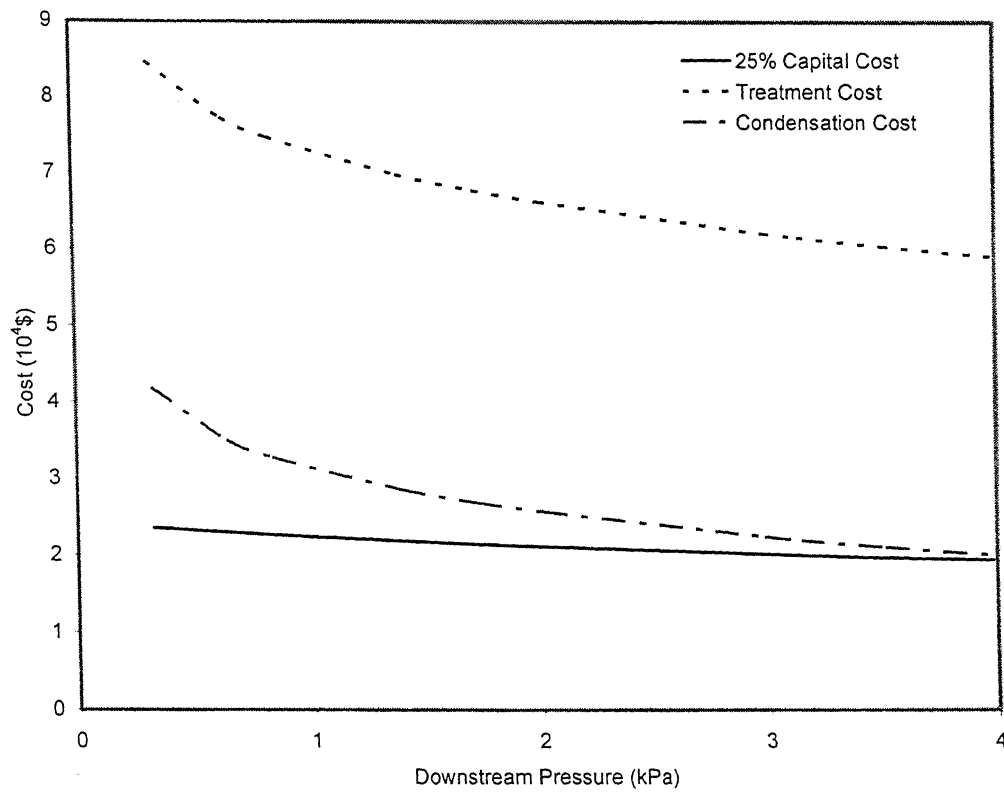**Figure 7.11 Effect of downstream pressure on cost for multi-component system.**

(at Re=161, q=16m^3/h, l=84μm, x$_{Tol}$=500ppm, x$_{TCE}$=720ppm,

x$_{MC}$=19400ppm, r$_i$=100μm.)
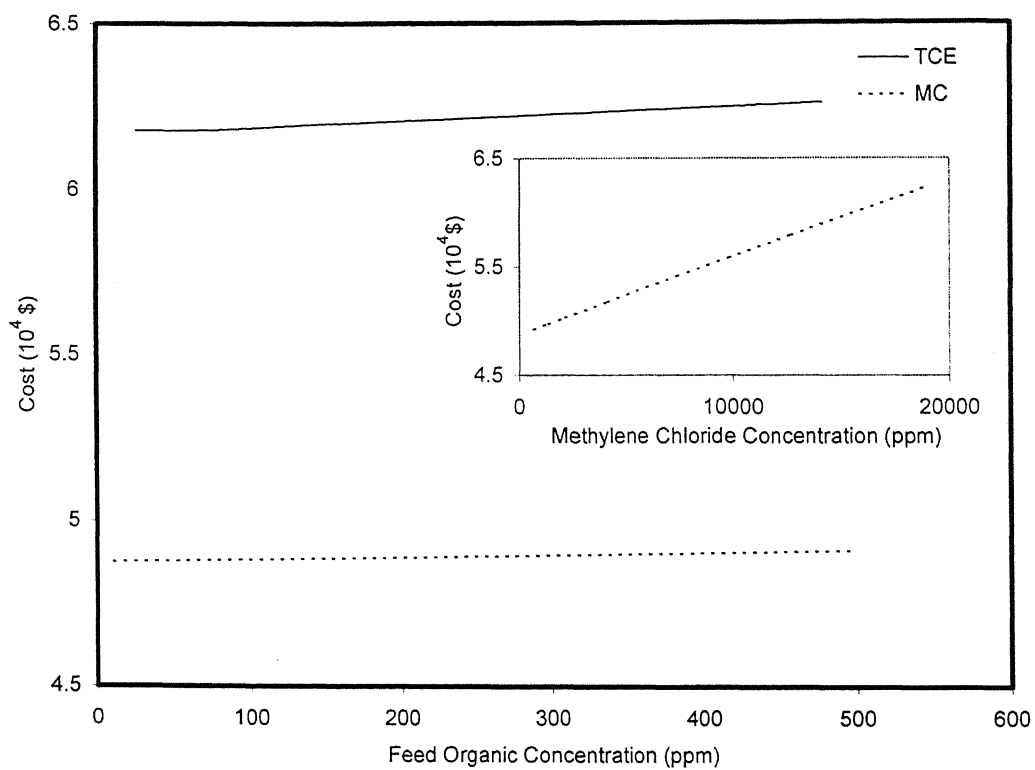
Figure 7.12 Effect of feed organic concentration on treatment cost.

(at Re=161,q=16m³/h, l=84μm, p=4kPa, x_{Tol}=720ppm, r_i=100μm.)

be concluded that the process of pervaporation may be more economical to deal with systems having multi-components as compared to the process of adsorption. In case of adsorption, presence of other components generally decrease number of adsorption sites and this increases treatment cost. Figure 7.12 shows that there is marginal effect on treatment cost with increase in the concentration of TCE in feed for 90% toluene removal. Similar trend is also observed for methylene chloride between 10 to 500 ppm concentrations. However, the effect of methyelne chloride concentration, beyond 10 to 19400 ppm, on treatment cost for 90% toluene removal has also been shown in the inset of Figure 7.12. There is now a linear increase in the treatment cost, although not significantly. This may be because of increase of flux of methylene chloride which increases its concentration in feed and hence, condensation and treatment costs also increase.

7.4.3.2 Global Optimum

The next objective of our study was to find global optimum for multi-component system by varying all variables simultaneously. Distribution of various costs at global optimum point is shown in the Figure 7.13. Table 7.4 shows the optimum values of variables for multi-component system and various costs associated at optimum points. From this Table 7.4 it is clear that the treatment cost for multi-component system is less than that of single component system at optimum point. This verifies that the separation of multi-component system by pervaporation process may be more economical. This is in contrast to conventional separation process of adsorption and air stripping, where treatment cost is more for multi-component system. Further, pervaporation process does not require any chemical reagents and/or regeneration. Unlike air stripping, it may not create any other pollution problems. Added to this, in pervaporation, removal efficiency is essentially a function of the affinity of organic
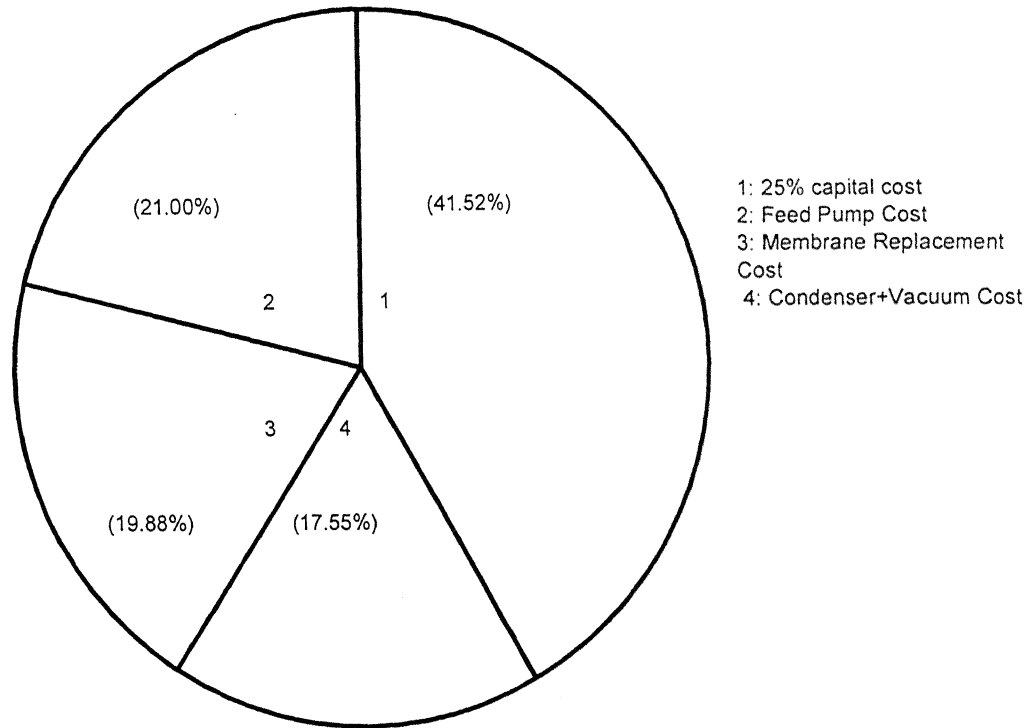
Figure 7.13 Distribution of various costs at global optimum point for multi-component system.

compounds for the polymeric membrane. A wide variety of polymers can, therefore, be used for a given separation.

7.5 Conclusions

An available [4] formulated optimized problem was solved to obtain process variables using real coded genetic algorithm for single component system. The problem was further extended for multi-component system for the purpose. The solution provided optimum process conditions for minimum annual treatment cost of waste water. It was observed that the global optimum existed in the laminar region. Further, studies on the effects of process variables on cost showed that for fixed removal fraction of toluene, treatment cost was not significantly affected by its concentration and presence of other components. The thickness of the selected PDMS membrane, a rubbery polymer (providing high organic flux), exhibited little influence on cost as compared to Reynolds number. Still, a value of 84μm was obtained as optimum thickness. In multi-component system, as total downstream pressure was shared by all components, it was observed that a low vacuum was required. Further, specific treatment cost was slightly decreasing with feed flow rate. Distribution of various costs at global optimum point for single and multi-component system has been found. The total treatment cost at optimum point was estimated to be less for multi-component system compared to single component system.

7.6 Notation

A   area (m^2)

b   module factor

C   concentration ($kmol/m^3$)

C_p specific heat capacity (kJ/kmol K)

D   diffusivity (m^2/s)

E   dimensionless number

e   price of electricity ($/kWh)

f   fugacity (kPa)

Fr   fraction

G   total permeate flow (kmol/s)

H_i Henry's law constant ($kPa\ m^3/mole$)

H   enthalpy (kJ/kmol)

N   permeation flux ($kmol/m^2\ s$)

K   overall mass transfer coefficient (m/s)

k_l mass transfer coefficient in the boundary layer (m/s)

k   heat capacity ratio

L   length of hollow fiber (m)

L_P permeability ($kmol\ m/m^2\ kPa\ s$)

l membrane thickness (m)

MC   methylene chloride

p   downstream pressure (kPa)

p^o saturated vapour pressure (kPa)

ΔP feed side pressure drop (kPa)

q   feed flow rate (m^3/s)

r_i inner radius of hollow fiber (m)

r_o outer radius hollow fiber (m)

R   universal gas constant (J/mol K)

Re   Reynolds number

Sc   Schmidt number

Sh   Sherwood number

T   temperature (K)

TCE   trichloroethane

Tol   toluene

t   time period (h)

U   overall heat transfer coefficient (kJ/s m^2 K)

W   energy consumption (kW)

x   mole fraction at feed side

y   mole fraction at permeate side

z   axial coordinate

Greek Symbols

γ activity coefficient

ρ total concentration of the feed (kmol/m^3)

Δ difference

μ viscosity (kg/m s)

η efficiency factor

$\not{c}$ cost ($)

Subscripts

F   feed side

254

i   organic compounds (i=1,2,3)

j   compounds (j=1,2,3 &water)

m   membrane

mod   module

P   permeate side

w   water

Superscripts

org   organic phase in permeate

References

[1]   J.J. Brown, M.D. Erickson, N.J. Beskid, Applying Membrane Technology to Air Stripping Effluent for Remediation of Ground Water Contaminated with Volatile Organic Compounds. Hazard Waste and Hazard. Mater. 10 (1993) 335-345.

[2]   Metcalf, Eddy. *Waste Water Engineering Treatment, Disposal and Reuse*; 1991 (3rd edition)

[3]   W. Ji, S.K. Sikdar, S.T. Hwang, Modeling of Multi-component Pervaporation for Removal Volatile Organic Compounds from Water. J. Membrane Sci. 93, (1994) 1.

[4]   W. Ji, A. Hilaly, S.K. Sikdar, Hwang, S. T. Optimization of Multi-component Pervaporation for Removal of Volatile Organic Compounds from Water. J. Membrane Sci. 97 (1994) 109-125.

[5]   C. Lipsi, P. Cote, The Use of Pervaporation for the Removal Organic Contaminants from Water. Environmental Progress. 9 (1990) 254.

[6]   D. E. Goldberg, *Genetic Algorithms in Search, Optimization and Machine Learning;* Addison-Wesley: Amsterdam, 2000.

[7]   K. Deb, *Optimization for Engineering Design*; Prentice Hall of India: New Delhi, 2000.

[8]   R. Dawkins, *The Selfish Gene*; Oxford University Press: New York, 1976.

[9]   K. Deb, *Multi-objective Optimization Using Evolutionary Algorithms*; John Wiley & Sons: New York, 2001.

[10]   F. Herrera, M. Lozano, J.L. Verdegay, Tackling Real Coded Genetic Algorithms Operators and Tools for Behavioural Analysis. Artificial Intelligence Review 12(4) (1998) 265-319.

[11] D. E. Goldberg, K. Deb, A Comparison of Selection Schemes used in Genetic Algorithms. In Foundations of Genetic Algorithms. 1 (1990) 69-93.

[12] K. Deb, R.B. Agrawal, Simulated Binary Crossover for Continuous Search Space. Complex Systems. 9(2) (1995) 115-148.

[13] K. Deb, A. Kumar, Real Coded Genetic Algorithms with Simulated Binary Crossover: Studies on Multi-modal and Multi-objective Problems. Complex Systems. 9(6) (1995) 431-454.

[14] K. Deb, S. Agrawal, A Niched – Penalty Approach for Constraint Handling in Genetic Algorithms. *In Proceedings of the International Conference on Artificial Neural Networks and Genetic Algorithms.* 1999, 235-243.

[15] E. E. B. Meuleman, B.Bosch, M.H.V. Mulder, H. Strathmann, Modelling of Liquid/Liquid Separation by Pervaporation: Toluene from Water. *AIChE.* 45 (1999) 2153-2160.

[16] E.L. Cussler, *Diffusion: Mass Transfer in Fluid Systems*; Cambridge University Press: NewDelhi, 1998 (First South Asian Edition).

[17] D. R. Woods, *Cost Estimation for the Process Industry*; McMaster University: Hamilton, 1983.

[18] I. Blume, J.G. Wijmans, R.W. Baker, The Separation of Dissolved Organics from Water by Pervaporation. J Membrane Sci. 36 (1990) 463.

[19] M. S. Peter, K.D. Timmerhouse, *Plant Design and Economics for Chemical Engineers;* McGraw-Hill: New York, 1990.

[20] W. L. McCabe, J.M. Smith, P. Harriott,. *Unit Operations of Chemical Engineering*; McGraw-Hill: New York, 1985.

[21] R.E. Trybal, *Mass-Transfer Operations;* McGraw-Hill: New York, 1986. (Third Edition).

[22] D.M. Himmelblau, *Basic Principles and Calculations in Chemical Engineering*; Prentice-Hall of India: New Delhi, 1995.

[23] S.K. Gupta, *Numerical Methods for Engineers*; New Age International: India, 1995.

[24] G. Harik, E. Cantu-Paz, D.E. Goldberg, B.L. Miller, The Gambler's Ruin Problem, Genetic Algorithms, and the Sizing of Populations. Evolutionary Computation J. 7(3) (1999) 231-254.

[25] C.Y. Chan, Aatmeeyata, S. K. Gupta, K.R. Ajay, Multi-Objective Optimization of Membrane Separation Modules using Genetic Algorithms. J. Membrane Sci. 176 (2000) 177-196.

[26] G. Ravi, S. K. Gupta, S. Viswanathan, M.B. Ray, Optimization of Venturi Scrubbers using Genetic Algorithm. Ind. Eng. Chem. Res. 41 (2002) 2988-3002.

[27] X. Qi, F. Palmieri, Adaptive Mutation in Genetic Algorithms. *In Proceedings of the Second Annual Conference on Evolutionary Programming.* 1993,192-196.

Chapter 8

Recommendations

Several experiences are gained, some of which are listed below as recommendations for future work.

[1]   Positron annihilation technique may be carried out for wet membranes to measure free volume parameters and this may be mathematically related to free volumes/pore sizes for their estimations in wet state. Further, atomic force microscope technique may be employed using smaller tip size of tip.

[2]   Positron annihilation data may be analysed with Laplace transform method for the estimation of pore size distribution.

[3]   Various hydrophobic and its modified form of polymeric membranes may be prepared for separation of hydrazine hydrate. Further, zeolites or other inorganics may be explored for dehydration of hydrazine hydrate. Such compounds may reduce swelling of the membrane and thus may increase selectivity along with higher fluxes.

[4]   Composite membranes are known to provide better flux; however, support layer properties like pore size, chemical nature of the layer (may be estimated contact angle and permeability measurements), etc., may be simulated or optimized to make them suitable for industrial applications.

[5] Online measurements of fluxes and concentrations may provide better quantitative estimation of air leaks. Alternative transport mechanism may be attempted to include Kelvin's equation. It is required to know the amount of water leakage as well as air leakage for the accurate calculations of pervaporation selectivity particularly for dehydration of mixtures.

[6] The permeate tubes, connecting downstream section of pervaporation cell and condenser, should be heated to desired temperature. This may enhance the quality of results, particularly if permeability depends on the concentration.

[7] Location of vaporization across membrane thickness during pervaporation is important. Existing models may be improved by identifying the location of vaporization. Magnetic resonance image with Anemogram may be utilised for the purpose.

[8] Hollow fiber (with tube side feed flow) pervaporation unit along with conventional distillation unit may attempted which may provide better cost effective design for hydrazine-water separation

[9] Multi objectives optimization including cost may be performed for different binary and multi component systems to analyse pervaporation cost efficiency.

[10] Simulation/optimizations of hollow fiber modules with different aspect ratio (length to diameter) may be studied.

List of Publications

Publication

1. S.V. Satyanarayana and P.K. Bhattacharya, "Real Coded Genetic Algorithm for Optimization of Pervaporation Process Parameters for Removal of Volatile Organics from Water" *Ind. Eng. Chem. Res.* 42(13) (2003) 3118-3128

Communications

1. S.V. Satyanarayana, V.S. Subrahmanyam, H.C. Verma, A. Sharma and P.K. Bhattacharya, "Positron Annihilation Study of Pervaporation Dense Membranes" *J. Membrane Sci.* (communicated).

2. S.V. Satyanarayana, A. Sharma and P.K. Bhattacharya, "Composite Membranes for Hydrophobic Pervaporation: Study with Toluene – Water System" *Chemical Eng. J.* (communicated).

3. S.V. Satyanarayana and P.K. Bhattacharya, "Dehydration of Hydrazine Hydrate by Pervaporation" *J. Membrane Sci.* (communicated).

4. Nazish Hoda, S.V. Satyanarayana and P.K. Bhattacharya, "Pervaporation of Hydrazine-Water through Hollow Fiber Module: Modelling and Simulation" *Ind. Eng. Chem. Res.* (communicated)

5. S.V. Satyanarayana, P.K. Bhattacharya and A. Sharma "Pervaporation From a Dense Membrane: Role of Permeant-Membrane Interactions, Kelvin Effect and Membrane Swelling" *Langmuir* (communicated).

Presentations

1. S.V. Satyanarayana, A. Sharma and P.K. Bhattacharya, "Prediction of Partial fluxes during Pervaporative Separation of Toluene- Water, Presented in IIChE National Conference, CHEMCON -2001, held at CLRI, Chennai during 19-22nd, December, 2001.

2. S.V. Satyanarayana, N. Hoda and P.K. Bhattacharya, "Removal of Volatile Organics from Water by Pervaporation: Optimization of Process Parameters using Real coded Genetic Algorithm," Presented in IIChE National Conference, CHEMCON -2001, held at CLRI, Chennai during 19-22nd, December, 2001.

3. S.V. Satyanarayana, V.S. Subrahmanyam, A. Sharma and P.K. Bhattacharya, Positron Annihilation Technique for Free Volume Parameters of Pervaporation Dense Membranes, presented in IIChE National Conference, CHEMCON-2002, held at Hyderabad during 19-22nd December, 2002.